Author:
Tang, Sophie

Title:
Does the IGF axis influence EMT to play a role in bladder cancer progression?

Does the IGF axis influence EMT to play a role in bladder cancer progression?

Zhen (Sophie) TANG

A dissertation submitted to the University of Bristol in accordance with the requirements for the award of the degree of

Doctor of Philosophy in the Faculty of Health Sciences

Insulin-like Growth Factors and Metabolic Endocrinology Group (IMEG), School of Clinical Sciences

October 2017

Word count 61570

Abstract

Bladder cancer is the most common malignancy of the urinary tract in humans with a high incidence and rate of recurrence. Poor prognoses are associated with disease progression including the development of resistance to chemotherapy. Epithelial-to-mesenchymal transition (EMT) and high insulin-like growth factor (IGF)-activity have been reported to facilitate tumour development in many cancer types including bladder. Insulin-like growth factor binding protein 2 (IGFBP-2), a member of the IGF system as well as the second most abundant IGFBP in human serum, can exert effects that either promote or suppress cancer progression in an IGF-dependent and/or -independent way. In this thesis, the levels of IGFBP-2, its regulation, role and the mechanisms underlying its actions were investigated in bladder cancer cell lines. The relationship between IGF/IGFBP-2-activity and their involvement in EMT was also assessed.

We observed that the epithelial-like RT4 cells had abundant levels of IGFBP-2 whereas the mesenchymal-like T24 and TCCSUP bladder cancer cells lines were null for IGFBP-2. We determined that IGFBP-2 was epigenetically silenced in the mesenchymal cell lines via DNA methylation, suggesting a reduction in IGFBP-2 was associated with more aggressive disease.

To investigate this further, we found that silencing IGFBP-2 in epithelial-like RT4 cells led to increased cell proliferation, cell invasion, as well as colony formation: along this was associated with a decrease in the levels of E-cadherin

(an epithelial marker) and the nuclear translocation of the β-catenin. Adding exogenous IGFBP-2 to mesenchymal-like T24 and TCCSUP cells had the opposite effects on all cell phenotypes that were associated with an increase in the levels of N-cadherin (a mesenchymal marker). The cell lines with higher levels of endogenous IGFBP-2 were also found to be more sensitive to cisplatin. As the data suggested that IGFBP-2 could act in both an IGF-dependent and independent manner, we also examined the actions of IGF-I and found that IGF-I induced an increase in cell proliferation, invasion, migration, colony formation and EMT-related cancer progression in both RT4 and T24 bladder cancer cell lines that appeared to involve the IGF-IR/PI3K/Akt signalling pathway.

IGFBP-2 appears to play an inhibitory role in the progression of bladder cancer by decreasing proliferation, invasion, migration, colony-formation and by modifying markers of EMT. We also observed that IGFBP-2 may represent a biomarker for chemo-sensitivity. IGFBP-2 achieves its effects on cell actions in both IGF-dependent and independent ways and as anticipated the addition of IGF-I alone had a stimulatory effect in all cell lines, on all cell phenotypes to promote bladder cancer progression.

Dedication and Acknowledgments

I dedicate this thesis to my parents, Haiming and Cuilan, who have been giving me unconditional love and ultimate support. And also to my fiancé, Xiaoshan, who is writing up his thesis at the moment and has shared with me almost half of my life with laughter and tears.

I would like to give my sincere gratefulness deep from my heart to all people who have ever helped me along the past five years. Many thanks to our great lab manager, Sue, and all IMEG members, especially Dr Claire Perks and Professor Jeff Holly, who are not only my supervisors but also super-stars shinning in my darkest days before this work was finished. Life is short; I would rather get my job beautifully done in the future with more peace and grace, not battle against time like cracking this thesis brutally in a "couple" of days…

I would like to say a special "THANK YOU!" to my dearest friends, Dr Khadija and Athba, who teach me what real friendship looks like.

At last, I would like to thank myself cheekily, for not giving up…

Never a mistake; always a lesson.

Author's Declaration

I declare that the work in this thesis was carried out in accordance with the regulations of the University of Bristol. The work is original, except where indicated by specific reference in the text, and no part of the thesis has been submitted for any other academic award. Any views expressed in this thesis are those of the author.

Signature: 

Date:

Zhen (Sophie) Tang

Email: zt12809@bristol.ac.uk

IGF and Metabolic Endocrinology Group
School of Clinical Sciences
University of Bristol
Learning and Research Building
Southmead Hospital
Bristol
BS10 5NB
United Kingdom

Table of Contents

List of Tables

List of Figures

List of Abbreviations

AJs	Adherens junctions
Akt	Also PKB, protein kinase B
ALS	Acid-labile subunit
APC	adenomatous polyposis coli
APS	Ammonium Persulphate
AZA	5-aza-dCyd
BAD	BCL-2-associated death promoter
BCA	Bicinchoninic Acid
BCG	Bacillus Calmette-Guérin
BCL-2	B-cell lymphoma 2
BdSMC	Primary human bladder smooth muscle cell line
BSA	Bovine serum albumin
BTA	Bladder tumour antigen
CDS	Cell Dissociation Solution
CER I	Cytoplasmic Extraction Reagent I
CER II	Cytoplasmic Extraction Reagent II
CFE	Colony forming efficiency
CIS	Carcinoma in situ
CIS	Cisplatin

CK1	Casein kinase 1
COBRA	Combined Bisulphite Restriction Assay
COBRA	Combined Bisulphite Restriction Assay
CS	Cadherin Switching
CT	Control
DAPI	Vectashield mounting medium for fluorescence with DAPI
Dlg5	Discs large homolog 5
DMSO	Dimethylsulphoxide
DNMT	DNA bases catalysed by methyltransferases
DPM	Disintegration per minute
EAU	European Association of Urology
ECM	Extracellular matrix
EGFR	Epidermal growth factor receptor
ELK1	ETS domain containing protein
EMT	Epithelial-to-mesenchymal transition
FBS	Foetal bovine serum
FDA	Food and Drug Administration
FGFR-3	Fibroblast growth factor receptor-3
FGFs	Fibroblast growth factors
FOXO	Forkhead box O
GA-1000	Gentamicin/Amphotericin B

GBM	Glioblastoma multiforme
GH	Growth hormone
GM	Growth Media
GSK-3β	Glycogen synthase kinase 3-β
Hegf	Human epidermal growth factor
HEPES-BSS	HEPES buffered saline solution
hFGF-B	Human epidermal growth factor-B
HPV	Guman papillomavirus
IF	Immunofluorescence
IGF	Insulin-like growth factor
IGF	Insulin-like growth factor II
IGFBP	insulin-like growth factor binding protein
IGFBPRs	insulin-like growth factor binding protein receptors
IGF-I	insulin-like growth factor I
IGF-IR	IGF-I Receptor
IGFR	Insulin-like growth factor receptor
IR	Insulin receptor
IR-A	Insulin receptor isoform A
IR-B	Insulin receptor isoform B
IRS-1	Insulin receptor substrate 1
IRS-2	Insulin receptor substrate 2

KD	Gene knocking down
KDa	Kilo Dalton
KRT 5	Keratin 5
KRT 14	Keratin 14
KSHV	Kaposi's sarcoma-associated herpesvirus
LEF	Lymphoid enhancer-binding factor
LMP	Low Melting Point
LSD	Least significant different
LY	LY294002
M6P	Mannose 6-phosphate
MAPK	Mitogen-activated protein kinase
MET	Mesenchymal-to-epithelial transition
MIBC	Muscle invasive bladder cancer
mTORC1	Mammalian target of rapamycin complex 1
mTORC2	Mammalian target of rapamycin complex 2
NaOH	Sodium Hydroxide
NBI	NBI-31772
NcRNAs	Non-coding RNAs
NER	Nuclear Extraction Reagent
NLS	Nuclear localization signal
NMIBC	Non-muscle invasive bladder cancer

NS	Non-silencing
NS*	Not significant
p-Akt	Phospho-Akt
PBS	Phosphate Buffered Saline
PCR	Polymerase chain reaction
PDAC	Pancreatic ductal adenocarcinoma
PDK1	3-phosphoinositide-dependent protein kinase 1
PFA	Formaldehyde
PI3K	Phosphoinositide-3 kinase
p-IGF-IR	Phospho-IGF-I Receptor
PIP2	phosphatidylinositol bisphosphate
PIP3	Phosphatidylinositol triphosphate
p-MAPK	Phospho-MAPK
PTEN	Phosphatase and tensin homologue deleted on chromosome ten
RGD	Arg-Gly-Asp integrin-binding motif
RTK	Receptor tyrosine kinase
SCC	Squamous cell carcinoma
SCCL	Squamous cell cancer-like
SDS-PAGE	Sodium Dodecyl Sulphate–Polyacrylamide Gel Electrophoresis
SE	Standard error
SFM	Serum Free Media

Shc	Src homology 2 domain containing proteins
siRNA	Small Interference RNA
TBE	Tris-Borate-EDTA buffer
TBST	Tris-buffered saline with Tween
TCA	Trichloroacetic acid
TCCB	Transitional cell carcinoma of bladder
TCF	Transcription factor
TE	Trypsin: EDTA Solution
TEMED	N,N,N,N-tramethyethylenediamine
TKI	Tyrosine kinase inhibitor
TTI	Tritiated Thymidine Incorporation
UNLMP	Neoplasm of low malignant potential
VEGF	Vascular endothelial growth factor
WB	Western Blotting

Chapter 1- General Introduction

1.1 Bladder Cancer

As the most common malignancy of the urinary tract, bladder cancer is a major clinical problem with its high incidence and recurrence, poor prognosis after progression, and great costs to both patients and the society.

1.1.1 Epidemiology

Based on GLOBOCAN estimates, 429,800 new cases of bladder cancer and 165,100 deaths occurred worldwide in 2012, making this disease the ninth most common cancer for both sexes combined (Ferlay, Soerjomataram et al. 2015, Siegel, Miller et al. 2015, Torre, Bray et al. 2015). In the UK, bladder cancer is also the ninth most common cancer, for both sexes combined, with 28 cases diagnosed every day (2013), and it is the fourth most common cancer in males, while the fourteenth most common cancer in females (2013) (Cancer Research UK 2016).

Bladder cancer is relatively common in more developed regions with a 10-fold variation in incidence rates internationally with the highest rates in Europe, Northern America, Western Asia, and Northern Africa, and lowest in Eastern, Middle and Western Africa (see Figure 1). In recent years, a slight decline or stability in both incidence and mortality rates, in general, have been observed in most western countries, whilst the opposite has been seen in some eastern European and developing countries. These patterns might partly reflect differences in the stage and extent of the tobacco epidemic, changes in coding

practices, schistosomiasis prevalence (Africa) and occupational exposure (Chavan, Bray et al. 2014, Torre, Bray et al. 2015).

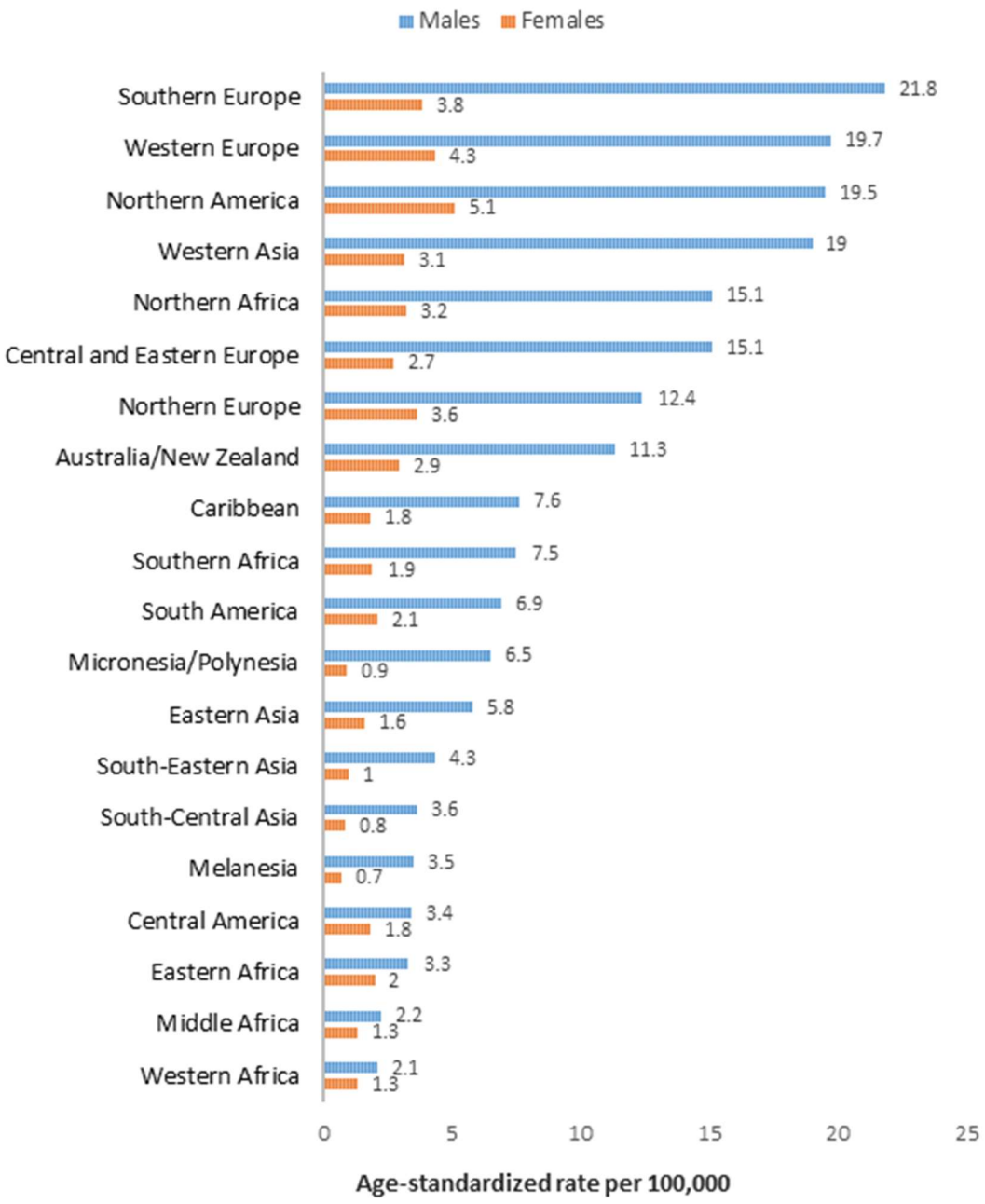

Figure 1: bladder cancer incidence rates by sex and world area (adapted from (Torre, Bray et al. 2015))

1.1.2 Risk factors

Cigarette smoking is the most well-established and the leading known risk factor for bladder cancer. It was reported that the risk among smokers is approximately 2- to 6-fold higher than among non-smokers, and smoking is estimated to be the cause of about 31% of bladder cancer deaths among males and 14% among females worldwide (Parkin 2008).

Workplace exposures such as industrial chemicals including aromatic amines (like benzidine which is used in the dye industry) and certain organic chemicals are reported to be another cause of bladder cancer if exposure is not limited by good workplace safety practices. Workplace exposures can act together with cigarette smoking to further increase the risk of developing bladder cancer (American Cancer Society 2016).

In less developed regions, especially Africa and Western Asia, another well-studied risk factor for bladder cancer is *chronic infection with Schistosoma hematobium*, which is a parasitic worm that causes urinary schistosomiasis, that accounts for nearly 50% of bladder cancers in some parts of Africa and around 3% of cases worldwide (Parkin 2006, Jemal, Bray et al. 2011, Oh and Weiderpass 2014).

During the past decade, emerging evidence has accumulated indicating a potential role of *oncogenic viruses*, including BK virus, Kaposi's sarcoma-associated herpesvirus (KSHV) and human papillomavirus (HPV), as possible cofactors in the development and progression of vesical neoplasm (Griffiths

and Mellon 2000, Cancer Genome Atlas Research 2014, Paradzik, Bucevic-Popovic et al. 2014, Alexander, Wang et al. 2015, Lee, Jeon et al. 2015, Yin, Lee et al. 2015).

Bladder cancer incidence is strongly *age-related* with highest incidence rates being in the elderly. For both sexes combined, more than half (54%) of bladder cancer cases in the UK each year are diagnosed in people aged 75 and over (Cancer Research UK 2016), and about 90% are older than 55 (American Cancer Society 2016). Studies of young patients, initially diagnosed at 40 years old or younger, have shown that the disease is mostly low grade and stage, and has a favourable prognosis; however, a small subset of patients with high-stage and high-grade tumours share similar clinical behaviours with the elderly group and have poor outcomes (Stanton, Xiao et al. 2013, Gunlusoy, Ceylan et al. 2015, Wang, Ji et al. 2016).

There is also a *gender difference* in bladder cancer incidence: males are three to four times more likely than females to develop bladder cancer (Ferlay, Soerjomataram et al. 2015, American Cancer Society 2016). However, it has been shown that women are generally diagnosed with the more advanced disease at presentation and have a worse prognosis (Henning, Wehrberger et al. 2013, Dobruch, Daneshmand et al. 2016). Differences in risk exposure, including smoking status, are independent of the difference in incidence between the sexes, and molecular mechanisms such as metabolism of carcinogens by hepatic enzymes and the activity of the sex steroid hormone pathways between the two sexes are suggested to be potential explanations (Lucca, Klatte et al. 2015, Dobruch, Daneshmand et al. 2016).

Obesity is associated with a linear increase in the risk of bladder cancer according to findings from a dose-response meta-analysis of fifteen cohort studies with 38,072 bladder cancer cases among 14,201,500 participants included (Sun, Zhao et al. 2015).

There is no strong epidemiological evidence for a *hereditary* cause of most cases of bladder cancer, although familial clusters of bladder cancer have been reported. The increased familial risk was indicated to be primarily in relatives who smoked (Tanaka, Miyazawa et al. 2011).

1.1.3 Classification

Bladder cancer can be classified into several different types according to different criteria.

1.1.3.1 Normal bladder

The bladder is a hollow organ located in the pelvis, and its main function is to store urine. Urine is generated by the kidneys and then carried to the bladder through ureters (see Figure 2). With flexible, muscular walls, an average adult bladder is able to hold approximately 300-400ml of urine without a significant rise in internal pressure, and the muscle contraction of bladder walls aids the process of urination in which urine is disposed of through the urethra (Lukacz, Sampselle et al. 2011).

The bladder wall consists of four main layers (see Figure 2).

- The innermost layer which lines the bladder wall is called the urothelium or transitional epithelium and is made up of cells called urothelial or transitional cells.

- The thin layer beneath the urothelium is called the lamina propria that comprises connective tissue, blood vessels and nerves.

- The third layer is a thick layer of muscles called the muscularis propria.

- The outermost layer is a layer of fatty connective tissue that separates the bladder from other nearby organs.

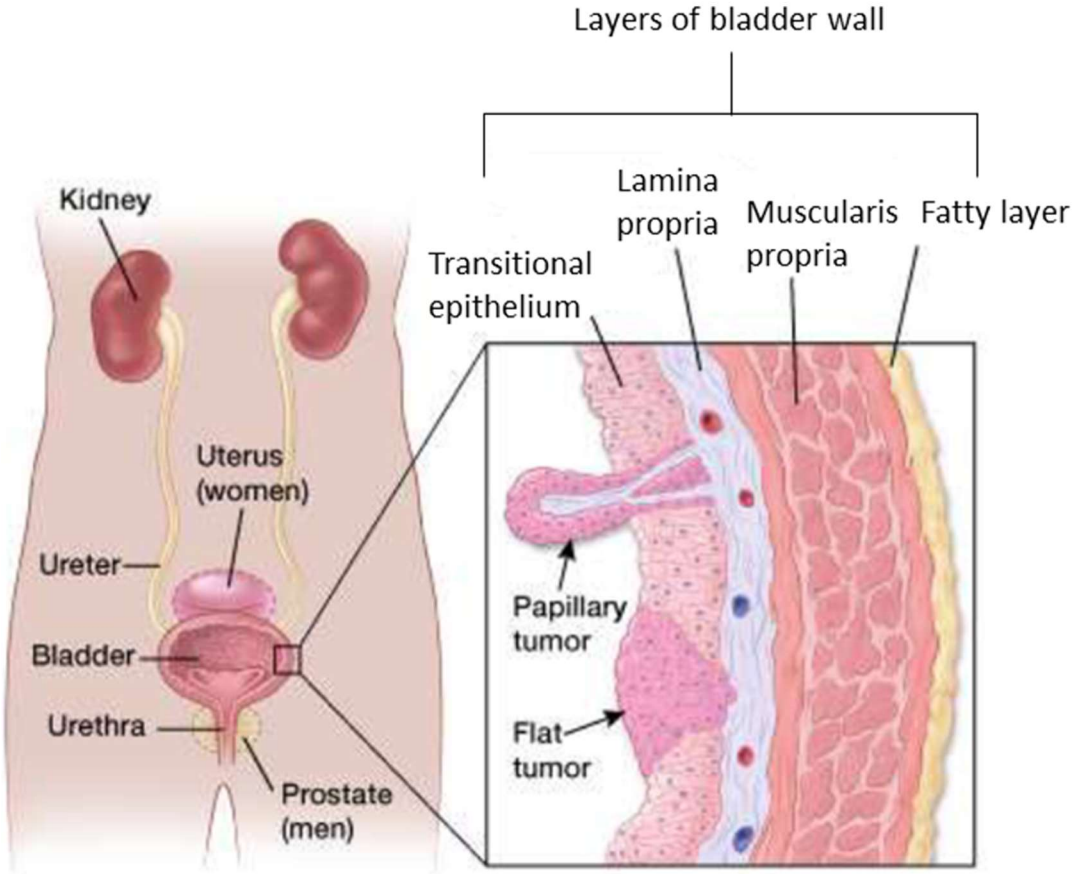

Figure 2: diagram of bladder location and bladder wall structure (adapted from (American Cancer Society 2016))

1.1.3.2 Bladder cancer of different histological types

Based on cellular characterisation, bladder cancers can be divided into several histological types. A very rare type is called sarcoma, where the cancer cells originate in the muscle cells of the bladder wall. There is another rare type, with an incidence of less than 1% in the US (American Cancer Society 2016), which starts in neuroendocrine cells, called small cell carcinoma that is also reported to develop in the urothelium (Zhao and Flynn 2012).

Greater than 90% of bladder cancers are of *urothelial* origin. Among those urothelial carcinomas, **transitional cell carcinoma of bladder (TCCB)** is by far the most prevalent (about 90%) histological type (Cancer Research UK 2016). About 8% of bladder cancer cases in the UK (Cancer Research UK 2016) and 1-2% in the US (American Cancer Society 2016) are squamous cell carcinoma (SCC) that originates in the flat cells. Approximately 1-2% of bladder cancers are adenocarcinoma which develop from cells that produce mucus (American Cancer Society 2016, Cancer Research UK 2016).

It has been indicated that squamous cell carcinoma (SCC) of the bladder is usually caused by schistosomiasis, and TCCB is associated with cigarette smoking (Torre, Bray et al. 2015).

Based on the growing pattern, TCCB can also be divided into two subtypes, papillary and flat. Papillary carcinomas grow toward the hollow centre of the bladder in a finger-like shape, and flat carcinomas, which are also called carcinoma in situ (CIS), are stemless tumours growing only in the urothelium (American Cancer Society 2016). CIS is often multifocal occurring not only in

the bladder but also in the upper urinary tract, prostatic ducts and prostatic urethra, and it can be missed at cystoscopy when not biopsied (Babjuk, Bohle et al. 2017).

At the molecular level, urothelial carcinomas of the bladder were classified into three major subtypes including the urobasal, the squamous cell cancer-like (SCCL) and the genomically unstable subtype according to the whole genome gene expression by the Lund group in 2013. The SCCL bladder cancer subtype was reported uniformly expressing keratin 5 (KRT 5), P-cadherin, keratin 14 (KRT 14), epidermal growth factor receptor (EGFR) and cell cycle genes through the tumour parenchyma, and it was associated with the worst disease-specific survival among the three defined subtypes (Sjodahl, Lovgren et al. 2013). In 2014, the Cancer Genome Atlas Research Network described a "basal/squamous-like" cluster of bladder cancers which is similar to that of basal-like breast cancers, as well as squamous cell cancers of the head and neck and lung (Cancer Genome Atlas Research 2014). And the KRT 5-expressing urothelial basal cells were demonstrated to be the likely progenitors of carcinoma in situ (CIS), squamous cell carcinoma (SCC) and muscle-invasive bladder cancers (Van Batavia, Yamany et al. 2014).

1.1.3.3 Bladder cancer of different clinical behaviours

Bladder cancers of urothelial origin are the most intensively studied, and they are divided into non-invasive and invasive cancers according to whether cancer cells have invaded into the lamina propria. The majority of bladder cancers (70%) are non-invasive tumours that do not penetrate the urothelium

and nearly all squamous cell carcinoma and adenocarcinoma are invasive (Genua, Xu et al. 2012, Stanton, Xiao et al. 2013, American Cancer Society 2016).

Based on the criterion of whether tumours have invaded the muscularis propria of the bladder wall, bladder cancers are also divided into non-muscle invasive (NMIBC) and muscle invasive (MIBC) cancers. Non-muscle invasive bladder cancers (NMIBC) include both non-invasive tumours and any invasive tumours that have not grown into the muscle layer of the bladder (American Cancer Society 2016). Among muscle-invasive bladder cancers, tumours which have spread to nearby organs are also called *advanced* bladder cancers (Cancer Research UK 2016).

1.1.3.4 Bladder cancer grade and stage

Tumour grade and stage are the most important factors for predicting disease behaviour and prognosis.

Tumours are graded according to cellular characteristics, and there are two bladder cancer classification systems currently in use. The widely used traditional World Health Organization (WHO) 1973 classification divides bladder cancers into three grades (G1-3) based on cell anaplasia and lesions with higher grade (poorly differentiated tumours) that are at a greater risk of recurrence and progression (World Health Organization 1973). A new histologic classification system was developed by WHO in 2004 introducing the terms *urothelial neoplasm of low malignant potential* (UNLMP) and papillary carcinoma of low and high grade (Eble 2004). The new system

expands the description of the categories of NMIBC aiming to improve standardised interpretation of pathological samples for better disease behaviour characterisation. For example, a tumour with particularly good prognosis (papillary urothelial neoplasm of low malignant potential) no longer carries the label of "cancer", and the use of ambiguous grading such as grade 1/2 or 2/3 (as done in the WHO 1973 classification) is avoided (Montironi and Lopez-Beltran 2005). However, a multicentre study in 328 bladder tumours showed that reproducibility of both the WHO 1973 and the WHO 2004 classifications are poor with the scoring of individual criteria poorly reproducible, indicating the descriptions of the criteria for grade are not specific, and the prognostic value of both classification differ per pathologist (Bosschieter, Hentschel et al. 2018).

The universal staging system of bladder cancer is the TNM classification (see Table 1) according to the depth of invasion (T) (see Figure 3), involvement of regional lymph nodes (N) and the presence or absence of distant metastases (M) (Turo, Cross et al. 2012, Knowles and Hurst 2015).

Table 1: TNM classification of bladder cancer (adapted from (Turo, Cross et al. 2012))

TNM classification of bladder cancer	**T*** (invasion depth)	**Tis**: transitional carcinoma in situ **T_a**: non-invasive papillary carcinoma **T_1**: invasive papillary carcinoma into the lamina propria **T_2**: invasive papillary carcinoma into the muscularis propria (**T_{2a}** into the superficial layer, and **T_{2b}** into the deeper layer) **T_3**: invasive papillary carcinoma out of the muscularis propria without contiguous organs affected **T_4**: invasive papillary carcinoma out of the muscularis propria with contiguous organs affected [* Tis – T_1 are included in non-muscle invasive bladder cancers (NMIBC), also called *superficial* bladder cancers; T_2 – T_4 are included in muscle-invasive bladder cancers (MIBC), and T_4 tumours are also called *advanced* bladder cancers.]
	N (lymph nodes)	**NX**: Regional lymph nodes cannot be assessed **N0**: No regional lymph node metastases **N1**: Metastasis to a single lymph node, ≤2cm in greatest dimension **N2**: Metastasis in a single lymph node, >2cm and ≤5cm in greatest dimension; Or multiple lymph nodes, none >5cm in greatest dimension **N3**: Metastasis in a lymph node, >5cm in greatest dimension
	M (distant metastasis)	**MX**: Distant metastasis cannot be assessed **M0**: No distant metastasis **M1**: Distant metastasis

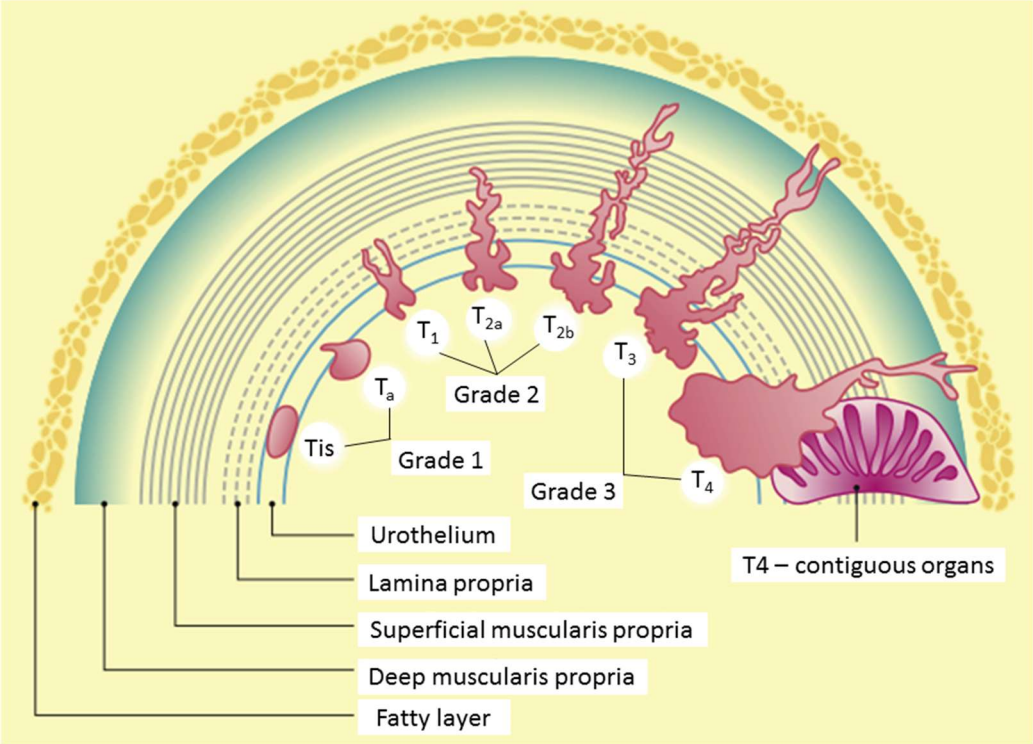

Figure 3: grading and staging of bladder cancer (adapted from (Turo, Cross et al. 2012))

TCCB is characterised by polychronotropism that is a tendency for a tumour to recur over time and in new locations in the urothelial tract, with a variable rate of progression (Turo, Cross et al. 2012). On average, about 70% of patients present with NMIBC at diagnosis, with CIS being 10%, T_a being 70% and T_1 being 20%. For patients with T_a tumours, high recurrence (up to 80%) is the main clinical issue. However, for the other 30% with CIS/T_1 tumours, progression is the main concern, occurring in up to 45%. Progression to, or presentation with, muscle-invasive disease (T_2 - T_4) indicates the critical step in the disease course of bladder cancer, necessitating more radical and aggressive therapies, and carrying a 5-year survival rate of only 27-50% (Wallace, Bryan et al. 2002, Kirkali, Chan et al. 2005, van Rhijn, Burger et al. 2009).

And updated guidenlines on non-muscle-invaisve bladder cancer (NMIBC) were released by the European Association of Urology (EAU) in 2016 stratifying patients into low-, intermediate- and high-risk groups in aid of the decisions about adjuvant intravesical instillations (Babjuk, Bohle et al. 2017). Notably, although tumours classified as stage CIS (Tis) and T_1 are grouped as NMIBC, highly malignant potential has been demonstrated by molecular biology techniques and clinical experience (Babjuk, Bohle et al. 2017).

1.1.4 Clinical information

1.1.4.1 Symptoms

The most common presenting symptom of bladder cancer is painless haematuria with approximately 80-85% of patients diagnosed with either visible or non-visible haematuria. Other urinary tract symptoms contribute to 15-20% of patients, especially those with CIS, are the same as that of bladder irritability which includes increased frequency of urination, urgency and dysuria (Amling 2001, Zhang, Han et al. 2015). For advanced bladder cancers which have grown large enough or have even spread to other parts of the body, urinary retention and weight loss are commonly observed (American Cancer Society 2016).

1.1.4.2 Diagnosis & Surveillance

In diagnosing bladder cancer, cystoscopy and urine cytology are two gold standard assays that are also applied in the follow-up surveillance. Cystoscopy is an endoscopy of the bladder via the urethra and is capable of identifying

most bladder tumours, but there are still false negative results due to operator errors or difficulty in detection of flat carcinoma *in situ* (CIS) presenting the sensitivity and specificity of white light cystoscopy range from 62-84% and 43-98%, respectively (Cauberg Evelyne, de la Rosette et al. 2011). It is a costly and quite traumatic procedure accompanied by significant discomfort and anxiety and constitutes a large part of the lifetime painful experiences of patients (Amling 2001, Tanaka, Miyazawa et al. 2011, Zhang, Han et al. 2015, Cancer Research UK 2016). Urine cytology, the examination of cellular changes from a urine specimen under a microscope, is successful in the diagnosis of most high-grade tumours in both non-muscle invasive and muscle invasive types, but has a major limitation with its low sensitivity in the detection of low-grade tumours, at about 4-31% (Zhang, Han et al. 2015).

Since bladder cancer can recur and progress, it requires lifelong surveillance after diagnosis and patients are mainly subjected to regular endoscopic check-ups which are not only painful but also costly. Although the incidence of the disease appears to have stabilised in most western countries over the past decades, it still poses a heavy economic burden to the society as a result of population ageing as well as growth worldwide. Therefore, more accurate markers for timely diagnosis are in urgent need. A few such markers have been approved for clinical use following clinical trials, but most still need more investigation.

With the advantage of being easily accessible in a rapid and non-invasive manner, urinary markers aid diagnosis by acting as predictive indicators of bladder cancer recurrence and survival in patients presenting with

haematuria. Most of the markers are still at the pre-clinical stage, and the prime tests approved by the Food and Drug Administration (FDA) are bladder tumour antigen (BTA) stat and BTA TRAK test, which provide semi- and complete quantitative detection of both complement factor H and complement factor H-related proteins, respectively, with relatively high sensitivity and specificity. Molecular markers including specific gene mutations and methylations, chromosome aberrations, and transcribed, non-protein-coding microRNA molecules, which play a key role in transcriptional regulation of gene expression, have also been studied in recent years in order to achieve better and earlier detection of bladder cancer (Tanaka, Miyazawa et al. 2011, Zhang, Han et al. 2015, Motawi, Rizk et al. 2016, Rodrigues, Jeronimo et al. 2016).

1.1.4.3 Treatments

1.1.4.3.1 Treatment for NMIBC

The primary treatment for NMIBC is transurethral endoscopic resection to remove the cancer. Perioperative intravesical therapy, chemotherapy or bacillus Calmette-Guérin (BCG) treatment into the bladder will be given to patients to reduce the risk of recurrence (Turo, Cross et al. 2012, Cancer Research UK 2016).

1.1.4.3.2 Treatment for MIBC

Partial or radical cystectomy to remove part of or the whole bladder as well as contiguous organs according to the area that the cancer cells have affected can be applied to treat invasive disease.

Compared with surgery, radiotherapy that uses high-energy rays to kill cancer cells has the advantage of keeping the bladder. However, it can cause side effects such as diarrhoea or inflammation of the bladder during treatment, and surgery would be highly recommended if cancer recurs.

With a response rate of 50-70% to frontline treatments, bladder cancer is considered to be a chemosensitive malignancy. Chemotherapy, especially those cisplatin-based combination therapies that represent the standard first-line therapy, is commonly used to destroy bladder cancer cells via the drugs' cytotoxic effects (von der Maase, Sengelov et al. 2005). It can be applied *before* surgery or radiotherapy to shrink the tumour size to improve the efficacy of subsequent treatments. Also, it can be used *during* radiotherapy (chemoradiation, with both therapies combined) to achieve better effects. When used *after* surgery, it may stop cancer recurrence. Side effects may happen depending on the dose of the drugs and the patient's' individual reaction (Cancer Research UK 2016).

1.1.4.3.3 Treatment for advanced bladder cancer

Advanced bladder cancer indicates MIBC has spread out of the bladder. For local spread (to nearby areas such as ureters, urethra, prostate or vagina) of advanced bladder cancer, surgery to remove cancer or radiotherapy are mainly used; for distant spread (to the lymph nodes in the pelvis, abdomen or neck, or to the lungs, the liver or the bones) disease, intensive chemotherapy and radiotherapy, or minor surgery to control as well as reduce symptoms are considered (Cancer Research UK 2016).

1.1.4.3.4 Targeted therapies

In recent years, bladder cancer has been recognized as a disease with several dysregulated cellular processes, and novel targeted therapies have been undergoing investigation. Molecules involved are of great interest to researchers to develop accurate biomarkers for better diagnosis, as mentioned in 1.1.4.2, as well as for more reliable prognostic tests to predict individual tumour behaviour (Nagata, Muto et al. 2016). Also, potential targeted therapies specific to the tumours will reduce treatment side effects as well as morbidity, and therefore bring notable impact to future cancer management (Mitra and Cote 2009, Turo, Cross et al. 2012).

Clinical trials in NMIBC are mainly assessing the role of immunotherapy and agents targeting molecules such as vascular endothelial growth factor (VEGF) and fibroblast growth factor receptor-3 (FGFR-3) which could be efficiently inhibited, leading to reduced tumour growth (Ghosh, Brancato et al. 2014, van Kessel, Zuiverloon et al. 2015). NMIBC with high recurrence is related to activation of the Ras-MAPK (mitogen-activated protein kinase) pathway, and the less common but more aggressive MIBC is linked to alterations in the p53 and retinoblastoma pathways (Mitra and Cote 2009, Tanaka, Miyazawa et al. 2011, Knowles and Hurst 2015). However, at present, none of the approved targeted agents for cancer therapy have been approved for the treatment of bladder cancer, and limited success was shown by the few clinical trials, due to a lack of efficacy and toxic effects (van Kessel, Zuiverloon et al. 2015).

1.1.4.4 Prevention

There are three major types of prevention defined for cancer, including bladder cancer. Primary prevention focuses on avoiding the development of cancer in the general healthy public. Secondary prevention concentrates on preventing premalignant lesions progressing to cancers. Moreover, tertiary prevention emphasises stopping cancer progression in patients who have already received treatment after being diagnosed with early cancer (Tanaka, Miyazawa et al. 2011).

Specifically for bladder cancer, it is highly recommended to avoid smoking and limit exposure to certain chemicals in the workplace to prevent the contact of certain carcinogenic chemicals with the urothelium. Drinking plenty of liquid, mainly water, and eating lots of fruit and vegetables are also advised. No routine screening is in place for the general public, however people at very high risk (certain birth defects of the bladder or those with a lot of work-related exposure to certain chemicals) are sent for screening (Tanaka, Miyazawa et al. 2011, American Cancer Society 2016).

1.2 Insulin-like Growth Factor (IGF) System

The insulin-like growth factor (IGF) family consists of two polypeptide ligands (IGF-I and IGF-II), two types of cell-surface receptors (IGFRs including IGF-I receptor and IGF-II receptor, with abbreviation of IGF-IR and IGF-IIR respectively) and six specific high-affinity binding proteins (IGFBP-1 to IGFBP-

6), as well as a large group of IGFBP proteases which cleave IGFBPs leading to the release of bound IGFs (Zha and Lackner 2010).

1.2.1 IGFs

An insulin-like factor which could not be removed by anti-insulin antibodies was discovered during the 1960s (Froesch, Buergi et al. 1963), and following sequencing, two peptides were identified (Rinderknecht and Humbel 1976) that were named insulin-like growth factor (IGF) I and II because of their structural and functional homology with insulin (Livingstone 2013).

IGF-I and IGF-II are both single-chain polypeptides mainly synthesized in the liver but they are also secreted locally by most tissues where they can act in an autocrine or paracrine manner (Le Roith 1997, Livingstone 2013). IGF-I is a basic protein of 70 amino acids with a molecular weight of 7.65 KDa, while IGF-II is a slightly acidic peptide of 67 residues with a molecular weight of 7.47 KDa (Stewart and Rotwein 1996). They have about 62% homology in their amino acid sequences and share high similarity of structure with proinsulin (Yu and Rohan 2000, Dung V. Nguyen 2013).

The location of the IGF-I and IGF-II genes are on chromosomes 12 and 11, respectively, with the IGF-II gene being 1.4 kilobases downstream from the insulin gene. The IGF-I gene has two promoter sites while the IGF-II gene has four, and it has been identified that both IGFs have multiple transcripts (Yu and Rohan 2000). While the expression of IGF-I gene is highly regulated by growth hormone (GH), IGF-II expression is much less GH-dependent but

mainly regulated by genetic factors such as genomic imprinting (Yu and Rohan 2000, Livingstone 2013). Expressions of both IGFs are also affected by other factors such as hormones (e.g. estrogens) as well as growth factors such as fibroblast growth factors (FGFs) (Yu and Rohan 2000).

Levels of IGFs in the blood present little difference between sexes but vary considerably with age. Serum IGF-I, which is required for maximal postnatal growth, are low at birth and increase progressively until puberty reaching a sharp upsurge, after which the concentration declines gradually with age. Different from IGF-I, serum IGF-II levels rise from birth until puberty, but then remain stable. IGF-II is considered to be the primary growth factor essential for embryonic and foetal growth (Stewart and Rotwein 1996, Yu and Rohan 2000). Nutritional status and dietary energy intake are critical regulators of IGF-I levels and nutrition is linked to growth via the IGF axis (Thissen, Ketelslegers et al. 1994).

Both IGF-I and IGF-II act as mitogens and can also inhibit apoptosis, thereby playing an important role not only in regulating normal cell proliferation and differentiation, but also in key aspects of neoplasia such as transformation and anti-apoptotic signalling (Yu and Rohan 2000, Zha and Lackner 2010).

1.2.2 IGFRs and cell signalling

The IGF-IR and the IGF-IIR are both located on the cell membrane and are both glycoproteins. However, they are completely different regarding structure as well as function. The IGF-IR is a tetramer consisting of two identical α subunits

and β subunits respectively, while the IGF-IIR is a monomer called the IGF-II/mannose 6-phosphate (M6P) receptor because it has three ligand-binding regions in its extracellular domain that can bind both IGF-II and M6P-containing molecules (Yu and Rohan 2000).

The IGF-IR is structurally and functionally homologous to the insulin receptor (IR). Insulin signals through the IR that exists in two isoforms (IR-A and IR-B) formed by the absence or presence of exon 11, respectively. It has been demonstrated that the expression of IR-A occurs in foetal cells as well as many tumour cells, and that signalling through IR-A leads to a more mitogenic effect compared with than that of signalling via IR-B. Hybrid receptors (see Figure 4) are composed of an α and β subunit of an IR (IR-A or IR-B) bound to the α and β subunit of the IGF-IR (Gallagher and LeRoith 2010).

IGFs and insulin can bind to each other's receptors, though the binding affinity is much weaker than that for the preferred ligand (Zha and Lackner 2010). IGF-I can bind to its specific IGF-IR as well as either type of the hybrid receptors, while IGF-II is able to bind to the IGF-IR, IGF-IIR as well as IR-A but only to the IGF-IR/IR-A hybrid. As for insulin, having negligible affinity for either IGF-IR containing hybrid, it can only bind to the IR as well as its specific IR-A/IR-B hybrids (see Figure 4) (Gallagher and LeRoith 2010).

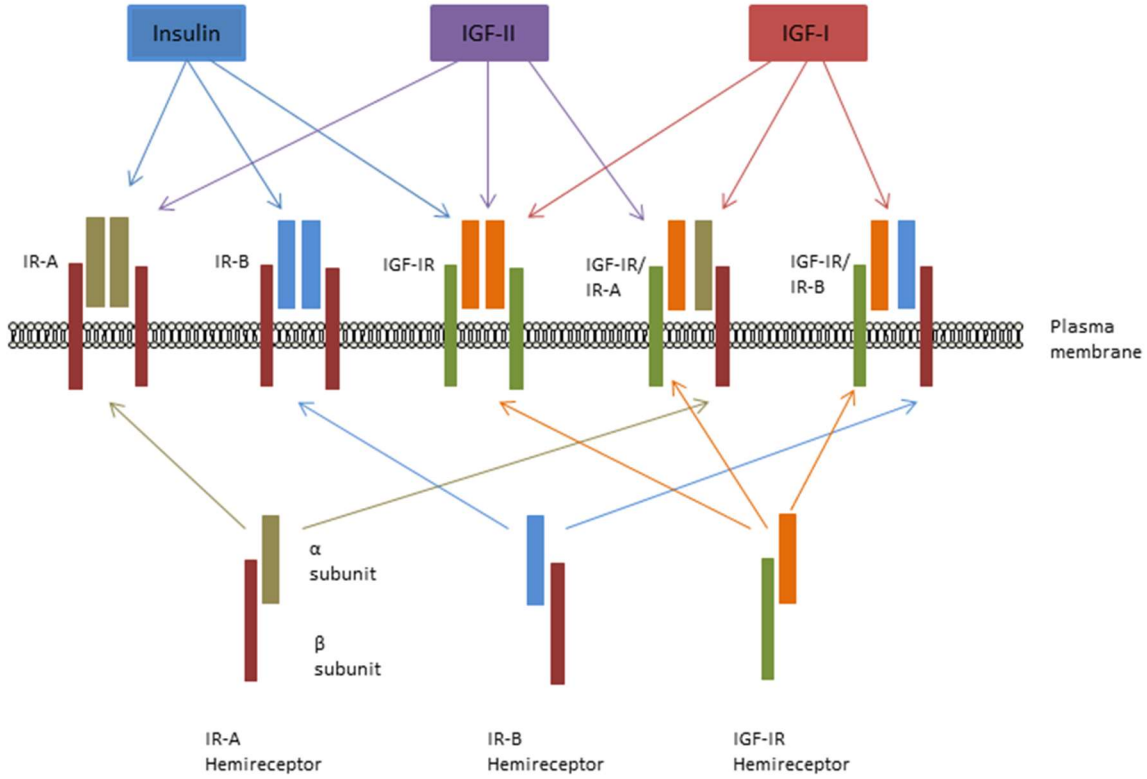

Figure 4: IGF-IR, IR, and hybrid receptors (adapted from (Gallagher and LeRoith 2010))

Compared with IGF-II, IGF-I has a higher affinity for the IGF-IR (Yu and Rohan 2000). The IGF-IR shares high structural similarity with the IR (60% homology). It is one of the cognate receptor tyrosine kinase (RTK) for the PI3K (phosphoinositide-3 kinase)/Akt (a serine/threonine kinase, also known as protein kinase B, or PKB) pathway and binding of IGFs to the IGF-IR can induce IGF-IR clustering and auto-phosphorylation resulting in activation of downstream signalling (Baselga 2011). In contrast, instead of mediating signalling, the main role of the IGF-IIR is to regulate extracellular IGF-II levels through receptor-mediated endocytosis followed by IGF-II degradation in lysosomes (Zha and Lackner 2010).

There are two main signal transduction pathways including the PI3K/Akt pathway and the mitogen-activated protein kinase (MAPK) pathway which have been well characterised for the IGF-IR (see Figure 5) (Zha and Lackner 2010).

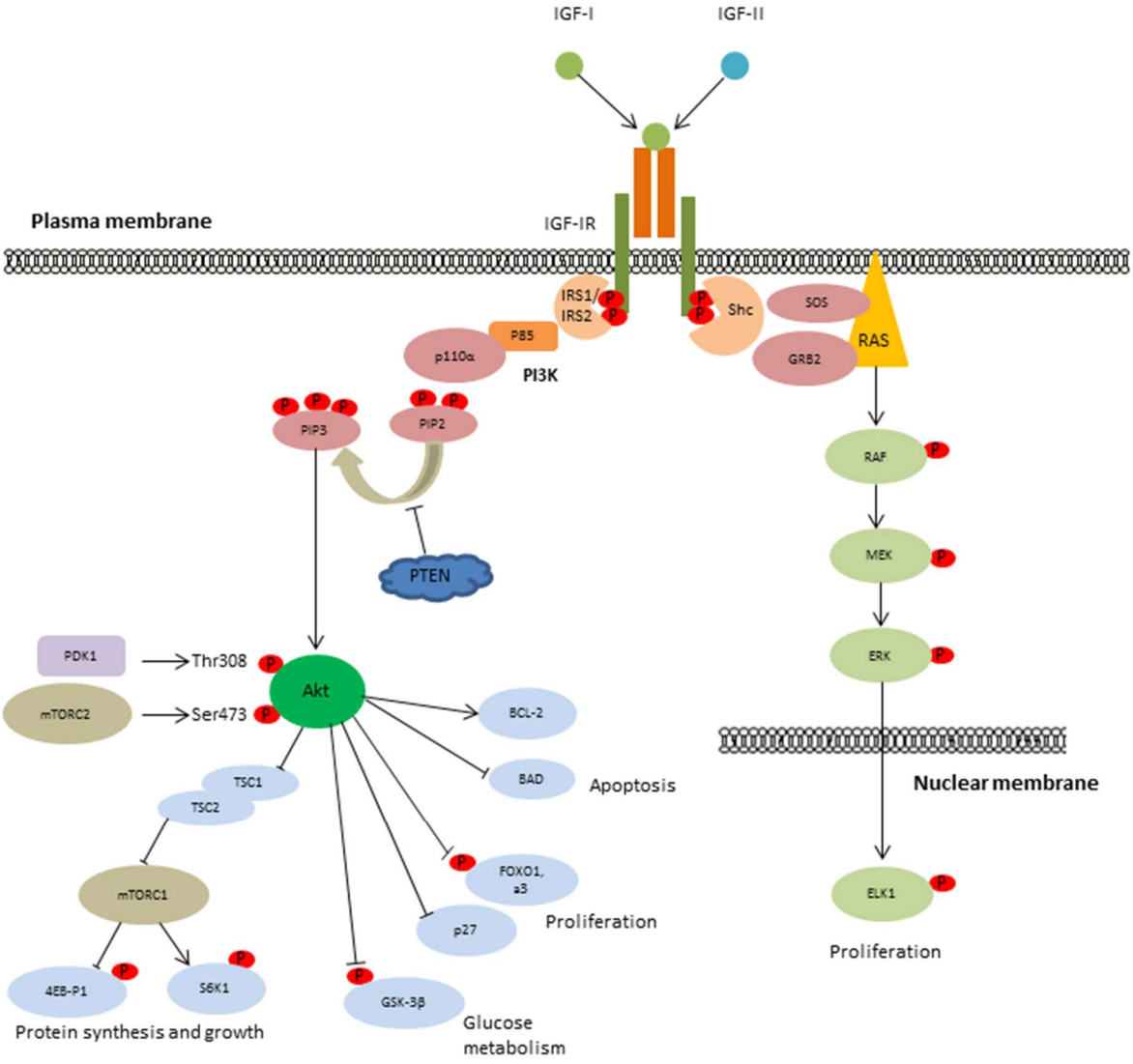

Figure 5: key components of IGF-IR signalling pathways (adapted from (Zha and Lackner 2010))

IGFs are both capable of binding to and stimulating the catalytic activity of the IGF-IR. Upon activation, phosphorylated IGF-IR stimulates the two signalling pathways by recruiting and activating their adaptor proteins, insulin receptor substrate 1/2 (IRS-1/IRS-2) and Src homology 2 domain containing proteins (Shc) respectively.

In the **MAPK pathway**, the stimulation of Shc initiates cascades that result in the activation of target nuclear genes such as ETS domain containing protein (ELK1) leading to an enhancement of cell proliferation (Zha and Lackner 2010, Baselga 2011). The **PI3K/Akt signalling pathway** is switched on by IRS-1 phosphorylation resulting from activation of the IGF-IR. Phosphorylated IRS-1 binds to p85, the regulatory subunit of PI3K, which results in the removal of the inhibitory effect of p85 on p110, the catalytic subunit of PI3K, and thus leads to full activation of PI3K. Activated PI3K catalyses the phosphorylation of phosphatidylinositol bisphosphate (PIP2) into phosphatidylinositol triphosphate (PIP3) which provides Akt with a docking site to move to the cell membrane to play a critical role as the central mediator of the PI3K/Akt pathway. Once localized, Akt is phosphorylated and activated by 3-phosphoinositide-dependent protein kinase 1 (PDK1) and mammalian target of rapamycin complex 2 (mTORC2) complex and then mediates a series of cell signalling events including increased cell survival and proliferation through activation or inhibition of key effectors such as B-cell lymphoma 2 (BCL-2), BCL-2-associated death promoter (BAD), Forkhead box proteins (Foxo, e.g. Foxo3a) transcription factors and p27, increased protein synthesis and cell growth by disinhibition of mammalian target of rapamycin complex 1

(mTORC1), and increased glycogen conversion from glucose after the inhibition of Glycogen synthase kinase 3-β (GSK-3β). Beside the stimulatory components, there are also some molecules acting in an intrinsic inhibitory way in the pathway, such as phosphatase and tensin homologue deleted on chromosome ten (PTEN) that converts PIP3 back into PIP2. PTEN is considered to be a tumour suppressor which modulates cell growth and apoptosis (Yamada and Araki 2001) and PTEN loss due to mutations also plays a role in activating this pathway (Zha and Lackner 2010, Sfakianos, Lin Gellert et al. 2014).

1.2.3 IGFBPs

Six IGFBPs (IGFBP-1 to 6) with specific binding affinities for IGFs have been identified through cloning and sequencing (Yu and Rohan 2000, Sandhu, Gibson et al. 2004). They are secreted proteins that are also found intracellularly, with evidence for nuclear translocation of some IGFBPs such as IGFBP-2 (Ahmad, Morton et al. 2011, Baxter 2014). All six IGFBPs are structurally similar consisting of three distinct domains, including N-terminal, linker, and C-terminal, and they have similar IGF binding determinants located in both the N- and C-domains. There are also other functional motifs, such as Arg-Gly-Asp (RGD) integrin-binding motif and nuclear localization signal (NLS) motif, which enable IGFBPs to engage in various interactions with ligands other than IGFs (Fukushima and Kataoka 2007, Forbes, McCarthy et al. 2012). Basic characteristics of IGFBPs are summarised in Table 2.

Table 2: summary of IGFBPs characteristics (adapted from (Fukushima and Kataoka 2007))

	IGFBP-1	IGFBP-2	IGFBP-3	IGFBP-4	IGFBP-5	IGFBP-6
Gene location	7p13-p12	2q33-q34	7p13-p12	17q12-q21.1	2q33-q36	12q13
Gene size (kbp)	5.3	31.0	9.0	14.0	23.0	4.7
mRNA size (kbp)	1.6	1.4	2.6	2.2	6.3	1.0
Molecular weight (KDa, mature protein)	25	31	43-45	24	29	28-30
Amino acids (mature protein)	234, 216	289	274	237	252	213
Serum concentration (nM)	2-15	2-15	100	2-15	2-15	2-15
RGD sequence	√	√				
NLS			√		√	√

Levels of most of the IGFBPs are stable in the circulation except for IGFBP-1, which is closely related to levels of insulin with a negative correlation (Yu and Rohan 2000). Like IGFs, levels of IGFBPs in blood show little variation between sexes but change significantly with age. Concentrations of IGFBP-1 and IGFBP-2 in blood are high at birth and then decline with age until puberty to reach a

nadir, after which the levels stay relatively constant or increase slightly. IGFBP-3 shows a similar age-specific distribution to that of IGF-1. There is limited data indicating that levels of IGFBP-5 decline with age, but strong evidence to show that concentrations of IGFBP-4 and IGFBP-6 increase with age (Yu and Rohan 2000).

Compared with the IGFRs, IGFBPs have a higher binding affinity for the IGFs. In the pool of circulating IGF-I and IGF-II, less than 1% are free in serum, while more than 99% are bound and restricted to IGFBPs. IGFBP-bound IGFs are more stable, whilst unbound/free IGFs have a circulating half-life of only a few minutes due to degradation (Yu and Rohan 2000). The predominant circulating form of IGFs in serum is a ternary complex consisting of IGF, IGFBP-3 (and, to a lower degree, IGFBP-5), as well as the acid-labile subunit (ALS) which is a glycoprotein staying in the circulation. The remaining bound IGFs are thought to be carried by IGFBPs of the smaller molecular weight in binary complexes without the involvement of ALS that can be carried out of the circulation (Baxter 2014).

IGFBPs can modulate cell function in both IGF-dependent and IGF-independent ways (Yu and Rohan 2000, Baxter 2014). In respect of IGF-dependent actions, IGFBPs regulate the availability of IGFs to their receptors by first binding and then either transporting or sequestering IGFs, resulting in either stimulation (Uzoh, Holly et al. 2011) or suppression of cell proliferation. In IGF-independent model, direct interaction of IGFBPs with cell surface molecules, such as integrin recptors and some have reported the existence of IGFBP receptors (IGFBPRs) and intracellular IGFBPs interactions with nuclear

hormone receptors (Beattie, Phillips et al. 2008, Perks and Holly 2008). Some preclinical studies have shown the paradoxical role of IGFBPs, such as IGFBP-2, both in tumour suppression (Hoflich, Lahm et al. 1998) and promotion (Foulstone, Zeng et al. 2013) in various cancers in different contexts.

1.2.4 IGF axis and bladder cancer

The IGF axis is a critical regulator of many physiological processes, including cell proliferation, differentiation, apoptosis and metabolism of glucose and is often found to be dysregulated in a number of different cancers and as such has been intensively investigated as a potential target to inhibit cancer progression.

Multiple components of the IGF axis haven been reported to be dysregulated in cancer.

High levels of circulating IGF-I are associated with an increased risk of certain types of cancers, including prostate (Roddam, Allen et al. 2008), colorectal (Rinaldi, Cleveland et al. 2010), and breast cancers (both pre- and post-menopausal women) (Endogenous, Breast Cancer Collaborative et al. 2010). Upregulated levels of IGF-II have been associated with Ewing's sarcoma (Manara, Landuzzi et al. 2007), a paediatric tumour type, as well as a worse prognosis in a variety of adult malignancies (Singer, Mogg et al. 2004, Lu, Katsaros et al. 2006). IGFs are suggested to influence tumour progression and metastases by promoting cancer cell proliferation, angiogenesis, survival and motility, as well as synergising with other molecules and growth factors

(Clayton, Banerjee et al. 2011). However, a pilot study demonstrated that levels of free IGF-I either in urine or serum are not helpful in predicting tumour development in patients with bladder cancer (Serel, Turan et al. 2003).

Overexpression of the IGF-IR has been reported in several cancers (Bergmann, Funatomi et al. 1995, Pandini, Vigneri et al. 1999, Hellawell, Turner et al. 2002, Weber, Fottner et al. 2002, Fottner, Minnemann et al. 2006). Hyper-activation of the IGF-IR pathway is considered to lead to promotion and progression of many cancer types including bladder cancer (Metalli, Lovat et al. 2010), and repressing IGF-IR signalling using microRNA-143 has been indicated to enhance cell chemo-sensitivity and reduce cell proliferation in bladder cancer (Wang, Li et al. 2017). With the development of research into novel agents targeting pathways, emerging studies have identified the IGF-IR as a therapeutic target (Sachdev and Yee 2007, Heidegger, Massoner et al. 2015).

Levels of IGFBP-1 and -2 can be suppressed by insulin, and low concentrations of both IGFBPs in obese people due to hyperinsulinemia have been suggested to elevate the potential mitogenicity of the IGFs, which leads to an increased risk of cancer in obese individuals (Renehan, Frystyk et al. 2006).

Conflicting data have been reported on IGFBP-2 expression levels in different disease settings and its role in cancers. It is considered to be an oncogenic protein with elevated expression observed in many cancers such as glioma (Moore, Holmes et al. 2009) and prostate (Karantanos, Corn et al. 2013), with inhibition of IGFBP-2 reported to improve cell sensitivity to cisplatin in bladder cancer (Zhu H 2015). In our laboratory, investigations have been

making in the field of how IGFs and related factors may mediate the effects of nutrition on chronic illness and major epithelial caners, and works focused on IGFBP-2 suggest its promoting role in the development of various cancers such as breast (Perks, Vernon et al. 2007, Foulstone, Zeng et al. 2013) and prostate (Uzoh, Holly et al. 2011). However, high levels of IGFBP-2 are observed in rapidly growing non-invasive brain tumours, whereas low/undetectable levels are found in invasive malignant tumours (Shelton, Mukherjee et al. 2010).

IGFBP-3, the most abundant IGFBP, is purported to play a protective role in cancer development as consequence of sequestering IGFs and decreasing the IGF-dependent signalling via the IGF-IR, thus causing cell cycle arrest and apoptotic signals upregulation (Jogie-Brahim, Feldman et al. 2009). It can also act in an IGF-independent manner exerting both positive and negative effects on cell functions (McCaig, Perks et al. 2002, Perks, Burrows et al. 2011).

1.3 Epithelial-to-Mesenchymal Transition (EMT)

1.3.1 Definition

Epithelial-to-mesenchymal transition (EMT) is defined as a series of events during which epithelial cells lose their epithelial characteristics like intercellular adhesion and cell polarity, and gain an enhancement of mesenchymal properties like cell motility (Guarino, Rubino et al. 2007, Gos, Miloszewska et al. 2009).

The EMT phenomenon was first observed during embryonic development (Savagner, Boyer et al. 1994) and described as "*epithelial-mesenchymal transformation*" using a model of chick primitive streak formation (Hay 1995). The term "*transformation*" has been changed to "*transition*" over time based on the difference of it between neoplastic transformation (Kalluri and Neilson 2003) and the nature of reversibility during this process (Chen, Han et al. 2012, Martyn-Hemphill, Mak et al. 2013).

Conversely, mesenchymal-to-epithelial transition (MET) describes the reverse process of EMT in which cells are switched from a mesenchymal-like to an epithelial-like phenotype by regaining key epithelial features like homotypic adhesion: this frequently occurs during early embryogenesis as well as the wound healing process (McConkey, Choi et al. 2009, Chen, Han et al. 2012).

1.3.2 Subtypes

EMT is categorised into three distinct types that are involved in different functional settings.

Type 1 EMT, which is also called *developmental* EMT, is associated with implantation, embryo formation as well as organ development, and generates diverse cell types which share common mesenchymal phenotypes in an organised manner (Kalluri and Weinberg 2009).

Type 2 EMT links to organ fibrosis and inflammation. In the situation of inflammation, as can be seen during wound healing and tissue regeneration, EMT ceases once inflammation is attenuated (Kalluri and Weinberg 2009).

Type 3 EMT is also called ***oncogenic*** EMT, and it occurs in neoplastic cells which have undergone genetic and epigenetic alterations previously, specifically in genes which favour clonal outgrowth and the development of localised tumours (Kalluri and Weinberg 2009, Yun and Kim 2013).

1.3.3 EMT and cancer

Invasion, as the mark of malignancy, encompasses the translocation of tumour cells from the original neoplastic focus into adjacent host tissues, and distant metastases take place when these invasive cells enter the circulation after intravasation through lymph or blood vessels (Guarino, Rubino et al. 2007, Son and Moon 2010).

EMT enables cells to change from an adherent epithelial-like into a highly motile mesenchymal-like phenotype, which allows cells to gain the ability to migrate and invade after being released from the parent epithelial tissue site, and thereby facilitates metastatic progression of cancer (Guarino, Rubino et al. 2007, Gos, Miloszewska et al. 2009, Tiwari, Gheldof et al. 2012, Smith and Bhowmick 2016).

In addition, MET, the reverse process of EMT plays a part in the establishment and stabilisation of distant metastases by allowing invasive cancerous cells to regain epithelial features and integrate into the secondary foci (Guarino, Rubino et al. 2007, Yang and Weinberg 2008).

So far, there is growing evidence supporting EMT with cancer progression, and it has become the most accepted explanation of distant metastases of epithelial

cancers including TCCB (Guarino, Rubino et al. 2007, De Wever, Pauwels et al. 2008, Acloque, Adams et al. 2009, McConkey, Choi et al. 2009, van der Horst, Bos et al. 2012, Zhu, Pan et al. 2012, Murai, Yamada et al. 2014, Wu, Sarkissyan et al. 2016).

1.3.4 Molecular mechanisms of EMT

The process of EMT comprises a form of epithelial plasticity that is categorised by changes in epithelial cells not only morphologically but also molecularly (Abba, Patil et al. 2016). Although the molecular basis has not been fully elucidated, some key molecules and transduction pathways that are potentially involved have been reported.

Typically, EMT is characterised by down-regulation of epithelial cell adhesion proteins, E-cadherin and cytokeratins and associated with up-regulation of mesenchymal proteins such as N-cadherin and vimentin (Ko, Yanai et al. 2009, Yao, Li et al. 2013, Wu, Sarkissyan et al. 2016). Transcription factors like Snail, Slug, Twist, and zinc finger E-box-binding homeobox (ZEB1 and ZEB2) are categorised as EMT inducers (Wu, Sarkissyan et al. 2016). Understanding the molecular mechanisms responsible for EMT-mediated tumour progression will be of great importance to disease management.

1.3.4.1 Cadherin switching

Cadherins are prime mediators of intercellular adhesion and are expressed ubiquitously in all tissues. By forming homodimers, they bind to their counterparts on adjacent cells at adherens junctions (AJs) and play key roles in embryonic development as well as in the maintenance of normal tissue architecture (Ko, Yanai et al. 2009, Mitra and Cote 2009).

Among classical cadherin family members, E-cadherin is expressed by most normal epithelial cells and plays a central role in facilitating the barrier functions of epithelial tissues by connecting epithelial cells through its interaction with β-catenin and the actin cytoskeleton (see Figure 6) (McConkey, Choi et al. 2009). N-cadherin is expressed by neural, endothelial and muscle cells and not normally by epithelial cells (Bryan 2015).

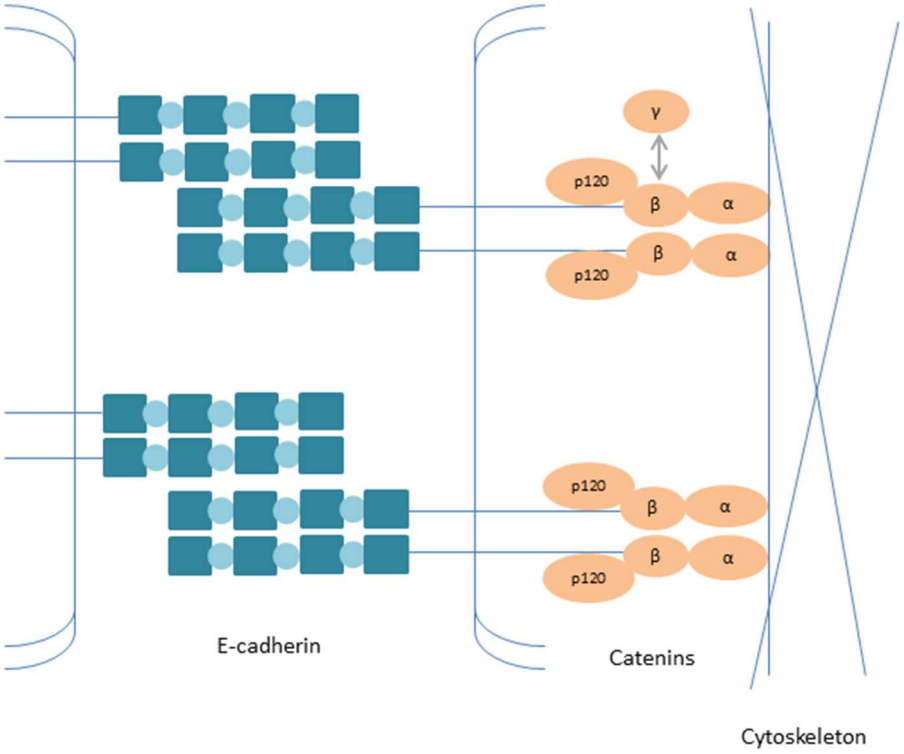

Figure 6: cell-cell adhesion in epithelial tissues (adapted from (McConkey, Choi et al. 2009))

Molecular structure of adherens junction showing the relationship between E-cadherin molecules and neighbouring cells, and among E-cadherin, catenins, and cytoskeleton.

The change of cadherins that occurs during the process of EMT is named "Cadherin Switching (CS)" indicating the switching in the expression of cadherins from one subclass to another, or the termination of expression of a certain cadherin subclass in a tissue (Bryan and Tselepis 2010).

In the context of epithelial malignancies including bladder cancer, CS is typically observed where normal expression of E-cadherin is replaced by the abnormal expression of N-cadherin, or N-cadherin expression is increased while E-cadherin levels do not change significantly. This switch may mediate the migration of cells into tissues with a similar cadherin expression profile

(e.g. vascular endothelium) and away from the epithelial compartment and it may also change intracellular signalling to enhance cell growth and invasion (Bryan 2015).

P-cadherin has also been demonstrated playing a very important role in TCCB with increased expression associated with higher grade and stage of tumours as well as worse prognosis, and similar findings were noted in breast cancers (Bryan, Atherfold et al. 2008). And an alternative switch from E-cadherin to P-cadherin instead of N-cadherin has been observed in cancers such as bladder, gastric and breast, although the role of P-cadherin in CS is less clear than that of N-cadherin (Bryan and Tselepis 2010). In addition, P-cadherin has also been shown to inhibit invasion and promote an epithelial instead of a mesenchymal phenotype in some malignancies such as malignant melanoma and oral squamous cell carcinoma (Bryan and Tselepis 2010).

1.3.4.2 Wnt/β-catenin signalling pathway

The Wnt/β-catenin signalling pathway is one of several signalling pathways that have been strongly implicated in inducing EMT in epithelial cells including bladder cancer urothelial cells, and its aberrations have been linked to many cancers (Loh, Hedditch et al. 2013, Gheidari, Bakhshandeh et al. 2014, Li, Ma et al. 2014). β-catenin interacts with E-cadherin directly and is confined by it to the cell adhesion complex as shown in Figure 6, and nuclear translocation of β-catenin presents a key step involved in Wnt/β-catenin signalling pathway (see Figure 7).

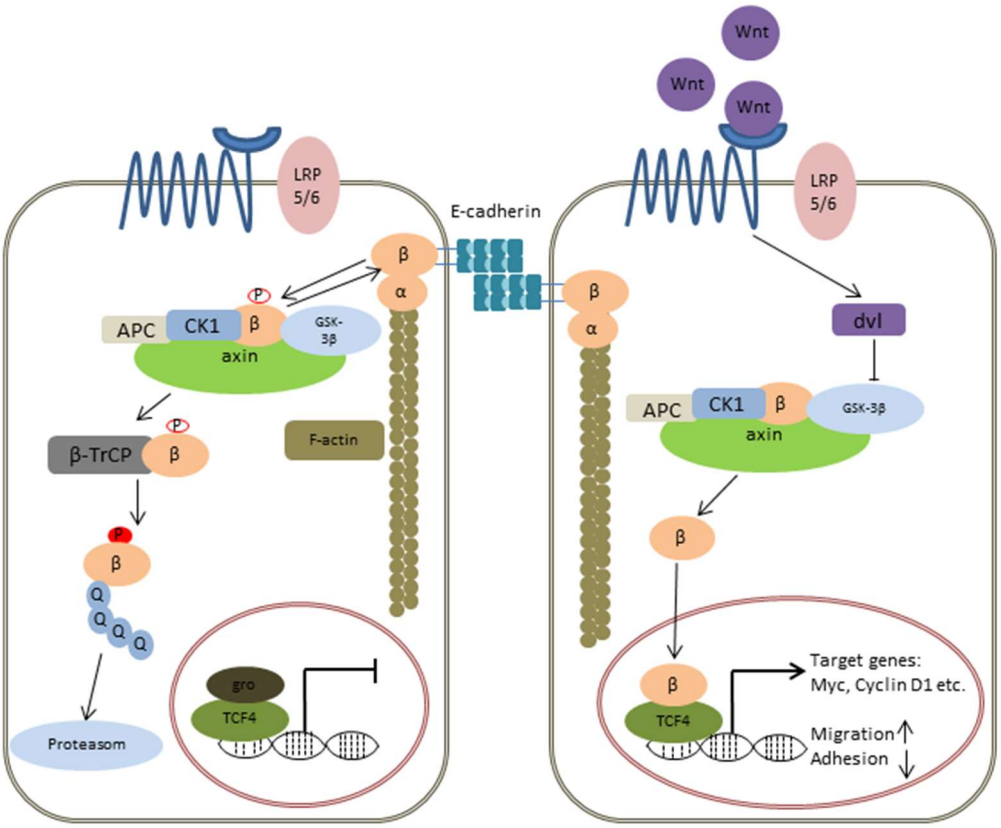

Figure 7: the Wnt/β-catenin pathway and the nuclear translocation of β-catenin (adapted from (Jin, George Fantus et al. 2008)).

In the absence of Wnt signalling, cytoplasmic β-catenin is phosphorylated and degraded by a multi-protein scaffolding complex consisting of adenomatous polyposis coli (APC), casein kinase 1 (CK1), GSK-3β, and axin. When the pathway is activated, by the binding of a Wnt ligand to its frizzled transmembrane receptor, GSK-3β is inactivated by phosphorylation of its serine and then the degradation of β-catenin is blocked. Thus β-catenin accumulates, translocates into the nucleus where it binds to Transcription factor (TCF)/Lymphoid enhancer-binding factor (LEF) members and transcriptionally regulates Wnt target genes including cyclin D1 and c-myc, resulting in promotion of cancer development (Jin, George Fantus et al. 2008, Ahmad, Morton et al. 2011).

As shown in Figure 5 in section 1.2.2, the inhibition of GSK-3β also occurs in PI3K/Akt pathway in IGF-signalling system, and accumulating evidence indicates that accumulation of Snail, a GSK-3 substrate, resulting from GSK-3β's inhibition leads to the downregulation of E-cadherin since Snail is a transcriptional repressor of E-cadherin (Bachelder, Yoon et al. 2005, Doble and Woodgett 2007). And a reduction of E-cadherin, as mentioned above in 1.3.4.1, is an important event in the EMT process.

1.3.5 EMT and IGF axis in cancer

In recent years, emerging evidence indicates a role of the IGF axis in EMT.

By upregulating certain molecules including transcription factors, such as ZEB-1, which lead to changes of EMT molecules, IGF-I/IGF-IR signalling, especially the PI3K/Akt pathway, has been implicated in inducing EMT in many types of cancer, including the breast (Walsh and Damjanovski 2011, Al Moustafa 2013, Liao, Wang et al. 2014, Taliaferro-Smith, Oberlick et al. 2015, Zielinska, Bahl et al. 2015), prostate (Graham, Zhau et al. 2008), gastric (Li, Li et al. 2015, Li, Xu et al. 2015), colorectal (Yao, Su et al. 2016), and non-small cell lung cancer (Nurwidya, Takahashi et al. 2014). Attenuation of IGF-IR signalling inhibits or even reverses EMT in cancers including breast (Lorenzatti, Huang et al. 2011), pancreatic (Subramani, Lopez-Valdez et al. 2014) and non-small cell lung cancer (Nurwidya, Takahashi et al. 2014, Zhou, Wang et al. 2015). Emerging evidence supports the significant correlation between decreased E-cadherin expression and tumour development, and it has been identified as an epithelial marker, with its downregulation

considered to be a critical event in EMT in association with increased risk of tumour recurrence and progression, as well as with shorter survival in bladder cancer patients (Bringuier, Umbas et al. 1993, Byrne, Shariat et al. 2001, Mahnken, Kausch et al. 2005, Mhawech-Fauceglia, Fischer et al. 2006).

It has also been reported that IGF-II, acting via the IGF-IR, promotes EMT by relocating E-cadherin from the membrane to the cytoplasm with increased degradation of E-cadherin (Morali, Delmas et al. 2001). A reduction of membrane E-cadherin can also release β-catenin into the cytoplasm, which can lead to its stabilization as well as translocation into nucleus activating Wnt signalling when it over-loads its degradation pathway, thereby stimulating tumour migration (see Figure 7) (Morali, Delmas et al. 2001, Ahmad, Morton et al. 2011). This, however, can only occur when the normal β-catenin degradation pathway is impaired which can be caused by inactivation of GSK-3β via its phosphorylation by Akt, which itself is activated by the PI3K/Akt signalling pathway. Also, the IGF-IR has been found to be within the same membrane complex as E-cadherin/β-catenin (Morali, Delmas et al. 2001). IGFBPs have also been reported to promote EMT: IGFBP-3 promotes EMT as well as invasion in transformed human oesophageal epithelial cells, by acting in an IGF-independent manner through TGF-β (transforming growth factor β) signalling, another critical EMT-mediating signalling pathway (Natsuizaka, Ohashi et al. 2010) and IGFBP-4 is reported to promote EMT in glioblastoma cells (Praveen Kumar, Sehgal et al. 2014).

The link between IGF-IR/PI3K and E-cadherin/β-catenin pathways and bladder cancer formation as well as progression was also supported by a

clinical study that reported the correlations between high levels of β-catenin/pAkt (activated Akt) and low levels of PTEN which blocks cell proliferation (Ahmad, Morton et al. 2011).

A further interaction between the IGF-IR/PI3K and E-cadherin/β-catenin pathways was realised when it became clear that β-catenin was able to bind in a complex with forkhead box O (FOXO) transcription factors in the nucleus. FOXO proteins mainly mediate ageing and stress signalling that promote cell cycle arrest, stress resistance, and apoptosis. Nuclear FOXO proteins compete with TCF transcription factors for binding to β-catenin and this competition determines the resultant transcriptional targets affected by β-catenin. Insulin/IGF induced activation of Akt results in phosphorylation of FOXO proteins leading to their binding to 14-3-3 proteins that then retains the FOXO proteins in the cytoplasm and thus promotes cell survival by reducing the nuclear actions of FOXO proteins (Jin, George Fantus et al. 2008).

However, a recent study in colon cancer showed opposite results that β-catenin binding to FOXO3a proteins diverts the affected target genes away from inducing genes associated with apoptosis to instead of genes associated with cell scattering and metastasis (Tenbaum, Ordonez-Moran et al. 2012). Consistent with this effect on metastasis, high levels of both β-catenin and FOXO3a in colorectal cancers are associated with reduced patient survival (Tenbaum, Ordonez-Moran et al. 2012).

In contrast with bladder cancer, low levels of FOXO3a have been associated with reduced patient survival, and knockdown of FOXO3a in bladder cancer

cells increased cell motility and reduced E-cadherin levels (Shiota, Song et al. 2010). Similarly, low levels of FOXA1 have been associated with high-grade bladder cancer, and knockdown of FOXA1 in bladder cancer cells decreased E-cadherin expression and increased cell proliferation (DeGraff, Clark et al. 2012).

These reports indicate that there are functional interactions between FOXO proteins and E-cadherin/β-catenin in bladder cancers but with different consequences to that reported in colon cancer cells. The interactions between FOXO proteins and β-catenin/TCF proteins in the nucleus and the consequences of such interactions in bladder cancer cells have yet to be examined.

1.4 Epigenetics

1.4.1 Definition

The term *epigenetics* was first introduced in the early 1940s, and its widely accepted definition is "the study of changes in gene function that are mitotically and/or meiotically heritable and that do not entail a change in DNA sequence" (Dupont, Armant et al. 2009).

Epigenetic regulation plays an important part in different stages of normal development, through which they gain the ability to develop cell- and tissue-type specific gene expressions, although most of their cells contain the same genome (Waterland and Michels 2007, Nickel and Stadler 2015).

1.4.2 Epigenetics and cancer

So far, epigenetic alterations described in the literature consist of DNA methylation, histone modifications, nucleosome remodelling, and non-coding RNAs (ncRNAs) (Dupont, Armant et al. 2009, Han, Wolff et al. 2012, Nickel and Stadler 2015).

In recent decades, epigenetic abnormalities have been widely studied and are considered to play a critical role in cancer initiation as well as progression (Han, Wolff et al. 2012). Abnormal epigenetic modifications which lead to gene aberrant expression and malfunction have been reported in many types of cancer, including liver (El Tayebi and Abdelaziz 2016), lung (Hwang, Kim et al. 2013), lymphoma (Hassler, Klisaroska et al. 2012), colorectal (Williams, Zhang et al. 2011), breast (Liu, Liu et al. 2014, Nickel and Stadler 2015) as well as bladder (Han, Wolff et al. 2012, Tahara, Shibata et al. 2014, Wu, Cao et al. 2015).

Dysregulation of members of the IGF family resulting from epigenetic modifications have also been demonstrated in many studies, among which genes of IGFBP family have consistently been reported to exhibit aberrant DNA methylations in tumours. Methylation is characterised as the predominant modification in mammalian DNA. Aberrant DNA methylation refers to a process by which methyl group are added to DNA bases catalysed by methyltransferases (DNMT 1-3), and it happens exclusively at cytosine and guanine nucleotides with the intervening phosphate group (CpG) dinucleotides in mammals (Dupont, Armant et al. 2009). For example, gene promoter hypermethylation of IGFBP-2 in hepatomas (Chiba, Yokosuka et al.

2005), and of the IGFBP-3 promoter in several types of cancer, such as renal (Morris, Gentle et al. 2008), ovarian (Wiley, Katsaros et al. 2006), breast (Zeng, Jarrett et al. 2013), and bladder (Christoph, Weikert et al. 2006). In a study of hepatocellular carcinoma, IGFBP-3 was considered to be a tumour suppressor with proof of cell growth inhibition after its reactivation (Baxter 2014), and DNA methylation of IGFBP-3 is proposed as a potential marker of disease stage as well as tumour aggressiveness (Perks and Holly 2015). Of the other IGFBP genes, IGFBP-4 was found hypermethylated in about 42% of lung adenocarcinomas, and IGFBP-6 in approximately 23% of gastric carcinomas (Baxter 2014).

Likewise, associations of EMT with aberrant epigenetic regulations, especially DNA methylations, have been suggested in cancers, for instance bladder (Han, Wolff et al. 2012, Tahara, Shibata et al. 2014, Varol, Konac et al. 2014, Wu, Cao et al. 2015) and breast (Liu, Liu et al. 2014, Nickel and Stadler 2015). For example, loss of expression of Discs large homolog 5 (Dlg5) has been reported to involve in the prostate cancer cell migration and invasion (Tomiyama, Sezaki et al. 2015), and hypermethylation of Dlg5 gene was found associated with silencing of Klg5 expression in bladder cancer cell lines and in bladder cancer tumours, especially in muscle-invasive tumours (Zhou, Guo et al. 2015). Moreover, some studies have elucidated underlying abnormal modulations of EMT-inducing transcription factors caused by epigenetic modifications (Huangyang and Shang 2013, Malouf, Taube et al. 2013, Bedi, Mishra et al. 2014, Carmona, Davalos et al. 2014, Diaz-Lopez, Diaz-Martin et al. 2015).

While most studies place emphasis on the research of tumours induced by silenced tumour suppressor genes due to abnormal hypermethylation of the promoters, global hypomethylation (losses of DNA methylation) has also been indicated in the development and progression of cancer (Chen and Wu 2016).

A genome-wide analysis of DNA methylation patterns in urothelial tumours showed distinct methylation patterns, with hypo- only in non-invasive tumours and widespread hyper- in invasive ones, implying different underlying epigenetic pathways (Wolff, Chihara et al. 2010).

Based on the nature of reversibility of epigenetic alterations, compared with genetic mutations, the accumulating findings of epigenetically regulated genes, as well as potentially involved transduction signalling pathways, provide the possibility of treating some tumour subtypes by reversing their phenotypes (Knowles and Hurst 2015), and all this information has shed light on possible epigenetic target cancer therapies. For example, drugs such as decitabine (5-aza-dCyd), and gemcitabine, which is a pillar in the treatment of MIBC (Kaneko, Kikuchi et al. 2011), could hypothetically be used as effective anticancer agent targeting the reversal of methylation-mediated silencing of critical genes in certain cancers (Ghoshal and Bai 2007, Gray, Baird et al. 2012).

1.5 Project Aims

With the background of emerging evidence indicating the potential involvement of the IGF axis and EMT in many cancers that has led to promising diagnostic/prognostic biomarkers and/or therapeutic treatments, it is

frustrating that there is limited literature regarding this for bladder cancer. Particularly as this is one of the most expensive malignancies due to its high recurrence in early stage tumours and high morbidity in advanced disease. Therefore, the principle objective of this project was to determine the role of the IGF axis in relation to EMT and progression of bladder cancer.

1.5.1 Project hypothesis

An increase of IGF-activity results in decreased levels of E-cadherin, induction of N-cadherin, and an increase in nuclear localisation of β-catenin, which promotes EMT and the progression of bladder cancer. IGFBP-2 acts as a protective factor in bladder cancer development, and so is suppressed in aggressive disease via gene promoter hypermethylation.

1.5.2 Project aims:

- To assess the levels and role of IGFBP-2 in bladder cancer.
- To explore the association of IGFBP-2 with cell sensitivity to cisplatin in bladder cancer.
- To investigate the regulatory and working mechanisms of IGFBP-2 in bladder cancer.
- To assess the effect of IGF-I on bladder cancer cells.
- To look into the relationship of EMT and IGFBP-2/IGF-I in bladder cancer.

Chapter 2- Materials and Methods

2.1 Cell Culture

2.1.1 Equipment

Incubator (SANYO MCO-18AIC, Panasonic Biomedical, Leicestershire, UK)

Hood (BIOMAT Class II, Medical Air Technology, Manchester, UK)

Cell Culture Plastics (Greiner Bio-one, Gloucester, UK)

Pasteur Pipettes (Fisher Scientific, Loughborough, UK)

Centrifuge (Centaur2, MSE, London, UK)

Syringe/Needles (Terumo, Leuven, Belgium)

Hemocytometer (Fisher Scientific, Leicestershire, UK)

Cryogenic vials (NUNC, Roskilde, Denmark)

Filters 0.2μm (Appleton Woods, Birmingham, UK)

2.1.2 Cell Lines

Four human urinary bladder cancer cell lines and one primary human bladder smooth muscle cell line (BdSMC), were used in this study, and their characteristics are listed below (see Table 3).

Table 3: Cell line characteristic

Cell line	Source info.	Obtainment info.
RT4	Organism: Homo sapiens (human) Tissue: urinary bladder Disease: transitional cell papilloma Age: 63 years Gender: male Ethnicity: Caucasian Morphology: epithelial Growth properties: adherent	Purchased from ATCC Catalogue No.: HTB-2 Lot No.: 59817519
UMUC3	Organism: Homo sapiens (human) Tissue: urinary bladder Disease: transitional cell carcinoma Age: unknown Gender: male Ethnicity: unknown Morphology: epithelial Growth properties: adherent	Purchased from ATCC Catalogue No.: CRL-1749
T24	Organism: Homo sapiens (human) Tissue: urinary bladder Disease: transitional cell carcinoma Age: unknown Gender: female Ethnicity: unknown Morphology: epithelial Growth properties: adherent	A kind gift from Professor Margaret Knowles (University of Leeds)
TCCSUP	Organism: Homo sapiens (human) Tissue: urinary bladder Disease: grade IV, transitional cell carcinoma Age: 67 years Gender: female Ethnicity: unknown Morphology: epithelial Growth properties: adherent	Purchased from ATCC Catalogue No.: HTB-5
BdSMC	Organism: Homo sapiens (human) Tissue: urinary bladder Disease: none (normal) Age: unknown Gender: female Race: black Morphology: fibroblastic Growth properties: adherent	Purchased from Lonza Product code: CC-25533T25 Lot No.: 0000450859

2.1.3 Cell Culture Solutions

2.1.3.1 Growth Media (GM)

Five different GM were used for the cell lines respectively as shown below (see Table 4).

Table 4: GM information

Cell line	GM	Supplements
RT4	McCoy's 5A Medium (Modified) (BioWhittaker)	• 10% foetal bovine serum (FBS, Gibco) • 1% Penicillin and streptomycin (50 IU/ml, Britannia Pharmaceuticals Ltd) • 1% L-glutamine solution (200mM, Sigma-Aldrich)
UMUC3	ATCC-formulated Eagle's Minimum Essential Medium (EMEM, BioWhittaker)	• 10% FBS (as above) • 1% Penicillin and streptomycin (as above)
T24	Dulbecco's Modified Eagle's Medium (DMEM, Bio-Whittaker), with 4500 mg/L glucose	• 10% FBS (as above) • 1% Penicillin and streptomycin (as above) • 1% L-glutamine solution (as above)
TCCSUP	Eagle's Minimum Essential Medium in Earle's BSS (BioWhittaker) with non-essential amino acids	• 10% FBS (as above) • 1% Penicillin and streptomycin (as above) • 90% 1mM sodium pyruvate (Sigma)
BdSMC	SmBM Basal Medium (Lonza) with no growth factors	SmGM-2 SingleQuots Kit (supplements and growth factors, Lonza): • Human epidermal growth factor (hEGF), 0.5ml • Insulin 0.5ml • Human fibroblast growth factor-B (hFGF-B) 1.0ml • FBS 25ml • Gentamicin/Amphotericin B using at 1:1000 ratio (GA-1000) 0.5ml

2.1.3.2 Serum Free Media (SFM)

SFM was used in all experiments unless otherwise stated, and bovine serum albumin (BSA) was added as a supplement to provide the necessary protein while depleting available growth factors to cause cells to quiesce in the G_0 stage. All cell lines used the same SFM shown below (see Table 5).

Table 5: SFM information

Cell Line	SFM	Supplements
All cell lines	Dulbecco's Modified Eagle Medium/Nutrient Mixture F-12 (DMEM/F-12, no Phenol Red)	• Apo-Transferrin (Sigma); 5mg: final concentration: 0.01mg/ml • Sodium bicarbonate (NaHCO3, Sigma); 600mg: final concentration: 1.2mg/ml • Bovine serum albumin (BSA, Sigma); 100mg: final concentration 0.2mg/ml • 1% L-glutamine solution (as above) • 1% Penicillin and streptomycin (as above)

2.1.3.3 Phosphate Buffered Saline (PBS)

PBS was prepared by dissolving 1 PBS tablet (Cat. # 524650-1EA, Calbiochem) tablet in 1L of dH_2O. Once dissolved, it was autoclaved and stored at room temperature.

2.1.3.4 HEPES buffered saline solution (HEPES-BSS)

HEPES-BSS was purchased from Lonza (Cat. #CC-5024). It was aliquotted and stored at -20˚C.

2.1.3.5 Cell Dissociation Solution (CDS)

CDS (non-enzymatic) was purchased from Biological Industries (Cat. # 03-071-1B) and stored at -4˚C.

2.1.3.6 Trypsin: EDTA Solution (TE)

Trypsin-versene EDTA 10X liquid (Lonza, Cat. # BE 02-007E) was diluted 1X with sterile dH_2O, aliquotted and stored at -20°C.

2.1.3.7 Trypan Blue Dye

Trypan blue dye (Sigma) was diluted with sterile PBS from 0.4% to 0.165% to form a working stock and this was stored at room temperature.

2.1.4 Cell Maintenance

2.1.4.1 Cell Passage

For stocks, 10-15ml of fresh GM was replenished every two or three days and cells were passaged when they reached approximately 80% confluency.

Solutions used for cell passaging were allowed to reach room temperature and then used in sufficient volume for different cell lines respectively (see Table 6).

Table 6: application of solutions in cell passaging

Step	Solution	Cell line	Volume for T75 flask (ml)
1. Pre-wash	PBS	RT4, UMUC3, T24, TCCSUP	10
	HEPES-BSS	BdSMC	10
2. Cell disassociation	CDS	RT4, UMUC3, TCCSUP	3
3. Trypsinisation	TE:CDS (1:1)	RT4, UMUC3, TCCSUP	3
	TE	T24, BdSMC	3
4. Trypsinisation termination	GM	All cell lines	10

1. Media was aspirated from the flasks and cells were pre-washed once with PBS or HEPES-BSS to neutralise the complex proteins in GM which may inactivate the trypsin during the trypsinisation procedure.
2. CDS was then applied to certain cell lines for 5-10 minutes at 37˚C before trypsinisation to disengage attached and clumped cells without the risk of damage associated with protein digestive enzymes like trypsin.
3. Cells were then incubated in TE with or without additional fresh CDS in a 1:1 (v/v) ratio at 37˚C for 5-10 minutes under observation until about 90% of cells were rounded up and detached.
4. After trypsinisation, fresh warm GM was added to neutralise the TE.

2.1.4.2 Determination of Cell Number and Viability

Cell pellets then were collected after the cell suspension was centrifuged at 1200rpm for 3-5 minutes, and then cells were resuspended in 15ml fresh GM with a 5ml syringe (Greiner Bio-One) and a 21G needle (Terumo).

50µl of cell suspension was added to an equal volume of working stock of trypan blue (0.165%) (1:1).

A 50µl trypan blue cell suspension was loaded onto a hemocytometer by capillary action. With the aid of a microscope, both viable and dead cells were observed. Viable cells remained colourless, and dead cells were stained blue because the trypan blue dye was taken up through a permeable plasma membrane.

Cells observed in the centre squares of both top and bottom grids were counted as N_t and N_b, and the number of cells per ml in the cell suspension (N) equals the sum of N_t and N_b and multiplied by $1x10^4$ (per ml) (see Figure 8).

Cell number was determined before a new passage was re-seeded into appropriate fresh vessels at specific densities as new stocks or for experiments (see Table 7). Cells were then incubated in humidified conditions of 5% CO_2 at 37˚C.

Table 7: cell seeding densities

Cell Line	T75 flasks ($x10^6$ cells in 10ml)		T25 flasks ($x10^6$ cells in 5ml)	6-well plates ($x10^6$ cells in 1ml)	24-well plates ($x10^6$ cells in 500µl)	Migration Assay Inserts ($x10^6$ cells in 70µl)	Invasion Assay Inserts ($x10^6$ cells in 500µl)	Colony Formation Assay Dishes ($x10^4$ cells per dish)
	Stocks	Experi-ments						
RT4	0.5	0.8	0.2	0.1	0.03	0.049	0.1	1.0
UMUC3	0.5	-	-	-	-	-	-	-
T24	0.2	0.4	0.1	0.05	0.02	0.028	0.08	0.5
TCCSUP	0.2	0.4	0.1	0.05	0.02	0.042	0.08	0.5
BdSMC	0.4	0.8	-	-	-	0.032	-	-

"-": not applicable in this study.

Trypan blue dye exclusion assay is a standard method that is commonly used to measure cell viability. However, imprecision and inconsistency could be caused by several factors such as sample preparation and subjective judgment. By dealing with samples carefully and determining cell-staining differences consistently, these problems could be largely overcome. Although this method does not distinguish apoptotic from necrotic cells, it does reflect cell viability.

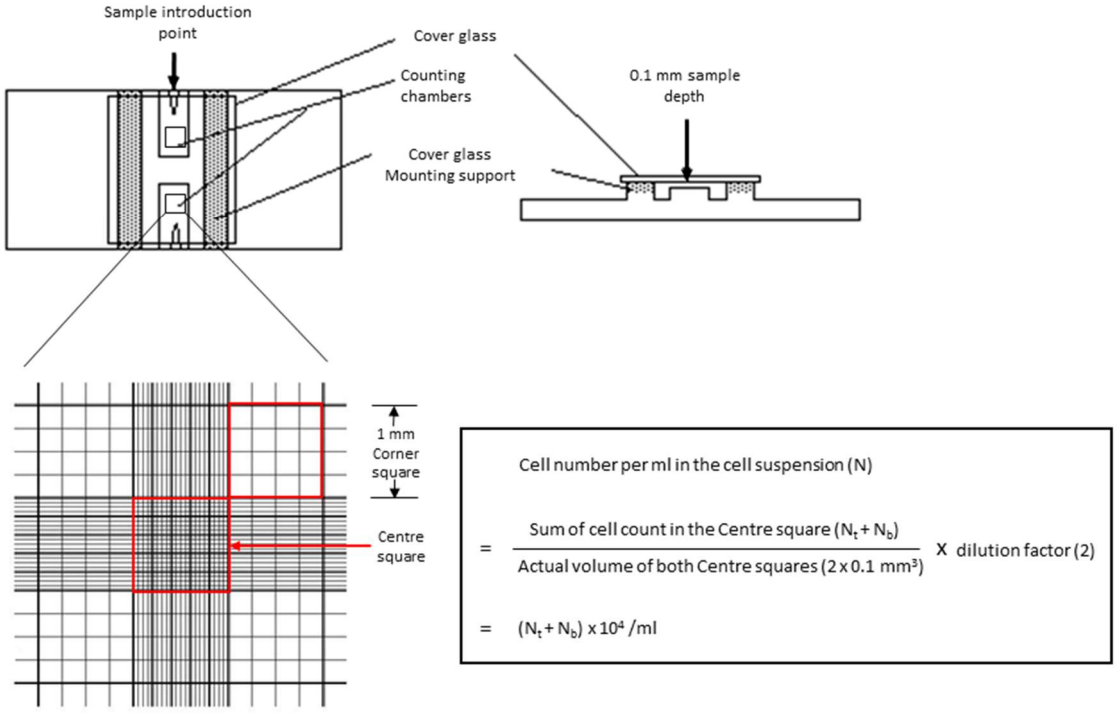

Figure 8: the structure of a hemocytometer and cell counting calculation equation

2.1.5 Cell Freezing and Retrieval

Cells needed to be periodically frozen down, especially at low passage numbers, for long term sustainability of the cell lines.

2.1.5.1 Cell Freezing Solution

The freezing solution is composed of GM supplemented with dimethylsulphoxide (DMSO, analytical grade, Fisher) and extra FBS in certain ratios for different cell lines respectively (see Table 8). The solution was left to cool before use.

Table 8: cell freezing solution

Freezing Solution		Volume per cryogenic vial (µl)	Ratio (v/v/v)	Cell line
Solution 1	GM	350	7:2:1	RT4, UMUC3, T24, TCCSUP
	DMSO	100		
	FBS	50		
Solution 2	GM	400	8:1:1	BdSMC
	DMSO	50		
	FBS	50		

2.1.5.2 Cell Freezing

0.5ml GM cell suspension containing 1-4x10^6 cells was mixed drop-wise with a 0.5ml freezing solution in each cryogenic vial.

Then the cryogenic vials were stored at -20°C first and then -80°C (for at least 24 hours) before being transferred to liquid nitrogen tanks.

2.1.6 Cell Retrieval

Cells taken from the liquid nitrogen tank were warmed at 37˚C till just defrosted, and then pre-warmed GM was gently added inside the wall of the cryogenic vial, 1ml/vial.

For BdSMC, the cell solution was transferred directly into a T25cm^2 flask with 4ml of pre-warmed GM and then incubated at 37˚C.

For the other four cancer cell lines, RT4, UMUC3, T24 and TCCSUP, the cell solution was transferred into a 30ml universal container with 15ml of pre-warmed GM and then centrifuged at 1200rpm for 3 minutes. After the supernatant was aspirated, the cell pellet was re-suspended

with 5ml fresh pre-warmed GM and the cell suspension was transferred into a T25cm^2 flask for incubation at 37°C.

All cells were allowed to adhere to the flask (several hours or overnight) before fresh GM was replenished.

2.1.7 Cell Treatment

Cells were split and re-seeded into appropriate vessels with GM for experiments. GM was removed after 24 hours and SFM was applied for the following 24 hours before treatments. Then cells were dosed with different chemicals and the treatment varied as detailed in the text.

2.2 Analysis of Cell Growth and Survival

2.2.1 Analysis of Cell Proliferation

Along with cell counting by Trypan Blue Exclusion Assay, which was described in 2.1.4.2, to assess total cell numbers; cell proliferation was also measured by a **Tritiated Thymidine Incorporation** (TTI) **Assay** by directly measuring DNA synthesis. TTI is based on determining the metabolic incorporation of [^{3}H]-Thymidine into new strands of chromosomal DNA during DNA replication in mitotic cell division.

2.2.1.1 Equipment

β-Scintillation Counter (Beckman, LS6500, CA, USA)

Scintillation vials (Pony vials, PerkinElmer, USA)

Plate Rocker Platform (Bellco Biotech, NJ, USA)

Incubator (Thermo Electron Corporation, REVCO, Asheville NC USA)

2.2.1.2 Reagents

[3H]-Thymidine: 1mCi/ml stock (GE Healthcare, Buckinghamshire, UK), stored at 4°C.

Trichloroacetic acid (TCA, Merck Ltd, Middlesex, UK) solution: 5% w/v; 5g TCA was added into 100mls dH2O and stored at 4°C.

Sodium Hydroxide (NaOH, Fisher Scientific Ltd, Leicestershire, UK) solution: 1M; 20g NaOH was dissolved into 500mls dH2O and stored at room temperature.

Scintillation fluid (Ultima Gold, Packard Bioscience Ltd, USA)

2.2.1.3 Method

3µl of the [3H]-Thymidine stock was diluted with 750µl SFM to make 0.004µCi/µl working solution. 25µl of the working solution was spiked into each well of a 24-well plate (0.1µCi/well).

The 24-well plates were incubated under normal cell culture conditions for the last 4 hours of the experiment.

The supernatant was aspirated and 500µl TCA solution was added to each well for 10 minutes at 4°C.

The TCA was aspirated and 500µl 1M NaOH was added for incubation at room temperature on a plate rocker for 1 hour.

The cell lysate suspension was transferred into labelled scintillation vials and 2mls of scintillation fluid were added in advance.

The vials were shaken vigorously and analysed using the β-Scintillation Counter. Raw data were recorded as disintegration per minute (DPM).

2.2.2 Assessment of Cell Death

All cells, both attached to cell culture vessels and in the supernatant, were harvested by trypsinisation (see 2.1.4.1) and spinning. Levels of cell death were determined by Trypan Blue Exclusion Assay as described in2.1.4.2. The number of cells staining positive for trypan blue dye were calculated as a percentage of the total cell number to give the percentage of dead cells.

2.3 Western Blotting (WB)

Western blotting, also called immunoblotting, is a widely used analytical technique to detect or confirm the change in levels of specific proteins of interest.

In this study, to measure proteins secreted by cells into culture media, a method of supernatant concentration was used to enhance the sensitivity of detection, and for non-secreted proteins, cells were lysed after treatment to release cellular compounds. Then protein samples were run on Sodium Dodecyl Sulphate–Polyacrylamide Gel Electrophoresis (SDS-PAGE) to separate the proteins, and then the proteins were blotted onto a nitrocellulose membrane and probed with corresponding antibodies.

2.3.1 Supernatant Concentration

The secretory protein that was assessed in this study was IGFBP-2 (36 KDa), and two sizes of centrifugal filter units with the same type of cellulose membrane (molecular weight cut-off: 30 KDa) were applied according to the difference in supernatant volume. Samples were concentrated 10 -60 times.

2.3.1.1 Equipment

For sample volume less than 3ml:

Amicon® Ultra-0.5 mL Centrifugal Filters (Merck Millipore, Cat #.UFC503024, Hertfordshire, UK)

Labnet Prism™ R Refrigerated Microcentrifuge (Labnet International, USA)

For sample volume more than 3ml:

Amicon® Ultra-4 Centrifugal Filter Units (Merck Millipore, Cat #.UFC803024, Hertfordshire, UK)

Centrifuge (see 2.1.1)

2.3.1.2 Reagent

PBS (see 2.1.3.3)

2.3.1.3 Method

Supernatant samples were placed into the centrifugal filter units in appropriate volumes and spun for 30 minutes at full speed.

The flow-through was removed and the filter units were topped with samples and spun again until the volume of the added sample was reduced to less than 10µl.

The concentrated samples were recovered and collected by reversing the filter units and spinning (for samples with an original volume less than 3ml, see Figure 9) or by using the appropriate volume of PBS to rinse the inside of the filter units.

The concentrated samples were transferred into labelled eppendorfs, ready to use for the next steps, or they were stored at -20˚C for later use.

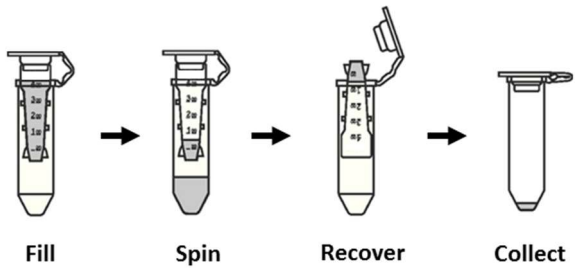

Figure 9: Supernatant concentration workflow demonstration

2.3.2 Non-secreted Protein Extraction of Samples

2.3.2.1 Equipment

Syringes/needles (Terumo, Leuven, Belgium)

Centrifuge (see 2.1.1)

2.3.2.2 Reagents

Lysis buffer

Tris HCL (Sigma, USA), 10mM

Sodium Chloride (Sigma, USA), 50mM

EDTA (Sigma, USA), 5mM

Sodium Pyrophosphate (Sigma, USA), 15mM

Sodium Fluoride (Sigma, USA), 50mM

Triton X-100 (Sigma, USA), 1%

Sodium Orthovanadate (Sigma, USA), 100µM

The lysis buffer was adjusted to pH 7.6 and then stored at 4°C. 10µl/ml of protease inhibitor cocktail (Sigma P8340) and 10µl/ml of phosphatase inhibitor cocktail (Sigma P5726) were added before use.

2.3.2.3 Method

Cell pellets were obtained following the same procedure as described in 2.1.4.1. The pellets were re-suspended in PBS and the cell suspensions were transferred into eppendorf tubes.

The supernatants were centrifuged and removed leaving the pellets as dry as possible to maximise the concentration of the protein extract.

An appropriate volume of lysis buffer was made up and added to the pellets.

The pellets were resuspended and incubated on ice for 5-10 minutes.

The eppendorf tubes were centrifuged at maximum speed (~ 16,000 x g) for 5 minutes to spin down the cellular debris. Then the supernatant (protein extract) was collected and transferred into another pre-chilled eppendorf tube and the debris was discarded.

The samples were stored at -20°C.

2.3.3 Protein Quantification

To ensure that samples were loaded equally onto gels for WB, the concentration of total protein in the samples prepared in 2.3.2 was determined via a colorimetric reaction using the Bicinchoninic Acid (BCA) Protein Assay Kit.

2.3.3.1 Equipment

96-well plates (Greiner Bio-one, Gloucester, UK)

Plate reader (LabSystem Multiskan, Thermo Scientific, Cheshire, UK)

2.3.3.2 Reagents

BCA Protein Assay Kit (Thermo Scientific, Cheshire, UK)

BCA reagent A containing sodium carbonate, sodium bicarbonate, bicinchoninic acid and sodium tartrate in 0.1 M sodium hydroxide.

BCA reagent B containing 4% cupric sulphate.

Albumin standard Ampules, 2.0 mg/ml, containing bovine serum albumin (BSA) at 2.0 mg/ml in 0.9% saline and 0.05% sodium azide.

2.3.3.3 Method

The standards were prepared by diluting Albumin Standard Ampules (stock, 2.0 mg/ml) with lysis buffer as described in Table 9.

Table 9: BCA standard set preparation

Vial	Standard Concentration (µg/ml)	BSA (µl)	Lysis buffer (µl)
A	2000	300 of stock	0
B	1500	375 of stock	125
C	1000	325 of stock	325
D	750	175 of vial B	175
E	500	325 of vial C	325
F	250	325 of vial E	325
G	125	325 of vial F	325
H	25	100 of vial G	400

5µl of the standards and 5µl of the protein extracts prepared in 2.3.1.3 were loaded into each well of the 96-well plate in duplicate.

Reagents A and B were mixed in a ratio of 50:1 and 200µl were added into each occupied well.

The plate was incubated at room temperature for 30 minutes.

The plate was read using Genesis Software package under 540nm filter.

2.3.4 Sodium Dodecyl Sulphate-Polyacrylamide Gel Electrophoresis (SDS-PAGE)

2.3.4.1 Equipment

Glass Plate (Bio-Rad, Hertfordshire, UK)

Clamps (Bio-Rad, Hertfordshire, UK)

Casting Base (Bio-Rad, Hertfordshire, UK)

Gel Tank (Bio-Rad, Hertfordshire, UK)

Power Pack (Pharmacia, LK-BPS 500/400, Bio-Rad, Hertfordshire, UK)

pH Meter (Whatman, PHA 230, Sigma, USA)

Magnetic Stirrer (SMI, Stuart Scientific, Germany)

2.3.4.2 Reagents

40% Acrylamide Gel Solution Bis-acrylamide 37.5:1(Severn Biotech, Worcestershire, UK), stored at 4°C.

1.5M Tris Base (Sigma, USA): 18.16g was added into 70mls dH_2O; pH adjusted to 8.9 before the solution was made up to 100mls; stored at 4°C.

1.1M Tris HCL (Sigma, USA): 17.33g was added into 70mls dH_2O; pH adjusted to 6.8 before the solution was made up to 100mls; stored at 4°C.

10% Sodium dodecyl sulphate (SDS) (Sigma, USA): 50g was added into 400mls dH_2O with gentle warming to assist dissolution; pH was adjusted to 7.2 before the solution was made up to 500mls; stored at room temperature.

10% Ammonium Persulphate (APS) (Sigma, USA): 1g was added into 10mls dH_2O; the solution was used up within 4 months; stored at 4°C.

N,N,N,N-tetramethyethylenediamine (TEMED) (Sigma, USA): stored at room temperature.

Butanol ((Fisher Scientific, UK): 50:50 mix of Butanol and dH_2O

Sample Buffer (Sigma, USA): Laemmli 2x Concentrate.

Precision Plus Protein Standards (BIO-RAD, Cat. # 161-0375)

10x Running Buffer:

- Dissolve the components shown below in Table 10 in 1 litre of dH_2O and adjusted to pH 9.65; stored at room temperature.
- 1x Running Buffer was prepared by diluting 10x Running Buffer with dH_2O in a ratio of 1:9.

Table 10: 10x Running buffer preparation

Tris Base (Sigma, USA)	30.3g
Glycine (Fisher Scientific, UK)	144g
SDS (Sigma, USA)	10g
dH_2O	Make up to 1 litre

Constituents of gels are listed below in Table 11.

- Percentage refers to the final percentage of acrylamide in the gel, and the thickness of all gels was 1.5mm.
- The interaction of APS and TEMED caused polymerisation of the gels and they were added at the last.

2.3.4.3 Method

2.3.4.3.1 Preparation of PAGE gels

Each gel is discontinuous consisting of a resolving or separating (lower) part and a stacking (upper) part. Proteins samples pass through the stacking gel to be concentrated before undergoing complete separation when entering the resolving gel.

Table 11: constituents of gels with different portion

Ingredients	Resolving Portion				Stacking Portion
	6%	**8%**	**10%**	**12%**	**5%**
dH_2O	11.6ml	10.6ml	9.6ml	8.6ml	6ml
40% Acrylamide	3ml	4ml	5ml	6ml	1.25ml
Tris Buffer	5ml (1.5M, pH8.8)	5ml (1.5M, pH8.8)	5ml (1.5M, pH8.8)	5ml (1.5M, pH8.8)	2.5ml (0.5M, pH6.8)
10% SDS	200µl	200µl	200µl	200µl	100µl
10% APS	200µl	200µl	200µl	200µl	100µl
TEMED	20µl	20µl	20µl	20µl	15µl

The spacer plates and short plates were assembled and clipped with clamps to be placed in casting bases.

The resolving portion was prepared according to Table 11 and poured into the gap between the spacers and short plates to a certain level, and then covered with a small volume of hydrated butanol (butanol:dH2O in a 1:1 ratio) to avoid air preventing the polymerization of the gels.

Gels were allowed to set for about 30 minutes and then butanol was washed off.

The stacking portion was also prepared according to the Table 11 and it was poured to the top. The 1.5mm thick combs were placed into the assembled gel sandwich.

Gels were allowed to set for another 30 minutes and then combs were removed, vertically with care.

The gels were moved from the clamps into the tank complex to be loaded.

2.3.4.3.2 Loading samples and running gels

- The amount of sample loaded was measured according to the result of the BCA protein assay. The samples were mixed with the same volume of 2x sample buffer.
- Mixed samples were boiled at 100°C for 5 minutes.
- Samples were loaded into each well of the gels slowly and gently to avoid cross contamination.

- Gels were run by limited volts of 125-200V depending on the number of gels being analysed and for approximately 35-90 minutes depending on the separation required and protein size.

2.3.5 Transfer

2.3.5.1 Equipment

Transfer tank (Bio-Rad, Hertfordshire, UK)

Power pack (Pharmacia, LK-BS5 500/400, Bio-Rad, Hertfordshire, UK)

Cassettes (Bio-Rad, Hertfordshire, UK)

Sponges (Pharmacia, LK-BPS 500/400, Bio-Rad, Hertfordshire, UK)

Nitrocellulose membrane (Amersham, GE Healthcare Life Sciences, Buckinghamshire, UK)

Filter paper (Whatman, Sigma, USA)

PH Meter (2.3.4.1)

Magnetic Stirrer (2.3.4.1)

2.3.5.2 Reagents

10x Transfer Buffer:

Dissolve the components shown in

- Table 12 in 1 litre of dH_2O and adjusted to pH 9.65; stored at 4°C.
- 1x Transfer Buffer was prepared by mixing 10x Transfer Buffer with Methanol (Fisher Scientific, UK) and dH_2O in a ratio of 1:2:7.

Table 12: 10x Transfer buffer preparation

Tris Base (Sigma, USA)	30.3g
Glycine (Fisher Scientific, UK**)**	144g
dH_2O	Make up to 1 litre

2.3.5.3 Method

Gels with separated proteins were made up into transfer sandwiches with other components inside of a transfer cassette, and the sequence below was followed to ensure that the current went from the gels to the membranes:

Black side

Sponge (1-2)

Thick filter paper (1)

Gel (1)

Nitrocellulose membrane (1)

Thin paper (2)

Sponge (1-2)

Clear side

The transfer occurred with the electronic current set to limited volts of 100V for about 1 hour.

2.3.6 Immunoblotting

2.3.6.1 Equipment

Orbital shaker (IKA, Sigma, USA)

Rotator (SB1, Stuart Scientific, Staffordshire, UK)

Polythene bag (Jencons, Leighton Buzzard, UK)

Bag sealer (Astrapac 500105, Walsall, UK)

2.3.6.2 Reagents

10x Tris-buffered saline with Tween (TBST), (pH 7.6):

- Dissolve Tris HCL and NaCl as shown in Table 13 in 1 litre of dH_2O. Add tween 20 after the solution was adjusted to pH 7.6; stored at room temperature.
- 1x TBST was prepared by adding 10x TBST with dH_2O in a ratio of 1:9.

Table 13: 10x TBST preparation

Tris HCL (Sigma, USA)	24.2g
NaCl (Sigma, USA)	80g
Tween 20 (polyoxyethylene sorbitan monolaurate, Sigma, USA)	5ml

TBST based Blocking Solutions:

- 1 X TBST with 5% milk: 2.5g skimmed dried milk in 50mls
- 1 X TBST with 2% milk: 1g skimmed dried milk in 50mls
- 1 X TBST with 1% milk: 0.5g skimmed dried milk in 50mls

- 1 X TBST with 5% BSA: 2.5g BSA (Sigma) in 50mls
- 1 X TBST with 3% BSA: 1.5g BSA (Sigma) in 50mls

Antibody solutions listed below in Table 14.

Table 14: antibody solutions information

Protein	Size (kDa)	Company & Cat. No.	Blocking	1° Ab	*2° Ab
Phospho-IGF-I Receptor (p-IGF-IR)	92	Cell Signaling #3024	3% BSA	1/750 3% BSA rabbit	1/2000 5% milk anti-rabbit
IGF-I Receptor (IGF-IR)	95	Cell Signaling #9750	5% BSA	1/1000 5% BSA rabbit	1/2000 5% BSA anti-rabbit
Insulin Receptor (IR)	95	Santa Cruz Sc-711	5% BSA	1/1000 5% BSA rabbit	1/2000 5% BSA anti-rabbit
Akt	60	Cell Signaling #9272	5% BSA	1/1000 5% BSA rabbit	1/2000 5% BSA anti-rabbit
Phospho-Akt	60	Cell Signaling #4060	5% BSA	1/1000 5% BSA rabbit	1/2000 5% BSA anti-rabbit
PTEN	54	Cell Signaling #9556S	5% milk	1/750 5% milk mouse	1/2000 5% milk anti-mouse
Phospho-MAPK	42, 44	Cell Signaling #9101	5% BSA	1/1000 5% BSA rabbit	1/2000 5% BSA anti-rabbit
Erk2	42	Santa Cruz Sc-154	5% milk	1/1000 5% milk rabbit	1/2000 5% milk anti-rabbit
Tubulin	55	Millipore (anti-α-Tubulin) #2016030	5% BSA	1/5000 1% milk mouse	1/5000 1% milk anti-mouse
GAPDH	35	Chemicon MAB 374	5% milk	1/5000 5% milk mouse	1/5000, 5%milk anti-mouse
IGFBP-2	36	Santa Cruz SC6001	5% milk	1/1000, 5% milk goat	1/2000, 5% milk anti-goat

*2° **Ab**: anti-rabbit (Sigma, #A0545); anti-mouse (Sigma, #A0944); anti-goat (Sigma, #A5420).

2.3.6.3 Method

The membranes with transferred proteins were cut into separate pieces according to the size of the proteins to be analysed, and they were blocked with the blocking solutions according to the Table 14 for over two hours at room temperature to prevent non-specific binding of proteins.

The membranes were then probed overnight in a cold room at 4°C with a primary antibody of interest in sealed bags on a rotator.

After incubation with a primary antibody, the membranes were washed 3 times for 5-15 minutes with TBST and then incubated with an appropriate secondary antibody for one hour at room temperature.

The membrane was subsequently washed 5-15 minutes for a further 3 times with TBST before visualisation.

2.3.7 Detection and Calculation

2.3.7.1 Equipment

ChemiDoc MP Imaging System (Bio-Rad, Hertfordshire, UK)

Image Lab™ Software (version 5.0)

ImageJ Software (version 1.46r)

2.3.7.2 Reagents

Super signal west dura substrate (Pierce Biotechnology, Cat.# 34075, Thermo Scientific, Cheshire, UK)

Super signal west femto substrate (Pierce Biotechnology, Cat.# 34094, Thermo Scientific, Cheshire, UK)

2.3.7.3 Method

Membranes were washed for 5 minutes with Super signal west dura substrate (West femto was used for antibodies requiring more sensitive detection).

The chemiluminescence signal was detected using Image Lab™ Software by the ChemiDoc MP Imaging System.

Densitometry was performed using ImageJ software.

2.4 Cellular Fractionation

The Thermo Scientific NE-PER Nuclear and Cytoplasmic Extraction Reagents enabled stepwise separation and preparation of non-denatured, active proteins of cytoplasmic and nuclear extracts from mammalian cultured cells or tissue in less than two hours. The first two reagents (CER I and CER II) were added to the cell pellets resulting in cell membrane disruption and release of cytoplasmic contents. And the third reagent (NER) was added to yield the nuclear extract.

All centrifugation steps were performed at 4°C and all samples and extracts, as well as reagents, were kept on ice to avoid protein degradation.

Protease inhibitors and phosphorylation inhibitors were added into CER I and NER to maintain extract integrity and function

2.4.1 Equipment

- Labnet Prism™ R Refrigerated Microcentrifuge (see 2.3.1.1)
- Autovortex Mixer SA2 (Stuart Scientific, UK)

2.4.2 Reagents

- Trypsin: EDTA Solution (TE) as described in 2.1.3.6.
- PBS as described in 2.1.3.3.
- NE-PER Nuclear and Cytoplasmic Extraction Reagents Kit (Thermo Scientific, Cheshire, UK)
  - Cytoplasmic Extraction Reagent I (CER I)
  - Cytoplasmic Extraction Reagent II (CER II)
  - Nuclear Extraction Reagent (NER)
- Lysis buffer with a protease inhibitor and phosphorylation inhibitor as described in 2.3.2.2.

2.4.3 Method

- Cells were harvested following the same procedure as described in 2.1.4.1 and 2.1.4.2 and then centrifuged at 500x g for 5 minutes.
- The cells were washed by suspending the cell pellets with PBS to wash off any traces of media and then the cell suspension was transferred into pre-chilled eppendorf tubes.

- The cell suspension was centrifuged again at 500 x g for 2-3 minutes.
- The supernatant was removed carefully and the pellets were left as dry as possible.
- The ice-cold CER I was added to the cell pellets and then Cytoplasmic and Nuclear Protein Extraction using the reagent volumes shown in Table 15 below was performed. The volume ratio of CER I: CER II: NER reagents was maintained at 200:11:100 respectively.

Table 15: reagent volumes for different packed cell volumes

Packed Cell Volume (µl)	CER I (µl)	CER II (µl)	NER (µl)
10	100	5.5	50
20	200	11	100
50	500	27.5	250
100	1000	55	500

After adding CER I, the tubes were agitated vigorously on a vortex on the highest setting (2500rpm) for 15 seconds to fully suspend the cell pellets, and then incubated on ice for 10 minutes.

The ice-cold CER II was added to the eppendorf tubes.

The tubes were agitated on the highest setting (2500rpm) for 5 seconds and then incubated on ice for 1 minute.

The tubes were agitated for another 5 seconds on the highest setting (2500rpm) and then centrifuged for 5 minutes at maximum speed (~ 16,000 x g).

The supernatants (cytoplasmic extract) were immediately transferred into clean pre-chilled eppendorf tubes and the tubes were placed on ice until used or were stored at -80˚C.

The pellets (intact nuclei) were washed with ice-cold PBS and centrifuged 2-3 times to remove leftover cytoplasmic extract to avoid contamination.

The ice-cold NER was added into the insoluble pellets that contained nuclei and was re-suspended.

The samples were agitated on the highest setting (2500rpm) for 15 seconds and then placed on ice for 10 minutes. The 15-second vortex and 10-minute incubation on the ice were repeated at least 4 times to release the nuclear extract.

The tubes were centrifuged at a maximum speed (~ 16,000 x g) in the microcentrifuge for 10 minutes.

The supernatant (nuclear extract) fraction was immediately transferred to a clean pre-chilled eppendorf tube and placed on ice till used or was stored at -80°C.

2.5 Immunofluorescence

Fluorescently labelled antibodies were utilised to detect specific target proteins of interest in cells by using immunofluorescent imaging.

2.5.1 Equipment

- Polylysine-coated coverslips (BD Biosciences, USA)

- 6-well plates (Greiner Bio-one, Gloucester, UK)
- Parafilm (Bemis Company, USA)
- Leica DMI 6000B microscope (Leica Microsystems, Germany)

2.5.2 Reagents

- PBS as described in2.1.3.3: 1ml/coverslip.
- Formaldehyde (PFA) (Polysciences, Germany): 3%, 500µl/coverslip, methanol free, stored at -20°C.
- Glycine (Fisher Scientific, Loughborough, UK): 30mM; 1ml/coverslip, decide volume by demand, e.g. weigh 22.5mg Glycine to resolve in 10ml PBS.
- Triton X-100 (see 2.3.2.2): 0.5%; 1ml/coverslip, decide volume by requirement, e.g. add 50µl from stock into 10ml PBS.
- BSA (Sigma, USA): 3%; made up in PBS, used for blocking (1ml/coverslip) as well as antibodies dilution, decide volume by requirement, e.g. weigh 0.3g BSA to resolve in 10ml PBS.
- Fluorescent secondary antibodies (Fisher Scientific, Loughborough, UK):
    - Alexa Fluor 568 Phalloidin: orange fluorescent, staining actin for the cytoskeleton.
    - Alexa Fluor 488 Goat Anti-Mouse IgG (H+L) (green fluorescent)
    - Alexa Fluor 568 Goat Anti-Mouse IgG (H+L) (red fluorescent)
    - Alexa Fluor 488 Donkey Anti-Rabbit IgG (H+L) (green fluorescent)

  - Alexa Fluor 568 Goat Anti-Rabbit IgG (H+L) (red fluorescent)
  - Alexa Fluor 488 Donkey Anti-Goat IgG (H+L) (green fluorescent)
  - Alexa Fluor 568 Donkey Anti-Goat IgG (H+L) (red fluorescent

- DAPI (Vectashield mounting medium for fluorescence with DAPI, Vector Laboratories, Peterborough, USA): preserves fluorescence, prevents rapid photobleaching of fluorescent reagents and retains fluorescence during prolonged storage.
- Nail varnish

2.5.3 Method

- Cells were seeded on poly-lysine coated coverslips in 6-well plates and allowed to grow prior to treating according to different experiments.
- The coverslips were washed with PBS in the plates by adding PBS to the side of the well gently for 3 x 5 minutes to remove any traces of media.
- The PBS was removed and 3% PFA was added gently directly to the edge of coverslips for 15 minutes to fix the cells.
- PFA was removed and PBS was added to wash off any traces of PFA.
- The PBS was removed and 30mM glycine was added to the sides of the wells and left for 5 minutes to quench the cells.
- The glycine was removed and PBS was added to wash the cells again.
- The PBS was removed and 0.5% Triton was added to permeabilize the cells. The permeability of an outer membrane would be achieved in 5 minutes and that of the nuclear membrane would be achieved in 15 minutes in total.

- The 0.5% Triton was removed and cells were washed with PBS.
- The PBS was removed and 3% BSA (1ml/coverslip) was added for 1 hour at room temperature to block the non-specific sites on the membranes.
- Primary antibodies were made up in 3% BSA on ice and details of the antibodies as well as dilution factors will be given in the relevant chapters.
- 50µl of antibody solution was dripped onto parafilm that was placed on the bench: each coverslip was placed onto the droplet of the antibody with cells facing towards the droplet.
    - The coverslips were covered with an inverted plastic box with a roll of damp tissue to create a humid chamber.
    - The primary antibody was left to incubate for 1 hour.
- The coverslips were taken back to 6-well plates, cell side up and then washed with PBS for 5 minutes, 3 times to remove any unbound antibody.
- Fluorescent secondary antibodies were also made up in 3% BSA on ice in dilution of 1:500, *avoiding light*. Together with the secondary antibody solutions, Phalloidin was added in dilution of 1:250 if needed.
- As with the primary antibody, a 50µl solution of secondary antibody was applied to each coverslip and left in *dark*, humid conditions for 1 hour at room temperature.
- The coverslips were taken back to the 6-well plates again with cell side up and then washed with PBS for a further 3 x 5 minutes in *dark* conditions.

- Coverslips were mounted in *darkness* onto slides with DAPI, cell side down and sealed with nail varnish to avoid movement.
- Coverslips were then imaged using a Leica DMI 6000B microscope.

2.6 Small Interference RNA (siRNA) Transfection

Small interfering RNA (siRNA) is also known as short interfering RNA or silencing RNA featuring a class of double-stranded RNA molecules with only 20-25 base pairs in length.

siRNA transfection is a technique to silence sequence-specific target genes by introducing exogenously derived antisense RNA molecules to interfere with the complementary messenger RNA followed by the degradation of the messenger RNA after transcription which results in no translation of target genes (Agrawal, Dasaradhi et al. 2003).

2.6.1 Equipment

- 6-well plates (Greiner Bio-one, Gloucester, UK)
- Pipette filter Tips (Starstedt, Germany)
- RNase, DNase and Pyrogen free microcentrifuge tubes (Appleton Wood, Birmingham, UK)

2.6.2 Reagents

Hs_IGFBP-2 _4 FlexiTube siRNA

- Target sequence: 5'-CCCGGAGCAGGTTGCAGACAA-3' (Qiagen, Cat #. SI02623859, Germany)

Non-silencing negative control (Qiagen, Cat #. 1027310, Germany)

SIRNA transfection reagent SAINT-RED Kit (Synvolux Therapeutics, Cat #. SR-1003-04, The Netherlands)

- SAINT-RED (transfection reagent)
- HBS 1x (siRNA suspension buffer)

2.6.3 Method

- A 20µM stock solution was made by re-suspending the lyophilised supplied siRNA (5nmol) in 250µl of siRNA suspension buffer.
- After re-suspension, the tube was heated to 90°C for 1 minute and then left at 37°C for 1 hour to remove aggregates. Then the stock solution was aliquoted and stored at -20°C.
- 2µM working stock of siRNA was prepared fresh by extracting 10µl of siRNA 20µM stock and adding to 90µl of HBS buffer.
- siRNA solutions were made by adding the 2µM siRNA/HBS dropwise into a mixture of SFM and SAINT-RED transfection reagent, giving a final concentration of 30nM of IGFBP-2 siRNA/SAINT-RED complex (15µl per well). Non-silencing negative control was made at the same concentration.
- The siRNA/SAINT-RED complex was incubated at room temperature for 20 minutes.

- Cells were seeded at 0.4 x 10^6 in 800µl GM per well of a 6-well plate.
- The siRNA/SAINT-RED complex was added dropwise with gentle agitation of the wells at 200µl per well according to the plate layout.
- The cells were incubated at 37°C for 24 hours.
- Cells were switched and exposed to SFM for another 48 hours.
- The impact of siRNA on the cells was assessed by WB as described in 2.3.

2.7 Combined Bisulphite Restriction Assay (COBRA)

DNA methylation is an epigenetic mechanism, which occurs through the addition of a methyl (-CH_3) group to DNA, that often results in gene silencing. Cytosine methylation of CpG dinucleotides happens commonly in mammals (Reinert, Modin et al. 2011). As a widely used molecular biology technique in cancer research and epigenetic studies, COBRA allows for sensitive quantification of DNA methylation levels at a specific gene locus in a small sample of genomic DNA. It introduces methylation-dependent sequence differences and combines bisulfite conversion based polymerase chain reaction (PCR) with restriction enzyme digestion to discriminate gene methylation levels according to the difference in DNA fragment production (see Figure 10).

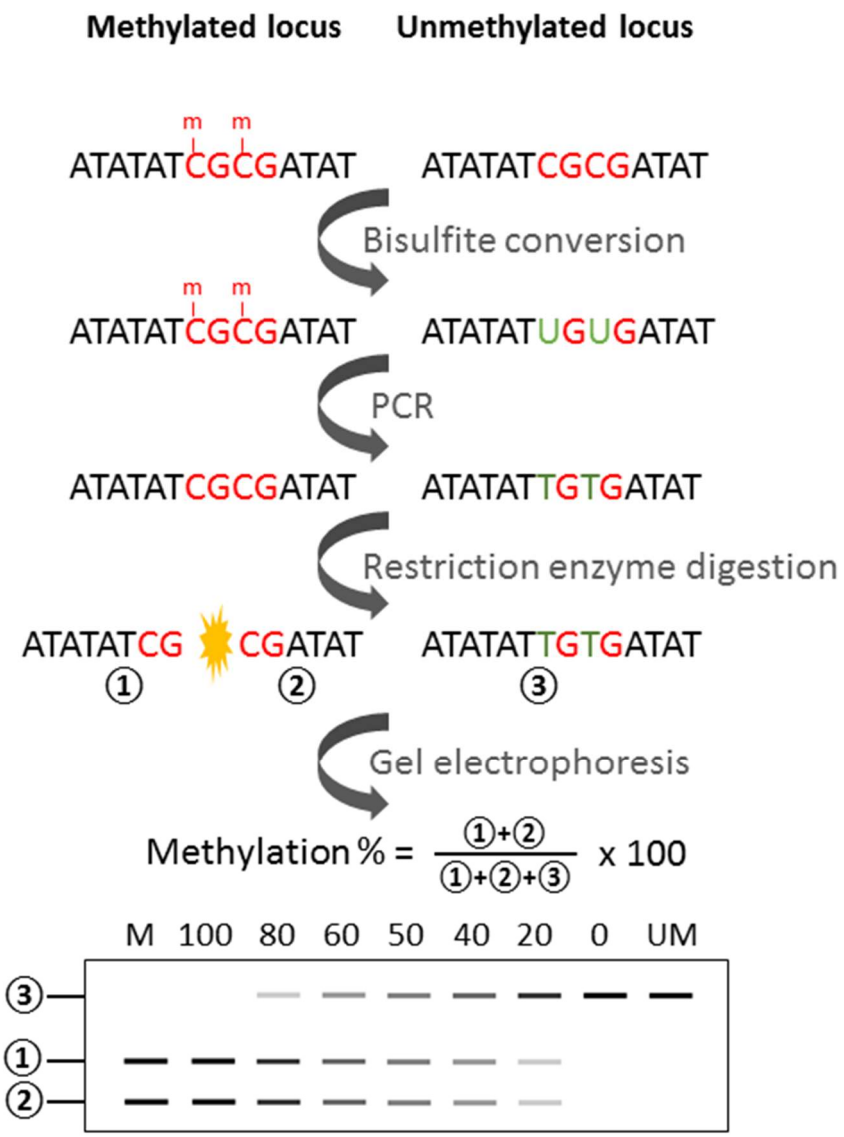

Figure 10: COBRA workflow

An example of DNA fragments cut from the digestion of BstUI, a restriction enzyme, of bisulfite conversion based PCR products with CpG sites. "**M**": completely methylated DNA control; "**UM**": completely unmethylated DNA control.

2.7.1 Equipment

Desktop centrifuge (Heraeus, Micro Centaur, UK)

1.5ml microcentrifuge tubes (Eppendorfs, Sigma, USA)

Water bath (GRANT, JB2, UK)

Vortex Mixer (Thermo Scientific, Cheshire, UK)

PCR machine (MJ RESEARCH, Bio-Rad, Hertfordshire, UK)

ChemiDoc MP Imaging System (see 2.3.7.1)

Image Lab™ Software (see 2.3.7.1)

2.7.2 Reagents

EZ DNA Methylation-Direct™ Kit (Zymo Research, Cat #. 5021, USA)

HotStarTaq Plus PCR Kit (Qiagen, Cat. # 203603, Germany)

IGFBP-2 primer (designed using MethPrimer tool and purchased from Thermo Fisher Scientific, UK)

- size: 263bp
- target sites: -413 to-150
- Sequences: **F**: 5'-GAT TGA AAT TTA TTT GAA GGT TAA AA-3'

  R: 5'-ACT CTA AAA ATT CCC TAC TCT TCC C-3'
- Anneal temperature: 57˚C

Restriction Enzyme BstUI, 10,000 U/ml (BioLabs, Cat.# R0518L, Hitchin, UK)

- Recognition site: 5´…. CG↓CG… 3´

  3´…. GC↑GC… 5´

Water – Rnase/Dnase/Protease free (Fisher Scientific, Cat. #HYC-001-218c, Loughborough, UK)

Tris-Borate-EDTA buffer (TBE), 5x (QIAGEN, Cat. # 129217, Germany)

50bp DNA ladder (Biolabs, Cat. # N3236S, Hitchin, UK)

Agarose (Melford, Cat. # MB 1200, Suffolk, UK)

Midori Green Advance (NIPPON Genetics EUROPE, Cat. # MG 04, Duren, UK)

2.7.3 Method

2.7.3.1 DNA Extraction and Bisulfite Conversion

Cultured cells were trypsinized and collected as described in 2.1.4.1, and then cell counting was performed as described in 2.1.4.2.

Cells were centrifuged and the supernatant was removed.

Cell pellets resuspended in a certain volume of PBS to reach a cell/PBS suspension containing $10x10^6$cells/ml.

10µl cell/PBS suspension was taken from each sample containing $0.1x10^6$ cells for DNA extraction.

Digestion solutions for each sample:

M-Digestion buffer (2x) (EZ DNA Methylation-Direct™ Kit)	13µl
Sample (containing 0.1x10^6 cells)	10µl
Proteinase K	2µl
Water	1µl
Total	26µl

All samples were then incubated in a water bath at 50˚C for 20 minutes. Samples were vortexed to mix the contents of the reaction thoroughly and then centrifuged at 10,000x g for 5 minutes.

20µl of supernatant were added to 130µl of pre-prepared CT Conversion Reagent solution in a PCR tube. All samples were vortexed again and centrifuged briefly to avoid droplets in the tube lid.

Samples in PCR tubes then were placed in a thermal cycle shown below:

98˚C	8 minutes
64˚C	3.5 hours
4˚C	up to 20 hours

Each Zymo-Spin IC Column was filled with 600µl of M-Binding buffer and then placed into a Collection tube. Samples were then loaded in the columns individually and mixed well.

Samples were centrifuged at full speed for 30 seconds, and the flow-through was discarded.

100µl of M-Wash buffer (EZ DNA Methylation-Direct™ Kit) was added to each sample and centrifuged again at full speed for 30 seconds.

200µl of M-Desulphonation buffer (EZ DNA Methylation-Direct™ Kit) were added to each sample and allowed to stand for 15-20 minutes at room temperature, and then once more centrifuged at full speed for 30 seconds.

Samples were then washed twice by adding 200µl of M-Wash buffer followed by 30 seconds full speed centrifugation.

The columns with samples were then placed into new 1.5ml eppendorf tubes. 10µl of M-Elution buffer (EZ DNA Methylation-Direct™ Kit) was added directly to the column matrix at the bottom of the columns and then centrifuged at full speed for 30 seconds to elute the DNA.

The DNA extraction was then stored at -20˚C.

2.7.3.2 PCR

A PCR Master Mix (MM) was made as below (see

Table 16, in a total volume of 10µl).

Table 16: PCR master mix constituent

Ingredients	**Final concentration**
10x Buffer	1x
10mM dNTP	0.1mM
25mM $MgCl_2$	2.0mM
10µM Forward primer	0.25µM
10µM Reverse primer	0.25µM
DMSO	5%
5 U/µl Taq	0.25 U/10µl
Water	Add up to the total volume of 10µl

PCR samples were prepared by adding 1µl of DNA sample extracted as in 2.7.3.1 into each PCR reaction tube pre-filled with 9µl of MM. Control DNA samples (**UM**: completely unmethylated DNA control; **M**: completely methylated DNA control; E: empty/water control) were prepared in the same way.

PCR reaction tubes were placed into a pre-warmed PCR machine run through the following programme:

94˚C	10 minutes	
94˚C	45 seconds	40x
57˚C	45 seconds	
72˚C	45 seconds	
72˚C	5 minutes	

The PCR products were ready for the following restriction enzyme digestion.

2.7.3.3 Restriction Enzyme Digestion and DNA Detection

An enzyme digestion solution was made as below (see Table 17, in a total volume of 10µl) and mixed with equal volume of PCR products.

The mixture of enzyme/PCR products was incubated for 4 hours at 60˚C.

A 2.5% agarose gel was made by melting 2 grammes of agarose into 100ml of 1x TBE buffer, with 5µl of Midori Green Advance added before pouring.

10µl of digested PCR samples and 50bp DNA ladder were loaded into wells after the gel was set, and run at 100 volts for approximately 30 minutes.

The migrated DNA on the gel was detected using Image Lab™ Software by the ChemiDoc MP Imaging System.

Table 17: restriction enzyme used for COBRA

Ingredients	Concentration before adding PCR products	Final concentration after adding PCR products
10,000 U/ml BstUI	2 U/µl	1 U/µl
10x Buffer	2x	1x
100x BSA	2x	1x
Water	Add up to the total volume of 10µl	---

2.7.3.4 DNA Methylation Level Calculation

Densitometry of DNA bands was performed using ImageJ software.

The percentage of DNA methylation level = sum of restricted enzyme cut DNA fragments/sum of the cut DNA fragments and uncut DNA x 100.

A linear response of the COBRA assays was validated by correlating the percentage of input of completely methylated DNA control versus the COBRA-measured percentage methylation.

2.8 Soft Agar Colony Formation Assay

In cancer progression, the ability of cells to grow in an anchorage-independent manner is an important criterion of cell malignant transformation. And the soft agar colony formation assay is considered to be one of the most well-established methods to test this capacity in vitro by suspending cells in agar

(see Figure 11), and it allows for semi-quantitative evaluation of cell transformation in response to various treatments. A colony is defined as a cluster of at least 50 cells and it is assumed to be the result of the anchorage-independent proliferation of an individual cell (Cai, Chattopadhyay et al. 2011). In this assay, cells were cultured in appropriate conditions for 3-4 weeks, and then colonies that were formed were analysed using ImageJ software after a cell stain.

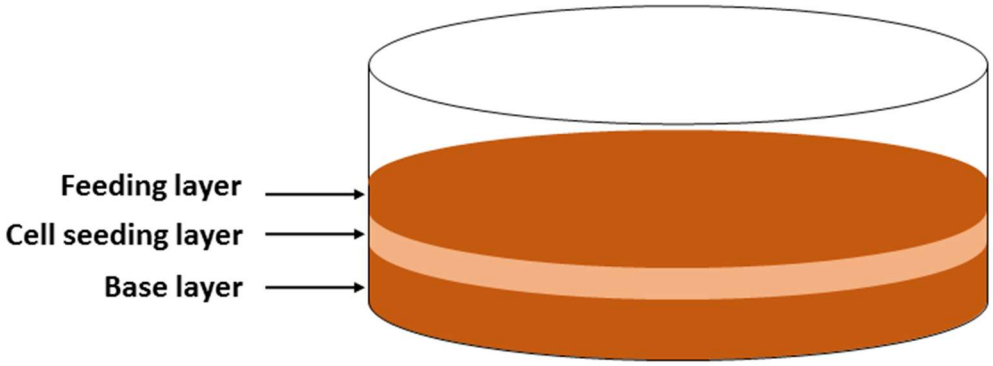

Figure 11: Soft agar colony formation assay dish demonstration

"**Base layer**": the bottom layer of agar prepared for set-up of experiments; "**Cell seeding layer**": the middle layer of agar containing cells; "**Feeding layer**": the upper layer of agar feeding cells with nutrients with or without chemicals as a treatment.

2.8.1 Equipment

Petri dishes (Corning, Cat #.430196, Sigma, USA)

LEICA DM IRB (Leica Microsystems, UK)

AxioCam ERc5s camera (Zeiss, Cambridge, UK)

ImageJ software (see 2.3.7.1)

2.8.2 Reagents

2x DMEM (see Table 18)

3.5% stock agarose solution (see Table 18)

FBS/L-glutamine solution/Penicillin and Streptomycin (see Table 4)

aliquots in small volume

10% FBS Medium Mix (see Table 18)

Crystal violet (Sigma, Cat #. C3886, USA)

Ethanol (Fisher Scientific, Cat #. 64-17-5, Loughborough, UK)

Table 18: soft agar colony formation solutions

	Ingredients	Volume	Preparation & Storage
2x DMEM	10x DMEM powder (Sigma)	1x	• The ingredients were mixed together and then adjusted to pH 7.4 by adding about 2ml of a sterile aqueous stock of 1M NaOH. • The mixture was filter sterilised and stored at 4˚C for at least 1 month.
	7.5% $NaHCO_3$ (Gibco BRL)	49.3ml	
	100mM sodium pyruvate (Gibco BRL)	5ml	
	Sterile tissue culture grade water	445.7ml	
3.5% stock agarose solution	Low Melting Point (LMP) agarose (Sea Plaque LMP agarose, Lonza)	3.5g	• Dissolve the agarose in the water in the microwave. • Aliquot the solution into 15ml per glass universal. • Autoclave and store at room temperature.
	Tissue culture grade water	100ml	
10% FBS Medium Mix	1x DMEM	36ml	• Recipe for 12 dishes. • Prepare fresh or refrigerate for later use up to 1 week. • Equilibrate to 37˚C before use.
	2x DMEM	15ml	
	FBS	7.5ml	
	L-glutamine solution	0.75ml	
	Penicillin and Streptomycin	0.75ml	
0.04% (w/v) Crystal violet	Crystal violet	10mg	• Weigh up and dissolve in pure ethanol. • Store at room temperature.
	Ethanol	25ml	

2.8.3 Method

2.8.3.1 Preparation of dishes with agar base layer

The stock agarose solution was pre-melted and equilibrated to 37˚C.

12.5ml of the agarose solution was added into 50ml of pre-warmed 10% FBS medium and pipetted up and down several times to mix well.

5ml of the base agar was added to each Petri dish. Any bubbles were removed by using a Pasteur pipette attached to a vacuum pump.

The dishes were placed in the fridge (4˚C) on a flat platform for at least 20 minutes to allow the agar to set. The dishes could be left in the fridge overnight for next step on the second day.

The set agar dishes were placed in the incubator (37˚C) to warm them before seeding the cells.

2.8.3.2 Cell seeding

Cells were trypsinized (see 2.1.4.1) and counted (see 2.1.4.2) in normal GM.

The desired cell number was calculated for each dish depending on the cell type (see Table 7) and the cells were placed into a 1.5ml eppendorf in a total volume of 0.5ml (top up with GM if not enough) individually and placed in an incubator at 37˚C before seeding into dishes.

2.5ml of pre-melted agarose solution was added to 10ml pre-warmed 10% FBS medium mix to prepare for the **cell seeding layer** (both equilibrated to 37˚C before mixing): the solution was pipetted up and down several times gently to avoid bubbles.

Relevant chemicals were added into the 10% FBS medium mix before mixing with the agarose solution if cells were being treated. The chemical calculation needs to take multiple step dilutions into consideration to reach desired final concentration.

1ml of 10% FBS medium mix/agarose (equilibrated to 37˚C) was added into each eppendorf containing cells and mixed gently to avoid bubbles. The 1.5ml cell/agarose medium mix was transferred into each pre-warmed dish and the dishes labelled on both the lid and the side.

The seeded dishes were placed in the fridge (4˚C) on a flat platform for about 20 minutes to allow the agar to set, and they were then returned to the incubator (37˚C) to complete cell seeding.

2.8.3.3 Cell feeding

Preparation of the **feeding layer** was the same as for the **cell seeding layer** described in 2.8.3.2: 4ml of stock agarose solution was added into 22ml of 10% FBS medium mix.

Any specific treatments were calculated and then added into the 10% FBS medium mix before mixing with the agarose solution.

2ml of the feeding agar/medium mix was added to each dish and bubbles removed.

The seeded dishes were placed in the fridge (4˚C) on a flat platform for about 20 minutes to allow the agar to set and then returned to the incubator (37˚C) to finish feeding.

Cells were fed once a week for about 3-4 weeks until colonies grew into suitable sizes for counting.

2.8.3.4 Colony staining

Colonies were stained using prepared 0.04% crystal violet by adding 0.5ml to each dish and leaving them on the bench for 30 minutes.

The dishes were rinsed a couple of times with distilled water until the background reached a suitable light colour for colony analysis.

2.8.3.5 Analysis of colonies using ImageJ

Colonies were observed under a LEICA DM IRB and pictures of the whole dish were taken individually using an AxioCam ERc5s camera.

The number and size of the colonies present were analysed using ImageJ software according to the protocol from Paul O'Gorman Lifeline Centre shown below (see Table 19 and Figure 12).

Table 19: procedures of using ImageJ to analyse colonies

Step	Aim	Procedure
1	Open a selected picture	"File" –- "Open"
2	Convert the image to greyscale	"Image" –- "Type" –- "8 bit"
3	Optimise image quality	"Process" --- "Sharpen"
4	Calibrate measurement scale applied to all images	Draw a straight line along the length of a scale bar (such as 5mm) --- Measure the line using a ruler as precise as possible --- "Analyze" --- "Set scale", enter "5000" into "known distance" box and change "unit of measurement" box to "microns" – "global"
5	Remove the particles unwanted to count	"Drawing tools" --- "Eraser tool"
6	Select particles wanted to count	"Image" --- "Adjust" --- "Threshold"
7	Check measure parameters	"Analyze" --- "Set measurements"
8	Take measurement	"Analyse" --- "Analyse particles" --- "OK" Note: set a minimum particle size to exclude noise (in this study, cell colonies with size being 2806μm^2 as the diameter of over 60μm is accepted as a colony).
9	Export data	The measurements will show up in a chart, and the results can be cut and paste into excel for analysing.

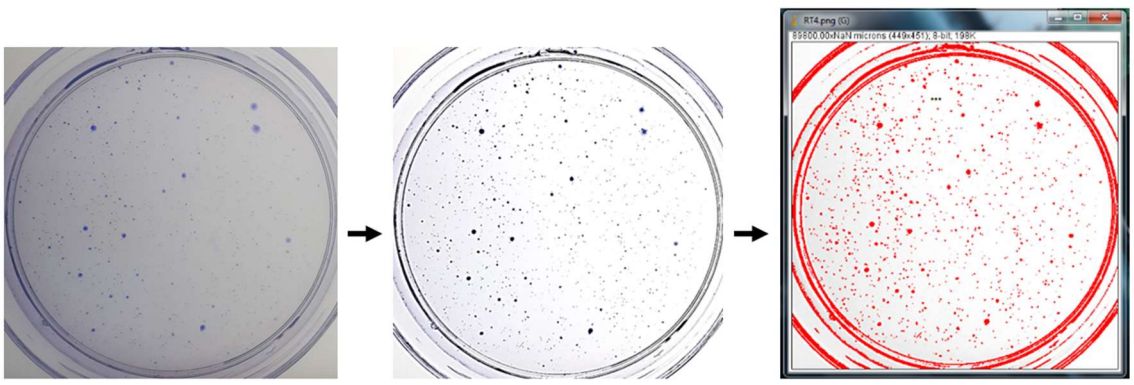

Figure 12: A sample of a colony picture processing using ImageJ

2.9 Migration Assay

Cell migration is defined as the movement of cells from one location to another individually or collectively (Vedula, Ravasio et al. 2013). It is of great importance in regulating various biological processes under either physiological conditions, such as cell growth and differentiation, or pathological ones, like cancer metastasis (Kramer, Walzl et al. 2013).

Migration assays measure differences in cell migration rates under different treatment conditions in vitro. In this study, a modified wound-healing assay was performed using a special sticky insert to create a defined gap across which cells migrate (see Figure 13), and it offered an alternative to traditional scratch assay with higher reproducibility. Cell migration can be monitored both in real time and at the end point.

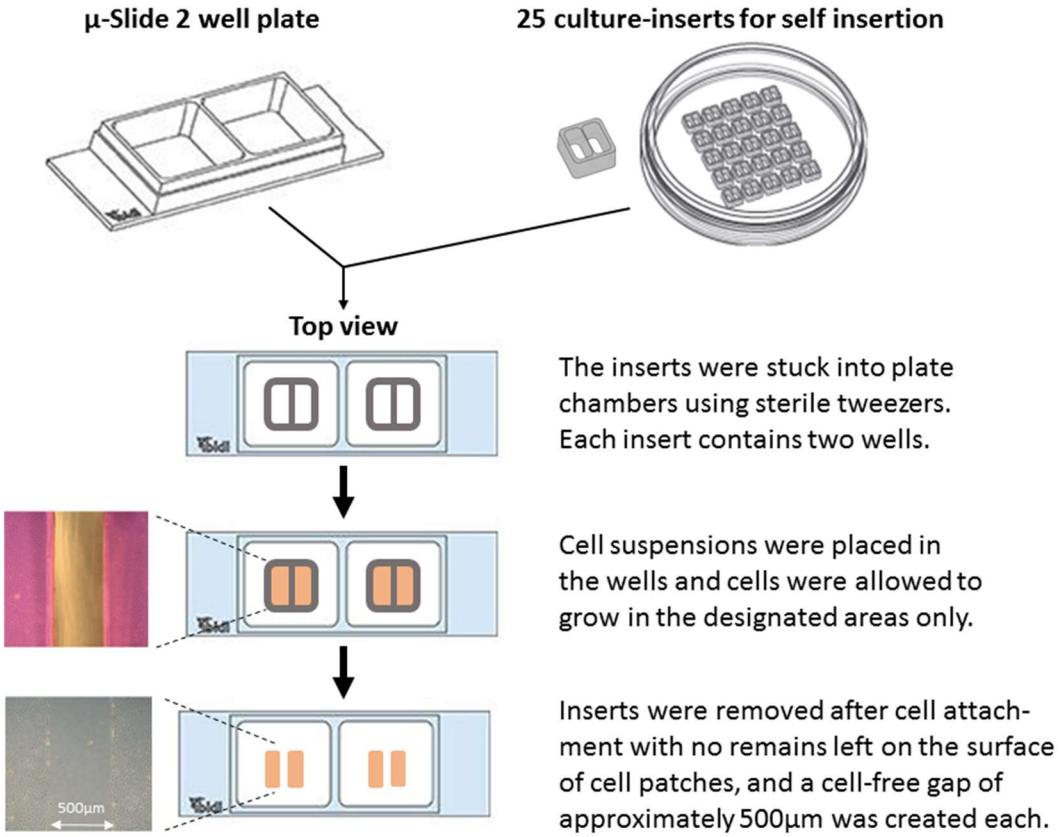

Figure 13: migration assay demonstration

2.9.1 Equipment

µ-Slide 2 well (Ibidi, Cat #. 80286, Germany)

Culture-Inserts (Ibidi, Cat #. 80209, Germany)

Tweezers (Fisher Scientific, Loughborough, UK)

LEICA DM IRB microscope/ AxioCam ERc5s camera (see 2.8.1)

ImageJ software (see 2.3.7.1)

2.9.2 Reagents

GM/SFM/PBS/CDS/TE (see 2.1.3)

2.9.3 Method

Inserts were placed into the wells of the slides one for each and secured.

Cells were trypsinized (see 2.1.4.1) and counted (see 2.1.4.2) in GM.

Cells were centrifuged and resuspended in certain volumes of GM to achieve stock cell suspensions of different densities suitable for seeding depending on cell type (see Table 7).

70µl of the stock cell suspension was added to each well of the inserts according to the experimental design and the outer area was filled with 1.5ml of GM for each well of the slides.

The slides were incubated at 37˚C for about 24 hours to let cells settle and reach approximately 70-80% confluency.

The GM was replaced with fresh SFM (70µl for the inside of the insert well and 1.5ml for outside) after washing with PBS gently twice and then cells were incubated at 37˚C for another 24 hours till the cells had reached 90-95% confluency. **Note**: over confluent cells should be avoided in case the cell-lawn is (partially) removed together with the inserts.

The inserts were removed carefully and each well of the slides was filled with 2ml of fresh SFM for **basal cell migration characterisation** or 2ml of SFM containing chemicals of certain concentrations for **experiments in which cells were treated**.

Cell migration was monitored under LEICA DM IRB microscope and pictures taken at the start point and every following 2 hours using AxioCam ERc5s camera focusing on the same area for each gap.

Cell migration rate was analysed using ImageJ software by measuring the area of the gap in the cell pictures (see Table 20 and Figure 14).

Table 20: procedure of using ImageJ to measure cell migration rate

Step	Aim	Procedure
1	Open a selected picture	"File" –- "Open"
2	Select the area to measure	"Freehand selections"
3	Check measure parameters	"Analyze" --- "Set measurements"
4	Take measurements	"Analyze" --- "Measure"
5	Export data	The measurements will show up in a chart, and the results can be cut and paste into excel for analysing.

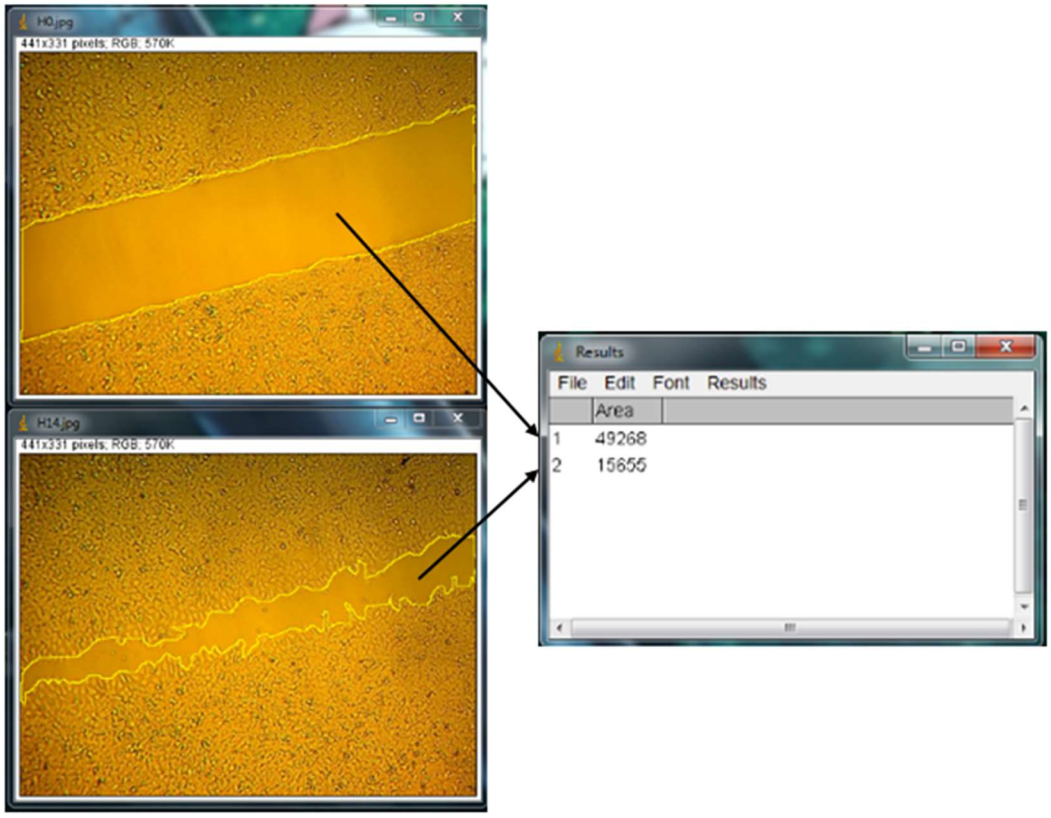

Figure 14: a sample of measurement of cell migration gap area using ImageJ

2.10 Invasion Assay

Compared with cell migration, invasion refers to cell invasive migration into neighbouring tissues involving degradation and proteolysis of extracellular matrix (ECM) (Kramer, Walzl et al. 2013). It is a fundamental function underlying many cellular processes such as cancer cell invasion.

Invasion assays monitor differences in cell movement through the extracellular matrix (ECM) under various treatment conditions in vitro. In this study, a model of trans-well migration assay with the collagen-coated porous membrane was used (see Figure 15). SFM was used for cell pre-starvation as well as preparation of cell suspensions seeded in the inserts, and GM supplemented with 10% FBS was placed in the lower chamber in the plate. The difference in the presence of cytokines and growth factors in the two compartments established a chemoattractant gradient which gave cells an incentive to invade the membrane. Cell invasion can only be examined at the end point.

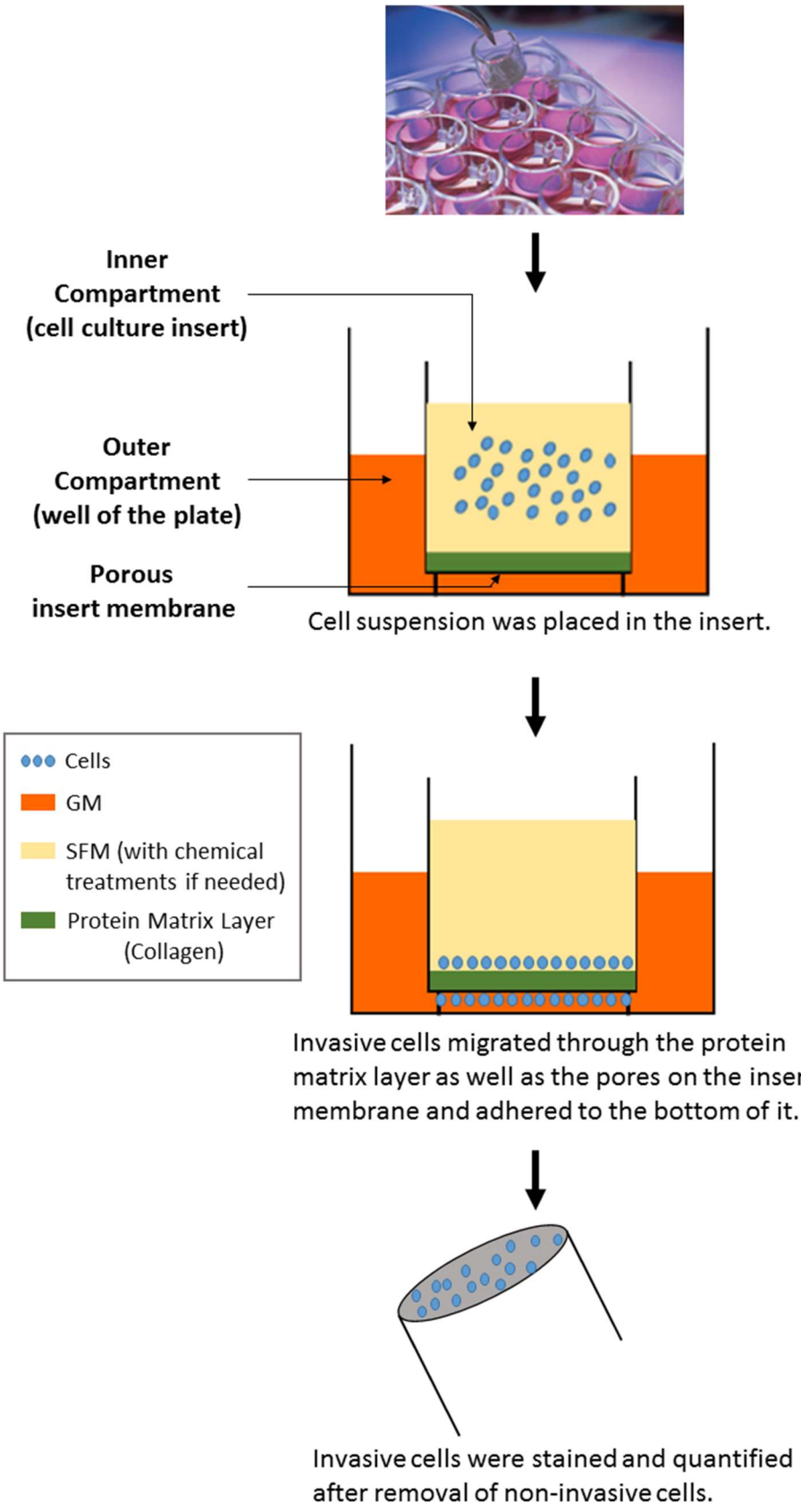

Figure 15: invasion assay demonstration

2.10.1 Equipment

24-well plate (Greiner Bio-one, Cat #. 662160, Gloucester, UK)

Millicell Cell Culture Insert (Merck Millipore, Cat #. PI8P01250, Hertfordshire, UK)

Tweezers (see 2.9.1)

Scalpel blade (Swann Morton, Cat #. 7471312, Sheffield, UK)

Leica DMI 6000B microscope (see 2.5.1)

ImageJ software (see 2.3.7.1)

2.10.2 Reagents

Purified Bovine Collagen Solution (Advanced BioMatrix, Cat #. 5005, USA)

GM/SFM/PBS/CDS/TE (see 2.1.3)

Triton X-100 (see 2.3.2.2)

Glycine/PFA/BSA/DAPI/Nail varnish (see 2.5.2)

2.10.3 Method

2.10.3.1 Coating cell culture inserts with collagen

One insert was placed in each well of a 24-well plate in the cell culture hood.

The purified bovine collagen solution was diluted with sterile dH_2O and mixed gently to make a working solution of 10µg/ml.

200µl of working collagen solution was added to the surface of the insert membrane ensuring that the entire surface was covered.

The plates containing coated inserts were left in the hood to stand overnight at room temperature until the surface was dry.

The coated surface was rinsed with PBS carefully to avoid scratching the surface.

Coated inserts can also be stored in the fridge (4˚C) for a short period of time as long as sterility is maintained.

2.10.3.2 Cell preparation

GM was replaced with fresh SFM to serum starve cells for about 15 hours.

2.10.3.3 Cell seeding

500µl of GM were added per well of the 24-well plates.

Cells were trypsinized (see 2.1.4.1) and counted (see 2.1.4.2) in SFM.

Cells were centrifuged and resuspended in specific volumes of SFM to achieve stock cell suspensions of different densities suitable for seeding depending on the cell type (see Table 7).

Stock cell suspensions were divided into several parts with treatments added to certain ones with appropriate final concentrations according to each experimental design.

500µl of stock cell suspensions were added to each insert carefully to avoid scratching the coated insert membranes.

The inserts were then transferred into wells of the 24-well plates with pre-filled GM, one for each well, carefully without causing bubbles under the inserts.

The cells were incubated at 37˚C for 18-24 hours depending on the cell type to allow for invasive migration through the collagen-coated membrane.

2.10.3.4 Cell staining with DAPI

Solutions used in this section were all applied to both compartments of the assay model.

Media was removed from both compartments and replaced with 500µl of PBS to wash both sides of the membrane.

The PBS was replaced with 300µl of PFA to fix cells and the plates were left covered to stand for 15 minutes at room temperature.

The PFA was removed and a PBS was performed.

The PBS was removed and 300µl of 30mM glycine was added for 5 minutes to quench the cells.

This was replaced with PBS to wash the cells again.

The cells were permeabilised by adding 300µl of 0.3% PBS-Triton solution and were left to stand for 20 minutes.

Cells were washed twice by replacing with 500µl of 0.05% PBS-Triton solution.

Any non-migrated cells were removed gently using a cotton bud.

The membrane was carefully cut out using a scalpel blade and placed on a cover slide with the migrated cells side up.

dH_2O was added dropwise gently by the side of the membrane and dried with tissue to wash away remaining floating cells.

In the *darkness*, the membrane was mounted in DAPI on the coverslip and then it was applied to a slide and sealed with nail varnish to avoid movement.

Membranes were then imaged using a Leica DMI 6000B microscope in 10 random fields with at least two of the views away from the membrane edge to avoid counting non-migrated/unremoved cells.

2.10.3.5 Analysis of invaded cells using ImageJ

Cell invasion was analysed by measuring the number of invaded cells under different treatments using ImageJ (see Table 21 and Figure 16).

Table 21: procedure of using ImageJ to measure invaded cell numbers

Step	Aim	Procedure
1	Open a selected picture	"File" –- "Open"
2	Convert the image to greyscale	"Image" –- "Type" –- "8 bit"
3	Remove background noise	"Process" --- "Subtract Background"
4	Select cells wanted to count	"Image" --- "Adjust" --- "Threshold"
5	Distinguish each cell from a cell cluster	"Process" --- "Binary" --- "Convert to Mask" --- "Binary" ---"Watershed"
6	Check measure parameters	"Analyse" --- "Set measurements"
7	Take measurement	"Analyse" --- "Analyse particles" --- "OK" Note: set a minimum particle size to exclude noise, and tick "Exclude on edges" to remove cells on edge
8	Export data	The measurements will show up in a chart, and the results can be cut and paste into excel for analysing.

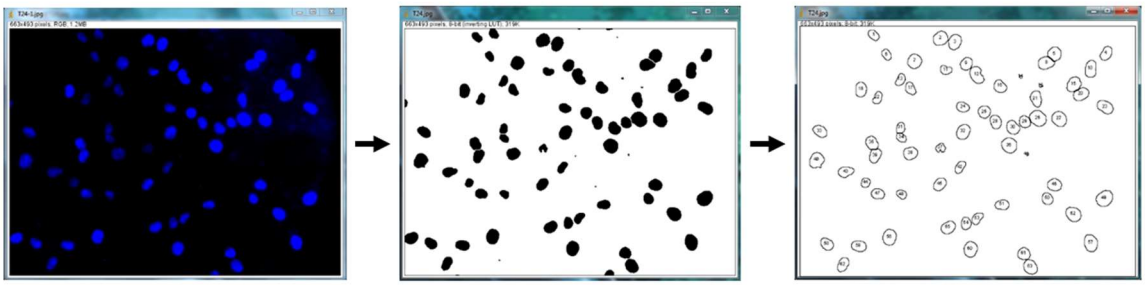

Figure 16: a sample of an invasion assay picture processing using ImageJ

2.11 Statistical Analysis

Unless otherwise stated, statistical analyses of all graphic results were performed by SPSS 23 statistical software (IBM, USA), and all data were from at least three independent experiments (n=3).

Data were analysed and expressed as mean ± standard error (SE). The significance of the difference between groups was evaluated by analysis of variance (ANOVA) followed by least significant different (LSD) post-hoc test and Student's t-test.

For all tests, a two-sided *p*-value was shown for statistical significance and was depicted in asterisks as a single one for *$p<0.05$ and a double for **$p<0.01$.

Chapter 3- The Levels and Role of IGFBP-2 in Bladder Cancer

3.1 Introduction

With accumulating evidence indicating a relationship between IGF-activity and EMT in bladder cancer, as well as based on the work about IGFBP-2 has been done on other tumours in our laboratory, this study was conducted to investigate the association of IGFBP-2, the second most abundant IGFBP in human serum, with bladder cancer development.

3.1.1 IGFBP-2 in cancer

The role that IGFBP-2 plays in cancer progression remains unclear.

Enhanced expression of IGFBP-2 is commonly observed in tumours with high grade, and it is thought to act as an oncogene to promote cancer development and progression. This has been observed in many cancers such as breast (Perks, Vernon et al. 2007, Mireuta, Darnel et al. 2010, Foulstone, Zeng et al. 2013), prostate (Degraff, Aguiar et al. 2009, Uzoh, Holly et al. 2011), and glioma (Fukushima and Kataoka 2007, Moore, Holmes et al. 2009).

However, contradictory results have also been reported in a number of studies, both *in vitro* and *in vivo*, even within the same cancer type: certain aggressive cancer types have little or no expression of IGFBP-2, that suggests IGFBP-2 may also act in a tumour suppressive way (Pickard and McCance 2015). For example, high levels of IGFBP-2 are found in rapidly growing non-invasive brain tumours, whereas low/undetectable levels are observed in malignant invasive tumours (Shelton, Mukherjee et al. 2010).

3.1.2 EMT in cancer

As mentioned in section 1.3, by allowing cells to alter from an adherent epithelial-like into a highly motile mesenchymal-like phenotype, oncogenic EMT is considered to play an essential part in cancer growth and progression.

There are a number of well-established epithelial and mesenchymal markers, including surface proteins (such as E-cadherin and N-cadherin), cytoskeletal markers (such as β-catenin), changes in which have been widely used to determine the occurrence of EMT (Zeisberg and Neilson 2009). Common changes in these markers include a reduction in E-cadherin (an epithelial marker mediating intercellular adhesion) (McConkey, Choi et al. 2009), the acquisition of N-cadherin (a mesenchymal marker providing a mechanism for cell transendothelial migration) (Ramis-Conde, Chaplain et al. 2009), and translocation of β-catenin (which interacts with E-cadherin in cellular adhesions) from the cell membrane in normal epithelial cells and non-invasive tumour cells into the nucleus of cells undergoing EMT, where it transcriptionally activates Wnt target genes (Bienz 2005, Zeisberg and Neilson 2009).

Cells undergoing EMT exhibit a series of changes in phenotype referring to the loss of epithelial features and gain of mesenchymal characteristics, such as an increase in cell proliferation, enhanced migration and invasion, and an increase in colony formation in terms of the quantity and the average size (Son and Moon 2010, Thiery and Lim 2013, Wu, Sarkissyan et al. 2016).

3.1.3 Cisplatin

Cisplatin is a member of a class of platinum-containing anticancer drugs triggering cell death by impeding DNA replication and transcription (Siddik 2003, Massari, Santoni et al. 2015, Michel, Vordos et al. 2018). Administered intravenously, it has been commonly used for the treatment of many types of malignancies including bladder cancer. Neoadjuvant platinum-based combination chemotherapy applied before radical cystectomy has been reported to shrink the tumour size which leads to a significant improvement in patients' overall survival at 5 yr after radical cystectomy (Sherif, Holmberg et al. 2004, International Collaboration of Trialists, Medical Research Council Advanced Bladder Cancer Working Party et al. 2011), and it is the established gold standard in the treatment of MIBC. Within the frontline chemotherapies for bladder cancer, cisplatin-based combination treatments represent the standard first-line therapy for patients suffering metastatic bladder cancer showing a relatively high response rate being approximately 50-70% (von der Maase, Sengelov et al. 2005).

However, cancer recurrence with very poor prognoses due to the development of drug resistance after first-line chemotherapy has become an emerging issue (Yafi, North et al. 2011), and no consensus in the management of cisplatin-resistant bladder cancer has been reached yet (Massari, Santoni et al. 2015).

3.2 Aims

In this study, I aimed to assess the basal levels of IGFBP-2 in bladder cancer cell lines and its relationship with cancer phenotype as well as sensitivity to cisplatin.

To achieve the aims above, I set the following goals:

To determine the basal levels IGFBP-2 in bladder cancer cell lines.

To manipulate the levels of IGFBP-2:

- To decrease the expression of IGFBP-2 through gene silencing using siRNA.
- To increase the abundance of IGFBP-2 by adding exogenous recombinant IGFBP-2.

To assess relative changes in EMT markers, including abundance and localisation, and cancer phenotype (proliferation, migration, invasion as well as colony formation) in bladder cancer cells.

To assess the sensitivity of bladder cancer cells to cisplatin in the presence or absence of IGFBP-2.

3.3 Materials and methods

3.3.1 Cell culture

Four human urinary bladder cancer cell lines including RT4, UMUC3, T24 and TCCSUP were used in this study. They were obtained and cultured as described in section 2.1.

3.3.2 Characterisation and optimisation of the antibodies for the assessment of EMT markers

Changes in the levels of E- and N-cadherin, as well as localisation of β-catenin, were used as markers of EMT in this study for the investigation relating to the levels of IGFBP-2. Since the antibodies for the three molecules were new to our laboratory, characterisation and optimisation using either Western blotting (WB, as described in section 2.3) or immunofluorescence (IF, as described in section 2.5) were carried out in RT4 and T24 cell lines by changing the solvent and/or the concentration of the antibody solutions, respectively. GAPDH and tubulin were used as loading controls in WB analyses.

Product details and the conditions optimised for the EMT markers used in this study are summarised in Table 22, and the known information of antibody solutions of IGFBP-2 and the reference proteins (GAPDH and tubulin) used as a loading control is shown below in Table 23.

Table 22: optimised antibody solutions information of EMT markers for WB/IF

Protein	Size (kDa)	Gel percentage (%)	Company & Cat. No.	Assay	Blocking	1° Ab	*2° Ab
E-cadherin	135	10	Cell Signaling (24E10), #3195	WB	5% milk	1/1000, 5% BSA, rabbit	1/2000, 5% BSA, anti-rabbit
N-cadherin	130	10	BD Biosciences, #610920	WB	5% milk	1/1000, 5% milk, mouse	1/2000, 5% milk, anti-mouse
β-catenin	92	10	Cell Signalling (683), #9582	WB	5% BSA	1/1000, 5% BSA, rabbit	1/2000, 5% BSA, anti-rabbit
		-		IF	3% BSA	1/50, 3% BSA, rabbit	1/500, 3% BSA, anti-rabbit, *avoid light*

2° Ab**: **E-cadherin**: anti-rabbit (Sigma, #A0545); **N-cadherin**: anti-mouse (Sigma, #A0944); **β-catenin**: ***WB: anti-rabbit (Sigma, #A0545); ***IF***: Alexa Fluor 488 Donkey Anti-rabbit IgG (H+L) (ThermoFisher, #A-21206).

Table 23: antibody solutions information of IGFBP-2 and reference proteins for WB

Protein	Size (kDa)	Gel percentage (%)	Company & Cat. No.	Blocking	1° Ab	*2° Ab
IGFBP-2	36	12	Santa Cruz, #SC6001	5% milk	1/1000, 5% milk, goat	1/2000, 5% milk, anti-goat
Tubulin	55	12	Millipore, (anti-α-Tubulin) #2016030	5% BSA	1/5000, 1% milk, mouse	1/5000, 1% milk, anti-mouse
GAPDH	35	12	Chemicon, #MAB 374	5% milk	1/5000 5% milk mouse	1/5000, 5%milk anti-mouse

***2° Ab**: anti-goat (Sigma, #A5420); anti-mouse (Sigma, #A0944).

3.3.3 Detection of protein abundance

Protein levels of E- and N-cadherin in whole cell lysates and the levels of IGFBP-2 both in whole cell lysates and in the supernatant were determined by performing WB analyses as described in section 2.3. Tubulin was used as a loading control. The information of antibody solutions is summarised in Table 22 and Table 23.

3.3.4 Detection of protein localisation

Cellular fractionation and IF were performed to look into the localisation of β-catenin as described in section 2.4 and 2.5, respectively.

Proteins of cytoplasmic and nuclear extracts from cultured cells were separated using cellular fractionation technique. Lamin and tubulin exist only in nuclei and cytoplasm, respectively, and they were therefore used as indicators of the efficiency of protein separation. The abundance of separated proteins was detected by WB as described above in 3.3.3. The information of antibody solutions of Lamin is listed below in Table 24, and the information of β-catenin and tubulin can be found in Table 22 and Table 23, respectively.

Table 24: antibody solutions information of Lamin for WB

Protein	Size (kDa)	Company & Cat. No.	Blocking	1° Ab	*2° Ab
Lamin A/C	70	Cell Signaling , #2032	5% milk	1/1000, 5% milk, rabbit	1/2000, 5% milk, anti-rabbit

***2° Ab**: anti-rabbit (Sigma, #A0545).

3.3.5 Transfection with IGFBP-2 siRNA

IGFBP-2 siRNA transfection was used to decrease IGFBP-2 expression by silencing the corresponding gene, and the technique was performed as described in section 2.6.

3.3.6 Cell treatment

3.3.6.1 Recombinant human IGFBP-2 protein

The recombinant human IGFBP-2 protein (GroPep, #BP2BU020) is biotechnologically generated in E.coli with the recombinant human IGFBP-2 gene. With correct amino acid sequence but non-glycosylated, it was used as an exogenous reagent in IGFBP-2 manipulation experiments.

Lyophilized human IGFBP-2 was reconstituted at 500µg/ml by re-suspending 20µg in 40µl sterile PBS and then aliquoted and stored at -20°C. 5000ng/ml working stock of IGFBP-2 was prepared fresh by extracting 15µl of 500µg/ml stock and adding to 1485µl of serum-free media (SFM: as described in section 2.1.3.2). Different final concentrations of IGFBP-2 were achieved by diluting the working stock further with SFM.

3.3.6.2 Cisplatin

Cisplatin (Merck Chemicals Ltd, #232120) was prepared fresh for each experiment by dissolving 2mg in 4ml of 0.9% saline solution (made by adding 45mg of NaCl to 5ml of dH_2O) to reach a 500µg/ml working stock solution. The stock solution was then sterilised with 0.2µm filters. Different final

concentrations of cisplatin were accomplished by diluting the working stock further with SFM. Exposure of cisplatin to light was avoided during the entire process.

3.3.7 Cell proliferation

Tritiated thymidine incorporation (TTI) assay was used to assess DNA synthesis, and Trypan Blue Exclusion assay was performed for cell counting to determine cell survival as described in section 2.2.

3.3.8 Cell migration

Cell migration assay was performed as described in section 2.9 to measure differences in cell migration rates in response to different treatments.

3.3.9 Cell invasion

To investigate the differences in cell movement through the extracellular matrix (ECM) under different treatments *in vitro*, a cell invasion assay was used as described in section 2.10.

3.3.10 Cell colony formation

A soft agar colony formation assay was used as described in section 2.8 to measure cell malignant transformation activity under various treatments.

For cells treated with siRNA, the first 24 hours of transfection were performed in universal tubes instead of 6-well plates to avoid the cells settling down: cells

were collected, resuspended and counted before being seeded in the soft agar plates with equivalent numbers of live cells.

3.3.11 Statistical analysis

Data were expressed as mean ± SEM and analysed with SPSS 23 for Windows using one-way analysis of variance (ANOVA) followed by least significant difference (LSD) post-hoc test and Student's test. A two-sided *p*-value was shown for statistical significance and was depicted in asterisks as a single one for $*p<0.05$ and a double for $**p<0.01$.

3.4 Results

3.4.1 Characterisation of EMT molecules: E-, N-cadherin and β-catenin

From the WB results we found that RT4 cells express abundant E-cadherin and undetectable amounts of N-cadherin; while T24 cells show the opposite having undetectable E-cadherin but abundant N-cadherin (see Figure 17-**A** & **B**). β-catenin was found in both RT4 and T24 cells with more present in RT4 cells (Figure 17-**C**). And based on the results above, 60μg was used as an appropriate amount to load for each of these proteins in the following experiments unless otherwise noted.

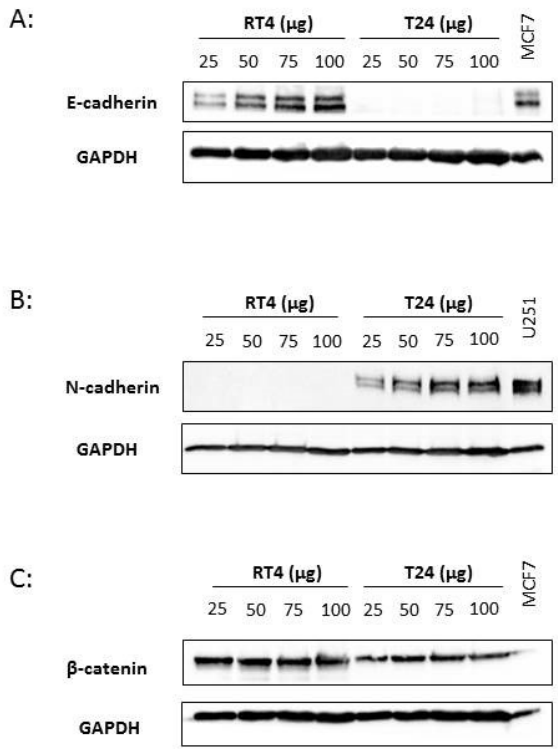

Figure 17: characterisation of the levels of E-, N-cadherin and β-catenin in RT4 and T24 cells

Figures (**A**), (**B**) and (**C**) show the western blots for E-, N-cadherin and β-catenin, respectively, in both RT4 and T24 cells detected using WB. RT4 and T24 cells were seeded in GM at the same density to grow for 24 hours and then were left in SFM for 48 hours before sample harvest. Proteins in whole lysates were loaded with increasing amounts from 25 to 100µg. Proteins from MCF7 (a human breast adenocarcinoma cell line) and U251 (a human glioblastoma cell line) cell lysates were used as positive controls for E-cadherin & β-catenin and N-cadherin, respectively. They were loaded equally at 50µg. GAPDH was used as a reference protein.

Basal localisation of β-catenin in RT4 and T24 cells was detected by cellular fractionation and IF.

From the cellular fractionation data shown in Figure 18, β-catenin was located only in the cytoplasm of RT4 cells with no trace in the nuclear extracts (Figure 18-**A**). It was found in both the nuclear and cytoplasmic extracts of T24 cells: with the most abundant levels observed in the cytoplasm (Figure 18-**B**). And the IF results presented in Figure 18-**C** confirmed that in RT4 cells, β-catenin

was mainly localised on the cell membrane with a small amount in the cytoplasm, while in T24 cells it was also found on the cell membrane but to a greater level in the cytoplasm compared with RT4 cells with some also observed in the nucleus.

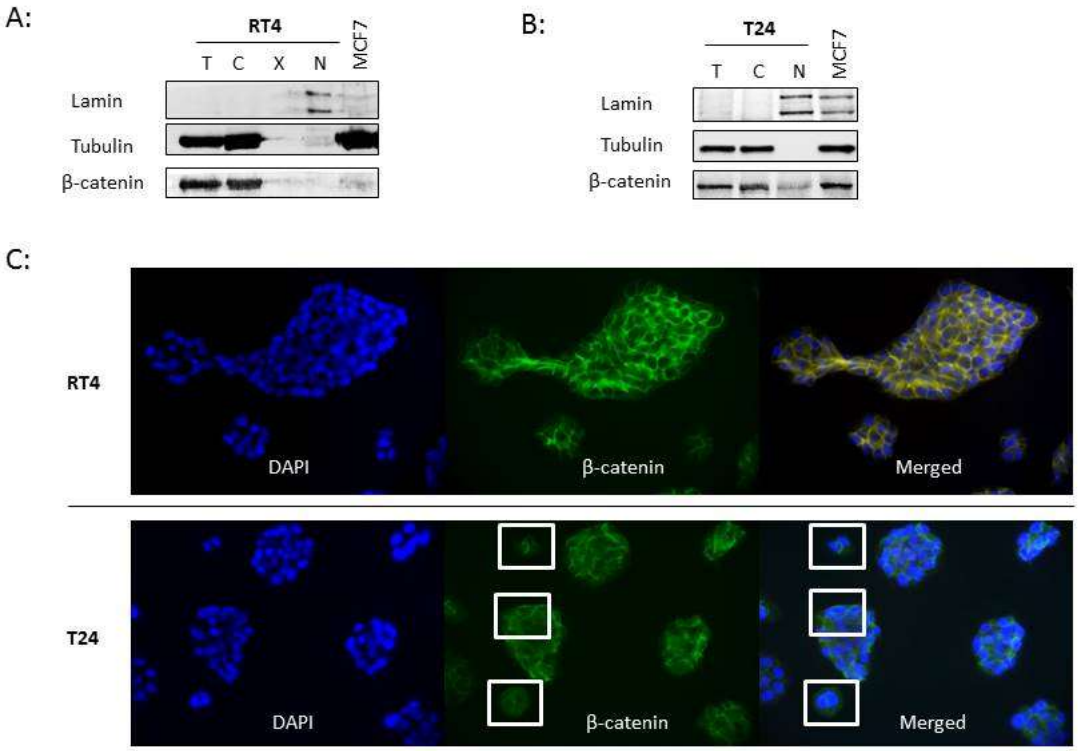

Figure 18: localisation of β-catenin in RT4 and T24 cells

(**A**) & (**B**): The WB blots show the characterisation of basal localisation of β-catenin in RT4 and T24 cells, respectively, using cellular fractionation. Both RT4 and T24 cells were seeded in GM at the same density to grow for 24 hours followed by serum starvation using SFM for another 24 hours, and then cells were trypsinized and harvested for performing cellular fractionation to separate proteins of cytoplasmic and nuclear extracts. Isolated proteins extracted from the total cell lysates were loaded equally for protein detection using WB. Lamin and Tubulin exist only in nuclei and cytoplasm, respectively, and they are indicators of the efficiency of protein separation. "T": total cell lysates; "C": cytoplasmic extract; "N": nuclear extract; "X": blank lane. Proteins of MCF7 (a human breast adenocarcinoma cell line) were used as a positive control for β-catenin. And the blots demonstrate the typical results from three experiments each performed at least in triplicate (n=3).

(**C**): Images show the characterisation of basal localisation of β-catenin in both RT4 and T24 cells using IF. Both RT4 and T24 cells were seeded in GM at the same density to grow for 24 hours and then were left in SFM for 48 hours before stained. Images show β-catenin (in green) with counterstaining for DAPI (nuclei in blue) and overlaid version labelled as "Merged". All images demonstrate the typical results from three experiments each performed in duplicate (n=3). All images shown are at x10 magnification.

3.4.2 Characterisation of basal levels of IGFBP-2

Initially, four human urinary bladder cancer cell lines were used to investigate the basal levels of IGFBP-2 by performing WB analyses (see Figure 19).

As shown in Figure 19, RT4 was the most epithelial-like phenotype cell line showing high levels of E-cadherin and no N-cadherin, and it was also shown to have the highest levels of IGFBP-2. T24 was the most mesenchymal-like phenotype demonstrating the highest levels of N-cadherin with undetectable levels of E-cadherin: we observed that this cell line had undetectable levels of IGFBP-2. Similarly, TCCSUP another mesenchymal cell line with low levels of N-cadherin and no E-cadherin also had very low levels of IGFBP-2. UMUC3 had low levels of IGFBP-2 with no E- or N-cadherin expression.

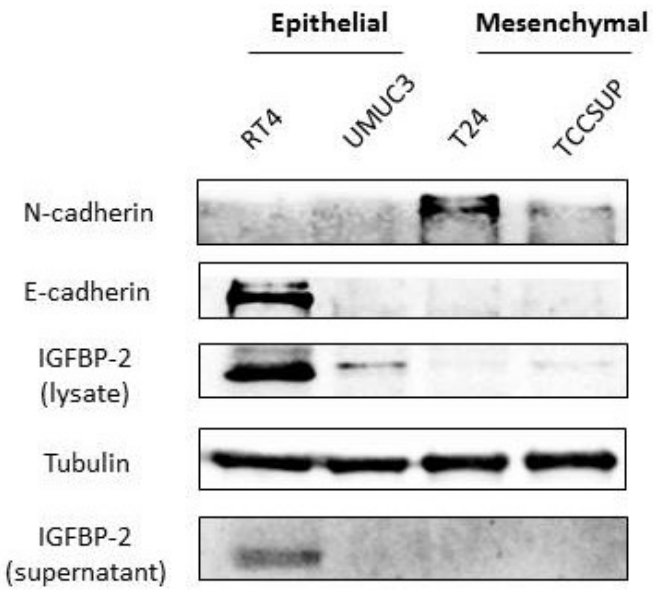

Figure 19: basal levels of IGFBP-2 and EMT markers in bladder cancer cell lines

Cells were seeded in GM at the same density and then were left in SFM for 48 hours before sample harvest. Proteins in whole lysates were loaded equally at 60µg and tubulin was assessed as the reference protein. IGFBP-2 in the supernatant was loaded equally at 25µl.

The levels of IGFBP-2 were reduced as the cells progressed to a more mesenchymal phenotype. To investigate a potential role for IGFBP-2, RT4 and T24 were selected as the two predominant cell lines exhibiting an epithelial-like and a mesenchymal-like phenotype, respectively. The less mesenchymal TCCSUP cell line was also investigated in the late stage of the study to complement the data observed in the T24 cell line. Showing only low levels of IGFBP-2 with no E- or N-cadherin expression, UMUC3 was, therefore not studied further.

As shown in Figure 20, these three cell lines all grew in discrete patches attaching to the substrate of the culture vessels. Compared with RT4 cells which proliferated slowly in clusters maintaining more epithelial characteristics, T24 and TCCSUP cells were faster growing in a less "organised" manner and presented with mesenchymal features such as diminution of the cell-to-cell adhesion with elongated structure.

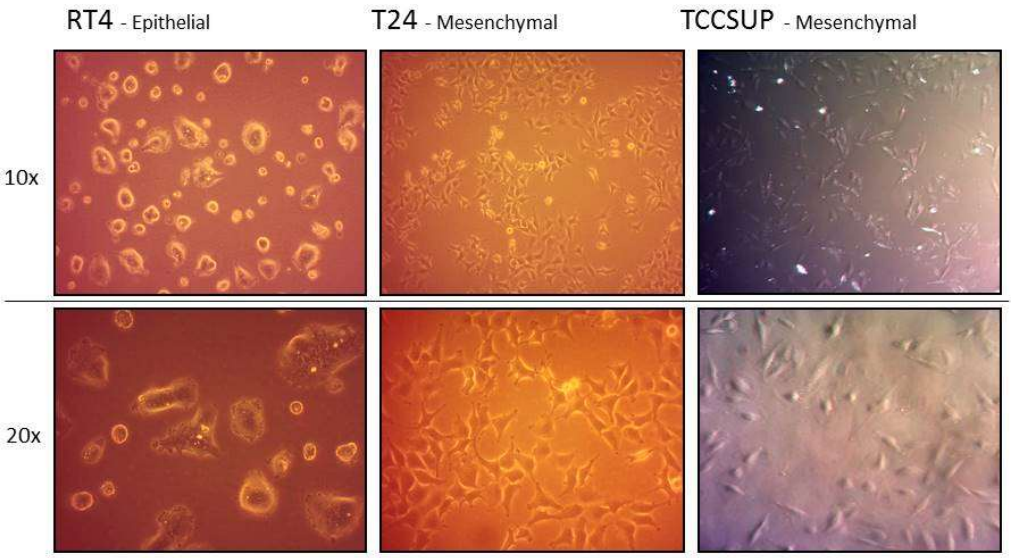

Figure 20: cell images of RT4, T24 and TCCSUP cells 24 hours-post-seeding

Cells were seeded in T75 flasks at a certain density ($0.5x10^6$ cells for RT4 and $0.2x10^6$ cells for both T24 and TCCSUP) in 10ml of GM. Images were taken at the 24^{th} hour after seeding. Images shown are at x10 and x20 magnification, respectively.

3.4.3 Using siRNA to silence IGFBP-2

As shown above in Figure 19, RT4 cells presented the strongest epithelial phenotypic characteristics along with abundant IGFBP-2 expression; therefore, specific siRNA for IGFBP-2 silencing was used in this cell line to examine the link between IGFBP-2 and cancer phenotype regarding cell growth, invasion, migration and colony formation. Changes in EMT markers were also investigated.

3.4.3.1 Optimisation of an effective dose of siRNA

Efficacy of IGFBP-2 siRNA for silencing IGFBP-2 was tested as described in section 2.6.3 by using different siRNA concentrations from 5nM to 30nM shown in Figure 21. WB analysis was performed after 72 hours of transfection

as this corresponded to the experimental set up for the phenotypic models. Using increasing concentrations of siRNA, 30nM was determined to be the most effective (about 70% silencing, $p<0.001$).

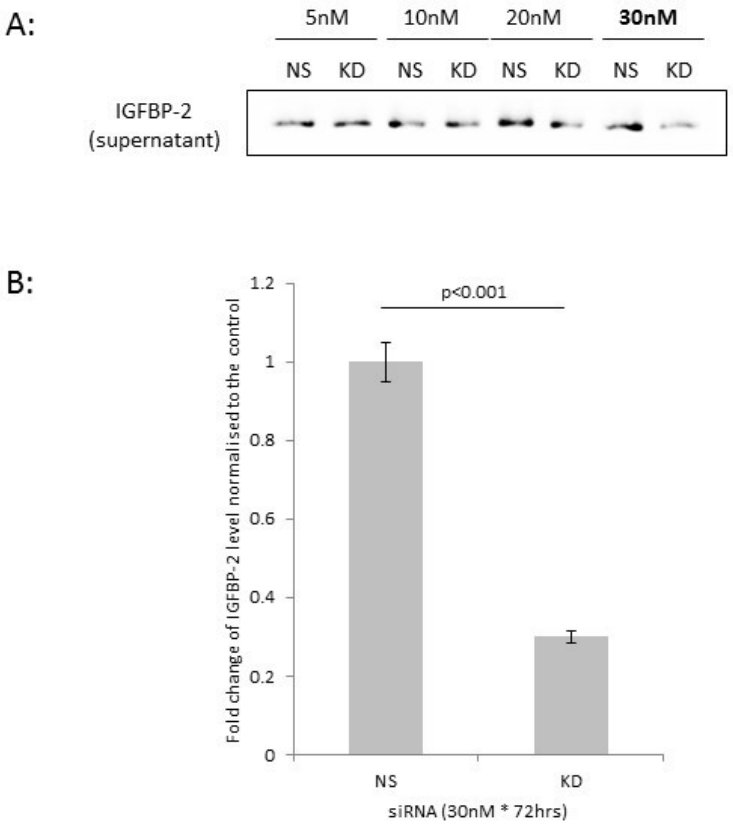

Figure 21: WB analysis of IGFBP-2 protein in cell culture supernatant of RT4 cells

Cells were seeded at the same density in GM, and the supernatant was harvest at 72 hours after transfection with IGFBP-2 siRNA at concentrations of 5nM, 10nM, 20nM, and 30nM, respectively. "NS": cells treated with non-silencing scrambled siRNA as control; "KD": cells treated with IGFBP-2 siRNA for silencing IGFBP-2. All supernatants under different treatments were loaded equally at 25µl.

(**A**): The blot presents levels of IGFBP-2 in cell culture supernatant under different treatments. (**B**): Graph shows the mean of the optical density measurements of IGFBP-2 from three experiments each performed at least in triplicate and error bars represent the standard error of the mean of experiments.

3.4.3.2 Effect of silencing IGFBP-2 on the growth of RT4 cells

Cell counting was performed to determine the effect of IGFBP-2 silencing on cell growth in RT4 cells. As shown in Figure 22, with efficient gene knockdown of IGFBP-2 (Figure 22-**A**), compared with cells treated with scrambled non-silencing siRNA, the growth of the cells with IGFBP-2 knocked down by IGFBP-2 siRNA showed an increase in both total cell number by 27.2% ($p<0.001$) and live cell number by 21.6% ($p<0.01$) (Figure 22-**B**), and no significant change in the level of cell death observed between the two groups (Figure 22-**C**).

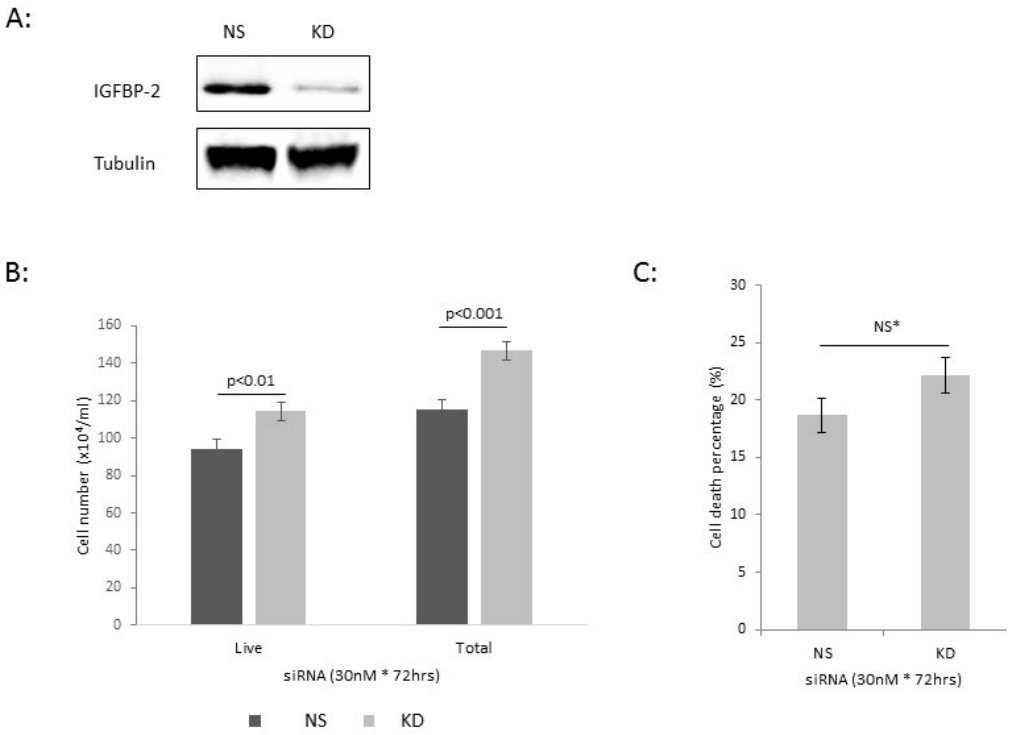

Figure 22: effect of silencing IGFBP-2 on the growth of RT4 cells

Cells were initially seeded into 6-well plates at a density of $0.1x10^6$ cells/well in GM. "NS": cells treated with non-silencing scrambled siRNA as control; "KD": cells treated with IGFBP-2 siRNA for IGFBP-2 knocking down (both at a concentration of 30nM for 72 hours).

(**A**): WB blot shows the efficiency of IGFBP-2 knockdown achieved. Proteins were harvested from whole cell lysates and loaded equally at 50µg. Tubulin was assessed as reference protein. (**B**): Graph shows cell counting of live and total cell numbers of RT4 cells treated with different siRNA both at 30nM for 72 hours. (**C**): Graph presents the percentage cell death under the different treatments described above. Graphs in (**B**) and (**C**) represent the mean of three experiments each performed at least in triplicate, and error bars represent the standard error of the mean of the experiments. "NS*": not significant.

3.4.3.3 Effect of silencing IGFBP-2 on cell invasion in RT4 cells

An invasion assay was conducted (as described in section 2.10) following 72 hours of siRNA transfection (as described in section 2.6) to examine the effect of silencing IGFBP-2 on cell invasion in RT4 cells. According to the results shown in Figure 23, with efficient IGFBP-2 silencing achieved (Figure 23-**A**), IGFBP-2 siRNA transfected RT4 cells invaded more (Figure 23-**B**) compared with cells treated with scrambled siRNA with a significant 68% increase in the fold change of invaded cells($p<0.05$) (Figure 23-**C**).

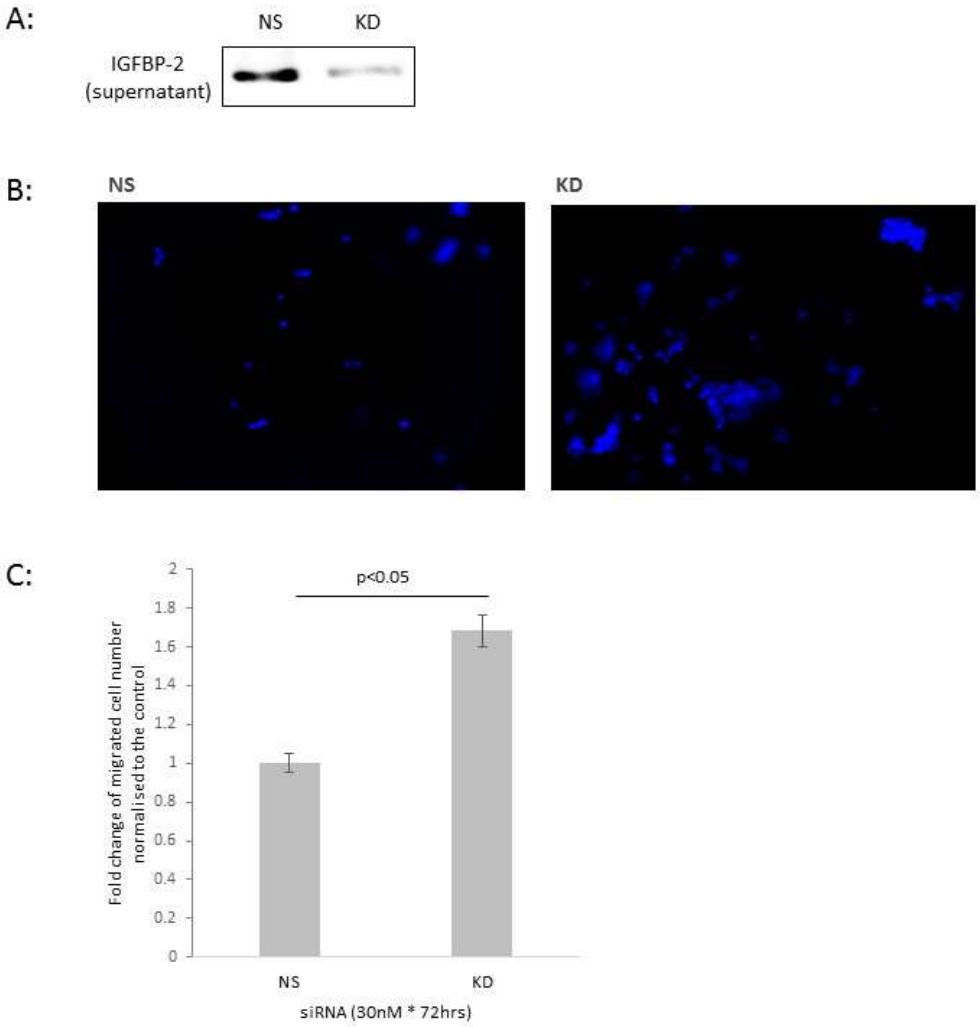

Figure 23: effect of silencing IGFBP-2 on cell invasion in RT4 cells

Cells transfected with either scrambled or IGFBP-2 siRNA ("NS" for non-silencing scrambled siRNA as control and "KD" for IGFBP-2 siRNA) at a concentration of 30nM for 72 hours were trypsinized and then seeded in the collagen-coated inserts at a density of $0.1x10^6$ cells/insert and allowed to invade for 24 hours. The supernatant was taken before cell trypsinization to assess levels of IGFBP-2 to determine the efficiency of IGFBP-2 silencing.

(**A**): The blot shows the efficiency of IGFBP-2 knockdown achieved by loading the supernatant collected under each treatment equally at 25µl; (**B**): The image shows transwell migrated cells with nuclei (in blue) stained by DAPI; all images shown are at x10 magnification; (**C**): the graph shows the fold change of invaded cells between RT4 cells transfected with different siRNA. The graph represents the mean of three experiments each performed in triplicate +/- the standard error of the mean (n=3).

3.4.3.4 Effect of silencing IGFBP-2 on cell migration of RT4 cells

By performing a migration assay as described in section 2.9, we observed that RT4 cells did not migrate with or without IGFBP-2 (see Figure 24 & Figure 25).

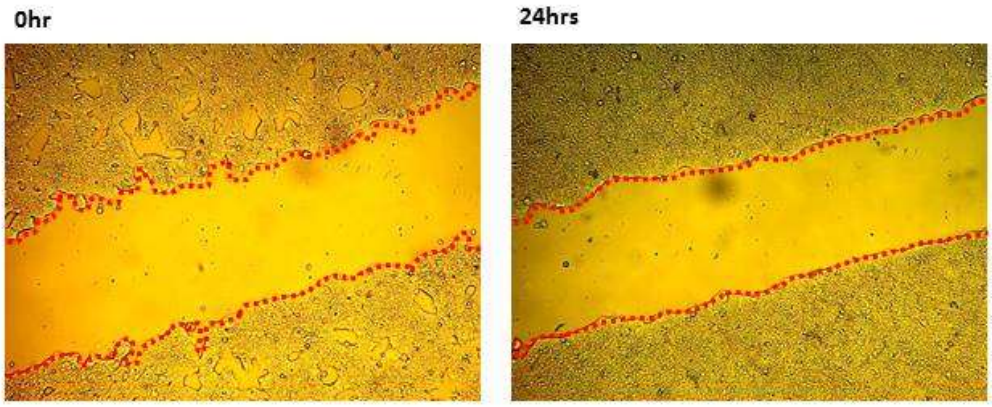

Figure 24: characterisation of cell migration of RT4 cells

Cells were seeded at a density of $0.049x10^6$ cells into each chamber in GM and allowed to grow for approximately 24 hours to reach about 80% confluence. Cells were allowed to reach 90-95% confluence during another 24 hours of serum starvation in SFM. Cell migration was investigated for up to 24 hours after the inserts were removed. "0hr": the start point after the removal of inserts; "24hrs": 24 hours after the removal of inserts. All images demonstrate the typical results from three experiments each performed in duplicate (n=3). All images shown are at x10 magnification, and the area of the gaps in the images was analysed using ImageJ software.

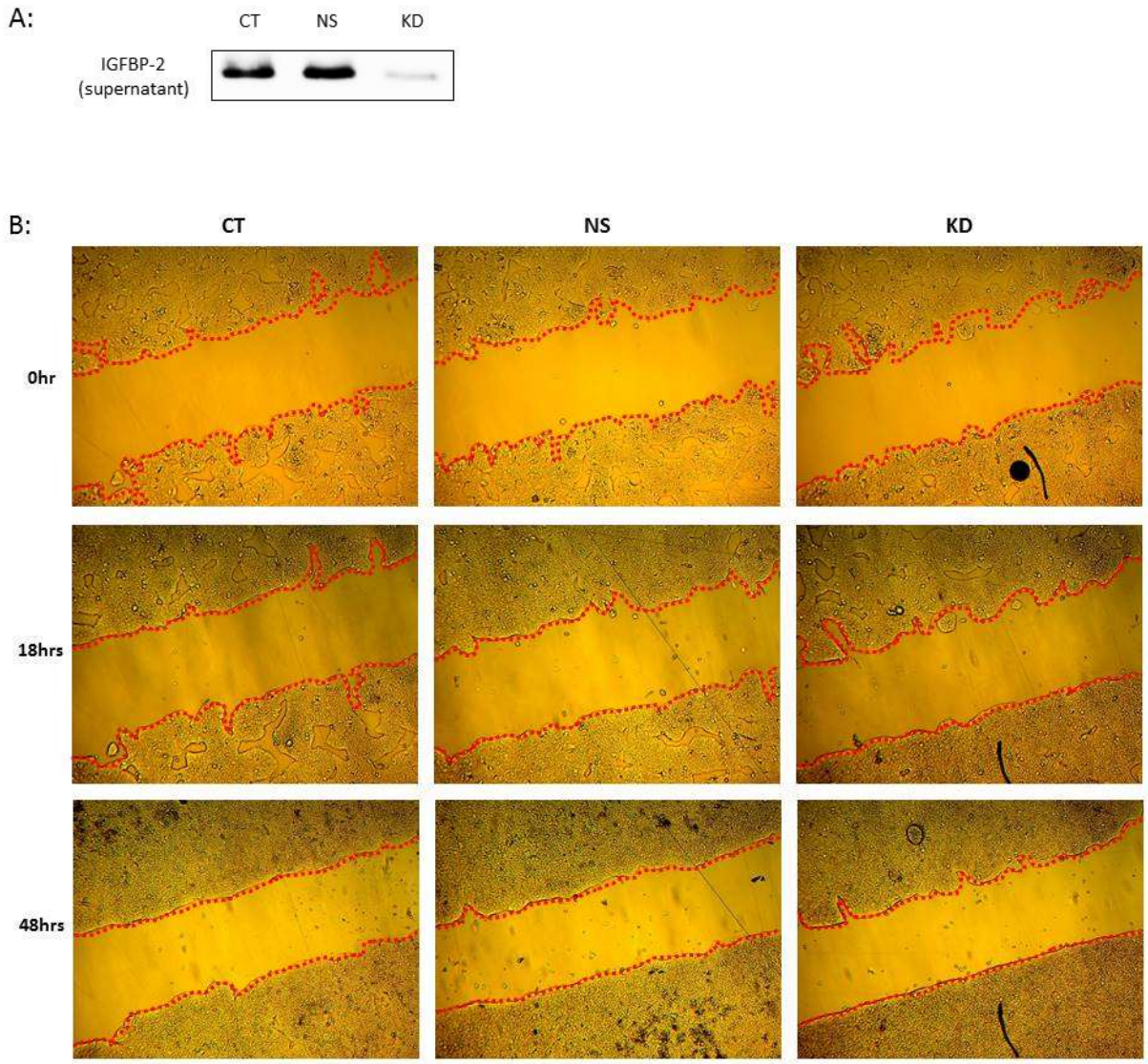

Figure 25: effect of silencing IGFBP-2 on cell migration in RT4 cells

Untreated control RT4 cells ("CT") and cells transfected with either scrambled or IGFBP-2 siRNA ("NS" for non-silencing scrambled siRNA and "KD" for IGFBP-2 siRNA) at 30nM were seeded at a density of $0.049x10^6$ cells into each chamber. Cells were allowed to grow for approximately 24 hours in GM to reach about 80% confluence and then were allowed to reach 90-95% confluence during another 24 hours of serum starvation in SFM. Then cell migration was investigated for up to 48 hours after the inserts were removed. The supernatant was taken at 24 hours after the removal of the inserts for determining the efficiency of IGFBP-2 silencing.

(**A**): The blot shows the efficiency of IGFBP-2 knockdown achieved by detecting IGFBP-2 in samples loaded equally at 25µl; (**B**): images show cell patches after the removal of inserts. "0hr": the start point after the removal of inserts; "18hrs": 18 hours after the removal of inserts; "48hrs": 48 hours after the removal of inserts. All images demonstrate the typical results from three experiments each performed in duplicate (n=3). All images shown are at x10 magnification.

3.4.3.5 Effect of silencing IGFBP-2 on cell colony formation in RT4 cells

After transfection with either scrambled or IGFBP-2 siRNA as described in section 2.6 , the ability of malignant transformation of RT4 cells was investigated by using a soft agar colony formation assay as described in section 2.8.

As shown below in Figure 26, with efficient IGFBP-2 silencing achieved (Figure 26-**A**), compared with cells treated with scrambled siRNA, the IGFBP-2 siRNA treated RT4 cells formed more colonies (Figure 26-**B**), and with a significant 15% increase in colony forming efficiency (CFE) ($p<0.01$) (Figure 26-**C**, left). In addition, IGFBP-2 silenced RT4 cells also formed bigger colonies with a fold change of 1.38 regarding the average size of each colony ($p<0.01$) (Figure 26-**C**, right).

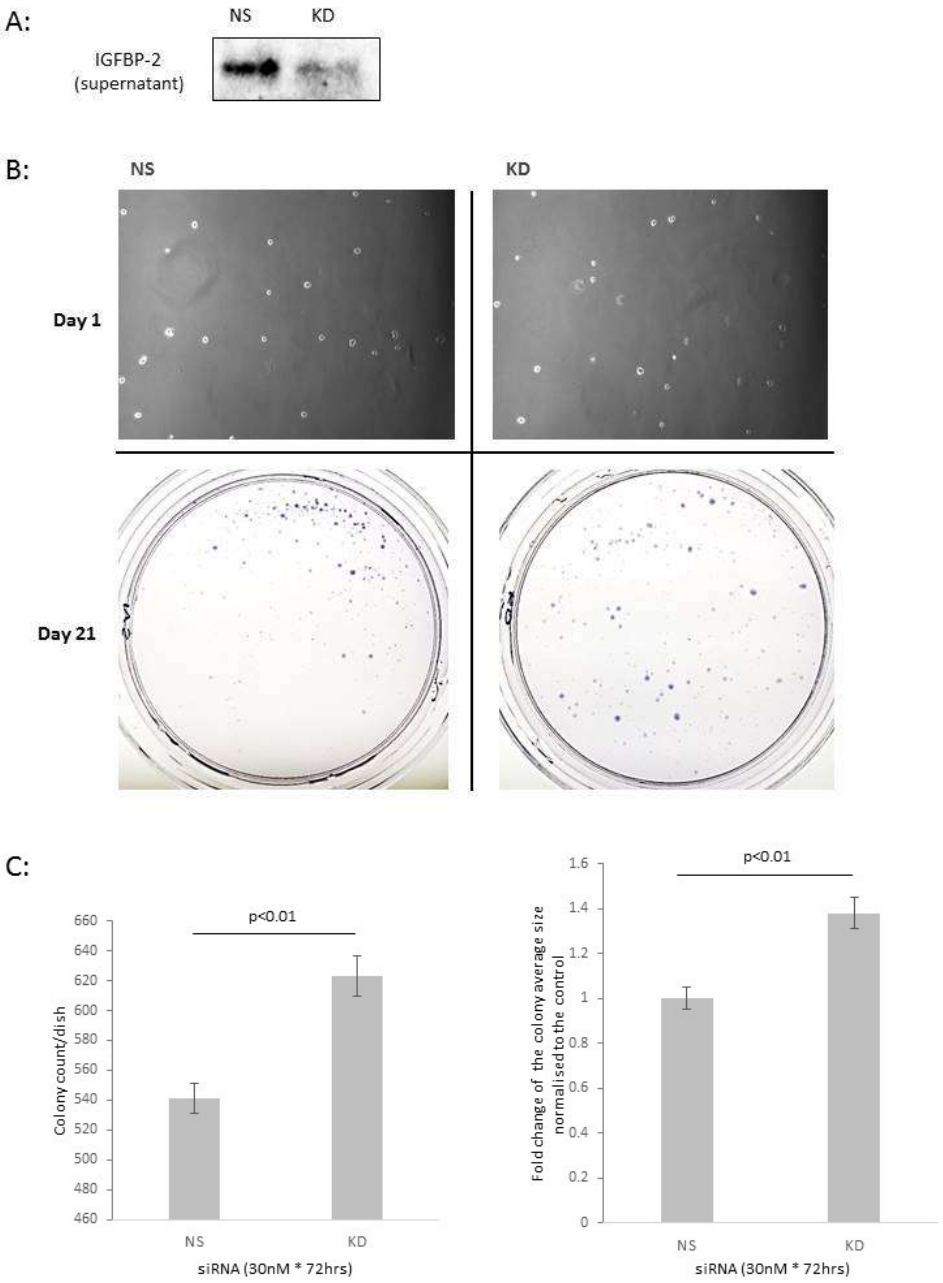

Figure 26: effect of silencing IGFBP-2 on cell colony formation in RT4 cells

Cells transfected with either scrambled or IGFBP-2 siRNA ("NS" for non-silencing scrambled siRNA as control and "KD" for IGFBP-2 siRNA) at a concentration of 30nM for 72 hours were trypsinized and then seeded in the dishes with an even density at 10,000cell/dish. After being fed once a week for 3 weeks in total, the numbers as well as the average size of the colonies were counted and calculated by ImageJ. The supernatant was taken before trypsinization for determining the efficiency of IGFBP-2 silencing.

(**A**): The blot shows the efficiency of IGFBP-2 knockdown achieved by detecting IGFBP-2 in samples loaded equally at 25µl; (**B**): images show cells were set up into dishes with even densities at the first day ("Day 1"), and colonies were stained at the end of the assay ("Day 21"); All images shown are at x10 magnification; (**C**): graphs present the difference in colony count (left) and fold change of the colony average size (right) normalised to the control. The graphs show the mean of three experiments each performed in triplicate, and error bars represent the standard error of the mean from three experiments (n=3).

3.4.3.6 Effect of silencing IGFBP-2 on EMT markers in RT4 cells

As shown in Figure 19, compared with mesenchymal-like T24 cells, epithelial-like RT4 cells express more abundant E-cadherin and β-catenin with undetectable N-cadherin, so WB analysis was performed to examine the change of these molecules regarding abundance following cell treatment with siRNA to silence IGFBP-2. Translocalisation of β-catenin from the membrane into the nucleus is considered an important indicator of cancer progression, so cellular fractionation and IF were conducted to examine the change in its distribution in RT4 cells under IGFBP-2 siRNA transfection.

3.4.3.6.1 Detection of changes in abundance of E-, N-cadherin and β-catenin

As shown in Figure 27, compared with control samples treated with scrambled siRNA, IGFBP-2 siRNA transfected RT4 cells demonstrated a significant 48% reduction in the abundance of E-cadherin ($p<0.05$) (Figure 27-**A** & **B**). No detectable induction of N-cadherin was observed (Figure 27-**B**), and no visible change in the abundance of β-catenin was noted (Figure 27-**C** & **D**).

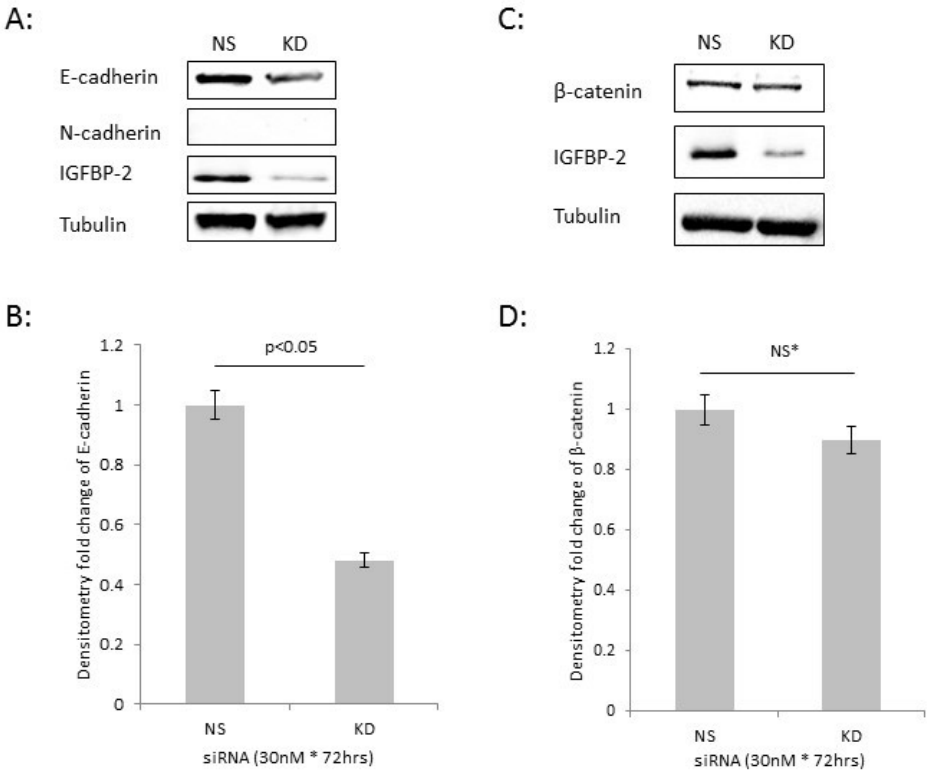

Figure 27: levels of EMT markers in RT4 cells with IGFBP-2 siRNA treatment

RT4 cells transfected with either scrambled or IGFBP-2 siRNA ("NS" for non-silencing scrambled siRNA as control and "KD" for IGFBP-2 siRNA) at the concentration of 30nM for 72 hours were trypsinized and harvested for the investigation of change of protein abundance using WB analysis. Samples from whole lysates were loaded equally at 60μg for protein detection, and tubulin was assessed as a reference protein in WB analysis. All blots demonstrate the typical results from three experiments each performed at least in triplicate (n=3).

The blots show levels of E- and N-cadherin (**A**) and β-catenin (**C**) under treatment of different siRNA. And the graphs (**B**) and (**D**) demonstrate the mean of the optical density of E-cadherin and β-catenin, respectively, from three experiments each performed at least in triplicate, and error bars represent the standard error of the mean of experiments (n=3). "NS*": not significant.

3.4.3.6.2 Detection of the change of localisation of β-catenin

With efficient IGFBP-2 gene knockdown achieved in RT4 cells (Figure 28-**A**), no translocation of β-catenin into the nuclei was observed in the blots (Figure 28-**B**) and this was confirmed by densitometry analysis which showed no significant difference between treated and untreated samples in the fold change of cytoplasmic β-catenin normalised to the β-catenin in total cell lysates (Figure 28-**C**).

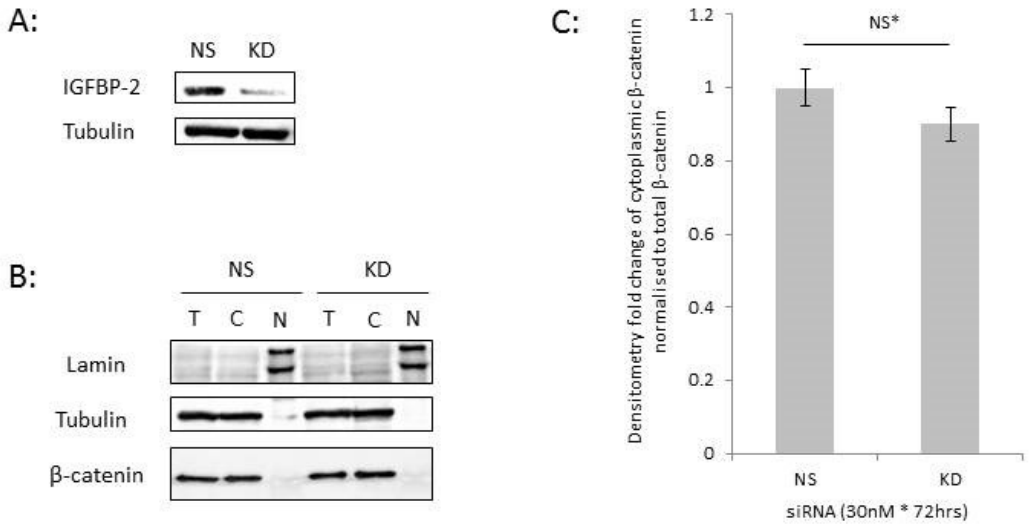

Figure 28: effects of silencing IGFBP-2 on the translocation of β-catenin in RT4 cells using cellular fractionation

RT4 cells were transfected with either scrambled or IGFBP-2 siRNA ("NS" for non-silencing scrambled siRNA as control and "KD" for IGFBP-2 siRNA) at the concentration of 30nM for 72 hours to look into the change in the localisation of β-catenin using cellular fractionation. Separate proteins were obtained as mentioned above and loaded equally for protein detection using WB. IGFBP-2 proteins from whole lysates were assessed for the efficiency of IGFBP-2 knocking down. All blots demonstrate the typical results from three experiments each performed at least in triplicate (n=3).

(**A**): The blot shows the achievement of efficient IGFBP-2 silencing. (**B**): The blot show localisation of β-catenin in the presence or absence of siRNA to IGFBP-2 in RT4 cells using cellular fractionation. Lamin and Tubulin exist only in nuclei and cytoplasm, respectively, and they are an indicator of the efficiency of protein separation. "T": total cell lysates; "C": cytoplasmic extract; "N": nuclear extract. (**C**): The graph presents the fold change of cytoplasmic β-catenin normalised to total β-catenin in the total cell lysates with error bars representing the standard error of the mean of experiments (n=3). "NS*": not significant.

To complement cellular fractionation, IF was also performed to examine any nuclear translocation in RT4 cells with IGFBP-2 siRNA transfection. With efficient gene knockdown of IGFBP-2 (Figure 29-**A**), an obvious translocalization of β-catenin from the cytoplasm into the nuclei was observed with RT4 cells as shown in Figure 29-**B**.

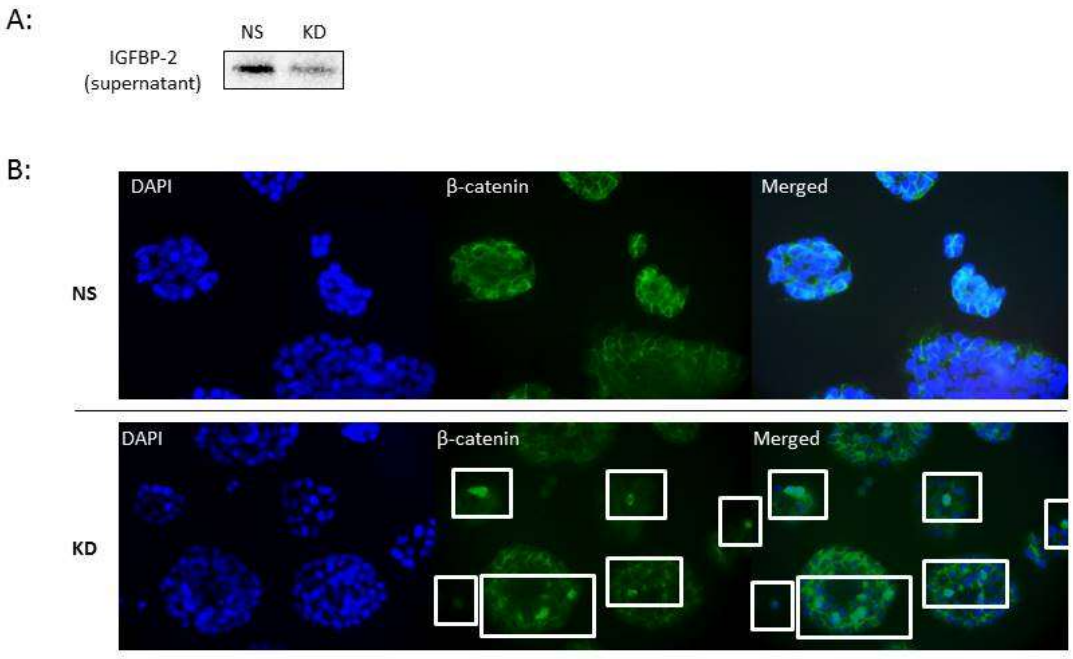

Figure 29: effects of silencing IGFBP-2 on the translocation of β-catenin in RT4 cells using IF

RT4 cells were transfected with either scrambled or IGFBP-2 siRNA ("NS" for non-silencing scrambled siRNA as control and "KD" for IGFBP-2 siRNA) at the concentration of 30nM for 72 hours to assess changes in the localisation of β-catenin using IF. The supernatant was collected before samples were washed with PBS to examine the efficiency of IGFBP-2 silencing by using WB analysis. All images and the blot demonstrate the typical results from three experiments each performed in duplicate (n=3).

(**A**): The blot shows the achievement of efficient IGFBP-2 silencing. (**B**) Images demonstrate the detection of translocation of β-catenin in RT4 cells using IF. Images show β-catenin (in green) with counterstaining for DAPI (nuclei in blue) and overlaid version labelled as "Merged". All images shown are at x10 magnification.

3.4.4 Exogenous IGFBP-2 treatment

With undetectable levels of IGFBP-2, T24 cells were used as the predominant cell line to investigate the relationship between IGFBP-2 and bladder cancer of a mesenchymal phenotype by treating cells with exogenous recombinant human IGFBP-2. Alterations in cell proliferation, invasion, migration, colony formation, as well as EMT-related molecules compared with untreated cells were assessed.

Another mesenchymal bladder cancer cell line, TCCSUP, was also used in the study with similar exogenous IGFBP-2 treatment, and the results of cells phenotypic changes were presented along with those of the T24 cells.

3.4.4.1 Optimisation of effective dose of exogenous IGFBP-2

TTI assay was used in T24 and TCCSUP cells to assess cell proliferation following the exogenous addition of IGFBP-2 (0-600ng/ml) for 24 hours.

As shown in Figure 30, both cell lines showed a decrease in cell proliferation with increasing concentrations of IGFBP-2: the maximal decreases were found to be at 600ng/ml (by 57% in T24 cells, $p<0.01$; by 59% in TCCSUP cells, $p<0.01$). Therefore, this dose was chosen as an effective concentration for further experiments.

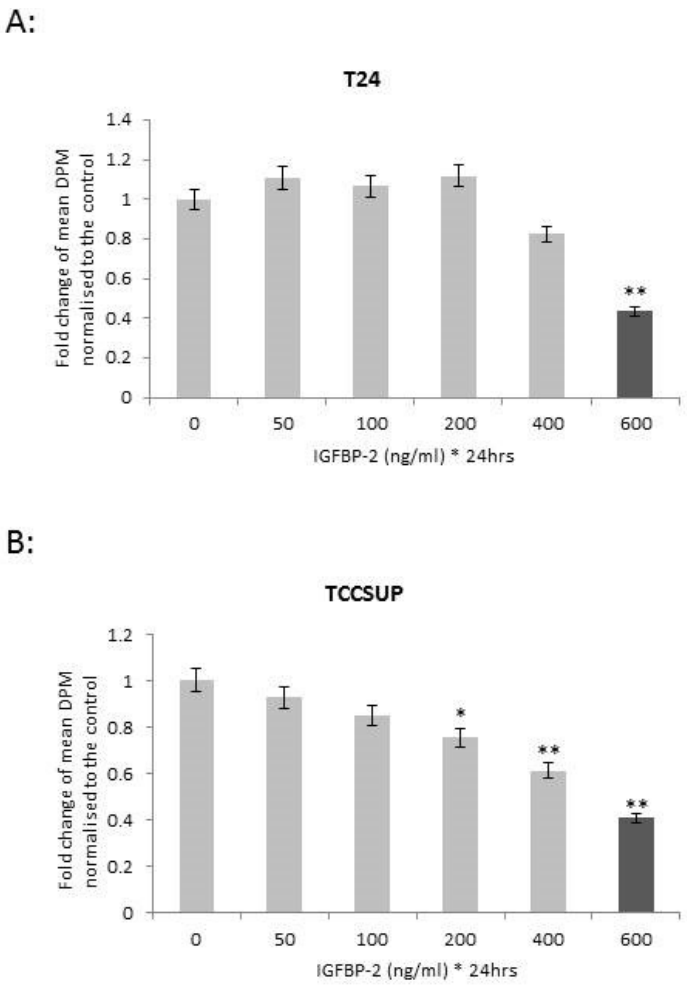

Figure 30: proliferative response to exogenous IGFBP-2 in T24 and TCCSUP bladder cancer cells

Both cells were seeded at a density of $0.02x10^6$ cells/well into 24-well plates in GM to grow for 24 hours followed by serum starvation for another 24 hours. Then TTI was performed to show the proliferative response to exogenous IGFBP-2 in T24 (**A**) and TCCSUP (**B**) cells at 0-600 ng/ml for 24 hours. The graphs represent the mean of three experiments each performed in quadruplicate, and error bars represent the standard error of the mean of the experiments (n=3). "*": $p<0.05$; "**": $p<0.01$. The bars in the darker colour represent the chosen effective concentrations for further experiments.

3.4.4.2 Effect of adding exogenous IGFBP-2 on cell growth in T24 and TCCSUP cells

Based on the effective dose of IGFBP-2 determined in 3.4.4.1, exogenous IGFBP-2 treatment experiments were conducted in both T24 and TCCSUP cells at the concentration of 600ng/ml for 48 hours, and cell growth was assessed by performing cell counting.

Significant decreases in both total and live cell numbers were observed in both cell lines. As to T24 cells, compared with the control group, cells treated with IGFBP-2 showed a 25.8% decrease in total cell number ($p<0.001$) and a 25.9% reduction in live cell number ($p<0.001$) (Figure 31-**A**). Similarly, a 20.2% decrease in total cell number ($p<0.001$) and in live cell number by 21.1% ($p<0.005$) was detected in IGFBP-2 treated TCCSUP cells compared with the untreated cells (Figure 31-**C**).In both experiments using T24 or TCCSUP cells, no significant change in cell death between the control and IGFBP-2 treated groups was observed (Figure 31-**B** & **D**).

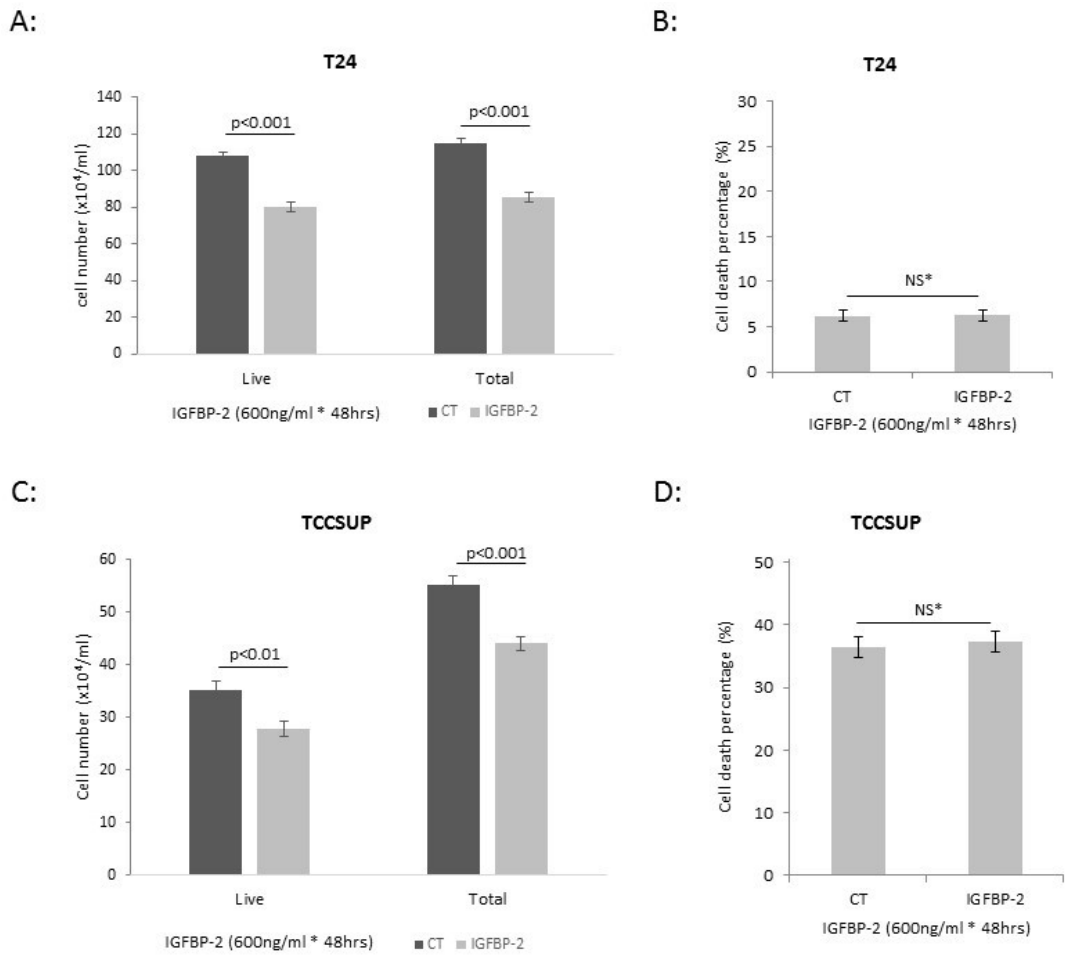

Figure 31: effect of dosing exogenous IGFBP-2 on cell growth in T24 and TCCSUP cells

Both T24 and TCCSUP cells were seeded into 6-well plates in GM at a density of $0.05x10^6$ cells/well. After 24 hours of serum starvation, cells were labelled according to different treatments ("CT" for control group without any treatment and "IGFBP-2" for IGFBP-2 treated cells at a concentration of 600ng/ml for 48 hours).

(**A**) & (**C**): Graphs show the cell counting of both live and total cell numbers under different treatments in T24 and TCCSUP cells, respectively. (**B**) & (**D**): Graphs represent the change in the percentage of cell death due to different treatments in T24 and TCCSUP, respectively. The graphs present the mean of three experiments each performed at least in triplicate, and error bars represent the standard error of the mean of the experiments (n=3). "NS*": not significant.

3.4.4.3 Effect of adding exogenous IGFBP-2 on cell invasion in T24 and TCCSUP cells

Invasion assays were performed to study the effect of exogenous IGFBP-2 on the invasive ability of T24 and TCCSUP cells.

Compared to untreated cells, cells treated with exogenous IGFBP-2 in both cell lines exhibited a decrease in the numbers of invaded cells (Figure 32-**A** for T24 and Figure 32-**C** for TCCSUP cells), and the reduction was significant in both T24 (by 55% in Figure 32-**B**) and TCCSUP (by 41% in Figure 32-**D**) cells.

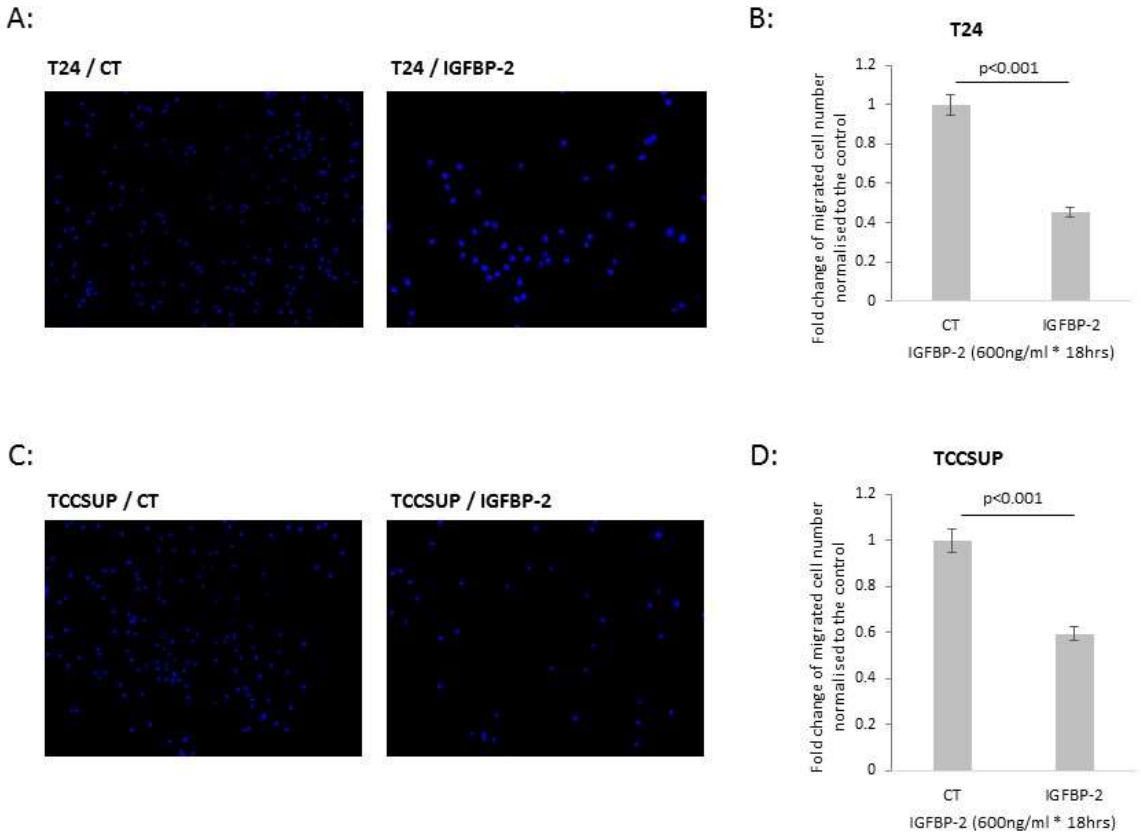

Figure 32: effect of adding exogenous IGFBP-2 on cell invasion of T24 and TCCSUP cells

Cells of both cell lines were previously seeded in GM for 24 hours and then changed to SFM for 16 hours before being prepared for an invasion assay. After serum-starvation, both T24 and TCCSUP cells were seeded into the collagen-coated inserts at a density of 0.08×10^6 cells/insert and allowed to migrate for 18 hours. Cells were labelled according to different treatments while seeding ("CT" for control cells without treatment, and "IGFBP-2" for cells treated with IGFBP-2 at the concentration of 600ng/ml).

(**A**) & (**C**): The images show migrated T24 and TCCSUP cells, respectively, with nuclei (in blue) stained with DAPI. All images shown are at x10 magnification. (**B**) & (**D**) The graphs show the fold change of invaded T24 and TCCSUP cells, respectively, between exogenous IGFBP-2 treatment group and control group. The graphs represent the mean of three experiments each performed in triplicate, up which the standard error of the mean of the experiments was presented (n=3).

3.4.4.4 Effect of adding exogenous IGFBP-2 on cell migration in T24 and TCCSUP cells

Characterization of basal cell migration of T24 and TCCSUP cells was performed as described in section 2.9. As shown in Figure 33, both T24 and TCCSUP cells migrated toward the centre of the gap area after the inserts were removed. Migration was observed in T24 cells after the removal of inserts, and the gap had been closed after about 9 hours. 0nly a few TCCSUP cells were detected with morphological movement at the same time.

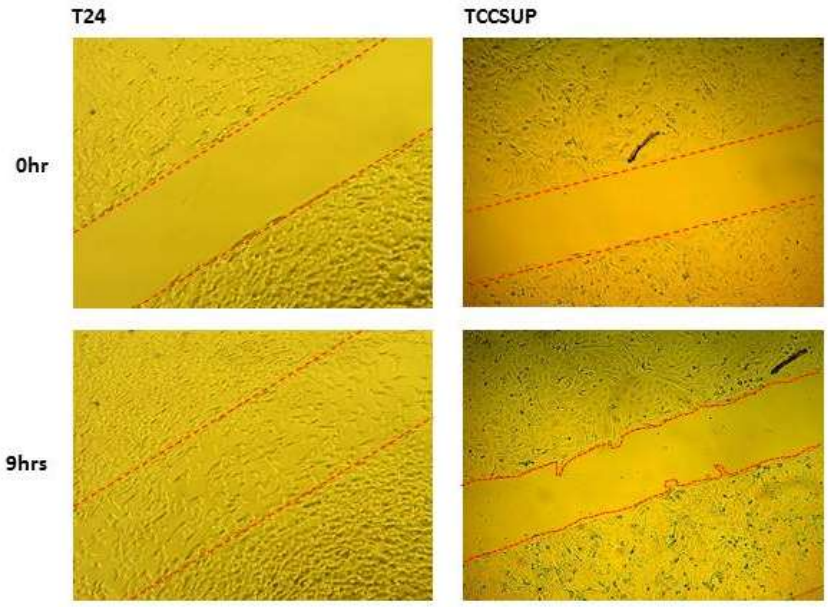

Figure 33: characterisation of the migrating ability of T24 and TCCSUP cells

Cells were seeded at a certain density ($0.028x10^6$ cells for T24 and $0.048x10^6$ cells for TCCSUP) into each chamber in GM and allowed to grow for approximately 24 hours to reach about 80% confluence. And then cells were allowed to reach 90-95% confluence during another 24 hours of serum starvation in SFM. Then cell migration was observed for up to 12 hours with the inserts removed. "0hr": the start point after the removal of inserts; "9hrs": 9 hours after the removal of inserts. All images demonstrate the typical results from three experiments each performed in duplicate (n=3). All images shown are at x10 magnification.

T24 cells migrated as a sheet, and cells treated with exogenous IGFBP-2 moved more slowly than the control group with the relative gap area showing a significant difference at the sixth ($p<0.001$), ninth ($p<0.01$) and twelfth ($p<0.001$) hour (Figure 34-**A** & **B**).

Although TCCSUP cells showed migration in individual cells only (Figure 34-**C**), a reduction in cell migration was still evident following exogenous IGFBP-2 treatment compared with the control group ($p<0.001$ at the third and ninth hour, and $p<0.01$ at the sixth and twelfth hour) (Figure 34-**D**).

A:

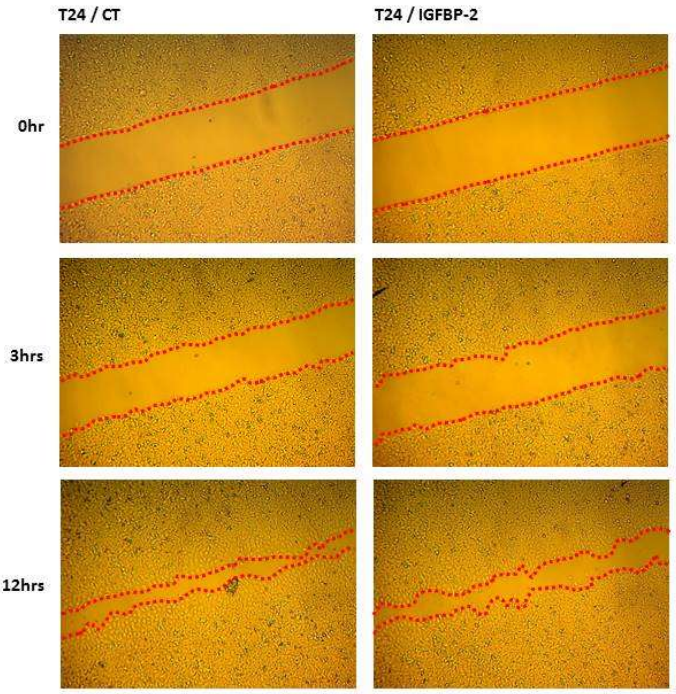

B:

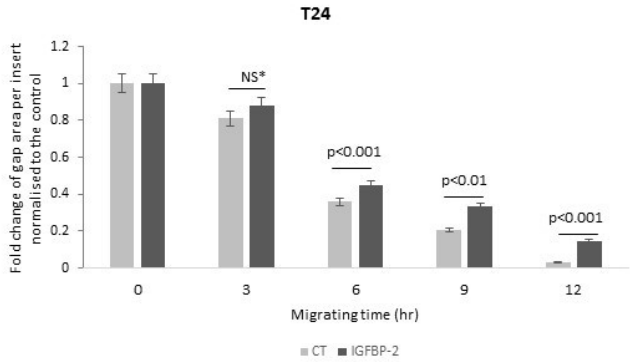

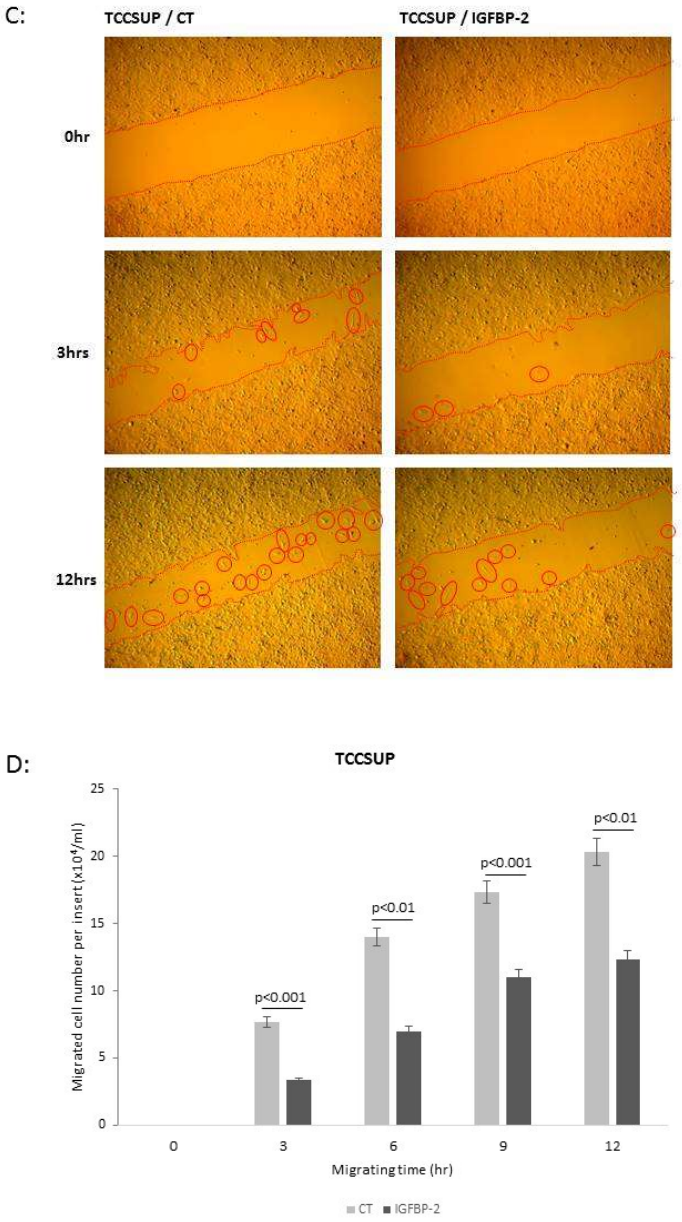

Figure 34: effect of adding exogenous IGFBP-2 on cell migration in T24 and TCCSUP cells

Cells were seeded at a certain density ($0.028x10^6$ cells for T24 and $0.048x10^6$ cells for TCCSUP) into relative chambers in GM and allowed to grow for approximately 24 hours to reach about 80% confluence. And then cells were allowed to reach 90-95% confluence during another 24 hours in SFM. Then the inserts were removed leaving cell patches observed and gap closing process recorded for up to 12 hours with different treatment ("CT": untreated cells as a control group; "IGFBP-2": cells treated with IGFBP-2 at the concentration of 600ng/ml). Images of cell gaps were taken at several times with relative labels. "0hr": the start point after the removal of inserts; "3hrs": 3 hours after the removal of inserts; "12hrs": 12 hours after the removal of inserts. All images demonstrate the typical results from three experiments each performed in duplicate (n=3). All images shown are at x10 magnification, and the area of the gaps in the images was analysed using ImageJ software.

(**A**) & (**C**) show the images of the gaps between cell patches of T24 and TCCSUP, respectively, with different treatments at the start point ("0hr"), 3 hours ("3hrs"), and 12 hours ("12hrs") after the removal of inserts. The red dashed lines in (**A**) present the outline of migrating T24 cells moving together, and the red circles in (**C**) show individual migrated TCCSUP cells. Accordingly, the graph in (**B**) shows the fold change of gap area per insert normalised to control with exogenous IGFBP-2 treatment in T24 cells, and the graph in (**D**) shows the number of migrated cells per insert (x10^4 cells/ml) in TCCSUP cells. The graphs represent the mean of three experiments each performed in duplicate, with the standard error of the mean of the experiments (n=3). "NS*": not significant.

3.4.4.5 Effect of adding exogenous IGFBP-2 on cell colony formation in T24 and TCCSUP cells

A soft agar colony formation assay was used as described in section 2.8 to assess the effect of exogenous IGFBP-2 on the ability of T24 and TCCSUP cell lines to form colonies in soft agar.

Visually, compared with untreated cells in control groups, both T24 (Figure 35-**A**) and TCCSUP (Figure 35-**D**) cells formed less and smaller colonies with exogenous IGFBP-2 treatment. Significant decreases both in colony forming efficiency (CFE) and in the average size of each colony were found in the two cell lines. Regarding CFE, a reduction of 78.8% ($p<0.001$) (Figure 35-**B**) and of 87.6% ($p<0.001$) (Figure 35-**E**) was found in IGFBP-2 treated T24 and TCCSUP cells, respectively. Similarly, the fold change of average size of each colony in IGFBP-2 treated T24 and TCCSUP cells were 0.60 ($p<0.001$) (Figure 35-**C**) and 0.57 ($p<0.01$) (Figure 35-**F**) of untreated cells, respectively.

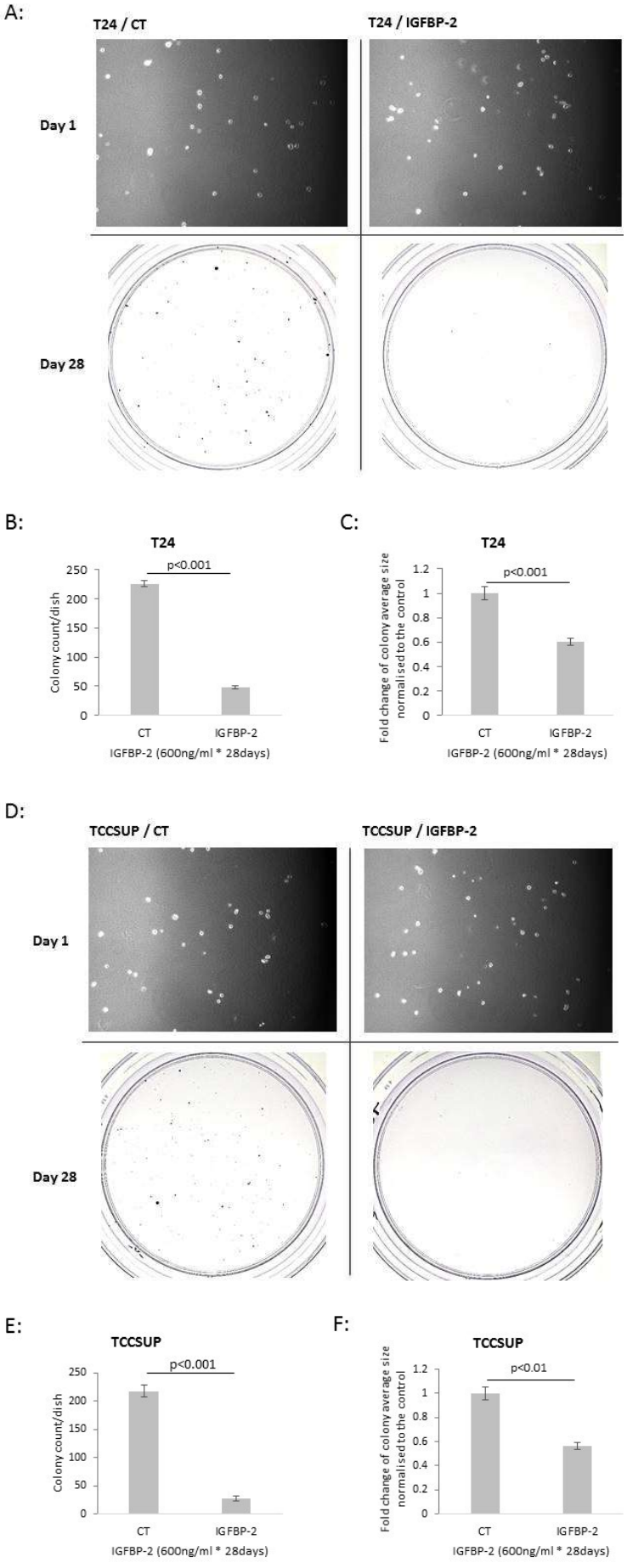
A:
T24 / CT
T24 / IGFBP-2
Day 1
Day 28
B:
T24
p<0.001
Colony count/dish
250
200
150
100
50
0
CT
IGFBP-2
IGFBP-2 (600ng/ml * 28days)
C:
T24
p<0.001
Fold change of colony average size normalised to the control
1.2
1
0.8
0.6
0.4
0.2
0
CT
IGFBP-2
IGFBP-2 (600ng/ml * 28days)
D:
TCCSUP / CT
TCCSUP / IGFBP-2
Day 1
Day 28
E:
TCCSUP
p<0.001
Colony count/dish
250
200
150
100
50
0
CT
IGFBP-2
IGFBP-2 (600ng/ml * 28days)
F:
TCCSUP
p<0.01
Fold change of colony average size normalised to the control
1.2
1
0.8
0.6
0.4
0.2
0
CT
IGFBP-2
IGFBP-2 (600ng/ml * 28days)

Figure 35: effect of adding exogenous IGFBP-2 on formation of colonies by T24 and TCCSUP cells in soft agar

Both T24 and TCCSUP cells were seeded in dishes under different treatments with corresponding labels ("CT": untreated cells as a control group; "IGFBP-2": cells treated with IGFBP-2 at the concentration of 600ng/ml 48 hours prior to seeding). All cells were seeded with an even density at 5,000cell/dish and fed once a week for four weeks in total, and then colony numbers, as well as average size, were measured by ImageJ software.

(**A**) & (**D**): Images show T24 and TCCSUP cells, respectively, were set up into dishes with even densities at the first day ("Day 1"), and colonies were stained at the end of the assay ("Day 28"); All images shown are at x10 magnification; (**B**) & (**E**): Graphs present the change of colony count per dish under different treatments for T24 and TCCSUP cells, respectively. (**C**) & (**F**): Graphs demonstrate the fold change of average size of colonies due to different treatments for T24 and TCCSUP cells, respectively. All graphs present the mean of three experiments each performed in triplicate, and error bars represent the standard error of the mean from three experiments (n=3).

3.4.4.6 Effect of adding exogenous IGFBP-2 on EMT markers in T24 cells

As for characterisation of basal levels of EMT markers shown in

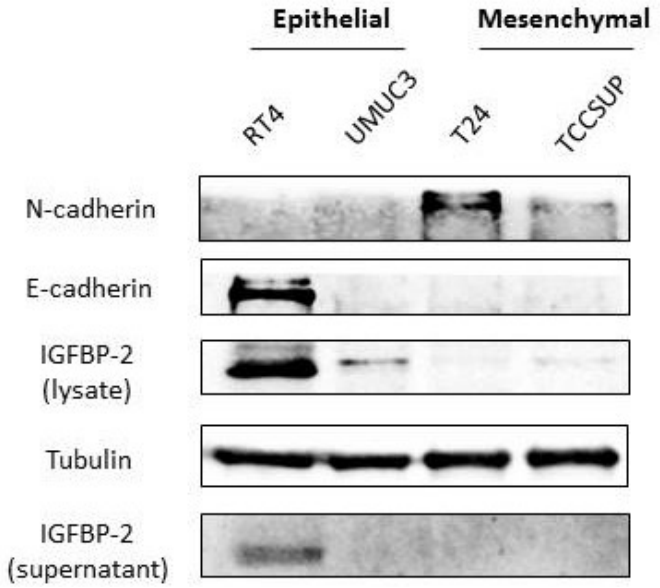

Figure 19, T24 cells expressed abundant N-cadherin and β-catenin with undetectable levels of E-cadherin (which is an epithelial marker). When treated with exogenous IGFBP-2 at 600ng/ml for 48 hours, compared with control samples, a reduction of 59% ($p<0.05$) in the abundance of N-cadherin was observed with no detectable induction of E-cadherin (see Figure 36-**A** &

B). And, again, no visible or statistically significant change in the abundance of β-catenin was noted (Figure 36-**C** & **D**).

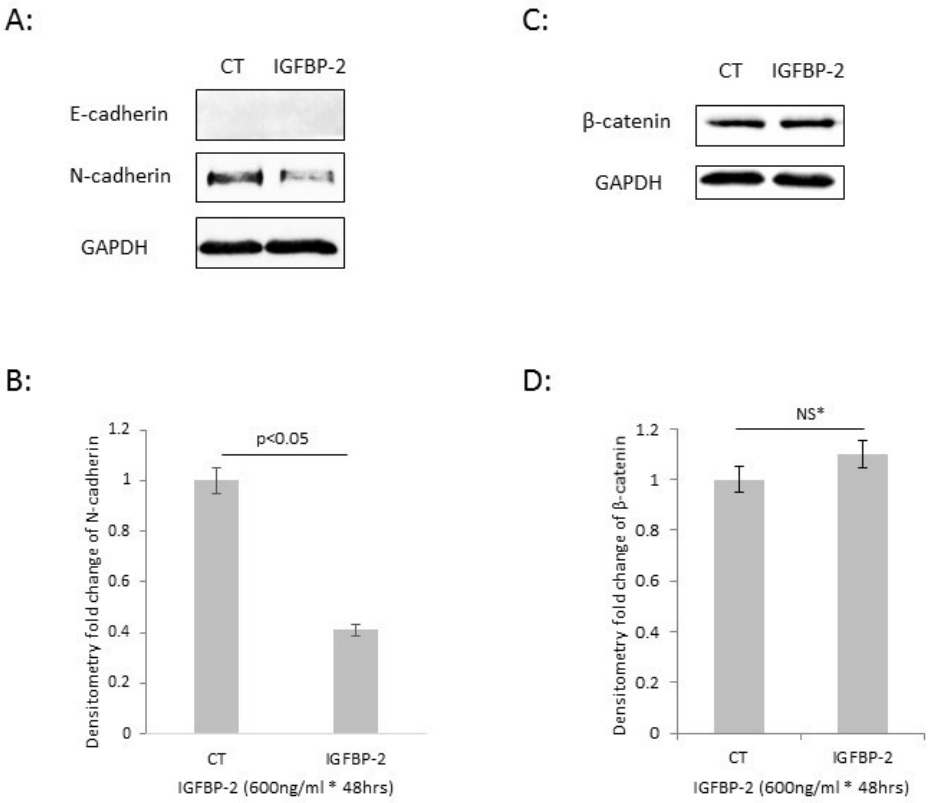

Figure 36: effect of adding exogenous IGFBP-2 on EMT markers in T24 cells

T24 cells were seeded in 6-well plates at a density of $0.05x10^6$ cells/well in GM for 24 hours and serum-starved with SFM for another 24 hours. Then cells were separated according to different treatments ("CT": untreated cells as a control group; "IGFBP-2": cells treated with IGFBP-2 at the concentration of 600ng/ml for 48 hours). After 48 hours of treatment, cells were harvested to investigate changes in protein abundance using WB analysis. Samples from whole lysates were loaded equally at 60µg for protein detection, and GAPDH was assessed as reference protein in WB analysis.

The blots show levels of E- and N-cadherin (**A**) and β-catenin (**C**) under different treatments. And the graphs (**B**) and (**D**) demonstrate the mean of fold change of the optical density of N-cadherin and β-catenin, respectively, from three experiments each performed at least in triplicate, and error bars represent the standard error of the mean of experiments (n=3). "NS*": not significant.

3.4.5 Relationship between IGFBP-2 and chemosensitivity

To look into the effect of IGFBP-2 on chemo-sensitivity of bladder cancer cells to cisplatin, two cell lines were used including IGFBP-2-abundant RT4 cells and IGFBP-2-absent T24 cells.

TTI assay was used to assess a dose response to cisplatin in RT4 and T24 cells regarding proliferation and cell counting was performed to examine changes in cell death.

As shown in Figure 37-**A**, both RT4 and T24 cells showed a significant decrease in cell proliferation with increasing concentrations of cisplatin. A reduction to about half of the control cells (dosage at 0μg/ml) was achieved in both cell lines at 5μg/ml ($p<0.001$ for both cell lines): this concentration was chosen for further experiments in this study.

Compared with the response in T24 cells, RT4 cells presented a sharper decrease in the fold change of cell proliferation with a relatively lower concentration of cisplatin treatment (1, 2.5μg/ml); however, the statistics showed no significant difference between the two cell lines at any dose of cisplatin.

The images (Figure 37-**B**) taken at the end of the TTI experiments showed that RT4 cells started to lose cell structure and detached from the surface of the culture vessels when treated with cisplatin, and more detached cells were observed as the concentration of cisplatin increased from 1μg/ml. Compared

with RT4 cells, T24 cells were more robust and presented less floating cells which only started to increase when the dose of cisplatin reached 5µg/ml.

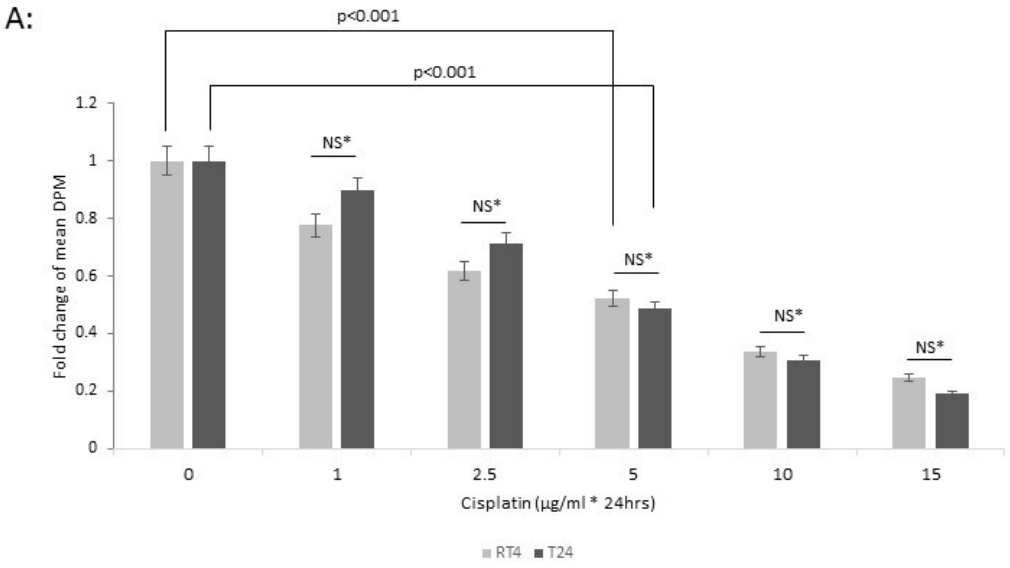

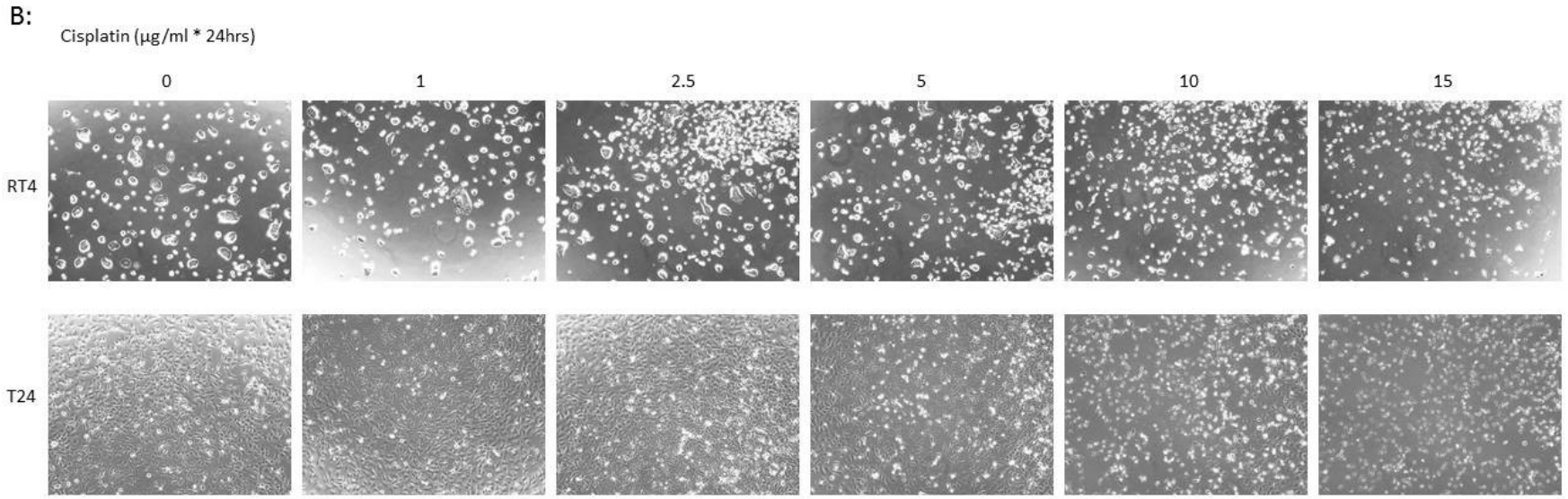

Figure 37: dose response to cisplatin in RT4 and T24 bladder cancer cells

Cells were seeded ($0.03x10^6$ cells/well for RT4, and $0.02x10^6$ cells/well for T24) into 24-well plates and TTI was performed to assess the dose response to cisplatin in both cell lines at the concentration of 0/1/2.5/5/10/15 µg/ml for 24 hours.

(**A**) The graph shows the mean of three experiments each performed in triplicate, and error bars represent the standard error of the mean from three experiments (n=3). "NS*": not significant. (**B**) Images were taken at the end point (24 hours) of the same TTI experiments representing the typical change of cells in response to Cisplatin treatment. All images shown are at x10 magnification.

To further investigate the sensitivity of both cell lines to cisplatin treatment, cell counting was performed after cells were treated with cisplatin at 5μg/ml for 24 hours or 48 hours.

As shown in Figure 38-**A**, with 24 hours treatment with cisplatin, there was a 1.8 ($p<0.001$) fold increase in the percentage cell death in RT4 cells compared with the control group, and a 1.2 fold increase in percentage cell death in T24 cells. With 48 hours of treatment shown in Figure 38-**B**, both cell lines demonstrated a greater fold increase in the sensitivity to cisplatin: compared to control group RT4 showed a 4.3 fold ($p<0.001$) higher percentage cell death than that of T24 cells being 3.1 fold higher ($p<0.001$).

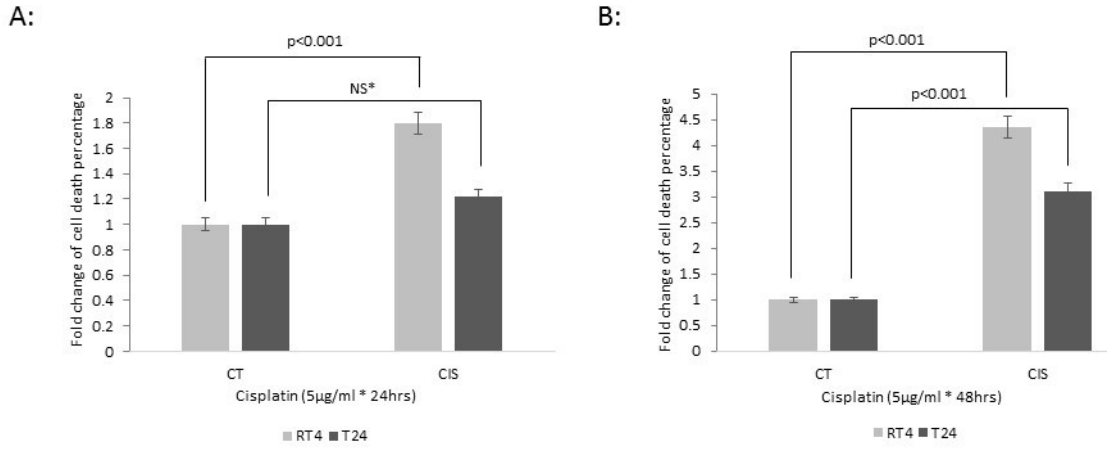

Figure 38: effect of Cisplatin on cell death in RT4 and T24 cells

Both RT4 and T24 cells were seeded into 6-well plates in GM at a density of $0.1x10^6$ cells/well and $0.05x10^6$ cells/well, respectively, to grow for 24 hours. After 24 hours of serum starvation, cells were labelled according to different treatments. "CT": control group without any treatment; "CIS": Cisplatin treated cells at a concentration of 5μg/ml for 24 (**A**) or 48 hours (**B**).

Graphs represent the fold change in the percentage of cell death due to cisplatin treatment in both RT4 and T24 cells for 24 and 48 hours, respectively. The graphs present the mean of three experiments each performed at least in triplicate, and error bars represent the standard error of the mean of the experiments (n=3). "NS*": not significant.

3.4.5.1 Effect of cisplatin treatment on cell death in RT4 cells following silencing of IGFBP-2

With IGFBP-2 abundant RT4 cells, treatment of cisplatin was combined with specific IGFBP-2 siRNA transfection to look into the effect of IGFBP-2 on cell chemosensitivity to cisplatin.

With efficient IGFBP-2 knockdown achieved (Figure 39-**A**), no significant change was observed between control cells with either scrambled siRNA ("NS") or IGFBP-2 siRNA ("KD") transfection only. In comparison, a subtle but significant alteration was shown between cells which were treated with cisplatin following siRNA transfection. Cells treated with cisplatin after IGFBP-2 siRNA transfection ("KD+CIS") demonstrated a smaller fold change of cell death percentage (3.2) compared with those after scrambled siRNA ("NS+CIS") (3.4) ($p<0.01$) (Figure 39-**B**).

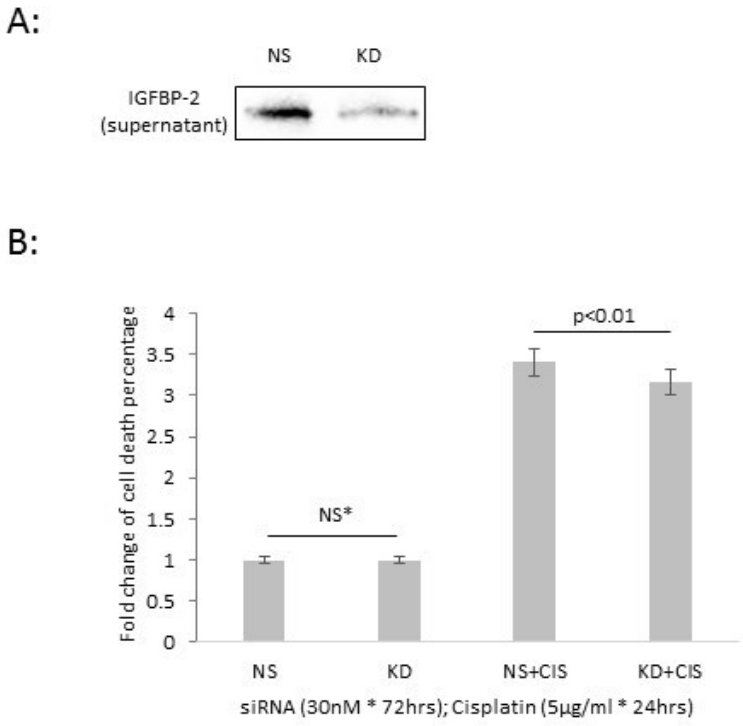

Figure 39: effect of silencing IGFBP-2 on response to cisplatin in RT4 cells

Cells were seeded into 6-well plates in GM at a density of $0.1x10^6$ cells/well to grow for 24 hours and were serum starved with SFM for another 24 hours. Then, after 72 hours of siRNA ("NS" for non-silencing scrambled siRNA as control and "KD" for IGFBP-2 siRNA) transfection, cisplatin ("CIS") was added to cells at 5µg/ml for another 24 hours. Cell death was determined by performing cell counting. The supernatant was taken before cisplatin treatment for the detection of the efficiency of IGFBP-2 silencing.

(**A**): The blot shows the efficiency of IGFBP-2 knockdown achieved by detecting IGFBP-2 in samples loaded equally at 25µl. (**B**): The graph shows the fold change of in percentage cell death due to different treatments in RT4 cells. "NS": cell group treated with non-silencing scrambled siRNA only as control; "KD": cell group treated with IGFBP-2 siRNA only; "NS+CIS": cell group treated with non-silencing scrambled siRNA transfection followed by another 24 hours of cisplatin dosing; "KD+CIS": cell group treated with IGFBP-2 siRNA transfection followed by another 24 hours of cisplatin dosing. The graph presents the mean of three experiments each performed in triplicate, and error bars represent the standard error of the mean of three experiments (n=3). "NS*": not significant.

3.4.5.2 Effect of adding exogenous IGFBP-2 on cell death in T24 cells in response to cisplatin treatment

Exogenous IGFBP-2 was applied to IGFBP-2 absent T24 cells to further investigate the effect of IGFBP-2 on cell chemosensitivity to cisplatin treatment.

As we can see in Figure 40, regarding fold change of percentage cell death, no significant difference was observed in IGFBP-2-alone-treated cells ("BP-2") compared with untreated control cells ("CT"). In comparison, when cells were treated with cisplatin, those with additional IGFBP-2 treatment ("BP-2 + CIS") presented more cell death (fold change being 3.0) compared with control than cells which were treated with cisplatin alone ("CIS") (fold change being 2.1) ($p<0.01$).

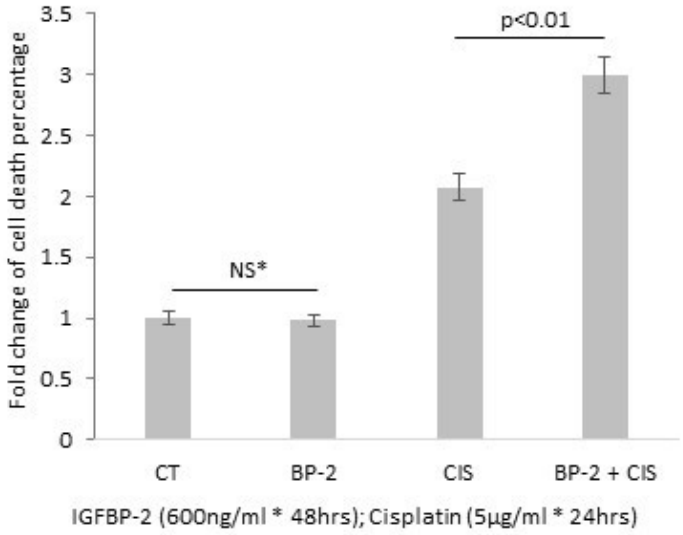

Figure 40: effect of adding exogenous IGFBP-2 response of T24 cells to cisplatin

Cells were seeded in 6-well plates in GM at a density of $0.05x10^6$ cells/well to grow for 24 hours and were serum starved with SFM for another 24 hours. Then, cisplatin ("CIS") was added to cells at 5µg/ml for another 24 hours of incubation with or without previous treatments of exogenous IGFBP-2 ("BP-2") for 24 hours at 600ng/ml. And then cell death was determined by performing cell counting. The graph represents the mean of three experiments each performed in triplicate, and error bars represent the standard error of the mean from three experiments (n=3). "NS*": not significant.

"CT": control group; "BP-2": cell group with only 48 hours of IGFBP-2 treatment; "CIS": cell group with only 24 hours of Cisplatin treatment; "BP-2 + CIS": cell group with previous 24 hours of IGFBP-2 treatment alone and then another 24 hours of combination of IGFBP-2 and cisplatin treatment.

3.5 Discussion

Three bladder cancer cell lines with the opposite phenotypes presenting distinct difference in the levels of IGFBP-2 were used in this study to examine the role that IGFBP-2 plays in bladder cancer progression. The epithelial-like RT4 cells express abundant IGFBP-2, while the mesenchymal-like T24 and TCCSUP cell lines possess little, which was found of the same pattern in Glioblastoma multiforme (GBM) (Shelton, Mukherjee et al. 2010).

Two distinct ways were used to manipulate the levels of IGFBP-2 in specific bladder cancer cell lines. In IGFBP-2 abundant epithelial-like RT4 cells, the levels of IGFBP-2 were reduced significantly by using specific IGFBP-2 siRNA. In contrast with mesenchymal-like T24 and TCCSUP cell lines that had negligible IGFBP-2 with, we added exogenous recombinant human IGFBP-2. Following manipulation of IGFBP-2 levels in these cell lines we assessed any phenotypic changes that occurred.

With IGFBP-2 knockdown in RT4 cells, a significant increase both in live and total cell number was observed with no difference in cell death. In contrast, by adding exogenous IGFBP-2, both live and total cell numbers were decreased significantly in T24 and TCCSUP cells, with again no significant changes in cell death. We observed that epithelial-like RT4 cells grow more slowly than mesenchymal-like T24 and TCCSUP cells and this has also been reported in the literature (Vallo, Michaelis et al. 2015). These data suggest that IGFBP-2 acts to inhibit cell proliferation in bladder cancer. Similar anti-proliferative effects

were reported in a human breast cancer cell line, Hs578T, by using an ELISA-based and a flow cytometry-based apoptosis assay (Frommer, Reichenmiller et al. 2006) and in human embryonic kidney fibroblasts by using an MTT assay (Hoflich, Lahm et al. 1998). Whereas the opposite results have also been reported in some cancers such as breast cancer of different cell lines, MCF7 and T47D, demonstrating the proliferative role of IGFBP-2 by using Trypan blue cell counting and Tritiated thymidine incorporation (TTI) assay (Foulstone, Zeng et al. 2013).

With invasion, silencing IGFBP-2 in RT4 cells led to a substantial increase in the numbers of invading cells. The exogenous addition of IGFBP-2 to T24 and TCCSUP cells resulted in a significant reduction in the number of invaded cells, which suggested IGFBP-2 might also act in an inhibitory way in the process of cell invasion in bladder cancer. Similarly, a reduction of IGFBP-2 was correlated with the promotion of epithelial invasion in the progression of cervical cancer (Adam Pickard 2015), and loss of IGFBP-2 was also found at the invasive front of glioblastoma with high grade suggesting its association with enhanced invasive potential (Hoelzinger, Mariani et al. 2005). However, another study in bladder cancer showed that over-expression of IGFBP-2 enhanced the invasive potential by generating an IGFBP-2 overexpressing cell subline, KoTCC/BP2, using cDNA transfection (Miyake, Hara et al. 2005).

Regarding cell migration, epithelial-like RT4 cells showed no migration either basally or with IGFBP-2 silenced. In contrast, mesenchymal bladder cancer cell lines were able to migrate basally and with different patterns. T24 cells migrated as a sheet that was significantly slowed down with the exogenous

addition of IGFBP-2. TCCSUP cells migrated individually, and the number of migrating cells was similarly reduced when dosed with IGFBP-2. In contrast to our work showing that exogenous addition of IGFBP-2 inhibited cell migration, inhibition of IGFBP-2 in some cancers such as glioma (Patil, Railkar et al. 2015) and leukaemia (Chen, Zheng et al. 2013)was reported to reduce cell migration.

Malignant transformation was investigated using a soft agar colony formation assay: the average colony counts formed per dish, and the average size of each colony were two quantitative read-outs from this assay reflected cell renewal and to measure the differences in cellular tumourigenicity in different contexts (Horibata, Vo et al. 2015). Considerable increases in both factors were observed in RT4 cells when IGFBP-2 was knocked down, and significant decreases were found in both T24 and TCCSUP cells with additional IGFBP-2. These data suggested that IGFBP-2 was playing a role in inhibiting malignant transformation in bladder cancer. In contrast, with certain human leukaemias inhibition of IGFBP-2 resulted in a reduction in cell colony formation activity in the mouse model (Chen, Zheng et al. 2013).

A number of changes occur in specific markers during EMT: for example, a reduction in the levels of E-cadherin, an increase in the abundance of N-cadherin as well as β-catenin nuclear translocation. With RT4 cells, the levels of E-cadherin were significantly reduced when IGFBP-2 was efficiently silenced. And compared with cellular fractionation, IF showed higher sensitivity presenting the detection of the β-catenin in the nuclei in IGFBP-2 silenced RT4 cells. Due to the marked difference between the results by these two techniques, more work would be required to be sure about the effects on

β-catenin localisation. Changes in RT4 cells indicated that silencing IGFBP-2 promoted a more EMT-like phenotype. While in mesenchymal-like T24 cells, adding exogenous IGFBP-2 led to a significant reduction of N-cadherin expression suggesting inhibition of EMT. These data indicate that the presence of IGFBP-2 may suppress EMT in bladder cancer. Again, different conclusions about the role of IGFBP-2 have been drawn in other types of cancers such as pancreatic ductal adenocarcinoma (PDAC), where IGFBP-2 promoted EMT: downregulation of N-cadherin and upregulation of E-cadherin followed knockdown of IGFBP-2 (Gao, Sun et al. 2016).

I also investigated the chemo-sensitivity of bladder cancer cells to cisplatin using epithelial-like RT4 and mesenchymal-like T24 cells representing cancer types with less and more aggressiveness, respectively. Even though there were no differences in the levels of DNA synthesis as shown in the TTI assay between these two cell lines in response to cisplatin treatment, cell images suggested that RT4 cells were more susceptible to death which was confirmed by examination of cell death using cell counting. The manner of RT4 cells growing into dense clusters might be the reason why detection of DNA synthesis was not as sensitive as the images or cell counting. Then I treated RT4 cells with cisplatin following IGFBP-2 gene silencing and observed less cell death than the control group, suggesting IGFBP-2 might act to enhance cell sensitivity to cisplatin, or reduce cell survival, with higher levels of IGFBP-2 indicating more sensitivity. To prove this hypothesis, I then conducted the experiments in T24 cells treated with exogenous IGFBP-2 and cisplatin, and the results showed that IGFBP-2 increased cisplatin-induced cell death in T24

cells, therefore, indicating the chemo-sensitivity of cancer to cisplatin was enhanced in the presence of IGFBP-2. However, another study in bladder cancer reported opposite results demonstrating increased levels of IGFBP-2 in a cisplatin-resistant subline (BIU87-CisR), with enhanced cell sensitivity to cisplatin resulted from the inhibition of IGFBP-2 by gene silencing (Zhu H 2015), which reflects the heterogeneity among cell lines.

In summary, in the present study, knocking down IGFBP-2 in IGFBP-2 abundant epithelial-like RT4 cells led to an increase in cell growth and promotion of cell invasion and colony formation, along with a reduction of E-cadherin and observation of β-catenin nuclear translocalization. And adding exogenous IGFBP-2 to mesenchymal-like T24 and TCCSUP cells with negligible basal IGFBP-2 resulted in decreased cell growth, invasion, migration, colony formation as well as the expression of N-cadherin. According to the results above, IGFBP-2 was considered to play an important inhibitory role in bladder cancer by inhibiting cell proliferation, invasion, migration, malignant transformation and EMT-related cancer progression. Also, IGFBP-2 may be used as an indicator of cell chemosensitivity to cisplatin in bladder cancer.

It is clear from my data and the literature that IGFBP-2 has the ability to act as a tumour promoter and tumour suppressor even in the same cancer. This can be the result of a number of different factors such as differences between cell types, culture conditions and in tumour stage, type and subtype. The most likely reason for these differences is the ability of IGFBP-2 to act in either an IGF-dependent or -independent manner, and each of these actions are context-dependent (Yau, Azar et al. 2015). Therefore, an understanding of the

mechanism by which IGFBP-2 is acting and the context in which this is occurring is key when comparing different studies. The IGF- dependency of my results is addressed in chapter 4.

Chapter 4- The Regulatory and Working Mechanisms of IGFBP-2

4.1 Introduction

Results of chapter 3 indicated that IGFBP-2 might act as an important inhibitor of a number of processes occurring during bladder cancer progression, including proliferation, invasion, migration, malignant transformation, and EMT development. Therefore, further studies were carried out to investigate how the levels of IGFBP-2 are regulated and by which means it plays an inhibitory role in these cell activities.

4.1.1 Regulation of the levels of IGFBP-2

IGFBP-2 is mainly expressed by tissues of the liver, adipose, reproductive and central nervous system (Shimasaki and Ling 1991) and the levels are influenced by various factors.

As a secreted protein, plasma IGFBP-2 levels are correlated with metabolic and dietary status including for example body fat and age. For instance, IGFBP-2 levels are inversely associated with the presence of obesity (Wheatcroft and Kearney 2009).

Compared with circulating plasma levels, local levels of IGFBP-2, which can be found in both epithelial and mesenchymal cancer cells, appear to provide a more accurate association with disease progression (Pickard and McCance 2015). And at the cellular level, levels of IGFBP-2 can be regulated in many different ways, including via epigenetic modifications such as gene

methylation (Yazawa, Sato et al. 2009), growth factors (Morrison, Liu et al. 2014) and by proteases (Berg, Bang et al. 2007).

4.1.2 DNA methylation of the *IGFBP-2* gene in cancer

Aberrant DNA methylation refers to a process by which methyl groups are added to DNA bases catalysed by methyltransferases (DNMT 1-3) (Dupont, Armant et al. 2009). Methylation modifies the genes, and potentially their expression, rather than introducing a change in the actual DNA sequence and hence is reversible (Dupont, Armant et al. 2009). It has mostly been studied due to its effects on transcriptional repression or even loss of gene function that has been widely reported in cancers (Chen and Wu 2016).

Methylation is characterised as the predominant modification in mammalian DNA (Dupont, Armant et al. 2009), and it happens exclusively at cytosine and guanine nucleotides with the intervening phosphate group (CpG) dinucleotides in mammals, with a methyl group added to carbon 5 of the cytosine (C) turning it into 5-methylcytosine (5mC). In the normal human genome, most (70-80%) cytosines within CpG dinucleotides are methylated, with unmethylated cytosines being located in specific GC-rich areas, named CpG islands (or CG islands, CGI) (Jabbari and Bernardi 2004). A CGI refers to a DNA patch of about 1,000 base pairs (bps), within which the CpG dinucleotide occupies a large percentage (about 65%) in base composition compared with the genome as a whole (about 40%) in humans (Suzuki and Bird 2008). CGIs are often associated with gene promoters, for instance, approximately 56% of human genes have CGI in their promoters (Suzuki and Bird 2008), and

aberrant hypermethylation in these promoters may lead to gene silencing by, for instance, preventing the binding of specific transcription factors to the gene (Dupont, Armant et al. 2009).

Due to the nature of reversibility of epigenetic modifications, the methylation can be inverted by DNMT inhibitors, such as 5-AZA-2,-deoxycytidine (5-AZA-dCyd, "AZA"). AZA can work as a demethylating agent removing the methyl groups from the CGIs of the DNA and therefore allows the re-expression of silenced genes (see Figure 41).

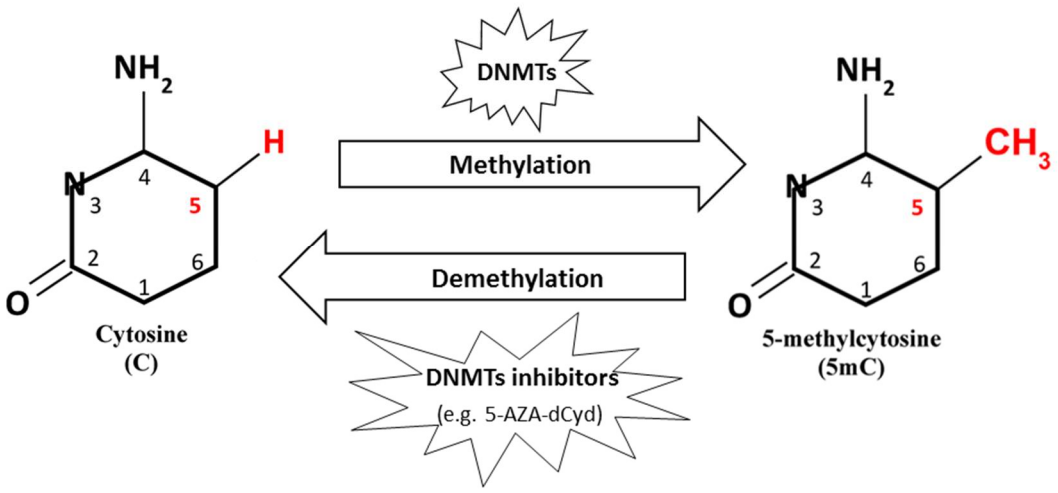

Figure 41: schematic diagram showing the methylation and demethylation of cytosine

Hypermethylation of the promoter region of *IGFBP-2* gene has been reported in several types of cancer including lung (Yazawa, Sato et al. 2009), breast (Liu, Liu et al. 2014, Nickel and Stadler 2015), colorectal (Simons, van den Brandt et al. 2014), and hepatomas (Chiba, Yokosuka et al. 2005). The rates even vary within a cancer with different histological types. For example, in lung cancer,

the *IGFBP-2* gene promoter was found to be methylated in 71% of adenocarcinomas and 29% of squamous cell carcinomas, with only 8% in small cell lung cancer (Yazawa, Sato et al. 2009).

4.1.3 The molecular working mechanism of IGFBP-2 in cancer

IGFBP-2 has been suggested to act in either an IGF-dependent or -independent manner.

IGFBP-2 acts in an IGF-dependent way by binding to IGFs operating as a carrier to either transport IGFs to their receptors triggering relevant signalling, or sequester them to prolong their bioactivity as well as to prevent their binding to the receptors (Yau, Azar et al. 2015). It has also been found to interact with certain components of the extracellular matrix (ECM)(Russo, Schutt et al. 2005) and cell surface proteoglycan receptors (Shen, Xi et al. 2012) offering a peri-cellular reservoir of bioactive IGFs.

The IGF-independent actions of IGFBP-2 refer to the intrinsic activities of it occurring without the presence of IGFs as ligands. IGFBP-2 has been suggested to influence tumorigenesis, by either binding to integrin receptors, including αVβ3 or α5β1, on the cell membrane activating intracellular signalling (Frommer, Reichenmiller et al. 2006, Perks, Vernon et al. 2007, Foulstone, Zeng et al. 2013), or translocating into the cell and entering the nucleus via distinct nuclear transportation complexes to affect the expression of some genes, such as VEGF (Miyako, Cobb et al. 2009, Azar, Azar et al. 2011, Azar, Zivkovic et al. 2014).

4.1.4 NBI-31772

NBI-31772 is a small non-peptide molecule (molecule weight: 341) which was identified almost two decades ago (Liu, Xie et al. 2001). With no biologic activity at the IGF receptors, it interacts with IGFBPs by competing specifically against IGF to bind all the six IGFBPs non-selectively with high affinity, and thus displaces free endogenous IGF-I and IGF-II from IGF:IGFBP complexes increasing the free levels of IGF-I and/or IGF-II (Liu, Xie et al. 2001). The freed IGF-I has been shown to be bioactive in both *in vivo* and *in vitro* studies (Mackay, Loddick et al. 2003, Choi, Gemberling et al. 2013); therefore, this molecule has been used as a nonspecific IGFBP inhibitor or IGF-potentiator enhancing IGF signalling.

Differences in the binding activity of NBI-31772 toward six IGFBPs were identified with the highest being to IGFBP-2 and IGFBP-4, and the lowest to IGFBP-6 (Liu, Xie et al. 2001).

4.2 Aims

To investigate the mechanism by which the level of IGFBP-2 is regulated and whether IGFBP-2 is working in an IGF-dependent or -independent manner to exert its effects on bladder cancer cells.

IGFBP-2-null, aggressive bladder cancer cell lines, T24 and TCCSUP, were treated with AZA, to assess whether the expression of IGFBP-2 is switched off by DNA hypermethylation.

- To determine the effect of AZA on the protein levels of IGFBP-2.
- To confirm DNA methylation status by performing Combined Bisulphite Restriction Assay (COBRA).
- To assess the associated phenotypic changes of bladder cancer cell lines in response to the treatment of AZA.

NBI-31772 was used to examine the working mechanism of IGFBP-2.

- To combine treatment of NBI-31772 with IGFBP-2 siRNA transfection in IGFBP-2-abundant epithelial-like RT4 cells.
- To combine treatment of NBI-31772 with exogenous recombinant IGFBP-2 and IGF-I in IGFBP-2-null mesenchymal-like T24 cells.

4.3 Materials and methods

4.3.1 Cell culture

Three human urinary bladder cancer cell lines including RT4 (an epithelial-like phenotype) and T24 as well as TCCSUP (mesenchymal-like phenotypes) were used in this study. They were obtained and cultured as described in section 2.1.

4.3.2 Cell treatments

4.3.2.1 AZA

0.5mg of AZA (Sigma, #A3656-50MG) were dissolved fresh in 0.5ml of sterile dH_2O to make a 4382µM stock solution. The stock solution was sterilised with a 0.2µm filter and then diluted with SFM to achieve a 500µM working stock. The working stock was then diluted further with SFM into different final concentrations for cell treatment.

4.3.2.2 NBI-31772

Protected from light during the whole process, NBI-31772 (Sigma; #N8289) was reconstituted at 100mM by re-suspending 34.1mg in 1ml sterile DMSO and then aliquoted and stored at -20°C. 1mM working stock was prepared fresh by mixing 10µl of the 100mM stock to 990 µl of SFM and then diluted further with SFM to reach a final concentration of 1µM. NBI-31772 was added to the cells 1 hour before other treatments. NBI-31772 is a non-peptide inhibitor of the binding of IGFs to all 6 IGFBPs (which have similar IGF-binding

sites) that was developed from screening chemical libraries and has no interactions with IGF receptors (Liu, Xie et al. 2001).

4.3.2.3 Recombinant human IGF-I

IGF-I (Gropep; receptor grade, #CM001) was made up to 1µg/µl stock solution following product instruction, aliquoted and stored at -20°C. A 10µg/ml working stock was made fresh by adding 3µl of stock solution to 297µl of SFM that was diluted further with SFM to achieve final working concentrations.

4.3.2.4 Recombinant human IGFBP-2 protein

A final concentration of 600ng/ml of IGFBP-2 was prepared as described in section 3.3.6.1.

4.3.1 Cell proliferation

TTI assay was used to measure DNA synthesis, and Trypan Blue Dye Exclusion assay was performed for cell counting to assess cell survival as described in section 2.2.

4.3.2 Cell colony formation

A soft agar colony formation assay was used with both T24 and TCCSUP cells as described in section in 2.8 to examine the change in malignant transformation activity in response to AZA treatment.

4.3.3 COBRA

COBRA was used to investigate the methylation status of the *IGFBP-2* gene promoter as described in section 2.7.

4.3.4 Detection of protein abundance

Protein levels of E-cadherin, N-cadherin and IGFBP-2 in either whole lysates or supernatant were detected using WB analyses as described in section 2.3. GAPDH was used as a loading control, and the antibody solution information is listed in Table 25.

Table 25 Antibody solutions information

Protein	Size (kDa)	Gel percentage (%)	Company & Cat. No.	Blocking	1° Ab	*2° Ab
E-cadherin	135	10	Cell Signalling (24E10), #3195	5% milk	1/1000, 5% BSA, rabbit	1/2000, 5% BSA, anti-rabbit
N-cadherin	130	10	BD Biosciences, #610920	5% milk	1/1000, 5% milk, mouse	1/2000, 5% milk, anti-mouse
IGFBP-2	36	12	Santa Cruz, #SC6001	5% milk	1/1000, 5% milk, goat	1/2000, 5% milk, anti-goat
GAPDH	35	12	Chemicon, #MAB 374	5% milk	1/5000, 5% milk, mouse	1/5000, 5% milk, anti-mouse

*2° **Ab**: anti-rabbit (Sigma, #A0545); anti-mouse (Sigma, #A0944); anti-goat (Sigma, #A5420).

4.3.5 Transfection with IGFBP-2 siRNA

IGFBP-2 gene knockdown in RT4 cells was achieved by performing IGFBP-2 siRNA transfection as described in section 2.6. Cells were transfected with IGFBP-2 siRNA at the concentration of 30nM for 72 hours as determined in section 3.4.3.1.

4.3.6 Statistical analysis

Data were expressed as mean ± SEM and analysed with SPSS 23 for Windows using one-way analysis of variance (ANOVA) followed by least significant difference (LSD) post-hoc test and Student's test. A two-sided *p*-value was shown for statistical significance and was depicted in asterisks as a single one for *$p<0.05$ and a double for **$p<0.01$.

4.4 Results

4.4.1 Optimisation of AZA Doses

TTI assay was performed in both T24 and TCCSUP cells to investigate the antiproliferative response to AZA treatment to try to establish an appropriate dose for further experiments in this study.

As shown in Figure 42 cell proliferation decreased with increasing concentrations of AZA in both cell lines: at 10μM proliferation was decreased by 63% in T24 cells, $p<0.01$ and by 48% in TCCSUP cells, $p<0.01$. This dose was selected for the following experiments.

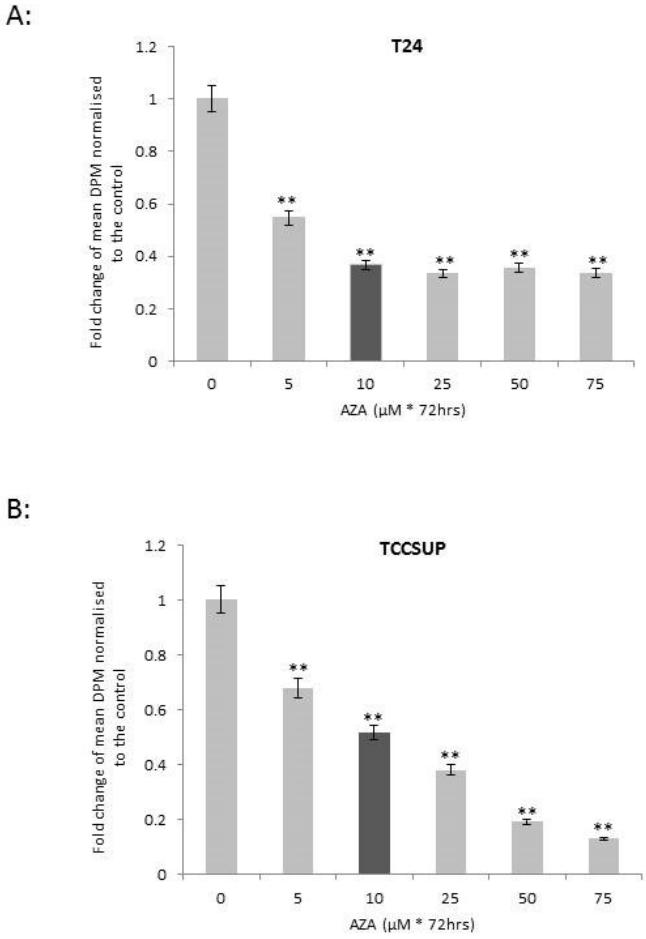

Figure 42: proliferative response to AZA in T24 and TCCSUP bladder cancer cells

Both T24 and TCCSUP cells were seeded at a density of $0.02x10^6$ cells/well into 24-well plates in GM to grow for 24 hours followed by serum starvation for another 24 hours. Then both cell lines were dosed with AZA at 0-75μM for 24 hours, and TTI was performed to show the proliferative response to AZA in T24 (**A**) and TCCSUP (**B**) cells.

The graphs represent the mean of three experiments each performed in quadruplicate, and error bars represent the standard error of the mean of the experiments (n=3). "**": $p<0.01$. The bars in the darker colour indicate the chosen concentration of AZA for both cell lines for further experiments.

4.4.2 Effect of AZA on the levels of IGFBP-2

Based on the chosen dose of AZA determined in 4.4.1, both T24 and TCCSUP cells were exposed to AZA (10μM) for 72 hours to investigate whether the loss of IGFBP-2 in bladder cancer potentially resulted from epigenetic regulation of

the gene promoter. The supernatant was collected, concentrated and analysed using WB to assess levels of IGFBP-2.

With T24 cells, as shown in Figure 43-**A**, IGFBP-2 was found at an undetectable level in the control with a trace in AZA-treated samples when un-concentrated ("Neat"). When concentrated either 10 or 20 times, we clearly observed an increase in the abundance of IGFBP-2 following AZA-exposure compared with the control. There were significant changes in the densitometry analysis (approximately 11-fold with 10-times and 8-fold with 20-times concentration, both $p<0.01$) (Figure 43-**C**).

Similar results were found with TCCSUP cells. According to the WB blot in Figure 43-**B**, little IGFBP-2 could be detected in the un-concentrated ("Neat") supernatant in both control and AZA-treated samples. When concentrated 30 times, a low level of IGFBP-2 was detected in the control sample with an induction observed in AZA-treated samples, with a more noticeable increase in IGFBP-2 when the supernatant was concentrated 60 times. Statistically, the levels of IGFBP-2 doubled under AZA treatment compared with the control samples ($p<0.01$) (Figure 43-**D**).

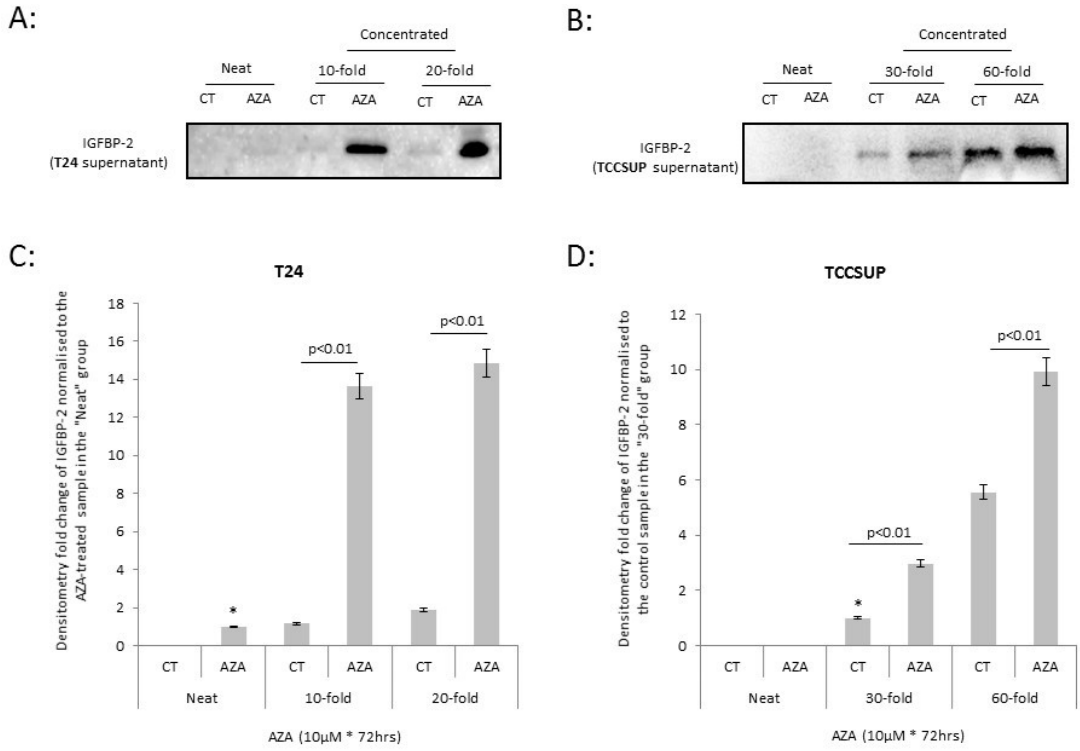

Figure 43: effect of AZA on the levels of IGFBP-2

Both T24 and TCCSUP cells were seeded in 6-well plates at a density of $0.05x10^6$ cells/well in GM to grow for 24 hours and serum starved in SFM for another 24 hours. Then cells were labelled according to different treatments ("CT": untreated cells as a control group; "AZA": cells treated with AZA at the concentration of 10μM for 72 hours). After 72 hours of treatment, the supernatant was collected and concentrated according to different concentrating factors ("Neat": un-concentrated supernatant samples; "Concentrated X-fold": X-times concentrated supernatant samples, "X" includes 10, 20, 30 and 60). WB was then performed to examine the levels of IGFBP-2 in the supernatant samples.

(**A**) & (**B**): The blots show the levels of IGFBP-2 detected in the supernatant samples in T24 and TCCSUP cells, respectively. (**C**) & (**D**): The graphs present the mean of fold change of optical density measurement of IGFBP-2 in T24 and TCCSUP cells, respectively, from three experiments each performed in triplicate, and error bars represent the standard error of the mean from three experiments (n=3). "*": the bar selected as the control of normalisation.

4.4.3 Assessment of the methylation status of *IGFBP-2* gene using COBRA

Having shown that IGFBP-2 was re-expressed in T24 and TCCSUP cells following AZA treatment, COBRA was then performed with these two cell lines to assess any alterations in gene methylation status of the *IGFBP-2* promoter

and to confirm whether the loss of IGFBP-2 in mesenchymal-like bladder cancer cell lines could be the result of methylation of the *IGFBP-2* gene promoter.

In T24 cells, as shown in Figure 44-**A**, the promoter region of the *IGFBP-2* gene was completely methylated in the control samples ("CT"), and the treatment of AZA led to the demethylation of this gene with a significant increase in the percentage of unmethylated DNA bands from 0 (in control cells) to 39.9% (in AZA-treated cells) ($p<0.001$) (Figure 44-**B**).

With TCCSUP cells, very low level of methylation was observed in the control cells. However, similar gene demethylation, but to a smaller extent than observed in T24 cells, was detected in TCCSUP samples upon AZA treatment (Figure 44-**C**), and the percentage of unmethylated DNA bands increased significantly from 74.8% (in control cells) to 88.6% (in AZA-treated cells) ($p<0.01$) (Figure 44-**D**).

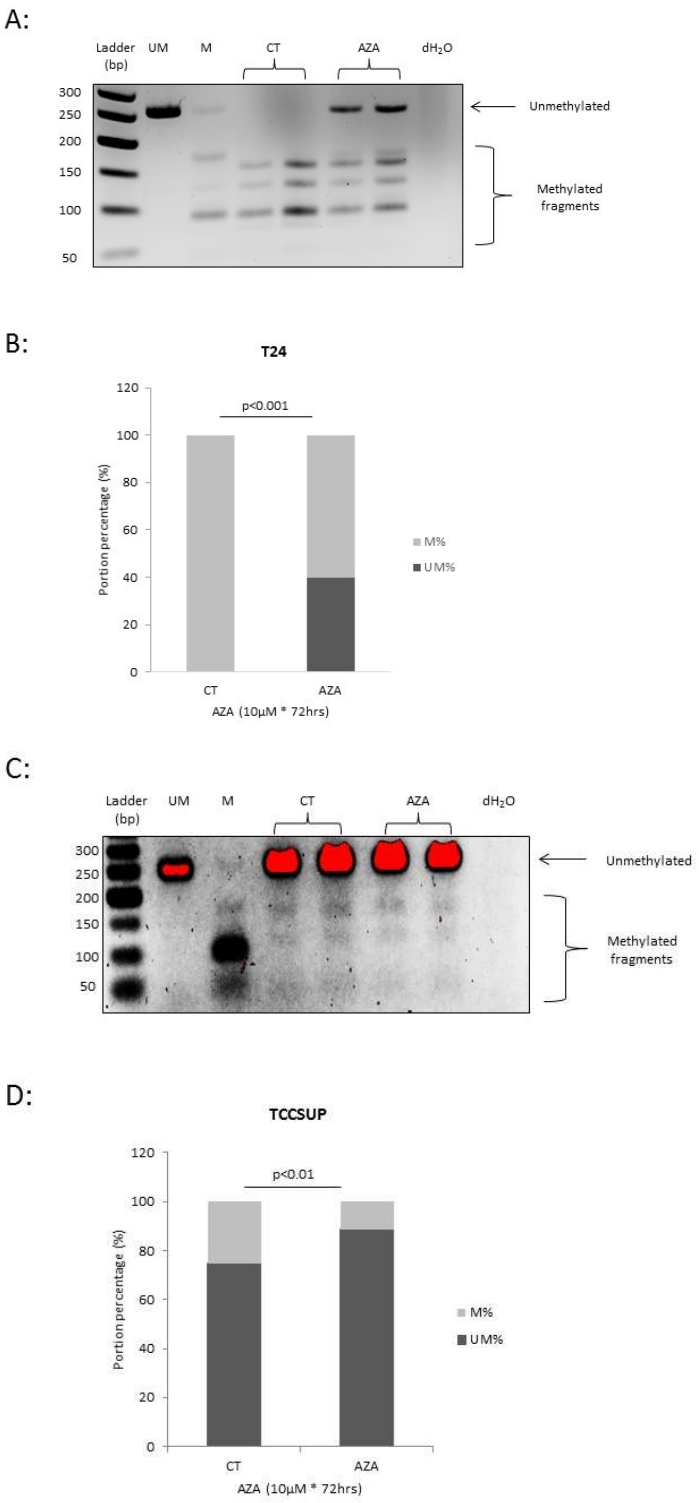

Figure 44: demethylation of the *IGFBP-2* gene in T24 and TCCSUP cells following AZA treatment using COBRA

T24 and TCCSUP cells were seeded in 6-well plates at a density of $0.05x10^6$ cells/well in GM for 24 hours and serum starved with SFM for another 24 hours. Then cells were labelled according to different treatments ("CT": untreated cells as a control group; "AZA": cells treated with AZA at the concentration of 10μM for 72 hours). After 72 hours of treatment, cells were harvested to investigate the methylation status of the *IGFBP-2* gene promoter using COBRA.

"Ladder(bp)": 50bp DNA ladder; "UM": positive control of completely unmethylated samples; "M": positive control of completely methylated samples; "CT": untreated samples; "AZA": AZA-treated samples; "dH_2O": distilled water samples as a negative control; "M%": percentage of methylated fragments; "UM%": percentage of unmethylated bands. Both CT and AZA samples were loaded in duplicate. The images of gels are representative of experiments with at least three repeats (n=3) each performed in triplicate, and the graphs demonstrate the mean of the optical density measurements of the percentage of uncut (unmethylated) and cut fragments (methylated) from the three experiments upon which statistical analysis was performed.

(**A**) & (**C**): A representative image of the gels shows the density of unmethylated and methylated bands in T24 and TCCSUP cells, respectively. The red colour indicates overexposure of the bands. (**B**) & (**D**): Graphs show the portion percentage of unmethylated and methylated bands in T24 and TCCSUP cell, respectively.

4.4.4 Effect of AZA on cancer phenotypes

With the confirmation of the methylation of the *IGFBP-2* gene promoter in mesenchymal-like bladder cancer cell lines using COBRA and the re-expression of IGFBP-2 in T24 and TCCSUP cells following treatment with AZA, I next examined how AZA affected the phenotype of the cells.

4.4.4.1 Effect of AZA on cell growth in T24 and TCCSUP cells

With the treatment of AZA, T24 cells presented significant decreases both in total cell number (by 34.3%, $p<0.001$) and in live cell number (by 36.4%, $p<0.001$) (Figure 45-**A**). More cell death was also observed in AZA-treated cells increasing from 0.6% in control cells to 1.2% in treated cells ($p<0.05$) (Figure 45-**B**).

However, in TCCSUP cells, no significant changes were found between control and AZA-treated cells either in cell numbers (Figure 45-**C**) or percentage cell death (Figure 45-**D**).

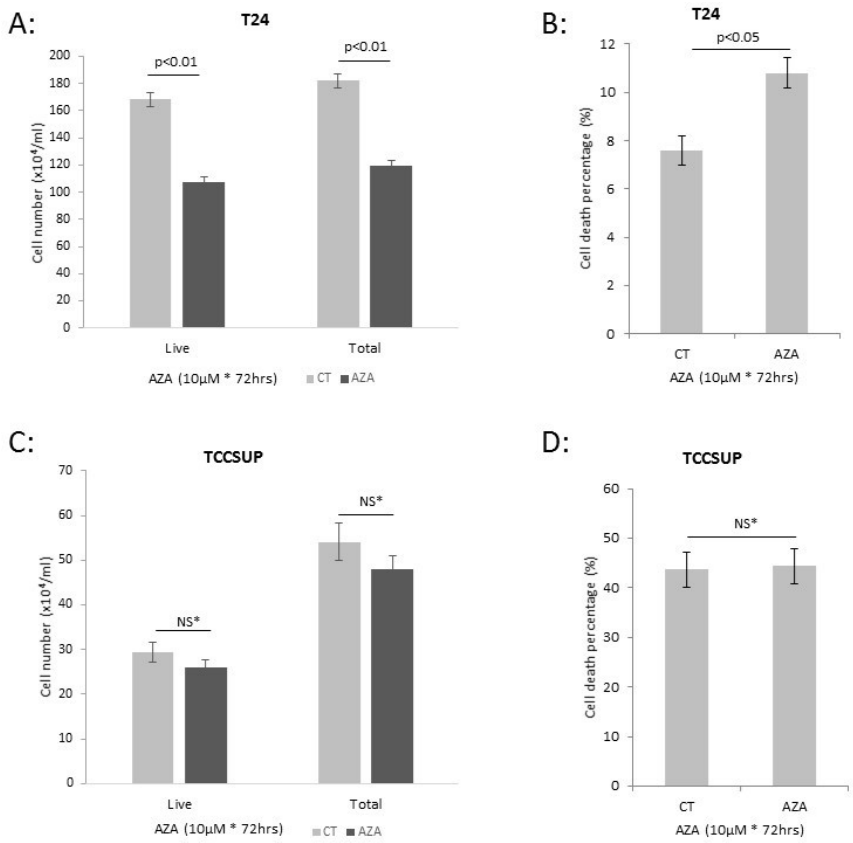

Figure 45: effect of AZA on cell growth in T24 and TCCSUP cells

Both T24 and TCCSUP cells were seeded in 6-well plates at a density of $0.05x10^6$ cells/well in GM to grow for 24 hours and serum starved in SFM for another 24 hours. And then cells were labelled according to the different treatments ("CT": untreated cells as a control; "AZA": cells treated with AZA at the concentration of 10μM for 72 hours). After 72 hours of treatment, cell numbers were determined by cell counting.

(**A**) & (**C**): Graphs show counting of both live and total cells after different treatments in T24 and TCCSUP cells, respectively. (**B**) & (**D**): Graphs represent the change in percentage cell death following different treatments in T24 and TCCSUP, respectively. The graphs present the mean of three experiments each performed at least in triplicate, and error bars represent the standard error of the mean of the experiments (n=3). "NS*": not significant.

4.4.4.2 Effect of AZA on cell colony formation in T24 and TCCSUP cells

To assess the influence of AZA on malignant cell transformation in T24 and TCCSUP cells, soft agar colony formation assays were performed.

As shown in Figure 46-**A** & **D**, with the treatment of AZA, less and smaller colonies were formed in both T24 and TCCSUP cells compared with the control, visually.

AZA-treated T24 cells presented a significant reduction in colony counts per dish. Colony forming efficiency (CFE) decreased by 36.7% ($p<0.01$) (Figure 46-**B**), and the average size of each colony showed a 0.6 fold decrease ($p<0.001$) relative to control cells (Figure 46-**C**).

Similarly, AZA-treated TCCSUP cells demonstrated a significant decrease in CFE of 67.4% ($p<0.001$) (Figure 46-**E**) and the same fold decrease in the average size of each colony (0.6, $p<0.05$) relative to untreated cells (Figure 46-**F**).

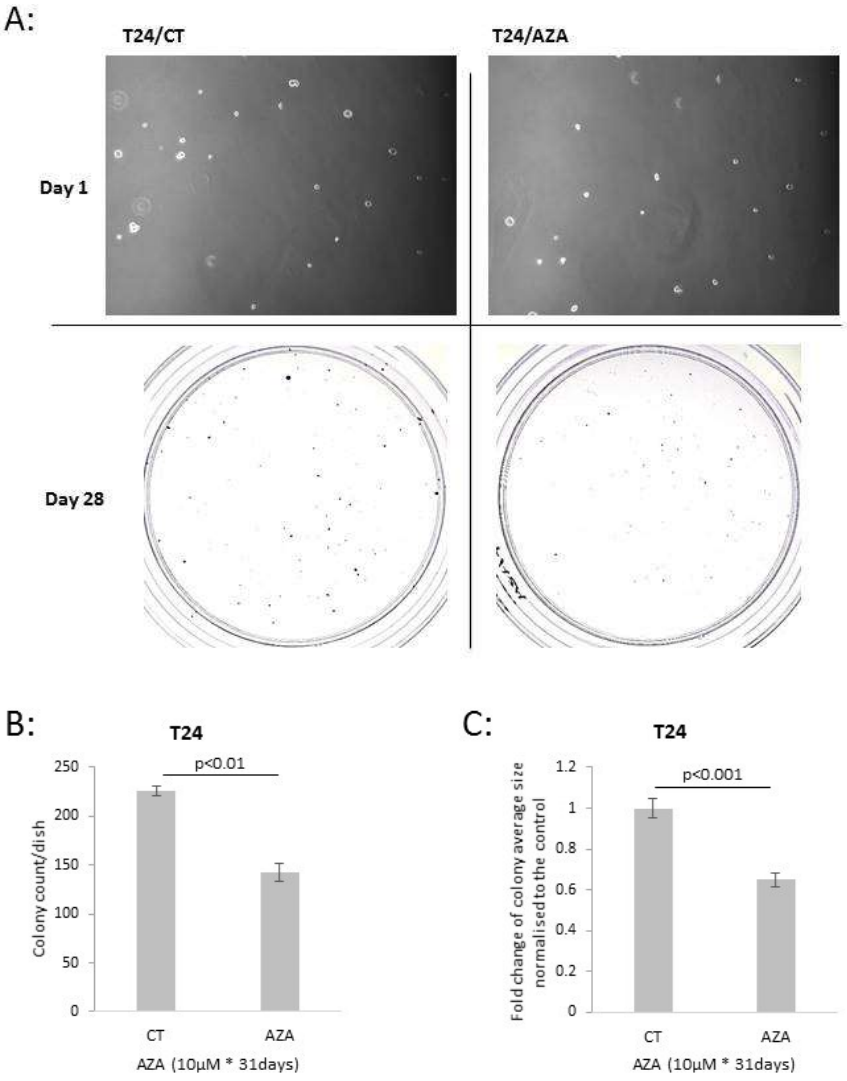
A:
T24/CT
T24/AZA
Day 1
Day 28
B:
T24
p<0.01
Colony count/dish
250
200
150
100
50
0
CT
AZA
AZA (10μM * 31days)
C:
T24
p<0.001
Fold change of colony average size normalised to the control
1.2
1
0.8
0.6
0.4
0.2
0
CT
AZA
AZA (10μM * 31days)

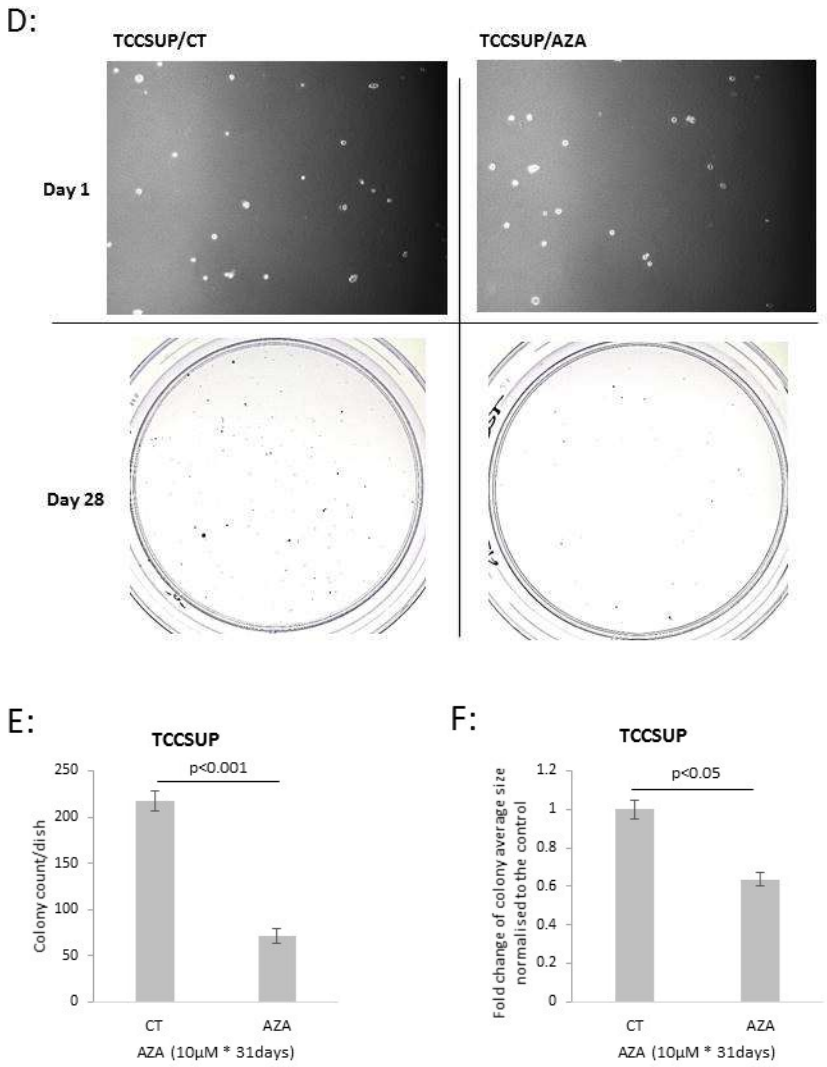

Figure 46: effect of AZA on the formation of colonies by T24 and TCCSUP cells in soft agar

Both T24 and TCCSUP cells were seeded in dishes under different treatments with corresponding labels ("CT": untreated cells as a control group; "AZA": cells treated with AZA at the concentration of 10μM for 72 hours before seeding). All cells were seeded at an even density of 5,000cells/dish and fed once a week for four weeks in total, and then colony numbers, as well as the average size, were measured by ImageJ software.

(**A**) & (**D**): Images show T24 and TCCSUP cells, respectively, that were seeded into dishes at even densities on the first day ("Day 1"), and colonies were stained at the end of the assay ("Day 28"); All images shown are at x10 magnification; (**B**) & (**E**): Graphs represent the change in colony count per dish under different treatments for T24 and TCCSUP cells, respectively. (**C**) & (**F**): Graphs demonstrate the fold change in the average size of colonies due to different treatments for T24 and TCCSUP cells, respectively. All graphs represent the mean of three experiments each performed in triplicate, and error bars represent the standard error of the mean from three experiments (n=3).

4.4.4.3 Effect of AZA on EMT markers in T24 cells

As mentioned in 3.4.1, T24 cells express abundant β-catenin and N-cadherin, a mesenchymal marker, with no trace of E-cadherin, an epithelial marker. WB analysis was used to assess changes in abundance of these molecules following AZA treatment. As nuclear translocation of β-catenin from the membrane and cytoplasm is considered another key indicator of cancer progression, cellular fractionation was also used to assess this after treatment with AZA.

4.4.4.3.1 Detection of changes in abundance of E-, N-cadherin and β-catenin

With the treatment of AZA at 10μM for 72 hours, the abundance of N-cadherin was reduced by of 65% ($p<0.05$) with no observed changes in E-cadherin (Figure 47-**A** & **B**). No visible or statistically significant change in the abundance of β-catenin was found (Figure 47**-C** & **D**).

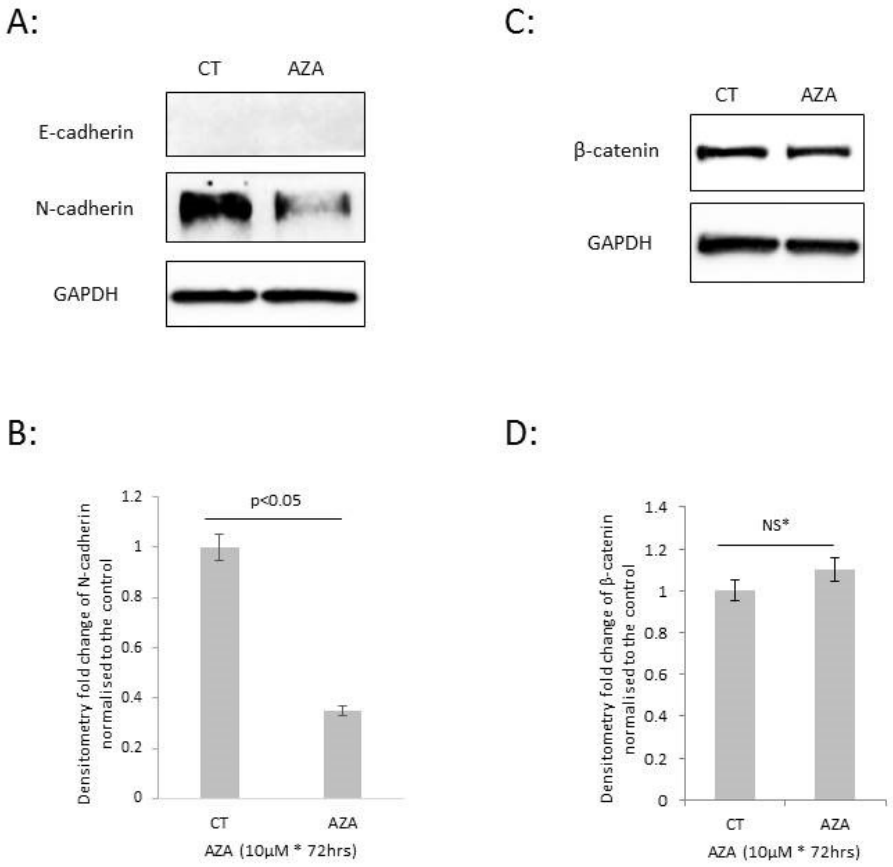

Figure 47: effect of AZA on EMT markers in T24 cells

T24 cells were seeded in 6-well plates at a density of $0.05x10^6$ cells/well in GM for 24 hours and serum starved with SFM for another 24 hours. Then cells were separated according to different treatments ("CT": untreated cells as a control group; "AZA": cells treated with AZA at the concentration of 10μM for 72 hours). After 72 hours of treatment, cells were harvested to investigate the changes in protein abundance using WB analysis. Samples from whole lysates were loaded equally at 60μg for protein detection, and GAPDH was assessed as reference protein.

The blots present the levels of E- and N-cadherin (**A**) and β-catenin (**C**) under different treatments. And the graphs (**B**) and (**D**) demonstrate the mean of fold change of the optical density measurements of N-cadherin and β-catenin, respectively, from three experiments each performed at least in triplicate, and error bars represent the standard error of the mean of experiments (n=3). "NS*": not significant.

4.4.4.3.2 Detection of a change in localisation of β-catenin

No prominent nuclear translocation of β-catenin was observed following AZA treatment (Figure 48-**A**), and no significant difference in the fold change of cytoplasmic β-catenin normalised to this protein in total cell lysates was found between control and AZA-treated cells by densitometry analysis (Figure 48-**B**).

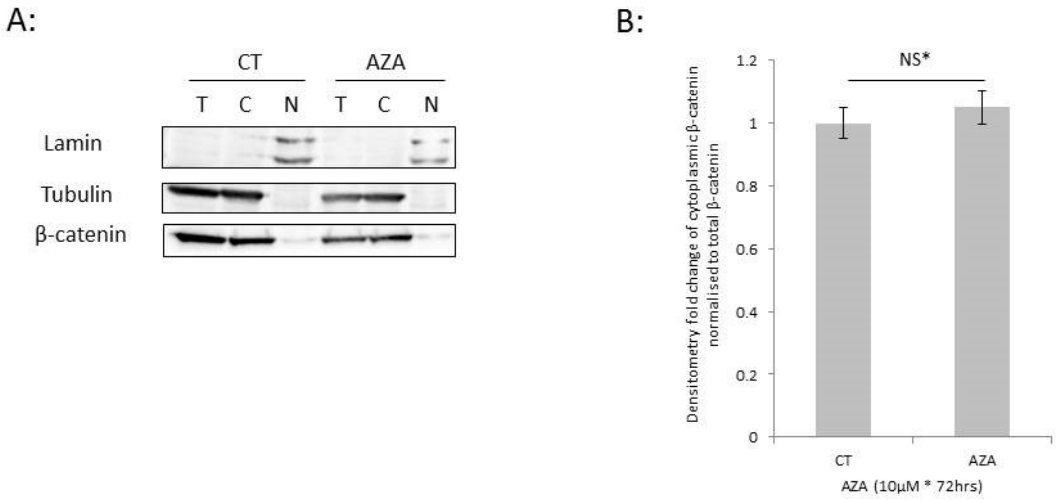

Figure 48: effect of AZA on nuclear translocation of β-catenin in T24 cells using cellular fractionation

T24 cells were seeded in 6-well plates at a density of $0.05x10^6$ cells/well in GM for 24 hours and serum starved with SFM for another 24 hours. Then cells were labelled according to different treatments ("CT": untreated cells as a control group; "AZA": cells treated with AZA at the concentration of 10μM for 72 hours). After 72 hours of treatment, cells were harvested to investigate the change in the localisation of β-catenin using cellular fractionation. Separate proteins were obtained and loaded equally for protein detection using WB. All blots demonstrate typical results from three experiments each performed at least in triplicate (n=3).

(**A**): The blot shows the localisation of β-catenin in the presence or absence of AZA treatment in T24 cells using cellular fractionation. Lamin and Tubulin exist only in nuclei and cytoplasm, respectively, and they are an indicator of the efficiency of protein separation. "T": total cell lysates; "C": cytoplasmic extract; "N": nuclear extract. (**B**): The graph presents the fold change of cytoplasmic β-catenin normalised to total β-catenin in the total cell lysates with error bars representing the standard error of the mean of experiments (n=3). "NS*": not significant.

4.4.5 Investigation of the mechanism of IGFBP-2 using NBI-31772

To examine the working mechanism of IGFBP-2 in bladder cancer, IGF-dependent or -independent, or even both, NBI-31772 was used as an IGFBP-2 inhibitor with RT4 and T24 cells by binding to six IGFBPs non-specifically and to IGFBP-2 with high affinity. Meanwhile, since using NBI-31772 could also elevate the level of bioactive IGF-I by displacing it from IGF-I:IGFBP complexes, exogenous recombinant human IGF-I was also used in the investigation. Alterations in cell proliferation and invasion were assessed.

4.4.5.1 Assessment of the working mechanism of IGFBP-2 in RT4 cells

In IGFBP-2-abundant epithelial-like RT4 cells, NBI-31772 was applied with or without IGFBP-2 siRNA transfection.

As shown in Figure 49, pre-treatment with NBI-31772 alone led to a significant increase in cell growth (21.7% in non-silenced cells between "NS" and "NS+NBI", $p<0.05$; see Figure 49-**B**), suggesting that IGFs had been released from IGFBPs, predominantly IGFBP-2 as this is the main one secreted by these cells, and was able to increase cell growth. This indicates that IGFBPs, predominantly IGFBP-2, acts at least partly by sequestering IGFs since when IGFs are displaced from the IGFBPs this stimulates cell growth and silencing IGFBP-2, when it can no longer sequester IGFs also results in cell growth.

Silencing IGFBP-2, as we observed previously, caused an increase in cell growth (by 40.9% in "NS" and "KD", $p<0.01$; Figure 49-**B**). In the presence of NBI-31772, silencing IGFBP-2 still induced a comparable increase in cell growth (36.7% in NBI-pre-treatment group between "NS+NBI" and "KD+NBI",

$p<0.001$; see Figure 49-**B**) which was additive to the effects of NBI-31772 alone on cell growth (66.3% between "NS" and "KD+NBI", $p<0.001$; see Figure 49-**B**). In the presence of NBI-31772, when any interaction of IGFBP-2 with IGFs is prevented, the observation that silencing IGFBP-2 still results in cell growth indicates that the presence of IGFBP-2 can inhibit cell growth independent of any interaction with IGFs. In combination these results suggest that the effects of IGFBP-2 on these cells are both IGF-dependent and -independent.

No significant changes in cell death were found under different treatments (Figure 49-**C**).

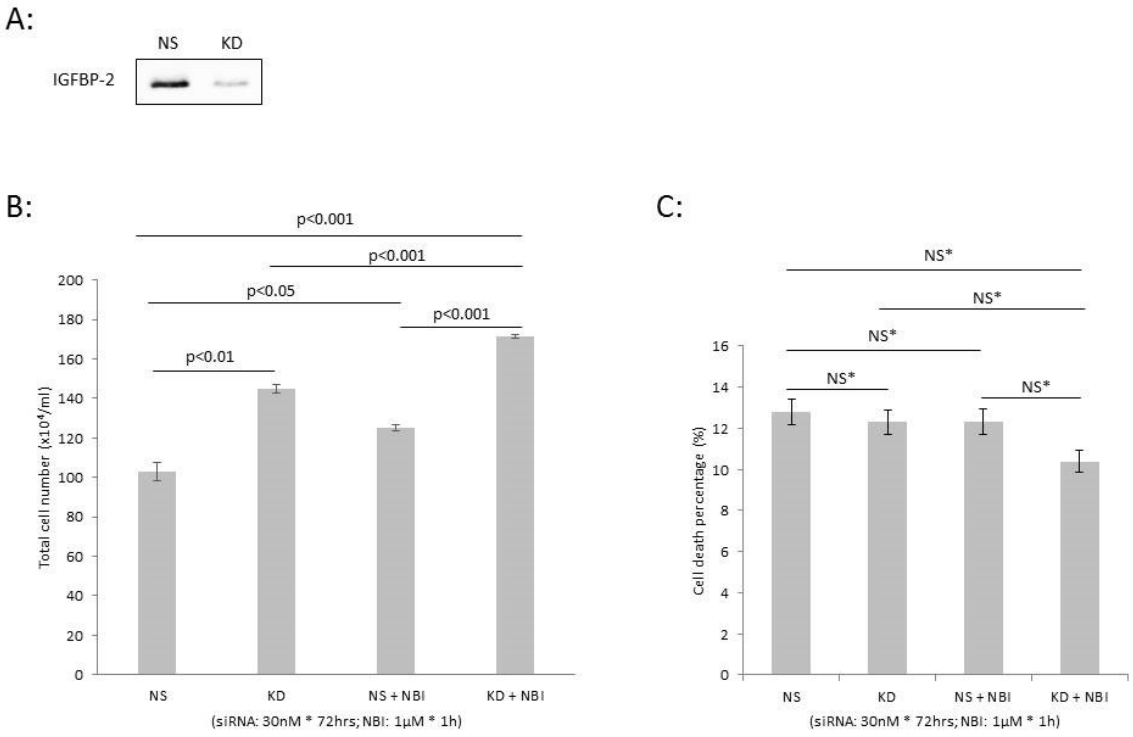

Figure 49: effect of NBI-31772 and IGFBP-2 siRNA transfection on cell proliferation in RT4 cells

RT4 cells were seeded into 6-well plates at a density of $0.1x10^6$ cells/well in GM for 24 hours. After 24 hours of serum starvation in SFM, cells were then dosed with scramble or IGFBP-2 siRNA (both at a concentration of 30nM for 72 hours) with or without 1 hour of pre-treatment of NBI-31772 at 1μM. "NS": non-silencing scramble siRNA only treated samples; "KD": IGFBP-2 siRNA treated samples; "NS+NBI": scramble siRNA treated samples with 1 hour of NBI-31772 pre-treatment; "IGFBP-2+NBI": IGFBP-2 siRNA treated samples with 1 hour of NBI-31772 pre-treatment.

(**A**): WB blot shows the efficiency of IGFBP-2 knockdown achieved by loading the supernatant collected under each treatment equally at 25μl; (**B**) & (**C**): Graphs represent the change in the counting of total cell numbers and the percentage cell death following different treatments in RT4 cells, respectively. The graphs show the mean of three experiments each performed at least in triplicate, and error bars represent the standard error of the mean of the experiments (n=3). "NS*": not significant.

Similarly, regarding cell invasion, as shown in Figure 50, a significant increase was observed with pre-treatment of NBI-31772 alone (17.3% in non-silenced cells between "NS" and "NS+NBI", $p<0.05$; see Figure 50-**B**), which confirmed the enhancing effect of released free IGF on cell invasion, similar to the effect observed on cell growth. Silencing IGFBP-2 alone increased cell invasion (by 33.1% in "NS" and "KD", $p<0.01$; see Figure 50-**B**. In the presence of NBI-31772, silencing IGFBP-2 still induced a comparable increase in invasion which was additive to the effects of NB1 alone on cell invasion growth (56.9% in "NS" and "KD+NBI", $p<0.01$; see Figure 50-**B**), suggesting again both IGF-dependent and -independent effects of IGFBP-2 on invasion in RT4 cells.

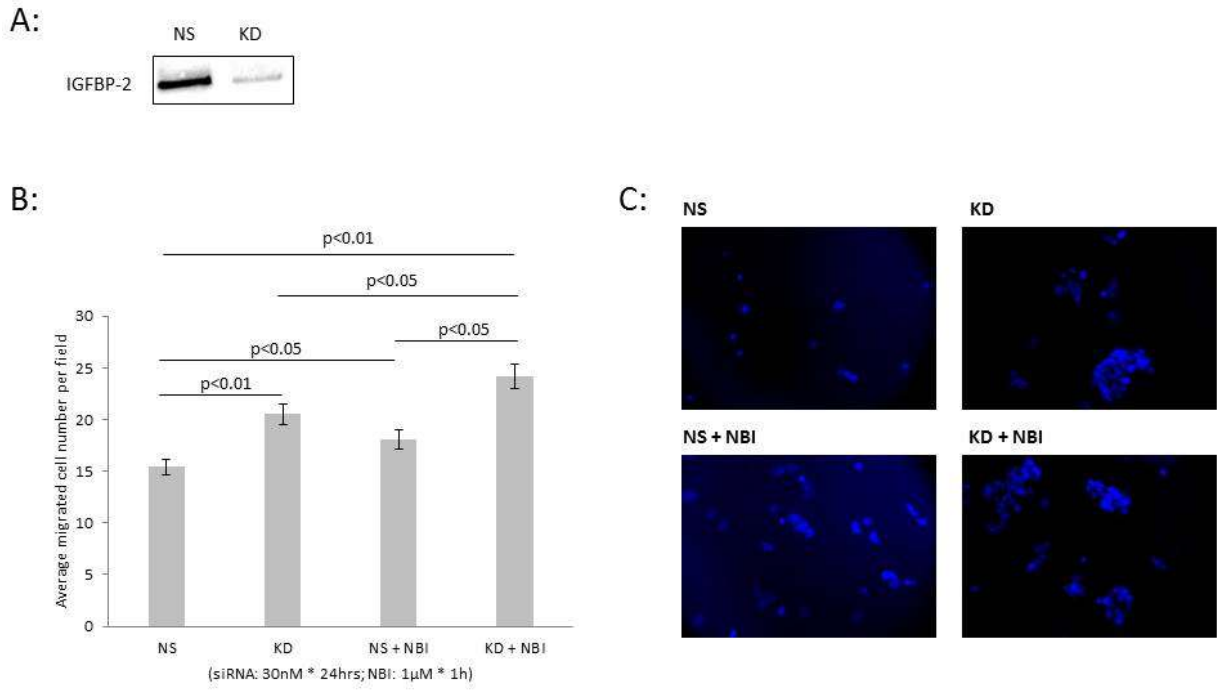

Figure 50: effect of NBI-31772 and IGFBP-2 siRNA transfection on cell invasion in RT4 cells

Cells were initially seeded into 6-well plates at a density of $0.1x10^6$ cells/well in GM for 24 hours. After 24 hours of serum starvation in SFM, cells were then transfected with non-silencing scramble or IGFBP-2 siRNA (both at 30nM for 72 hours) with or without 1 hour of pre-treatment of NBI-31772 at 1μM. And then cells were trypsinised and then seeded in the collagen-coated inserts at a density of $0.1x10^6$ cells/insert and allowed to invade for 24 hours. The supernatant was taken before cell trypsinisation to assess levels of IGFBP-2 to determine the efficiency of IGFBP-2 silencing. "NS": non-silencing scramble siRNA only treated samples; "KD": IGFBP-2 siRNA treated samples; "NS+NBI": scramble siRNA treated samples with 1 hour of NBI-31772 pre-treatment at 1μM; "IGFBP-2+NBI": IGFBP-2 siRNA treated samples with 1 hour of NBI-31772 pre-treatment at 1μM.

(**A**): WB blot shows the efficiency of IGFBP-2 knockdown achieved by loading the supernatant collected under each treatment equally at 25μl; (**B**): The graph shows the change of average invaded RT4 cells under different treatments; the graph represents the mean of three experiments each performed at least in triplicate, and error bars represent the standard error of the mean of the experiments (n=3); (**C**): The images show transwell invaded cells with nuclei (in blue) stained by DAPI; all images shown are at x10 magnification;

4.4.5.2 Assessment of the working mechanism of IGFBP-2 in T24 cells

4.4.5.2.1 Optimisation of an effective dose of IGF-I

TTI assay was used in T24 cells to assess cell proliferation following the exogenous addition of IGF-I (0-200ng/ml) for 24 hours.

As shown in Figure 51, an increase in cell proliferation was observed with increasing concentration of IGF-I: the maximal increase was found to be at 50ng/ml (by 105%, $p<0.01$). Therefore, this dose was chosen as an effective concentration to act as a control for further experiments.

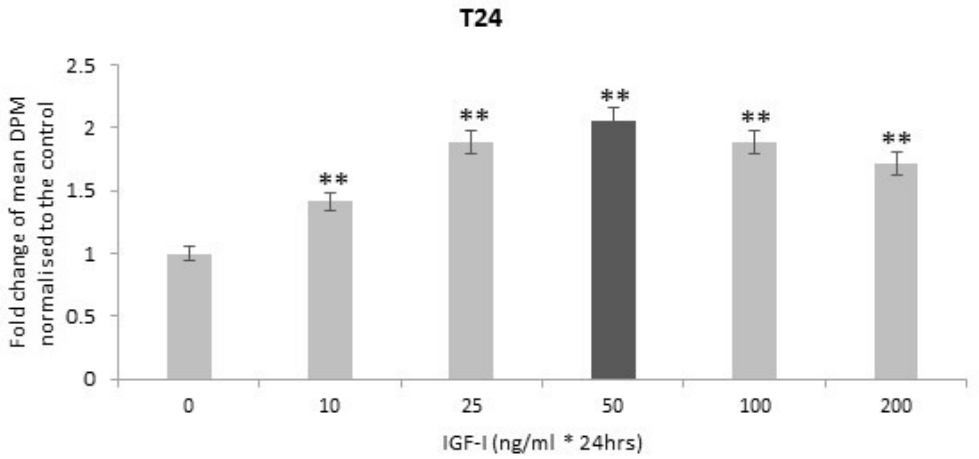

Figure 51: proliferative response to exogenous IGF-I in T24 bladder cancer cells

T24 cells were seeded at a density of $0.02x10^6$ cells/well into 24-well plates in GM to grow for 24 hours followed by serum starvation for another 24 hours. Then TTI was performed to show the proliferative response to exogenous IGF-I in T24 cells at 0-200 ng/ml for 24 hours. The graph shows the means of three experiments each performed in quadruplicate, and error bars represent the standard error of the mean of the experiments (n=3). "**": $p<0.01$. The bar in the darker colour represents the chosen effective concentration for further experiments.

4.4.5.2.2 Alterations in cell proliferation and invasion induced by NBI-31772 and IGFBP-2

As shown in Figure 52-**A**, compared with control cells ("CT"), exogenously added IGF-I induced a significant increase in total cell number (28.6%, $p<0.001$) while NBI-31772 did not (unnoticeable difference with non-significant p-value), suggesting that no IGF was released from any IGFBPs present. Exogenous IGFBP-2 led to a decrease in cell growth compared with control cells (35.3%, $p<0.001$), and this effect was negated in the presence of NBI-31772, suggesting that exogenously added IGFBP-2 reduces cell growth through sequestering endogenous IGFs and can no longer do this in the presence of NBI-31772: this implies an IGF-dependent action of the exogenously added IGFBP-2.

No significant changes in percentage cell death were observed among cells under different treatments (Figure 52-**B**).

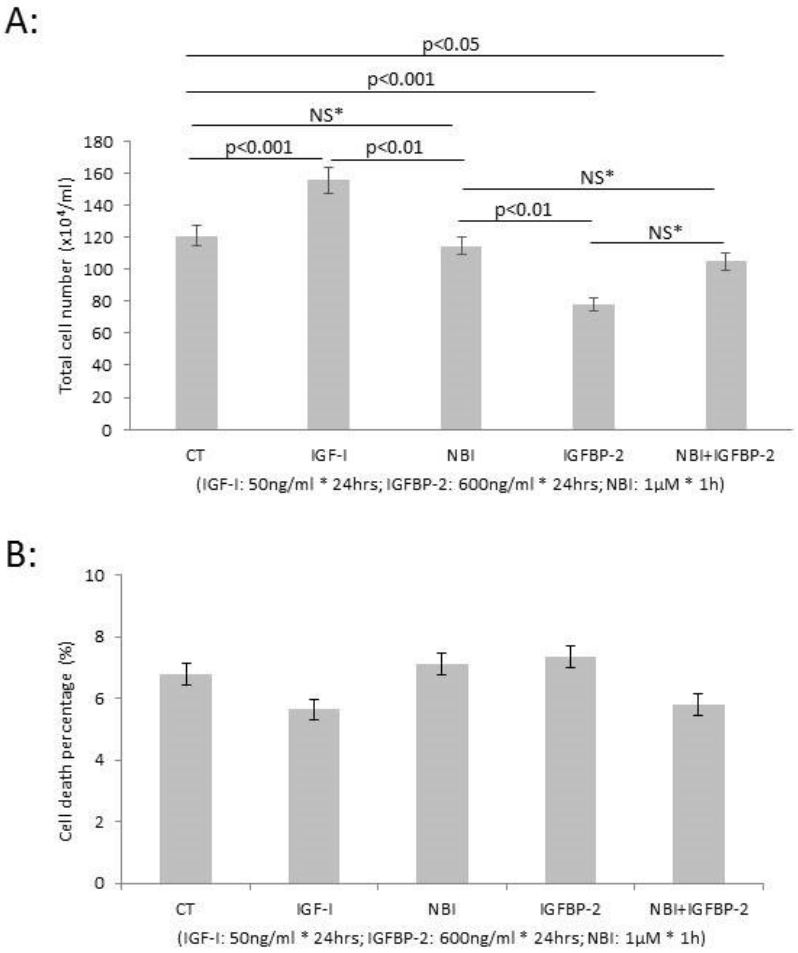

Figure 52: effect of IGF-I, exogenous IGFBP-2 and NBI-31772 on cell proliferation in T24 cells

T24 cells were seeded into 6-well plates at a density of $0.05x10^6$ cells/well in GM for 24 hours. After 24 hours of serum starvation in SFM, cells were then dosed with IGF-I (at 50ng/ml) or IGFBP-2 (at 600ng/ml) for 24 hours with or without 1 hour of pre-treatment of NBI-31772 at a concentration of 1μM. "CT": control cells without treatment; "IGF-I": cells treated with IGF-I only at a concentration of 50ng/ml for 24 hours; "NBI": cells treated with NBI-31772 only at 1μM for 1 hour; "IGFBP-2": cells treated with IGFBP-2 only at a concentration of 600ng/ml for 24 hours; "NBI + IGFBP-2": cells dosed with 1 hour of pre-treatment of NBI-31772 followed by the treatment of IGFBP-2 at a concentration of 600ng/ml for 24 hours).

(**A**) & (**B**): Graphs represent the change in the counting of total cell numbers and the percentage cell death following different treatments in T24 cells, respectively. The graphs show the mean of three experiments each performed at least in triplicate, and error bars represent the standard error of the mean of the experiments (n=3). "NS*": not significant.

Regarding cell invasion, as shown in Figure 53-**A**, similar to data observed for cell proliferation, IGF-I induced a significant increase compared with control

cells (45.5%, $p<0.001$) while NBI-31772 did not (unnoticeable difference with non-significant p-value).

Exogenous IGFBP-2 treatment ("IGFBP-2") led to a decrease in cell invasion compared with control cells (35%, $p<0.001$), and this was unaffected by the presence of NBI-31772 ("NBI+IGFBP-2") suggesting that IGFBP-2 effects on invasion not be blocked by NBI-31772 and were therefore independent of IGFs.

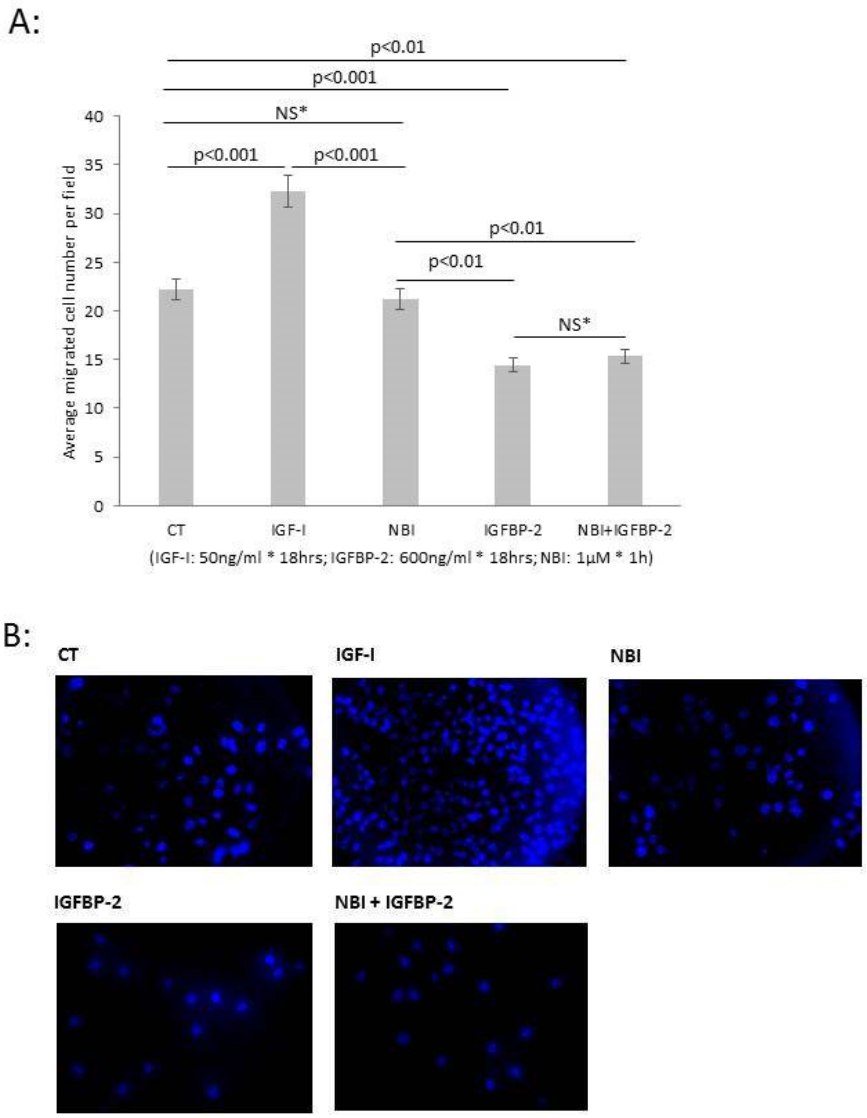

Figure 53: effect of IGF-I, exogenous IGFBP-2 and NBI-31772 on cell invasion in T24 cells

Cells were previously seeded into 6-well plates at a density of $0.05x10^6$ cells/well in GM for 24 hours and then changed to SFM for 16 hours before being prepared for an invasion assay. After serum-starvation, cells were dosed with or without 1 hour of pre-treatment of NBI-31772 at 1 μM, and then trypsinised and seeded into the collagen-coated inserts at a density of $0.08x10^6$ cells/insert and allowed to migrate for 18 hours. Cells were labelled according to different treatments while seeding ("CT": control cells without treatment; "IGF-I": cells treated with IGF-I only at a concentration of 50ng/ml for 18 hours; "NBI": cells treated with 1 hour of NBI-31772 at 1μM followed by no other treatment; "IGFBP-2": cells treated with IGFBP-2 only at a concentration of 600ng/ml for 18 hours; "NBI + IGFBP-2": cells dosed with 1 hour of pre-treatment of NBI-31772 followed by the treatment of IGFBP-2 at a concentration of 600ng/ml for 18 hours).

(**A**): The graph shows the change of average invaded T24 cells under different treatments; the graph represents the mean of three experiments each performed at least in triplicate, and error bars represent the standard error of the mean of the experiments (n=3); (**B**): The images show transwell invaded T24 cells with nuclei (in blue) stained by DAPI; all images shown are at x10 magnification.

4.5 Discussion

We observed in the previous chapter that IGFBP-2 plays an inhibitory role in the ability of bladder cancer cells to proliferate, invade, migrate and form colonies. In addition, its levels were altered depending on the aggressiveness of the cells, being abundant in the less advanced and absent in the most aggressive cells. Dysregulation of IGFBPs as a result of epigenetic modifications has been identified in many tumours, such as aberrant DNA methylation of the promoter of *IGFBP-2* and *IGFBP-3* genes in hepatomas and breast cancers respectively (Chiba, Yokosuka et al. 2005) (Zeng, Jarrett et al. 2013). We next investigated if altered methylation may be the mechanism by which IGFBP-2 levels were being regulated in bladder cancer cells.

The mesenchymal-like IGFBP-2-negative cell lines, T24 and TCCSUP, were exposed to AZA, a commonly used demethylating agent: re-expression of IGFBP-2 was observed in both cell lines, and the increase in abundance of IGFBP-2 was more significant in T24 cells. In addition to enabling the re-expression of IGFBP-2, treatment with AZA also led to similar phenotypic changes that were observed on addition of exogenous IGFBP-2: with T24 cells, a reduction in abundance of the mesenchymal marker (N-cadherin), significant decreases in cell proliferation, colony formation together with an increase in cell death. With TCCSUP cells, however, only a reduction in colony formation was noted with no notable change in cell growth or death, which indicates the heterogeneity among cell lines with similar phenotypes. To build a clearer picture, future work should assess other phenotypic changes (such

as cell invasion and migration and changes in EMT-related molecules) affected by AZA in T24 and TCCSUP cells and additional bladder cancer cell lines.

The application of COBRA confirmed that this increase in AZA-induced IGFBP-2 was specifically due to changes in the methylation status of the promoter region of *IGFBP-2* gene in the T24 cells. In TCCSUP cells, as the increase in demethylation in response to AZA was small, we suggest that other epigenetic changes such as histone modification, which has been reported in prostate cancer (Biernacka, Uzoh et al. 2013), might also contribute to the loss of IGFBP-2 which requires further investigation.

Based on the reversible nature of epigenetic modifications, compared with genetic mutations, these findings suggest IGFBP-2 is switched off in advanced bladder cancer which eliminates the inhibitory effects of this protein on cell proliferation, invasion, migration as well as colony formation in cancer development. Moreover, IGFBP-2 is considered as a potentially key mediator of the anti-tumorigenic effects of AZA on bladder cancer cells. This may provide the possibility of epigenetic-target cancer therapies for certain bladder cancer subtypes by aiming for the reversal of the phenotypes (Singh, Treas et al. 2012, Knowles and Hurst 2015).

As it has been reported that IGFBP-2 can act in either an IGF-dependent or -independent or both manners, NBI-31772, as an inhibitor of IGF/IGFBP-2 interactions, was used to study how it works in bladder cancer.

Stimulatory effects of pre-treatment with NBI-31772 alone on both cell growth and invasion of RT4 cells indicated that NBI-31772 freed endogenous IGFs from IGF:IGFBP complexes, mainly IGF:IGFBP-2, to act on the cells to promote growth and invasion alone. This suggested that endogenous IGFBP-2 was acting in an inhibitory manner in part through interactions with IGFs.

Silencing IGFBP-2 in RT4 cells also exerted promoting effects on both cell growth and invasion, and this stimulatory effect the same percentage change in the presence or absence of NBI-31772, but the percentage change was additive to the effects of NBI-31772 lone, which suggested that IGFBP-2 has the ability to act in both an IGF-dependent and -independent manner in epithelial-like bladder cancers.

In IGFBP-2-null mesenchymal-like T24 cells, compared with the increase in cell growth and invasion following the addition of exogenous IGF-I, no notable difference was found when cells were treated with NBI-31772 alone, which indicated little endogenous IGFs were released from IGF:IGFBP complexes in these cells.

Exogenously added recombinant IGFBP-2 led to a significant reduction both in cell growth and invasion of T24 cells. The inhibitory effect on growth was inhibited by the addition of NBI-31772. This suggested exogenous IGFBP-2 inhibited cell growth by sequestering endogenous IGFs and was no longer able to do this in the presence of NBI-31772, which implied an IGF-dependent action of the exogenously added IGFBP-2 on T24 cell proliferation which has been reported in colon cancer (Hoflich, Lahm et al. 1998). However, the

inhibitory effect of IGFBP-2 on cell invasion was not affected by adding NBI-31772, thus indicating that IGFBP-2 acted in an IGF-independent manner to inhibit invasion of T24 cells.

In summary, the results of the present study suggest that hypermethylation of the promoter region of the *IGFBP-2* gene plays an important part in the loss of IGFBP-2 in progressive mesenchymal bladder cancers, which raises the possibility of epigenetic-target anti-cancer therapies for aggressive bladder cancers.

IGFBP-2 acts in both IGF-dependent and -independent ways in bladder cancers despite the cancer phenotypes. In the presence of IGFs, IGFBP-2 reduces the effects of IGFs by sequestering free bioactive IGFs into inactive IGF:IGFBP-2 complexes (Liu, Xie et al. 2001), and the intrinsic effects have been demonstrated in many cancers by binding, via their RGD sequence, to integrin receptors, similar to that reported in prostate (Uzoh, Holly et al. 2011). Thus more work to unravel the molecular basis is required. The IGFs are widespread regulators of most cell functions; their interactions with IGFBPs can reduce the clearance of IGFs, sequester IGFs in the extracellular matrix or on cell surfaces, via interactions with proteoglycans, and hence enhance targeting of the IGFs to specific sites of action and also constrain receptor binding by competition. In addition they can also have intrinsic actions for example through binding to integrin receptors. The different effects of IGFBPs depend on interactions with extracellular matrix, cell surfaces and extracellular proteases; all of which can vary in a tissue specific manner and therefore confer specificity, depending on context, to the multiple potential IGF actions (Holly and Perks 2012).

Chapter 5- Effects of IGF-I on Bladder Cancer Cells

5.1 Introduction

Results from Chapter 4 showed that exogenous IGF-I promoted cell growth and migration of the T24 cell line. In addition, that some of the effects of IGFBP-2 in bladder cancer cell lines were at least in part mediated via an interaction with IGFs.

5.1.1 IGF axis

The IGF axis is a multifactorial system consisting of three ligands (IGF-I, IGF-II and insulin) and their receptors including the IGF-I receptor (IGF-IR), IGF-II receptor (IGF-IIR) and the insulin receptor (IR) (Foulstone, Prince et al. 2005, Samani, Yakar et al. 2007).

IGFs and insulin can bind to each other's receptors, though the binding affinity is much weaker than that of the preferred ligand (Zha and Lackner 2010). Compared with IGF-II, IGF-I has a higher affinity for the IGF-IR (Yu and Rohan 2000). Meanwhile, in contrast with the IGF-IIR which mainly regulates levels of extracellular IGF-II through receptor-mediated endocytosis, the IGF-IR is structurally and functionally homologous to the IR and it has been found to play an important role in mediating signalling upon IGF-I binding, activating phosphatidylinositol 3-kinase (PI3K) (Baselga 2011) and mitogen-activated protein kinase (MAPK) pathways (Hermanto, Zong et al. 2000) which lead to activation of downstream substrates.

5.1.2 IGF-I and cancer

As a critical regulator of many physiological processes such as cell proliferation and differentiation (Stewart and Rotwein 1996), the IGF axis is dysregulated in many different cancers exhibiting associations with increased risk of cancer formation and development. For example, high levels of circulating IGF-I are associated with an increased risk of certain types of cancers such as breast (Endogenous, Breast Cancer Collaborative et al. 2010), colorectal (Rinaldi, Cleveland et al. 2010) and prostate (Roddam, Allen et al. 2008). Moreover, accumulating evidence has suggested that IGF-I induces EMT, which is involved in the progression of many cancers such as breast (Walsh and Damjanovski 2011, Liao, Wang et al. 2014).

As there is very limited literature regarding the role of IGF-I in bladder cancer, I examined potential actions of IGF-I in bladder cancer cell lines, based on the increasing evidence indicating a role for IGF-I in other cancers and the results of previous chapters in my study suggesting its involvement.

5.2 Aims

In chapters 3 & 4 it was determined that RT4 cells contain high levels of IGFBP-2 compared with T24 cells and that the role of IGFBP-2 in these cell lines was both dependent and independent of IGF-I. To understand these data further, the effects of exogenously added IGF-I to these cells were examined.

- To assess the effect of IGF-I on phenotypic changes in bladder cancer cells including cell growth, invasion, migration, and colony formation.
- To assess which IGF signalling pathways (by PI3K/MAPK) may be involved in mediating the actions of IGF-I on cell phenotypes.
- To investigate whether IGF-I induces EMT in bladder cancer cell lines.

5.3 Materials and methods

5.3.1 Cell culture

Two human urinary bladder cancer cell lines including RT4 and T24 were used in this study. They were obtained and cultured as described in section 2.1.

5.3.2 Characterisation and optimisation of the antibodies for the assessment of EMT-related molecules

Changes in the levels as well as localisation of ZEB-1, FOXO3a, FOXA1, and 14-3-3 β in response to IGF-I were investigated in this study. Since the antibodies for these four molecules were new to our laboratory, characterisation and optimisation using Western blotting (WB, as described in section 2.3) were performed initially in RT4 and T24 cell lines by changing the solvent and/or the concentration of the antibody solutions, respectively. GAPDH and tubulin were used as loading controls in WB analyses.

Product details and the conditions optimised for the EMT-related molecules used in this chapter are summarised in Table 26, and details of the reference proteins (GAPDH and tubulin) used as a loading control are shown in Table 2 in section 3.3.2.

Table 26: optimised antibody solutions information of EMT-related molecules for WB

Protein	Size (kDa)	Gel percentage (%)	Company & Cat. No.	Blocking	1° Ab	*2° Ab
ZEB-1	200	8	Cell Signaling (D80D3), #3396	5% BSA	1/1000, 5% BSA, rabbit	1/2000, 5% BSA, anti-rabbit
FOXO3a	80	10	Cell Signaling (75D8), #2497	5% BSA	1/1000, 2% milk, rabbit	1/2000, 2% milk, anti-rabbit
FOXA1	49	12	Abcam, #ab55178	5% milk	1/500, 3% BSA, mouse	1/2000, 3% BSA, anti-mouse
14-3-3 β	28	12	Santa Cruz (k-19), #sc-629	5% milk	1/500, 3% BSA, goat	1/2000, 3% BSA, anti-goat

***2° Ab**: **ZEB-1** & **FOXO3a**: anti-rabbit (Sigma, #A0545); **FOXA1**: anti-mouse (Sigma, #A0944); **14-3-3 β**: anti-goat (Sigma, #A5420).

5.3.3 Antibody solutions for assessment of IGF signalling pathways involved in the study

IGF signalling pathways involved in mediating actions of IGF-I on bladder cancer cells were assessed in this study. The molecules potentially participating in the signalling activities have been identified in our laboratory, and the information of the antibody solutions is listed below in Table 27.

Table 27: antibody solutions information of IGF signalling pathway related molecules for WB

Protein	Size (kDa)	Gel percentage (%)	Company & Cat. No.	Blocking	1° Ab	*2° Ab
IGF-IR	95	10	Cell Signaling #9750	5% BSA	1/1000 5% BSA, rabbit	1/2000 5% BSA, anti-rabbit
Insulin Receptor (IR)	95	10	Santa Cruz Sc-711	5% BSA	1/1000 5% BSA, rabbit	1/2000 5% BSA, anti-rabbit
Phospho-IGF-IR	92	10	Cell Signaling #3024	3% BSA	1/250 3% BSA, rabbit	1/2000 5% milk, anti-rabbit
Akt	60	12	Cell Signaling #9272	5% BSA	1/1000 5% BSA, rabbit	1/2000 5% BSA, anti-rabbit
Phospho-Akt	60	12	Cell Signaling #4060	5% BSA	1/1000 5% BSA, rabbit	1/2000 5% BSA, anti-rabbit
Phospho-MAPK	42, 44	12	Cell Signaling #9101	5% BSA	1/1000 5% BSA, rabbit	1/2000 5% BSA, anti-rabbit
ERK2	42	12	Santa Cruz Sc-154	5% milk	1/1000 5% milk, rabbit	1/2000 5% milk, anti-rabbit

***2° Ab**: anti-rabbit (Sigma, #A0545).

5.3.4 Detection of protein abundance

Levels of target proteins in whole cell lysates were determined by performing WB analyses as described in section 2.3. Tubulin and GAPDH were used as loading controls, and the information of antibody solutions are summarised in Table 26 above and Table 2 in section 3.3.2.

5.3.5 Detection of protein localisation

Cellular fractionation was performed as described in section 2.4 to examine the localisation of target proteins including β-catenin, FOXO3a, FOXA1, and 14-3-3 β.

Proteins of cytoplasmic and nuclear extracts from cultured cells were separated using cellular fractionation. Lamin and tubulin exist only in nuclei and cytoplasm, respectively, and they were therefore used as indicators of the efficiency of protein separation from each fraction. The abundance of separated proteins was detected by WB as described in 5.3.3. The information of antibody solutions of Lamin is listed in Table 24 in 3.3.4 and the information of target proteins and tubulin can be found in Table 26 and Table 23 in section 3.3.2, respectively.

5.3.6 Cell treatment

5.3.6.1 Recombinant human IGF-I

Recombinant human IGF-I (Gropep; receptor grade, #CM001) was made up to a 1000μg/ml stock solution following product instructions, aliquoted and stored at -20°C. A 10μg/ml working stock was made fresh by adding 3μl of stock solution to 297μl of SFM that was diluted further with SFM to achieve final concentrations.

5.3.6.2 AG1024

AG1024 (Santa Cruz, sc-205907) is a selective tyrosine kinase inhibitor (TKI) which inhibits IGF-IR signalling through interfering with its auto-phosphorylation (Kisielewska, Ligeza et al. 2008).

The concentration of stock AG1024 when purchased was 3267.8μM. The stock solution was aliquoted and stored at -20°C. A 200μM working stock was made fresh by adding 18.36μl of stock solution to 281.64μl of SFM which was diluted further with SFM to achieve final concentrations.

5.3.6.3 LY294002

2-(4-morpholinyl)-8-phenyl-chromone (LY294002; Millipore, #440204) is a specific signal transduction molecule inhibitor of PI3K (Zhu, Qi et al. 2011).

10,000μM of LY stock solution was made up by dissolving 1mg LY294002 in 325μl DMSO following the instructions. The stock solution was aliquoted and stored at -20°C. The LY stock solution was then made fresh by adding 3μl of stock solution to 297μl of SFM to make a 50μM final concentration and cells were pre-treated with LY for 30 minutes before treatment with other reagents.

5.3.7 Cell proliferation

A TTI assay was used to measure DNA synthesis, and Trypan Blue Dye Exclusion assay was performed for cell counting to examine both live and dead cells, from which the percentage cell death could be calculated as described in section 2.2.

5.3.8 Cell migration

A cell migration assay was performed as described in section 2.9 to measure differences in cell migration rates in response to relevant treatments.

5.3.9 Cell invasion

A cell invasion assay was used as described in section 2.10 to investigate the differences in cell movement through the extracellular matrix (ECM) under different treatments *in vitro*.

5.3.10 Cell colony formation

A soft agar colony formation assay was used with both RT4 and T24 cells as described in section 2.8 to assess the change in malignant cell transformation in response to IGF-I treatment.

5.3.11 Statistical analysis

Data were expressed as mean ± SEM and analysed with SPSS 23 for Windows using one-way analysis of variance (ANOVA) followed by least significant difference (LSD) post-hoc test and Student's test. A two-sided *p*-value was shown for statistical significance and is depicted as asterisks; a single one for $*p<0.05$ and a double for $**p<0.01$.

5.4 Results

5.4.1 Phenotypic changes observed in bladder cancer cells following IGF-I treatment

RT4 and T24 cells were used to investigate the effects of IGF-I on bladder cancer cell proliferation, invasion, migration and colony formation.

5.4.1.1 Optimisation of an effective dose of IGF-I in RT4 cells

A dose-response to IGF-I (0-200 ng/ml) was performed previously for T24 cells, and changes in cell proliferation were assessed using a TTI assay (described in 4.4.5.2.1). And this indicated that 50ng/ml IGF-I was an effective dose. The same experiment was performed in RT4 cells to assess cell proliferation following the exogenous addition of IGF-I (0-200 ng/ml) for 24 hours.

As shown in Figure 54, an increase in cell proliferation was observed with increasing concentrations of IGF-I, and the maximal increase was found to be at 50ng/ml (by 27%, $p<0.01$). Therefore, this dose was chosen as an effective concentration for further experiments.

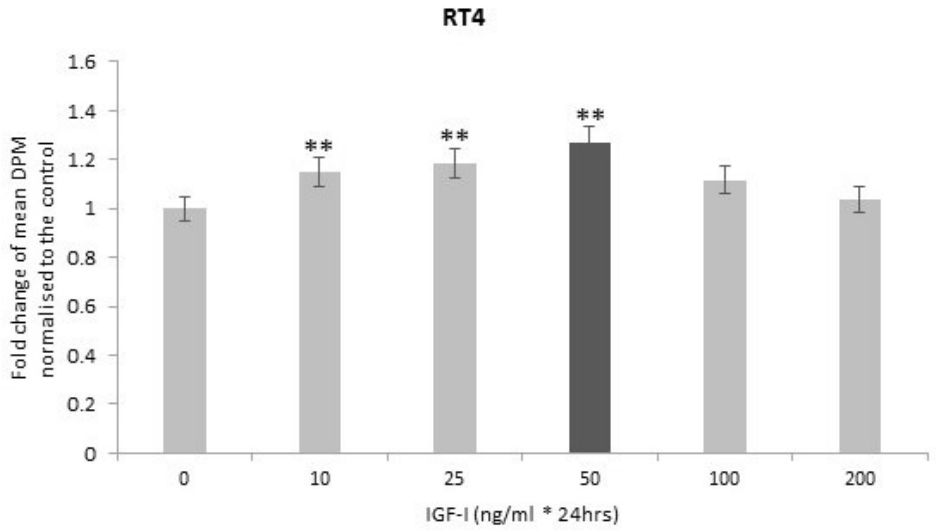

Figure 54: proliferative response to exogenous IGF-I in RT4 bladder cancer cells

RT4 cells were seeded at a density of $0.03x10^6$ cells/well in 24-well plates in GM and allowed to attach and grow for 24 hours followed by serum starvation for another 24 hours. Then TTI was performed to assess the proliferative response to exogenous IGF-I in RT4 cells at 0-200 ng/ml for 24 hours. The graph shows the means of three experiments each performed in quadruplicate, and error bars represent the standard error of the mean of the experiments (n=3). "**": $p<0.01$. The bar in the darker colour represents the chosen effective concentration for further experiments.

5.4.1.2 Effect of adding exogenous IGF-I on cell growth in RT4 and T24 cells

Based on the effective dose of IGF-I determined previously (in 4.4.5.2.1 and above in 5.4.1.1), dosing of exogenous IGF-I was conducted in both RT4 and T24 cells at the concentration of 50ng/ml for 48 hours to assess changes in total cell number by performing cell counting.

In RT4 cells, no significant changes were found between control and IGF-I-treated cells either in total or live cell number (Figure 55-**A**) or the percentage of cell death (Figure 55-**B**).

However, compared to untreated cells, IGF-I-treated T24 cells showed a significant increase both in total cell number (by 20.8%, $p<0.05$) and in live cell number (by 19.5%, $p<0.05$) (Figure 55-**C**). No significant change in percentage cell death was observed between control and treated cells (Figure 55-**D**).

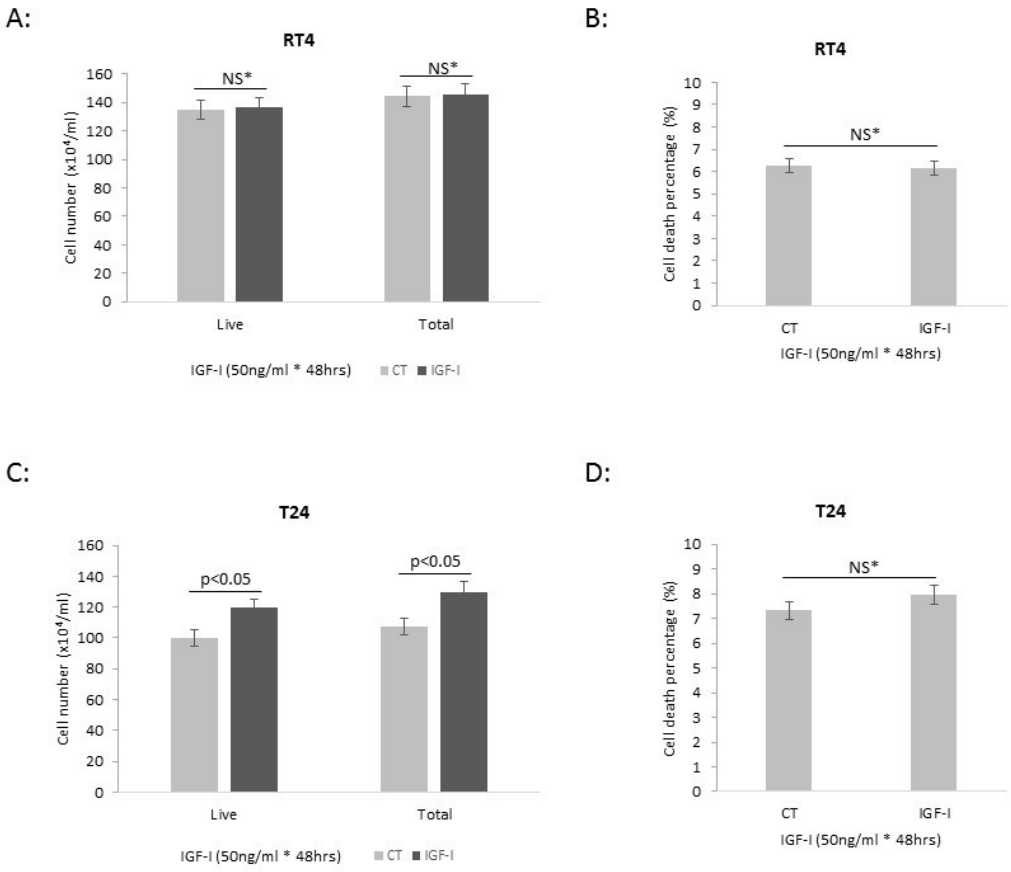

Figure 55: effect of dosing exogenous IGF-I on cell growth in RT4 and T24 cells

RT4 and T24 cells were seeded into 6-well plates in GM at a density of $0.1x10^6$ cells/well and $0.05x10^6$/well, respectively. After 24 hours of serum starvation, cells were labelled according to different treatments ("CT" for control group without any treatment and "IGF-I" for IGF-I treated cells at a concentration of 50ng/ml for 48 hours).

(**A**) & (**C**): Graphs show the cell counting of both live and total cell numbers under different treatments in RT4 and T24 cells, respectively. (**B**) & (**D**): Graphs represent the change in the percentage of cell death due to different treatments in RT4 and T24, respectively. The graphs present the mean of three experiments each performed at least in triplicate, and error bars represent the standard error of the mean of the experiments (n=3). "NS*": not significant.

5.4.1.3 Effect of adding exogenous IGF-I on cell invasion of RT4 and T24 cells

An invasion assay was conducted to assess the effect of adding IGF-I on the ability of RT4 and T24 cells to invade.

With the treatment of IGF-I, both RT4 and T24 cells exhibited an increase in the numbers of invaded cells compared with control cells (Figure 56-**A** for RT4 and Figure 56-**C** for T24 cells), and the increase was significant in both RT4 (by 46.9% in Figure 56-**B**) and T24 (by 111.6% in Figure 56-**D**) cells.

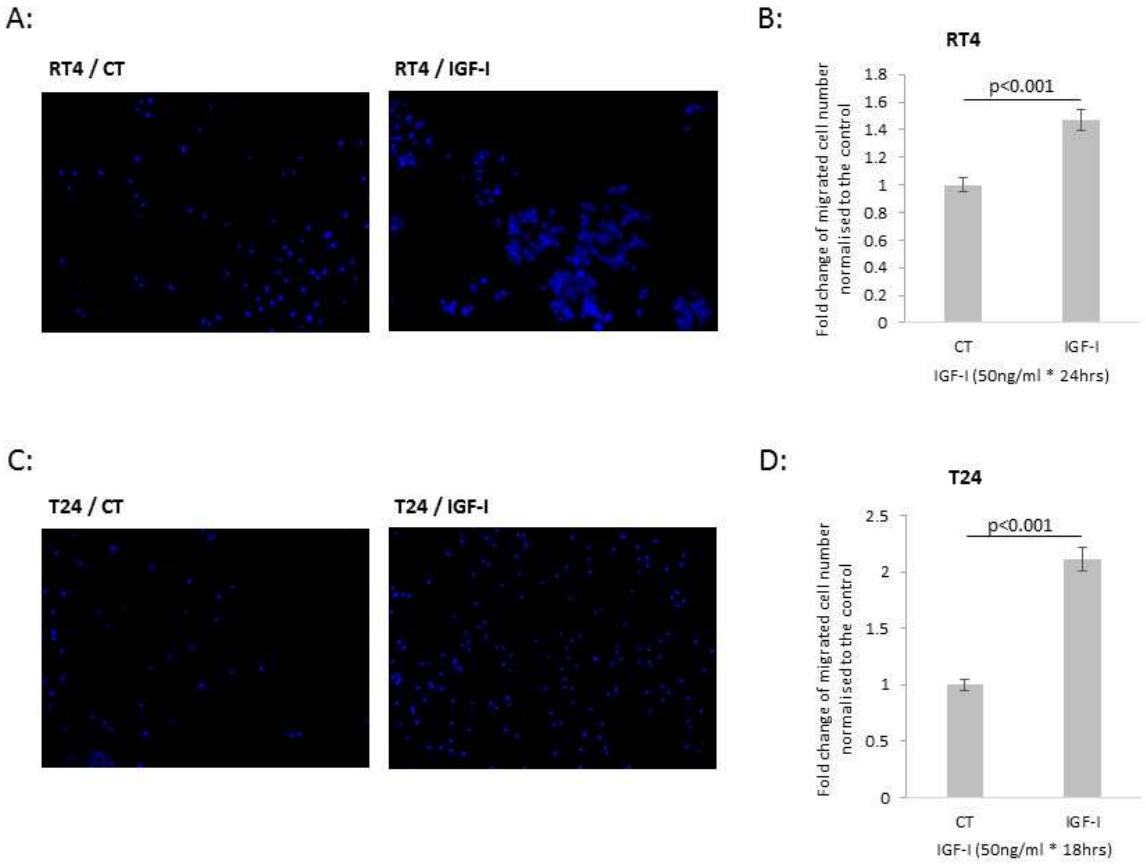

Figure 56: effect of adding exogenous IGF-I on cell invasion of RT4 and T24 cells

Both cell lines were previously seeded in GM for 24 hours and then changed to SFM for 16 hours before being prepared for an invasion assay. After serum-starvation, both RT4 and T24 cells were trypsinised and then seeded into the collagen-coated inserts at a certain density (RT4: $0.1x10^6$ cells/insert and T24: $0.08x10^6$ cells/insert) and allowed to invade (RT4: 24 hours and T24: 18 hours). Cells were labelled according to different treatments while seeding ("CT" for control cells without treatment, and "IGF-I" for cells treated with IGF-I at the concentration of 50ng/ml).

(A) & (**C**): The images show invaded RT4 and T24 cells, respectively, with nuclei (in blue) stained with DAPI. All images shown are at x10 magnification. (**B**) & (**D**) The graphs show the fold change of invaded RT4 and T24 cells, respectively, between exogenous IGF-I treatment group and control group. The graphs represent the mean of three experiments each performed in triplicate, upon which the standard error of the mean of the experiments was presented (n=3).

5.4.1.4 Effect of adding exogenous IGF-I on cell migration in RT4 and T24 cells

A migration assay was performed to examine the effect of IGF-I on cell migration in RT4 and T24 cells.

As characterised in the previous chapter (see 3.4.3.4 in chapter 3), RT4 cells did not migrate with or without IGFBP-2. With the treatment of IGF-I, still, no cell migration was observed compared to the control cells (see Figure 57).

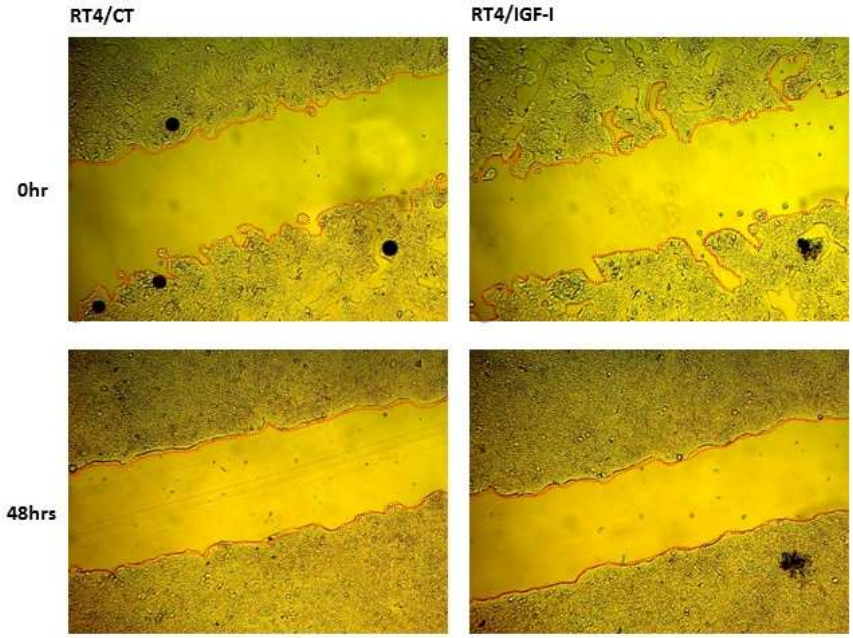

Figure 57: effect of adding exogenous IGF-I on cell migration in RT4 cells

RT4 cells were seeded at a density of $0.049x10^6$ cells into each chamber in GM and allowed to grow for approximately 24 hours to reach about 80% confluence. Cells reached 90-95% confluence during an additional 24 hours in SFM. The inserts were removed leaving an observed gap, and gap closure was recorded for up to 48 hours with different treatment ("CT": untreated cells as a control group; "IGF-I": cells treated with IGF-I at the concentration of 50ng/ml).

Images of cell gaps were taken at different times with relative labels. "0hr": the start point after the removal of inserts; "48hrs": 48 hours after the removal of inserts. All images demonstrate the typical results from three experiments each performed in duplicate (n=3). All images shown are at x10 magnification, and the area of the gaps in the images was analysed using ImageJ software.

In T24 cells, cells treated with IGF-I moved faster than the control group with the gap being significantly reduced at the sixth ($p<0.001$), ninth ($p<0.01$) and twelfth ($p<0.001$) hour (Figure 58-**A** & **B**).

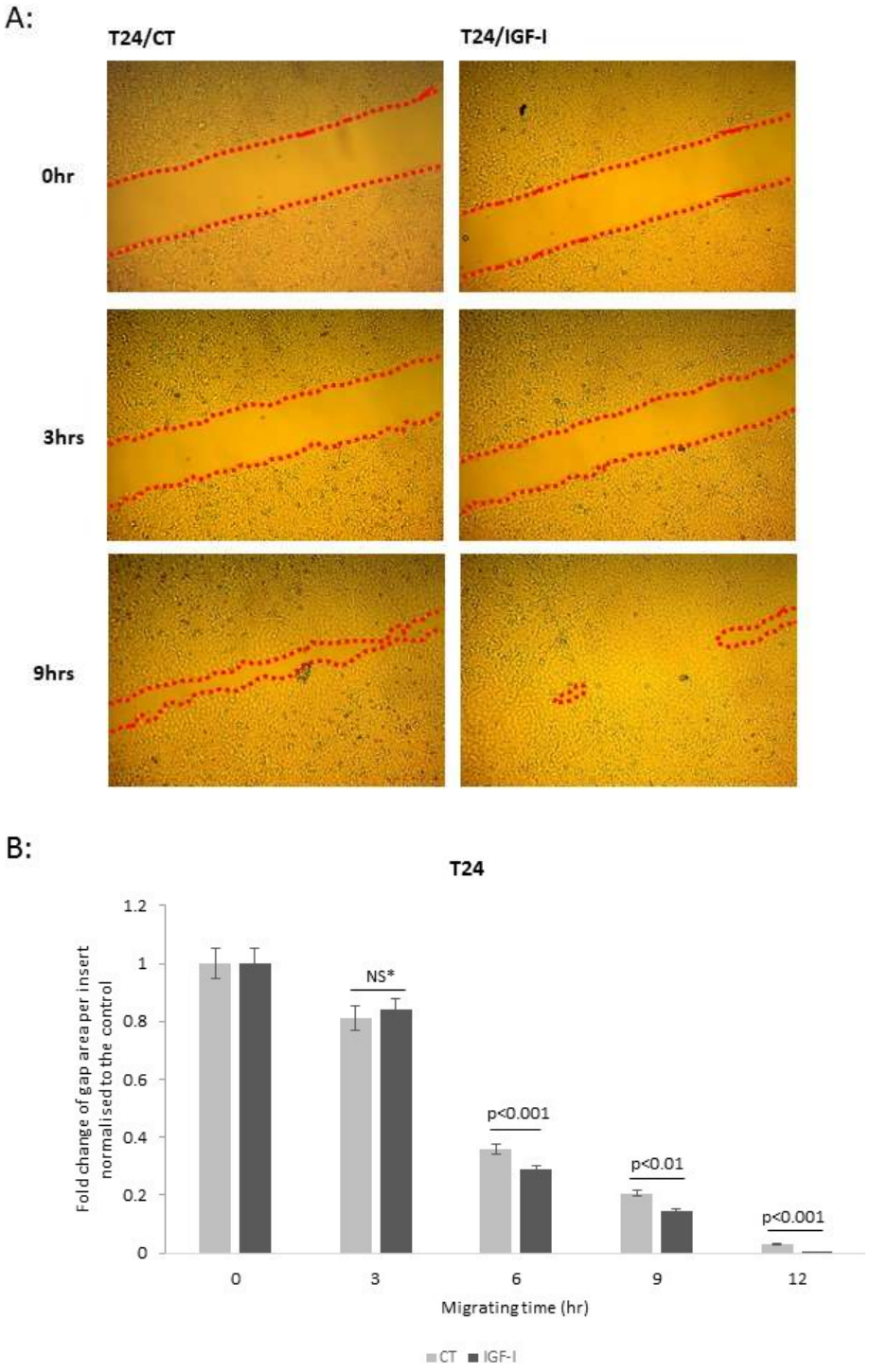

Figure 58: effect of adding exogenous IGF-I on cell migration in T24 cells

T24 cells were seeded at a density of $0.028x10^6$ cells into each chamber in GM and allowed to grow for approximately 24 hours to reach about 80% confluence. Cell reached 90-95% confluence during an additional 24 hours in SFM. The inserts were removed leaving an observed gap, and gap closure was recorded for up to 12 hours with different treatment ("CT": untreated cells as a control group; "IGF-I": cells treated with IGF-I at the concentration of 50ng/ml).

Images of cell gaps were taken at different times with relative labels. "0hr": the start point after the removal of inserts; "3hr", "4hr", "6hr", "9hr" and "12hr": 3, 4, 6, 9 and 12 hours after the removal of inserts. All images demonstrate the typical results from three experiments each performed in duplicate (n=3). All images shown are at x10 magnification, and the area of the gaps in the images was analysed using ImageJ software.

(**A**) shows the images of the gaps between cell patches of T24 cells with different treatments at the start point ("0hr"), 4 hours ("4hrs"), and 12 hours ("12hrs") after the removal of inserts. The red dashed lines present the outline of migrating T24 cells moving together. (**B**) shows the fold change of gap area per insert normalised to control with exogenous IGF-I treatment in T24 cells. The graph represents the mean of three experiments each performed in duplicate, with the standard error of the mean of the experiments (n=3). "NS*": not significant.

5.4.1.5 Effect of adding exogenous IGF-I on cell colony formation in RT4 and T24 cells

A soft agar colony formation assay was conducted to assess the effect of IGF-I on the ability of RT4 and T24 cells to form colonies in soft agar.

Visually, compared with control groups, both RT4 (Figure 58-**A**) and T24 (Figure 58-**D**) cells formed more and larger colonies with the treatment of IGF-I.

Statistically, the average size of each colony formed was significantly increased in IGF-I-treated cells in both cell lines with the fold change in IGF-I-treated RT4 and T24 cells being 1.31 ($p<0.05$) (Figure 58-**C**) and 1.13 ($p<0.05$) (Figure 58-**F**), respectively, compared with the control cells. As to colony forming efficiency (CFE), a significant induction of 59.4% ($p<0.01$) (Figure 58-**E**) was found in IGF-I-treated T24 cells compared with control cells. However, no significant change was found in RT4 cells (Figure 58-**B**).

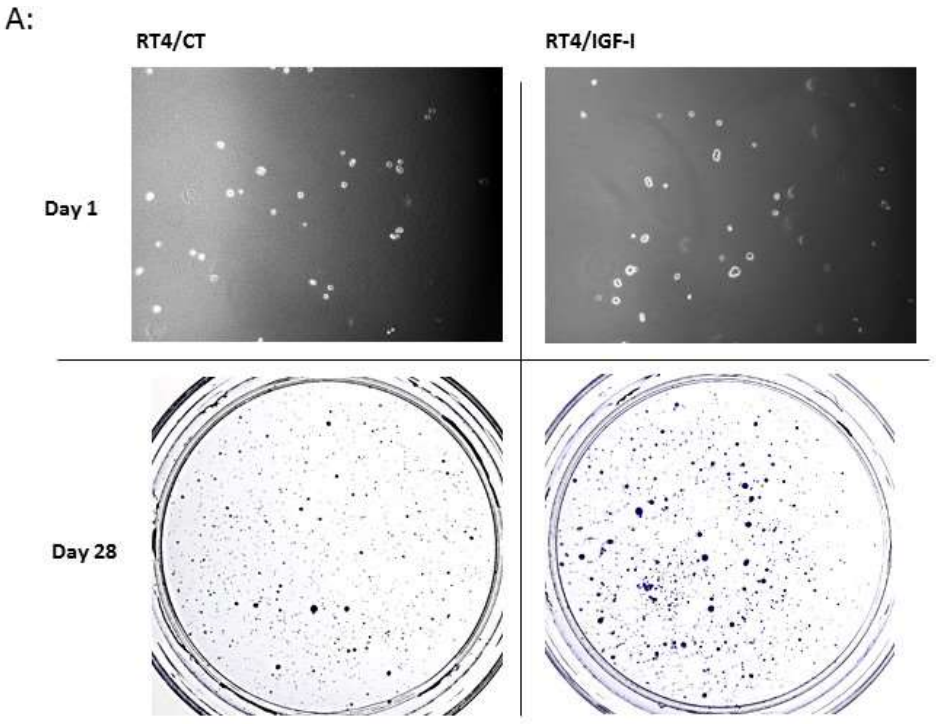
A:
RT4/CT
RT4/IGF-I
Day 1
Day 28

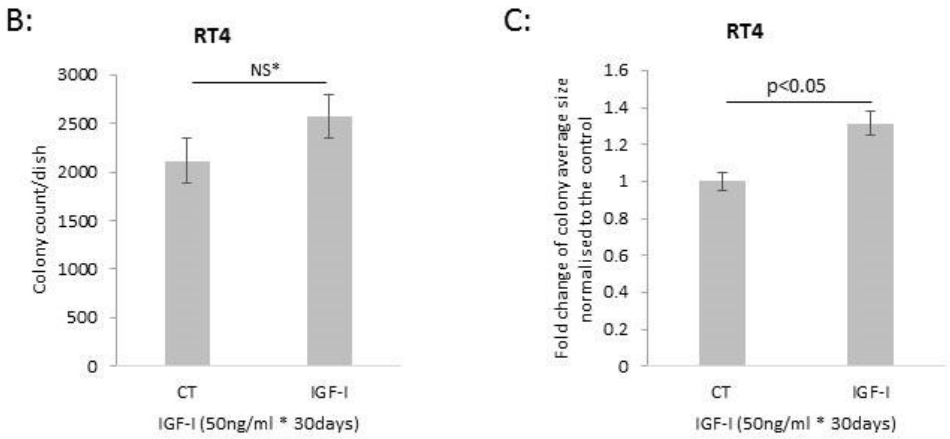
B:
RT4
NS*
Colony count/dish
3000
2500
2000
1500
1000
500
0
CT
IGF-I
IGF-I (50ng/ml * 30days)
C:
RT4
p<0.05
Fold change of colony average size normalised to the control
1.6
1.4
1.2
1
0.8
0.6
0.4
0.2
0
CT
IGF-I
IGF-I (50ng/ml * 30days)

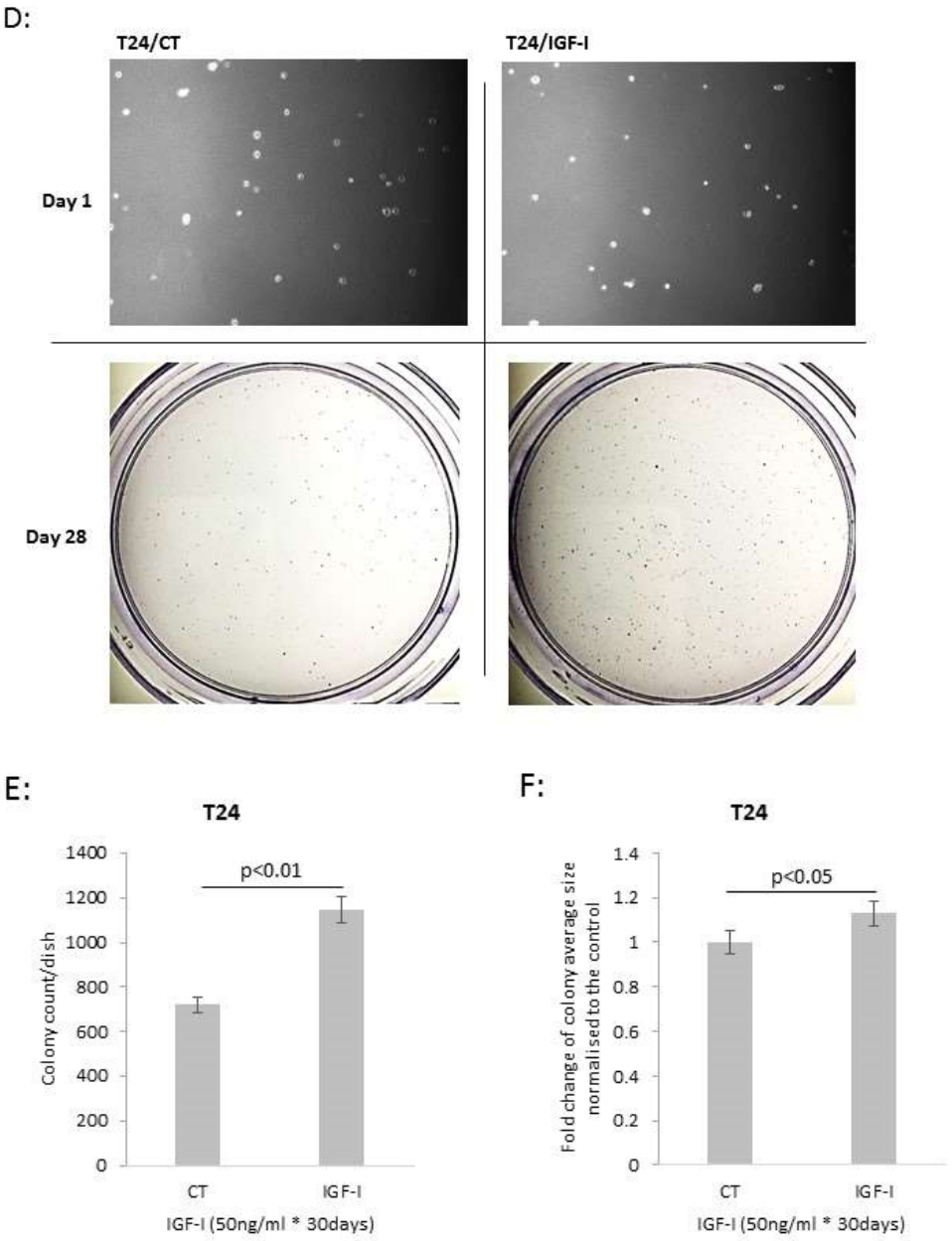

Figure 59: effect of adding exogenous IGF-I on formation of colonies by RT4 and T24 cells in soft agar

Both RT4 and T24 cells were seeded in dishes under different treatments with corresponding labels ("CT": untreated cells as a control group; "IGF-I": cells treated with IGF-I at the concentration of 50ng/ml 48 hours before seeding). Cells were seeded at an even density at 10,000 cells/dish and 5,000 cells/dish, respectively, and fed once a week for four weeks in total, and then colony numbers, as well as average size, were measured by ImageJ software.

(**A**) & (**D**): Images show RT4 and T24cells, respectively, were set up into dishes with even densities at the first day ("Day 1"), and colonies were stained at the end of the assay ("Day 28"). All images shown are at x10 magnification; (**B**) & (**E**): Graphs present the change of colony count per dish under different treatments for RT4 and T24 cells, respectively. (**C**) & (**F**): Graphs demonstrate the fold change of average size of colonies due to different treatments for RT4 and T24 cells, respectively. All graphs present the mean of three experiments each performed in triplicate, and error bars represent the standard error of the mean from three experiments (n=3).

5.4.2 Assessment of the IGF signalling pathway involved in mediating the actions of IGF-I on cell phenotype in bladder cancer cells

Assessment of activation, as well as specific inhibition, of IGF/PI3K/Akt and IGF/MAPK/ERK signalling pathways, was carried out to investigate how IGF-I induced phenotypic changes in bladder cancer.

5.4.2.1 Characterisation of IGF/PI3K/Akt and IGF/MAPK/ERK signalling pathways

I characterised the basal abundance of IGF-IR and IR in both RT4 and T24 cells and treated both cell lines with exogenous IGF-I for 5, 10, and 30 minutes, respectively, to assess IGF-IR activation by monitoring phosphorylation of the IGF-IR, of Akt and MAPK - key downstream molecules of the IGF-IR.

Both the IGF-IR and IR were expressed in both bladder cancer cell lines being more abundant in RT4 than that in theT24 cells (see Figure 60).

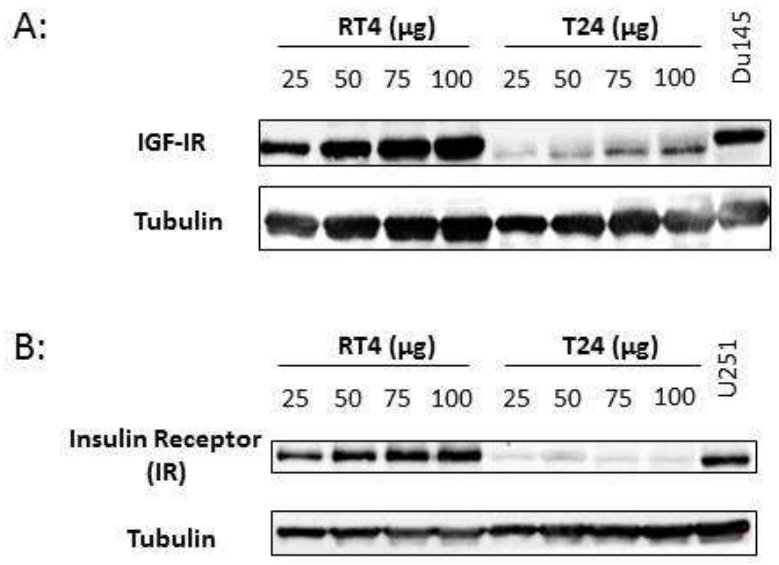

Figure 60: characterisation of the levels of IGF-IR and IR in RT4 and T24 cells

(**A**) and (**B**) show the western blots for IGF-IR and IR, respectively, in both RT4 and T24 cells detected using WB. RT4 and T24 cells were seeded in GM at the same density to grow for 24 hours and then were left in SFM for 48 hours before sample harvest. Proteins in whole lysates were loaded with increasing amounts from 25 to 100µg. Proteins from Du145 (a human prostate carcinoma cell line) and U251 (a human glioblastoma cell line) cell lysates were used as positive controls for IGF-IR and IR, respectively. They were loaded equally at 60µg. Tubulin was used as the reference protein.

As shown in Figure 61, in response to IGF-I treatment (up to 30 minutes), activation of phosphorylation of the IGF-IR was observed in RT4 cells from 5 minutes to 30 minutes with the total amount of the IGF-IR being significantly decreased at the 30-minute time point. In T24 cells, the activation of the IGF-IR (p-IGF-IR) was not stimulated until 30 minutes by IGF-I treatment, but the total amount of the IGF-IR was decreased from 5 minutes to 30 minutes.

Both RT4 and T24 cells expressed Akt, and a significant increase in activated Akt (p-Akt) activation from 5 to 30 minutes was shown in both cell lines in response to IGF-I treatment, with no changes observed in the total amount of Akt (see Figure 61).

MAPK presents as a double band with p44 (ERK 1) and p42 (ERK 2) which can be phosphorylated through activation of loop residues Thr202/Tyr204 and Thr185/Tyr187, respectively. ERK 2 was measured in this study to represent the total amount of MAPK. As shown in Figure 61, no activation of phospho-MAPK (p-MAPK) or changes in the levels of ERK 2 was observed in either RT4 or T24 cells following treatment with IGF-I.

Therefore, the IGF-IR/PI3K/Akt appears to be a dominant signalling pathway associated with the actions of IGF-I on bladder cancer cells, with the MAPK/ERK axis not seeming to be playing a role.

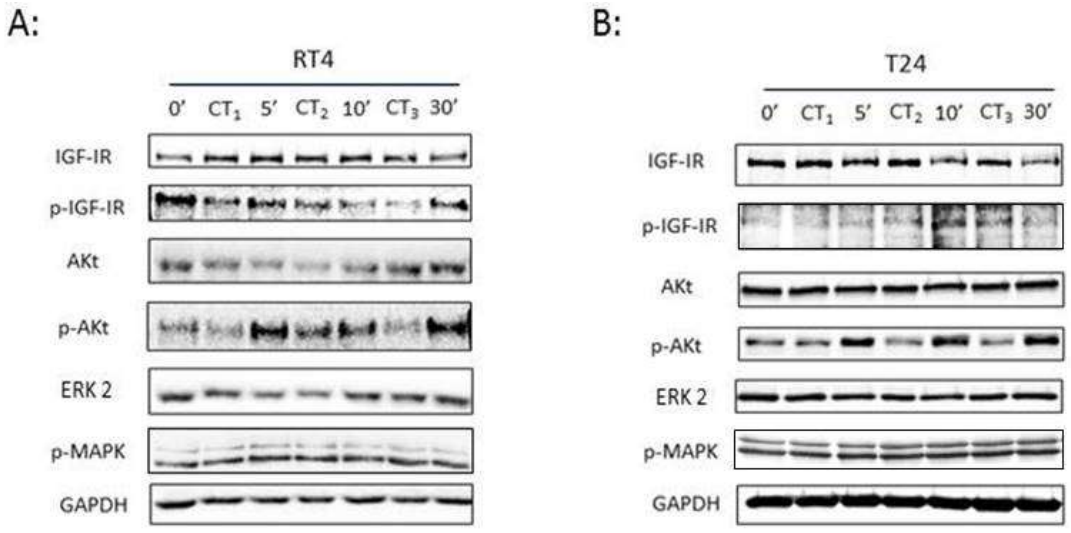

Figure 61: analysis of IGF-IR activation in RT4 and T24 cells following treatment with IGF-I at 50ng/ml for 5, 10 and 30 minutes, respectively, using WB

RT4 and T24 cells were seeded in 6-well plates at a density of 0.1 and $0.05x10^6$ cells/well, respectively, in GM for 24 hours and serum starved with SFM for another 24 hours. Then cells were separated according to different treatments ("0'": untreated cells harvested at the beginning of the experiment as a control group; "CT_1", "CT_2" and "CT_3": untreated cells harvested along with IGF-I-treated cells for 5, 10, and 30 minutes, respectively, as a control; "5'", "10'" and "30'": cells treated with IGF-I at 50ng/ml for 5, 10, and 30 minute, respectively). Samples from harvested cells were used to investigate the changes in protein abundance of molecules involved in IGF signalling using WB ("p-Akt": phospho-Akt; "p-MAPK": phospho-MAPK). Proteins in whole lysates were loaded equally at 60µg with GAPDH being used as the reference protein. All blots demonstrate typical results from three experiments each performed at least in triplicate (n=3).

5.4.2.2 Effects of inhibition of IGF/PI3K/Akt signalling pathway

Having identified in both cell lines that activation of the IGF-IR was associated with increased phosphorylation of the IGF-IR and Akt, a specific IGF-IR tyrosine kinase inhibitor (TKI), AG1024, and a specific PI3K inhibitor LY294002, were used to examine whether the effects of IGF-I on cell phenotype were mediated by these changes in signalling molecules.

5.4.2.2.1 Effects of inhibiting the IGF-IR on bladder cancer cell phenotype

Alterations in cell proliferation, invasion, migration and colony formation were assessed to examine the effects of inhibiting the IGF-IR using AG1024, a specific IGF-IR inhibitor, on bladder cancer cells.

5.4.2.2.1.1 Optimisation of an effective dose of AG1024 in RT4 and T24 cells

A TTI assay was used in RT4 and T24 cells to assess cell proliferation following treatment with AG1024 (0-10 μM) for 24 hours.

As shown in Figure 62, a decrease in cell proliferation in response to a dose of increasing concentrations of AG1024 was observed in both RT4 and T24 cells. At a dose of AG1024 at 1.25μM, a reduction of 63.7% ($p<0.01$) and 55.7% ($p<0.01$) was found in RT4 and T24 cells, respectively. As both cell lines were maximally inhibited by 96% ($p<0.01$) at 2.5μM, 2μM was selected as an effective concentration for further experiments.

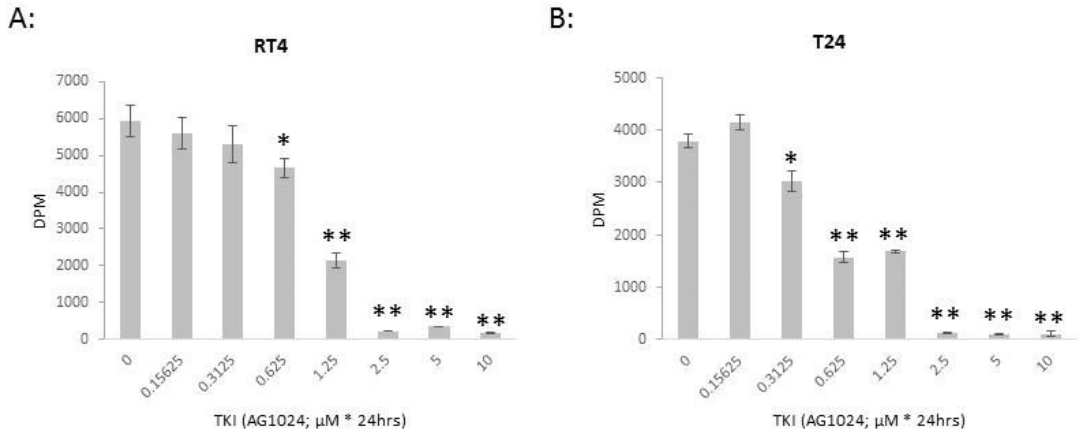

Figure 62: assessment of the proliferative response to AG1024 in RT4 and T24 bladder cancer cells using TTI

RT4 and T24 cells were seeded at a density of 0.03 and 0.02x10^6 cells/well into 24-well plates in GM to grow for 24 hours followed by serum starvation for another 24 hours. Then both cell lines were dosed with AG1024 at 0-10 µM for 24 hours, and TTI was performed to show the proliferative response to AG1024 in RT4 (**A**) and T24 (**B**) cells.

The graphs represent the mean of three experiments each performed in quadruplicate, and error bars represent the standard error of the mean of the experiments (n=3). "*": $p<0.05$; "**": $p<0.01$.

5.4.2.2.1.2 Characterisation of the effectiveness of AG1024

Based on the chosen dose of AG1024 determined above, both RT4 and T24 cells were treated with a short exposure to IGF-I at 50ng/ml for 10 minutes with or without 1 hour of pre-treatment with AG1024 at 2µM.

As shown in Figure 63-**A**, activation of phospho-IGF-IR (p-IGF-IR) by IGF-I was clearly observed in both RT4 and T24 cells without the pre-treatment of TKI. When pre-dosing TKI for 1 hour, the ability of IGF-I to activate its receptor was attenuated in both cell lines. Similar activation of phospho-Akt (p-Akt) by IGF-I was observed in both cell lines with more abundance shown in T24 cells. Moreover, no changes were observed in phospho-MAPK (p-MAPK) in either cell line.

No obvious changes in the total amount of the IGF-IR, Akt and ERK 2 were found in either RT4 or T24 cells (see Figure 63-**B**).

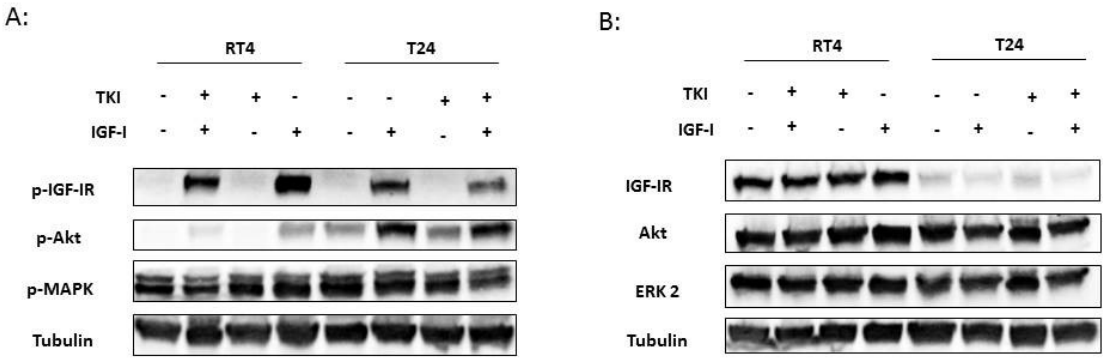

Figure 63: effect of AG 1024 on the activation of IGF-IR in RT4 and T24 cells

RT4 and T24 cells were seeded at a density of 0.1 and 0.05x10^6 cells/well into 6-well plates in GM to grow for 24 hours followed by serum starvation for another 24 hours. Cells were then pre-dosed with or without AG1024 ("TKI", IGF-IR tyrosine kinase inhibitor) at 2μM for 1 hour before spiked with or without IGF-I (50ng/ml) for 10 minutes. Samples from harvested cells were used to investigate the changes in protein abundance of molecules involved in IGF signalling using WB ("p-IGF-IR": phospho-IGF-IR; "p-Akt": phospho-Akt; "p-MAPK": phospho-MAPK). Proteins in whole lysates were loaded equally at 60μg with Tubulin being used as the reference protein. All blots demonstrate typical results from three experiments each performed at least in triplicate (n=3).

5.4.2.2.1.3 Effect of inhibiting the IGF-IR on cell proliferation in RT4 and T24 cells

Both RT4 and T24 cells were treated with IGF-I at 50ng/ml for 48 hours with or without pre-treatment of AG1024 at 2μM for 1 hour to assess the effects on cell proliferation upon inhibition of the IGF-IR.

With RT4 cells, no significant changes in either total cell number (see Figure 64-**A**) or percentage cell death (see Figure 64-**B**) were found when cells were treated with IGF-I ("IGF-I"), AG1024 ("TKI") alone or in combination ("TKI+IGF-I") compared to the control cells ("CT").

In T24 cells, compared to control cells ("CT"), a dose of IGF-I alone ("IGF-I") induced a significant increase in total cell number (by 22.7%, $p<0.05$; see Figure 64-**C**). Both the treatment of AG1024 alone ("TKI") and in combination with IGF-I ("TKI+IGF-I") led to a significant decrease in total cell number (by 22.2%, $p<0.05$ and 20.6%, $p<0.05$, respectively; see Figure 64-**C**) compared with the control cells ("CT"), associated with a similar increase in percentage cell death by 40% ($p<0.05$) (see Figure 64-**D**), suggesting that IGF-I could not increase growth when the receptor was inhibited, and that inhibition of the IGF-IR alone reduced cell growth by promoting cell death.

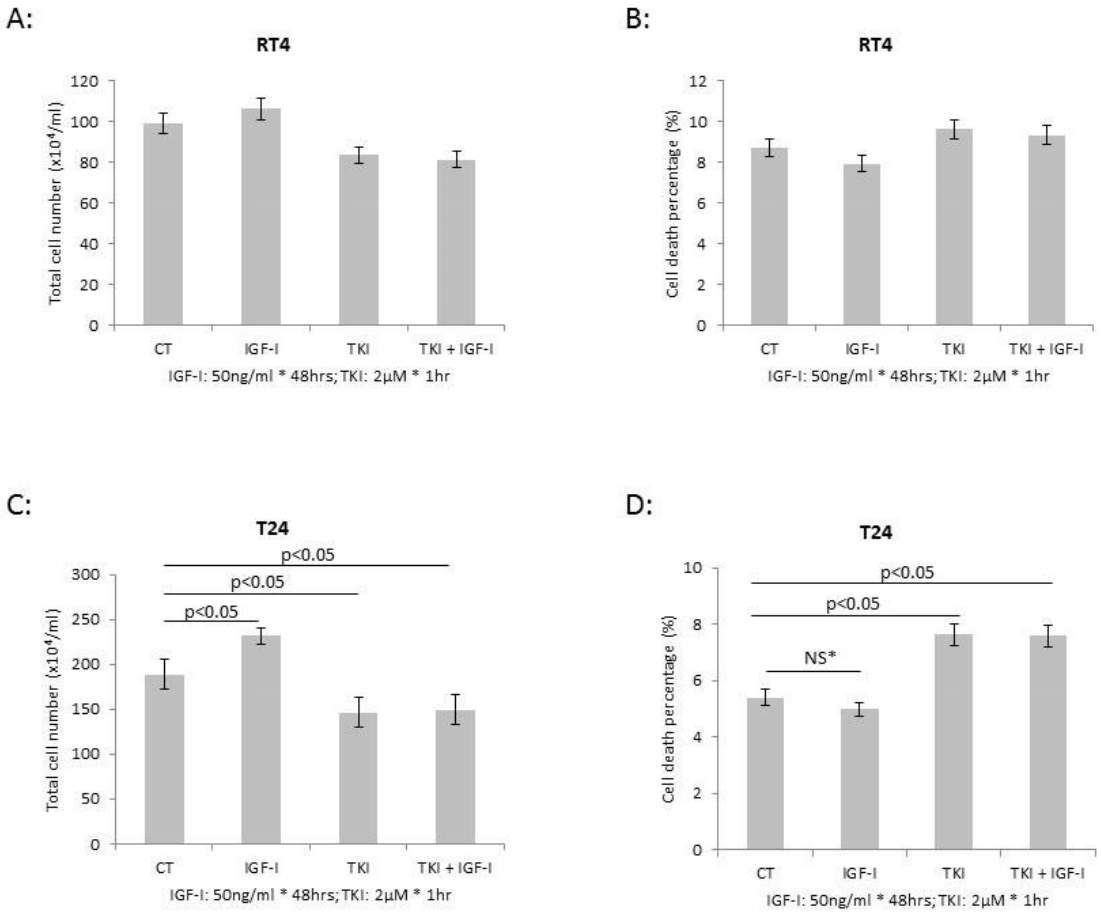

Figure 64: effect of AG1024 and IGF-I on cell proliferation in RT4 and T24 cells

RT4 and T24 cells were seeded at a density of 0.1 and 0.05x10^6 cells/well into 6-well plates in GM to grow for 24 hours followed by serum starvation for another 24 hours. Cells were then dosed with IGF-I (at 50ng/ml) with or without 1 hour of pre-dose of AG1024 at a concentration of 2μM. "CT": control cells without treatment; "IGF-I": cells treated with IGF-I alone at a concentration of 50ng/ml for 48 hours; "TKI": cells treated with AG1024 ("TKI", IGF-IR tyrosine kinase inhibitor) alone at 2μM for 48 hours; "TKI+IGF-I": cells dosed with 1 hour of pre-treatment of AG1024 at the concentration of 2μM followed by addition of IGF-I at 50ng/ml for 48 hours.

Graphs represent the change in the counting of total cell numbers (**A** & **C**) and the percentage cell death (**B** & **D**) following different treatments in RT4 and T24 cells, respectively. The graphs show the mean of three experiments each performed at least in triplicate, and error bars represent the standard error of the mean of the experiments (n=3). "NS*": not significant.

5.4.2.2.1.4 Effect of inhibiting the IGF-IR on cell invasion in RT4 and T24 cells

An invasion assay was conducted to assess the effect of dosing with AG1024 to inhibit the IGF-IR on the ability of RT4 and T24 cells to invade in response to IGF-I.

As shown previously in 5.4.1.3, dosing with IGF-I alone ("IGF-I") induced a significant increase in cell invasion in both RT4 (by 56.1%, $p<0.01$; see Figure 65-**B**) and T24 cells (by 93.1%, $p<0.01$; see Figure 65-**D**). Treatment of AG1024 alone ("TKI") led to a significant decrease in cell invasion in both RT4 (by around 50%, $p<0.01$; see Figure 65-**B**) and T24 cells (by around 50%, $p<0.01$; see Figure 65-**D**) and in combination ("TKI+IGF-I") the ability of IGF-I to increase invasion in both cell lines was blocked.

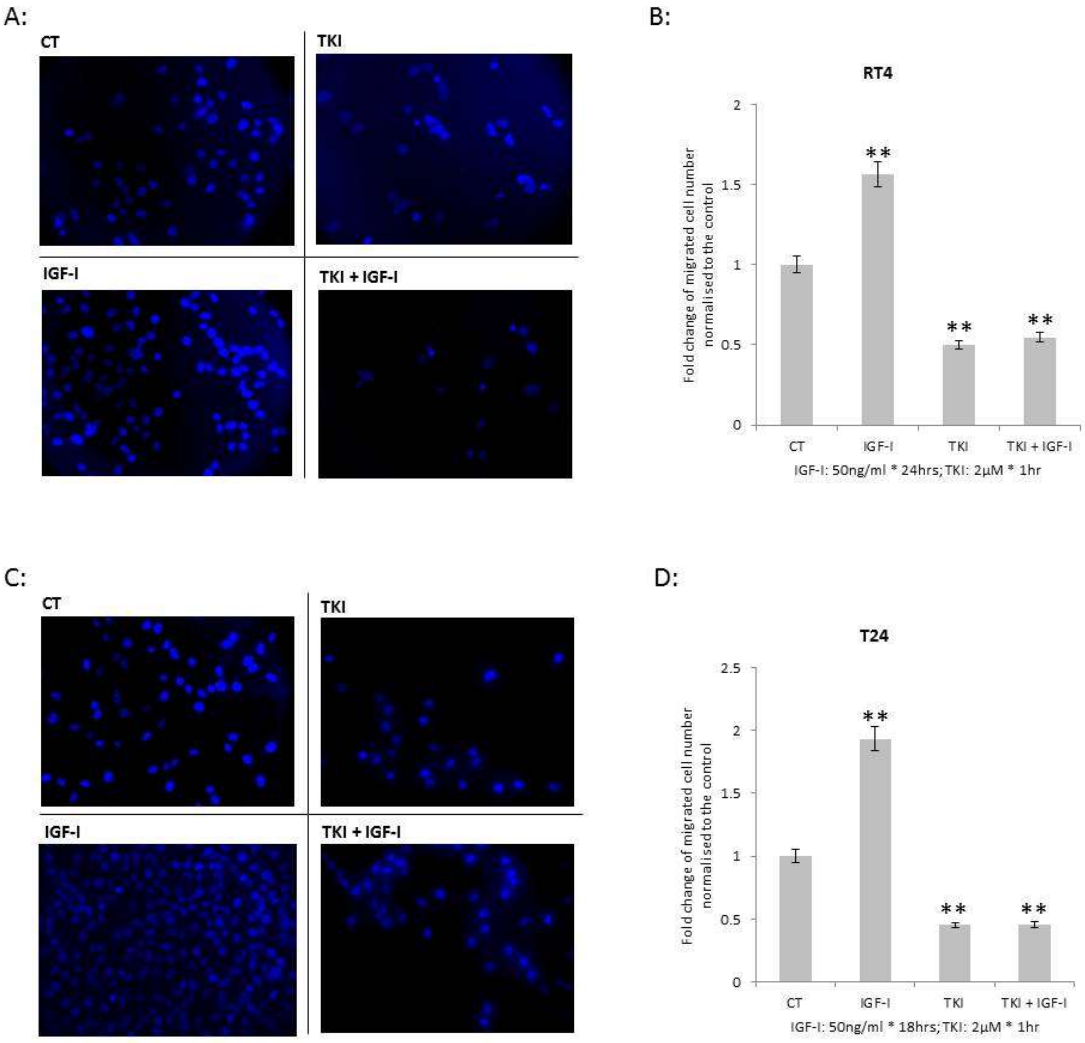

Figure 65: effect of AG1024 and IGF-I on cell invasion in RT4 and T24 cells

Cells of both cell lines were previously seeded in GM for 24 hours and then changed to SFM for 16 hours before being prepared for an invasion assay. After serum-starvation, 1 hour of pre-treatment of AG1024 at a concentration of 2μM was performed in both cells accordingly. Cells were then trypsinised and then seeded into the collagen-coated inserts at a certain density (RT4: 0.1x106 cells/insert and T24: 0.08x106 cells/insert) and allowed to invade (RT4: 24 hours and T24: 18 hours). Cells were labelled according to different treatments while seeding : "CT": control cells without treatment; "IGF-I": cells treated with IGF-I alone at a concentration of 50ng/ml (RT4: 24 hours and T24: 18 hours); "TKI": cells treated with AG1024 ("TKI", IGF-IR tyrosine kinase inhibitor) alone at 2μM (RT4: 25 hours and T24: 19 hours); "TKI+IGF-I": cells dosed with 1 hour of pre-treatment of AG1024 at the concentration of 2μM followed by addition of IGF-I at 50ng/ml (RT4: 24 hours and T24: 18 hours).

(**A**) & (**C**): The images show invaded RT4 and T24 cells, respectively, with nuclei (in blue) stained with DAPI. All images shown are at x40 magnification. (**B**) & (**D**) The graphs show the fold change of invaded RT4 and T24 cells, respectively, normalised to the control group. The graphs represent the mean of three experiments each performed in triplicate, upon which the standard error of the mean of the experiments was presented (n=3). "*": $p<0.05$; "**": $p<0.01$.

5.4.2.2.1.5 Effect of inhibiting the IGF-IR on cell migration in T24 cells

A migration assay was performed to investigate the effect of inhibiting the IGF-IR using AG1024 on cell migration in T24 cells in response to IGF-I.

As determined previously in 5.4.1.4, the treatment of IGF-I alone ("IGF-I") enhanced cell migration causing the gap to close faster compared with the control group (see Figure 66-**B**). In contrast, compared to the control, the dosing of AG1024 alone ("TKI") led to a slower decrease in the gap area, this was unaffected following the addition of IGF-I ("TKI + IGF-I") (Figure 66-**B**).

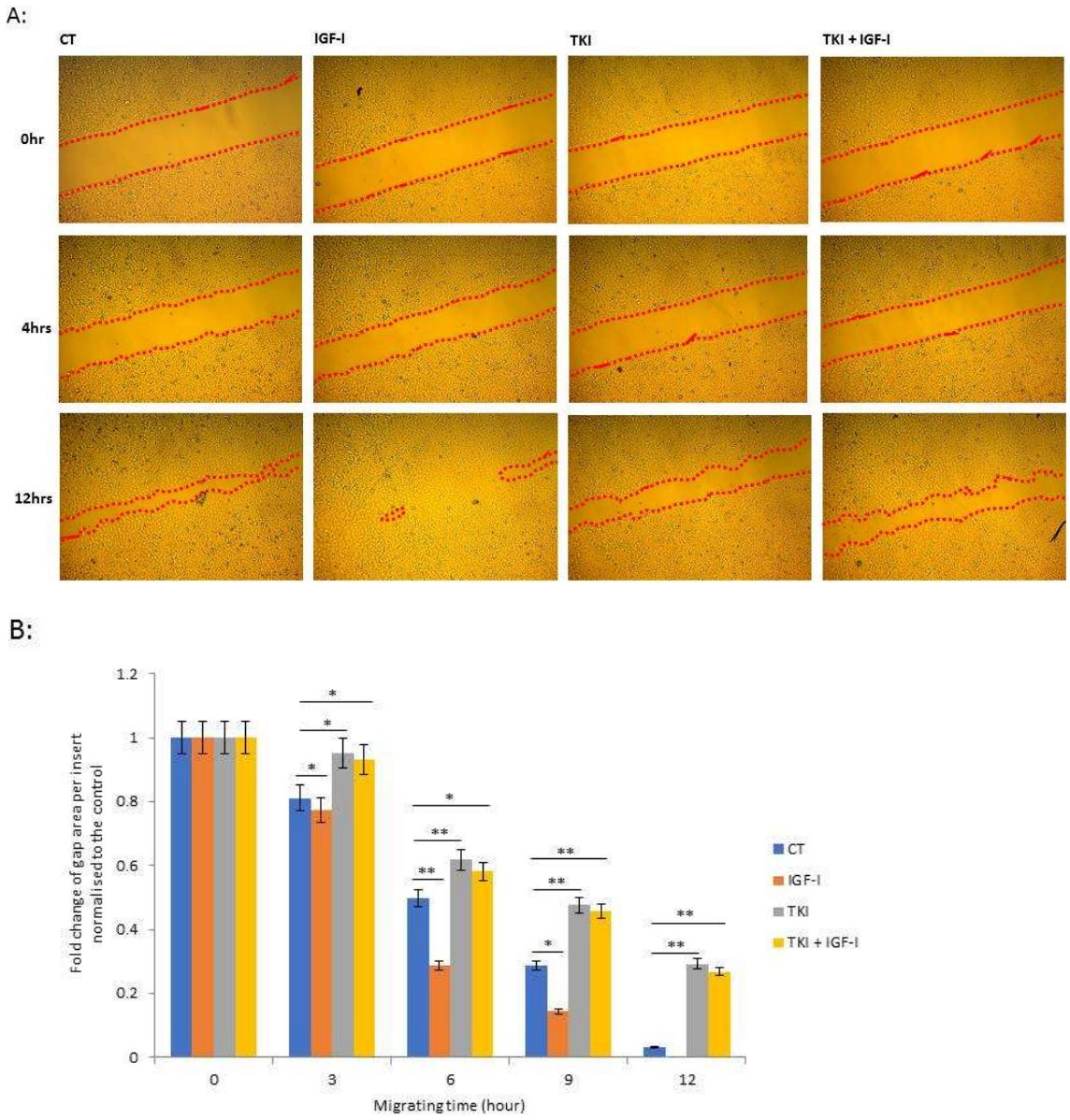

Figure 66: effect of AG1024 and IGF-I on cell migration in T24 cells

T24 cells were seeded at a density of $0.028x10^6$ cells into each chamber in GM and allowed to grow for approximately 24 hours to reach about 80% confluence. Cell reached 90-95% confluence during an additional 24 hours in SFM. After 1 hour of pre-dosing with fresh SFM or AG1024 at 2μM, the inserts were removed leaving an observed gap, and gap closure was recorded for up to 12 hours with different treatment ("CT": untreated cells as a control group; "IGF-I": cells treated with IGF-I alone at the concentration of 50ng/ml; "TKI": cells treated with AG1024 alone at the concentration of 2 μM; "TKI+IGF-I": cells dosed with 1 hour of pre-treatment of AG1024 at the concentration of 2μM followed by addition of IGF-I at 50ng/ml).

Images of cell gaps were taken at different times with relative labels. "0hr": the start point after the removal of inserts; "3hr", "4hr", "6hr", "9hr" and "12hr": 3, 4, 6, 9 and 12 hours after the removal of inserts. All images demonstrate the results from three experiments performed in duplicate (n=3). All images shown are at x10 magnification, and the area of the gaps in the images was analysed using ImageJ software. "*": $p<0.05$; "**": $p<0.01$.

5.4.2.2.1.6 Effect of inhibiting the IGF-IR on cell colony formation in RT4 and T24 cells

A soft agar colony formation assay was performed to assess the effect of inhibiting the IGF-IR on the ability of RT4 and T24 cells to form colonies in response to IGF-I.

In RT4 cells, the treatment of IGF-I alone ("IGF-I") induced a significant increase in the average size of each colony formed (with the fold change of colony average size normalised to the control increased by 37%, $p<0.05$, see Figure 67-C), but no significant changes in the colony forming efficiency, "CFE" compared to the control (see Figure 67-**B**). Dosing with AG1024 alone ("TKI") led to a significant decrease in both fold change of CFE (by 38%, $p<0.01$; see Figure 67-**B**) and average colony size (by 25%, $p<0.05$; see Figure 67-**C**) normalised to the control. Adding IGF-I in the presence of AG1024 ("TKI + IGF-I") could still increase CFE ($p<0.05$) (Figure 67-**B**) but did not affect the fold change of average colony size (Figure 67-**C**) when compared to the control cells.

In T24 cells, the treatment of IGF-I alone ("IGF-I") led to a significant increase in both CFE (by 73%, $p<0.01$, see Figure 67-**E**) and average colony size (by 13%, $p<0.05$, see Figure 67-**F**). AG1024 alone ("TKI") induced a significant decrease in both fold change of CFE (by 84%, $p<0.01$; see Figure 67-**E**) and colony average size (by 13%, $p<0.05$; see Figure 67-**F**) normalised to the control. Moreover, these reductions by AG1024 were not negated following co-treatment with IGF-I ("TKI + IGF-I") (Figure 67-**E** & **F**).

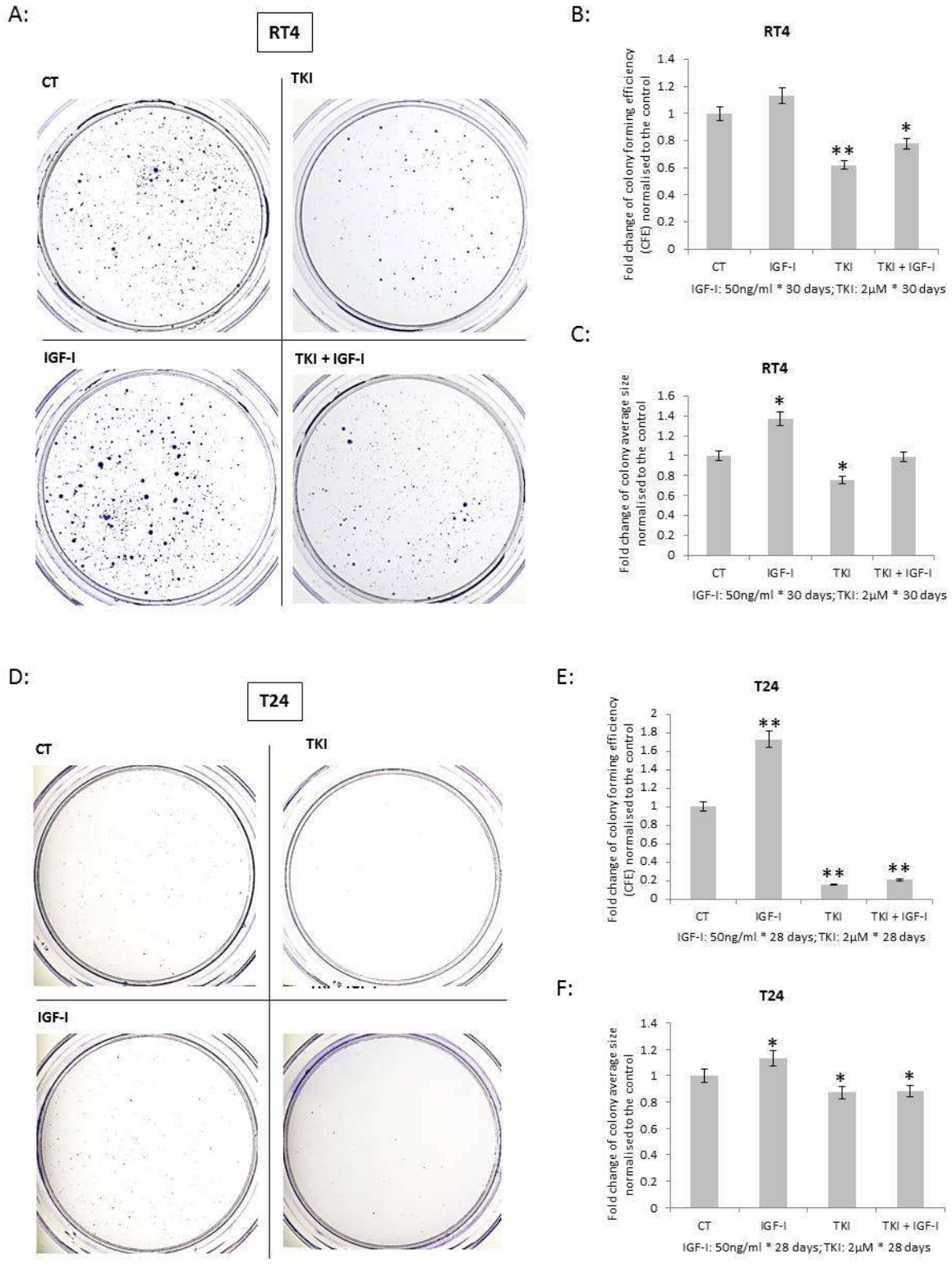

Figure 67: effect of AG1024 and IGF-I on cell colony formation in RT4 and T24 cells

Both RT4 and T24 cells were seeded in dishes under different treatments with corresponding labels ("CT": untreated cells as a control group; "IGF-I": cells treated with IGF-I alone at the concentration of 50ng/ml 48 hours before seeding; "TKI": cells treated with AG1024 alone at the concentration of 2 μM for 48 hours before seeding; "TKI+IGF-I": cells dosed with 1 hour of pre-treatment of AG1024 at the concentration of 2μM followed by addition of IGF-I at 50ng/ml

for 48 hours before seeding). Cells were seeded at an even density at 10,000 cells/dish and 5,000 cells/dish, respectively, and fed once a week for four weeks in total, and then colony numbers, as well as average size, were measured by ImageJ software.

(**A**) & (**D**): Images show RT4 and T24cells, respectively, with colonies were stained at the end of the assay ("Day 28"). All images shown are at x10 magnification; (**B**) & (**E**): Graphs present the fold change of colony forming efficiency (CFE) normalised to the control under different treatments in RT4 and T24 cells, respectively. (**C**) & (**F**): Graphs demonstrate the fold change of average size of colonies due to different treatments for RT4 and T24 cells, respectively. All graphs present the mean of three experiments each performed in triplicate, and error bars represent the standard error of the mean from three experiments (n=3). "*": $p<0.05$; "**": $p<0.01$.

5.4.2.2.2 Effects of inhibiting PI3K on bladder cancer cell phenotype

Changes in cell invasion and migration were examined to investigate the effect of inhibiting PI3K using LY294002 on bladder cancer cells in response to IGF-I.

5.4.2.2.2.1 Characterisation of effectiveness of LY294002

Both RT4 and T24 cells were treated with a short exposure to IGF-I at 50ng/ml for 10 minutes with or without 1 hour of pre-treatment of LY294002 at 50μM.

As characterised in 5.4.2.1, activation of the IGF-IR (p-IGF-IR) by IGF-I was clearly observed in RT4 cells and to a lesser extent in T24 cells in the presence or absence of LY294002 (Figure 68-**A**). The activation of p-IGF-IR led to a high induction of phospho-Akt (p-Akt) in both RT4 and T24 cells in response to IGF-I which was reduced by the pre-treatment with LY294002: the reduction in p-Akt was more obvious in T24 cells than that in RT4 cells suggesting higher efficiency of inhibition of activation of PI3K in T24 cells by LY294002 (Figure 68-**A**). Abundant p-Akt was observed in the control group of T24 cells with

little found in the control of RT4 cells showing a higher basal level of activation of PI3K in T24 cells (Figure 68-**A**).

No obvious changes in phospho-MAPK (p-MAPK) (Figure 68-**A**), the total amount of IGF-IR, Akt and ERK 2 (Figure 68-**B**) were found in RT4 or T24 cells.

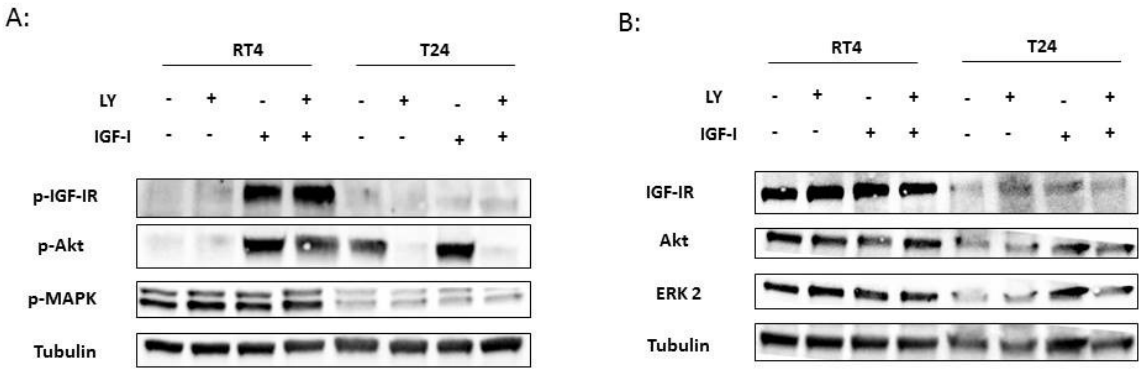

Figure 68: effect of LY294002 on the activation of PI3K in RT4 and T24 cells

RT4 and T24 cells were seeded at a density of 0.1 and 0.05x10^6 cells/well into 6-well plates in GM to grow for 24 hours followed by serum starvation for another 24 hours. Cells were then pre-dosed with or without LY294002 ("LY") at 50μM for 1 hour before spiked with or without IGF-I (50ng/ml) for 10 minutes. Samples from harvested cells were used to investigate the changes in protein abundance of molecules involved in IGF signalling using WB ("p-IGF-IR": phospho-IGF-IR; "p-Akt": phospho-Akt; "p-MAPK": phospho-MAPK). Proteins in whole lysates were loaded equally at 60μg with Tubulin being used as the reference protein. All blots demonstrate typical results from three experiments each performed at least in triplicate (n=3).

5.4.2.2.2.2 Effect of inhibiting PI3K on cell invasion in RT4 and T24 cells

An invasion assay was performed to assess the effect of inhibiting PI3K on cell invasion in both RT4 and T24 cells.

Similar to the pattern of results obtained for inhibiting the IGF-IR using AG1024 described in 5.4.2.2.1.4, the dosing of IGF-I alone ("IGF-I") induced a significant increase in cell invasion in both RT4 (by 58%, $p<0.01$; see Figure 69-**B**) and T24 cells (by 90%, $p<0.01$; see Figure 69-**D**). Treatment of

LY294002 alone ("LY") significantly decreased in cell invasion in both RT4 (by around 49%, p<0.01; see Figure 69-**B**) and T24 cells (by around 57%, p<0.01; see Figure 69-**D**) and the effect of IGF-I on invasion was negated when in combination with LY.

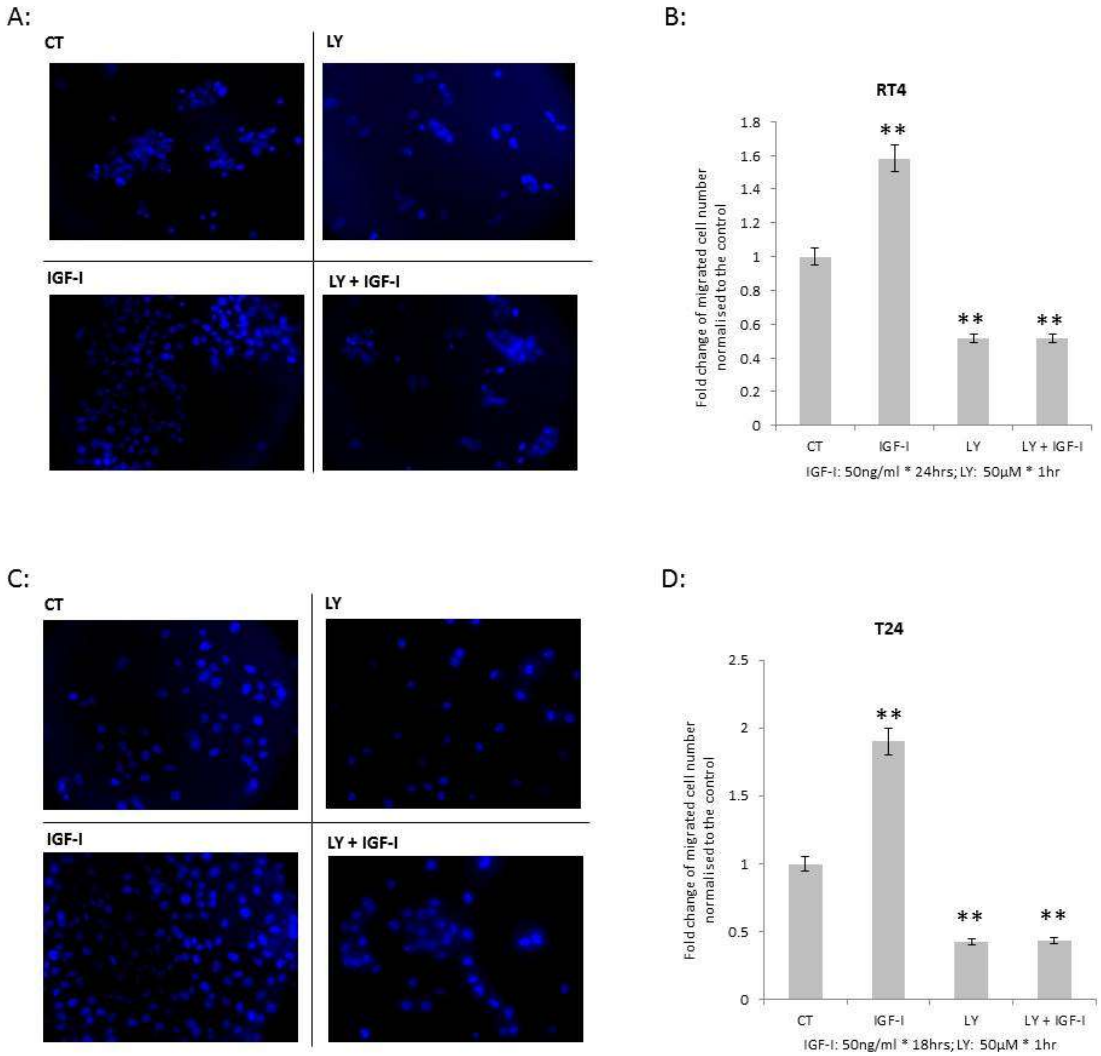

Figure 69: effect of LY294002 and IGF-I on cell invasion in RT4 and T24 cells

Cells of both cell lines were previously seeded in GM for 24 hours and then changed to SFM for 16 hours before being prepared for an invasion assay. After serum-starvation, 1 hour of pre-treatment of LY294002 at a concentration of 50μM was performed in both cells accordingly. Cells were then trypsinised and then seeded into the collagen-coated inserts at a certain density (RT4: 0.1x106 cells/insert and T24: 0.08x106 cells/insert) and allowed to invade (RT4: 24 hours and T24: 18 hours). Cells were labelled according to different treatments while seeding : "CT": control cells without treatment; "IGF-I": cells treated with IGF-I alone at a concentration of 50ng/ml (RT4: 24 hours and T24: 18 hours); "LY": cells treated with LY294002 alone at 50μM (RT4: 25 hours and T24: 19 hours); "LY+IGF-I": cells dosed with 1

hour of pre-treatment of LY294002 at the concentration of 50μM followed by addition of IGF-I at 50ng/ml (RT4: 24 hours and T24: 18 hours).

(**A**) & (**C**): The images show invaded RT4 and T24 cells, respectively, with nuclei (in blue) stained with DAPI. All images shown are at x40 magnification. (**B**) & (**D**) The graphs show the fold change of invaded RT4 and T24 cells, respectively, normalised to the control group. The graphs represent the mean of three experiments each performed in triplicate, upon which the standard error of the mean of the experiments was presented (n=3). "**": $p<0.01$.

5.4.2.2.2.3 Effect of inhibiting PI3K on cell migration in T24 cells

A migration assay was performed to investigate the effect of inhibiting PI3K using LY294002 on cell migration in T24 cells in response to IGF-I.

The treatment of IGF-I alone ("IGF-I") enhanced the migration showing a significantly faster reduction in the gap area compared to the control group (see Figure 70-**B**). In contrast, compared to the control, LY294002 alone ("LY") significantly slowed the decrease in the gap area showing the migratory activity of cells was inhibited. However, the inhibitory effect of LY294002 was attenuated upon treatment with IGF-I ("LY + IGF-I") (Figure 70-**B**).

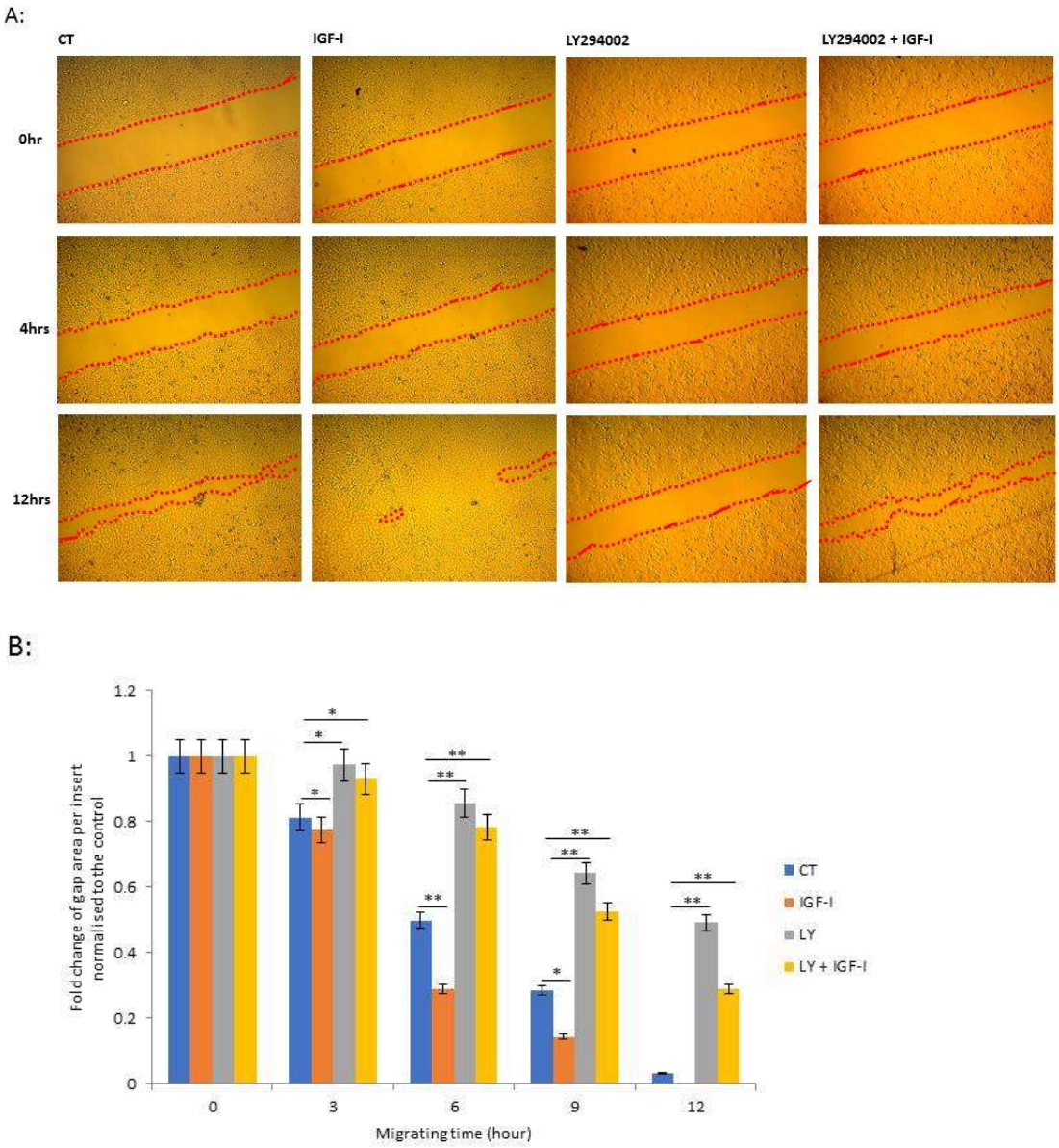

Figure 70: effect of LY294002 and IGF-I on cell migration in T24 cells

T24 cells were seeded at a density of 0.028×10^6 cells into each chamber in GM and allowed to grow for approximately 24 hours to reach about 80% confluence. Cell reached 90-95% confluence during an additional 24 hours in SFM. After 1 hour of pre-dosing with fresh SFM or LY294002 at 50μM, the inserts were removed leaving an observed gap, and gap closure was recorded for up to 12 hours with different treatment ("CT": untreated cells as a control group; "IGF-I": cells treated with IGF-I alone at the concentration of 50ng/ml; "LY": cells treated with LY294002 alone at the concentration of 50μM; "LY+IGF-I": cells dosed with 1 hour of pre-treatment of LY294002 at the concentration of 50μM followed by addition of IGF-I at 50ng/ml).

Images of cell gaps were taken at different times with relative labels. "0hr": the start point after the removal of inserts; "3hr", "4hr", "6hr", "9hr" and "12hr": 3, 4, 6, 9 and 12 hours after the removal of inserts. All images demonstrate the results from three experiments performed in duplicate (n=3). All images shown are at x10 magnification, and the area of the gaps in the images was analysed using ImageJ software. "*": $p<0.05$; "**": $p<0.01$.

5.4.3 Does IGF-I induce changes in EMT-related molecules in bladder cancer cells?

In addition to E, N-cadherin and β-catenin that were examined in the previous chapters, changes in ZEB-1, FOXO3a, FOXA1, and 14-3-3 β were also assessed in response to IGF-I.

5.4.3.1 Characterisation of ZEB-1, FOXO3a, FOXA1, and 14-3-3 β in RT4 and T24 cells

A range of protein concentrations was used to identify the optimum amount for each antibody in each cell line. T24 cells express high levels of ZEB-1; while RT4 cells show the opposite having undetectable amounts (see Figure 71-**A**). Both RT4 and T24 cells express FOXO3a, FOXA1 and 14-3-3 β (see Figure 71-**B** & **C** & **D**), with both FOXO3a and FOXA1 being more abundant in the RT4 cells (see Figure 71-**B**). It was also determined that 60μg would be an appropriate amount to load for each of these proteins unless noted otherwise.

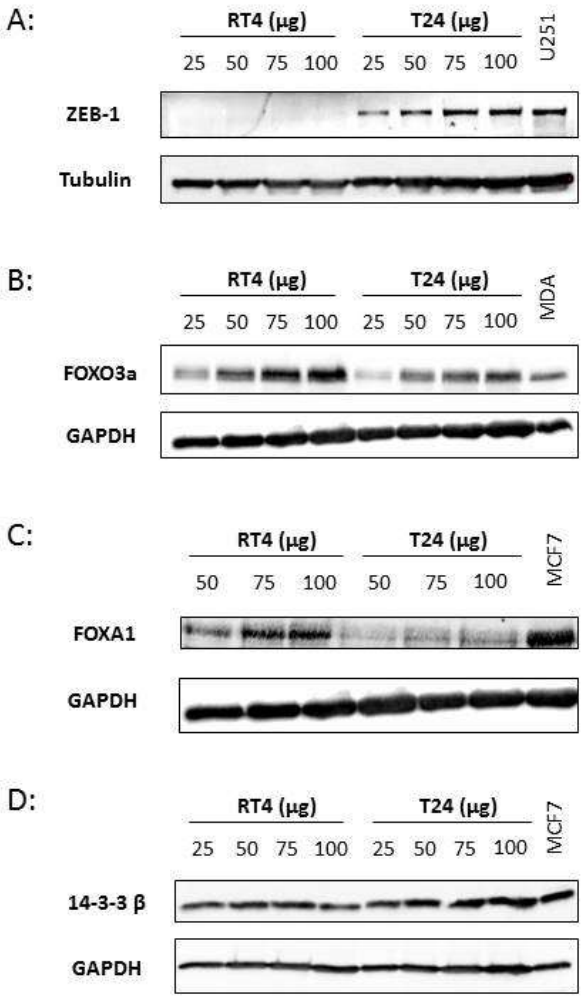

Figure 71: characterisation of the levels of ZEB-1, FOXO3a, FOXA1, and 14-3-3 β in RT4 and T24 cells

Figures (**A**), (**B**), (**C**) and (**D**) show the western blots for ZEB-1, FOXO3a, FOXA1 and 14-3-3 β, respectively, in both RT4 and T24 cells detected using WB. RT4 and T24 cells were seeded in GM at the same density to grow for 24 hours and then were left in SFM for 48 hours before sample harvest. Proteins in whole lysates were loaded with increasing amounts from 25 to 100µg. Proteins from U251 (a human glioblastoma cell line), MDA (MDA-MB-231, a human breast cancer cell line), and MCF7 (a human breast adenocarcinoma cell line) cell lysates were used as positive controls for ZEB-1, FOXO3a, and FOXA1 & 14-3-3 β, respectively. They were loaded equally at 50µg. Tubulin and GAPDH were used as the reference protein.

Basal localisation of these molecules in RT4 and T24 cells was detected by cellular fractionation. Consistent with the results of western blotting (Figure 71-**A**), no ZEB-1 was detected in RT4 cells (see Figure 72-**A**); and in T24 cells, ZEB-1 was located only in the nuclear fraction (Figure 72-**C**). FOXO3a was

found both in the nuclei and cytoplasm of RT4 and T24 cells, and it was more abundant in the nuclear component in both cell lines (see Figure 72-**B** & **C**). FOXA1 was located both in the nuclei and cytoplasm of T24 cells with more abundance observed in the nuclei (see Figure 72-**C**); while in RT4 cells, FOXA1 was detected at high levels but only in the nuclei (see Figure 72-**B**). 14-3-3 β was found only in the cytoplasm in RT4 cells (see Figure 72-**B**); 14-3-3 β was also located in the cytoplasm of T24 cells, with an almost undetectable presence in the nuclear fraction (see Figure 72-**C**).

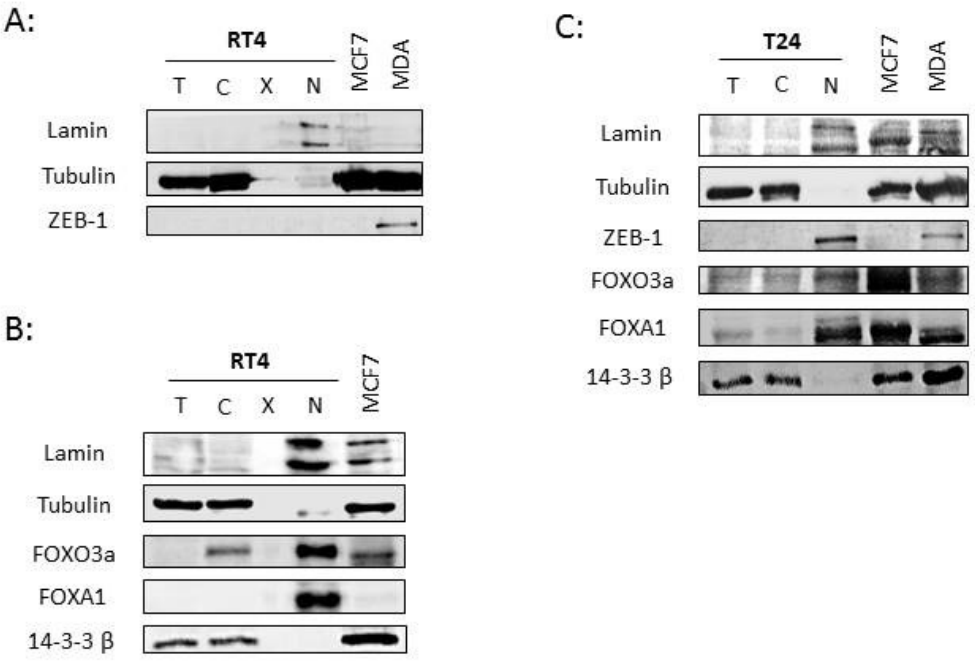

Figure 72: characterisation of the localisation of ZEB-1, FOXO3a, FOXA1 and 14-3-3 β in RT4 and T24 cells using cellular fractionation

Figure (**A**), (**B**) and (**C**) show western blots characterising the basal localisation of ZEB-1, FOXO3a, FOXA1 and 14-3-3 β in RT4 and T24 cells, respectively, using cellular fractionation. Both RT4 and T24 cells were seeded in GM at the same density to grow for 24 hours followed by serum starvation using SFM for another 24 hours, and then cells were trypsinised and harvested for performing cellular fractionation to separate proteins of cytoplasmic and nuclear extracts. Isolated proteins extracted from the total cell lysates were loaded equally for protein detection using WB. Lamin and Tubulin exist only in nuclei and cytoplasm, respectively, and they are indicators of the efficiency of protein separation. "T": total cell lysates; "C": cytoplasmic extract; "N": nuclear extract; "X": blank lane. Proteins of MCF7 (a human breast adenocarcinoma cell line) and MDA (MDA-MB-231, a human breast cancer cell line) were used as a positive control for target molecules. And the blots demonstrate the typical results from three experiments each performed at least in triplicate (n=3).

5.4.3.2 Assessment of changes in EMT-related molecules following IGF-I treatment

RT4 and T24 cells were dosed with exogenous IGF-I at a concentration of 50ng/ml for 48 hours, and changes in abundance and localisation of EMT-related molecules including N- and E-cadherin, β-catenin, ZEB-1, FOXO3a, FOXA1 as well as 14-3-3 β in both cell lines were investigated using cellular fractionation and WB analysis.

As we determined previously, N-cadherin, the mesenchymal marker, was expressed abundantly in aggressive mesenchymal-like T24 cells, with no detectable levels found in epithelial-like RT4 cells. With the treatment of increasing concentrations of IGF-I, an enhancement of N-cadherin expression was observed in T24 cells (by 21.4% at the concentration of 50ng/ml, $p<0.05$; see Figure 73-**A** & **C**) compared to the control, with no observed changes in E-cadherin (Figure 73-**A**). Enhanced expression of N-cadherin in both total cell lysates and the cytoplasmic extract in response to exogenously added IGF-I was confirmed in the cellular fractionation analysis (see Figure 73-**B**). With no N-cadherin in cell nuclei, the fold change of cytoplasmic N-cadherin normalised to untreated controls in T24 cells presented a similar increase (by 25%, $p<0.05$; see Figure 73-**D**) to that observed in whole lysates.

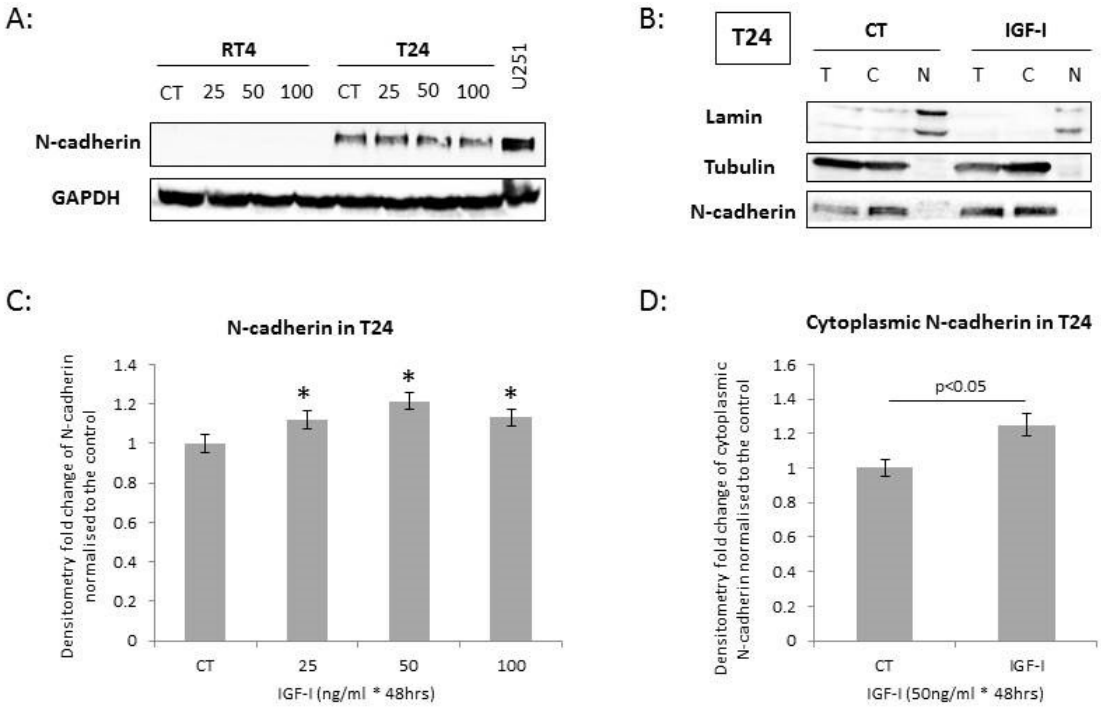

Figure 73: effect of IGF-I on N-cadherin in RT4 and T24 cells

RT4 and T24 cells were seeded in 6-well plates at a density of 0.1 and $0.05x10^6$ cells/well, respectively, in GM for 24 hours and serum starved with SFM for another 24 hours. Then cells were separated according to different treatments ("CT": untreated cells as a control group; "25", "50", "100": cells treated with IGF-I at the concentration of 25, 50, and 100ng/ml for 48 hours, respectively; "IGF-I": cells treated with IGF-I at the certain concentration of 50ng/ml for 48 hours). After 48 hours of treatment, cells were harvested to investigate the changes in protein abundance and localisation using WB and cellular fractionation analysis, accordingly. All blots demonstrate typical results from three experiments each performed at least in triplicate (n=3).

(**A**): The blot shows the abundance of N-cadherin in RT4 and T24 cells in response to an increased dosage of IGF-I treatment. Samples from whole lysates were loaded equally at 60µg for protein detection, and GAPDH was assessed as reference protein. Proteins from U251 (a human glioblastoma cell line) cell lysates were used as positive controls for N-cadherin. (**B**): The blot presents the localisation of N-cadherin in the presence or absence of IGF-I treatment in T24 cells using cellular fractionation. Lamin and Tubulin exist only in nuclei and cytoplasm, respectively, and they are an indicator of the efficiency of protein separation. "T": total cell lysates; "C": cytoplasmic extract; "N": nuclear extract. (**C**): The graph shows the mean of fold change of the optical density measurements of N-cadherin in response to increased dosage of IGF-I (from 0 to 100ng/ml for 48 hours) from three experiments each performed at least in triplicate; and error bars demonstrate the standard error of the mean of experiments (n=3). "*": $p<0.05$. (**D**): The graph represents the mean of fold change of the optical density measurements of N-cadherin in cytoplasmic extracts in response to treatment with and without the presence of IGF-I (at 50ng/ml for 48 hours), from three experiments each performed at least in triplicate; and error bars demonstrate the standard error of the mean of experiments (n=3).

In response to increasing doses of IGF-I, the levels of E-cadherin, the epithelial marker, in RT4 cells was reduced (see Figure 74-**A**): the fold change normalised to the control showed a significant reduction of 12% ($p<0.05$) when treated with exogenous IGF-I at 50ng/ml for 48 hours (see Figure 74-**C**). With no presence in the nuclear extract, E-cadherin demonstrated an 11% ($p<0.05$) reduction in fold change of cytoplasmic expression compared with the control (see Figure 74-**B** & **D**). No induction of E-cadherin in T24 cells was observed in response to the treatment with IGF-I (see Figure 74-**A**).

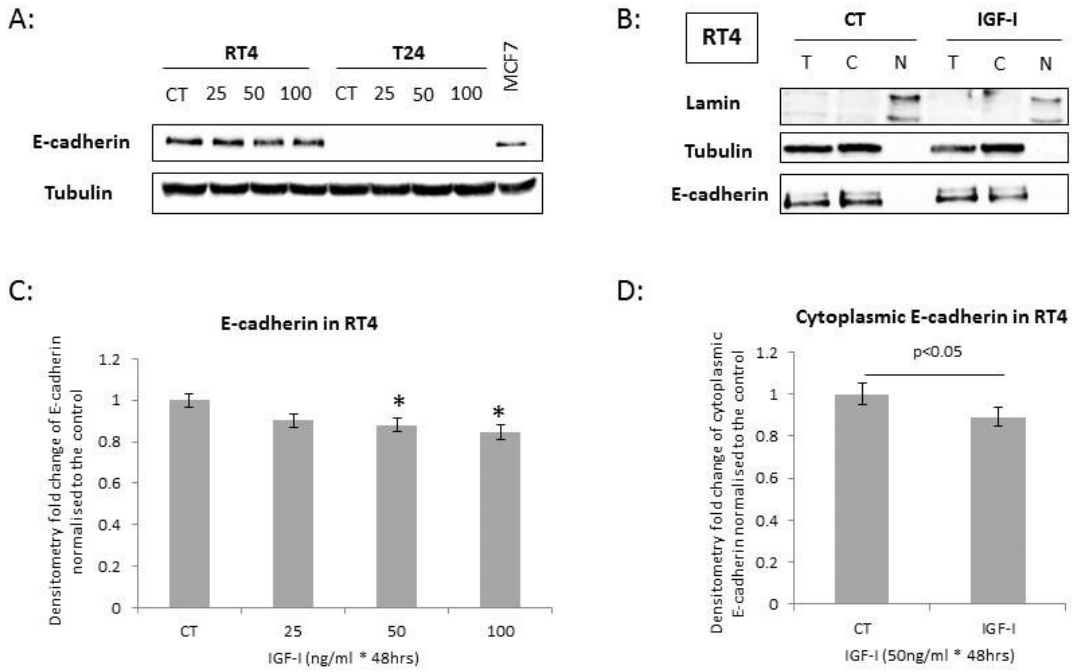

Figure 74: effect of IGF-I on E-cadherin in RT4 and T24 cells

RT4 and T24 cells were seeded in 6-well plates at a density of 0.1 and $0.05x10^6$ cells/well, respectively, in GM for 24 hours and serum starved with SFM for another 24 hours. Then cells were separated according to different treatments ("CT": untreated cells as a control group; "25", "50", "100": cells treated with IGF-I at the concentration of 25, 50, and 100ng/ml for 48 hours, respectively; "IGF-I": cells treated with IGF-I at the certain concentration of 50ng/ml for 48 hours). After 48 hours of treatment, cells were harvested to investigate the changes in protein abundance and localisation using WB and cellular fractionation analysis, accordingly. All blots demonstrate typical results from three experiments each performed at least in triplicate (n=3).

(**A**): The blot shows the abundance of E-cadherin in RT4 and T24 cells in response to an increased dosage of IGF-I treatment. Samples from whole lysates were loaded equally at 60µg

for protein detection, and Tubulin was assessed as reference protein. Proteins from MCF7 (a human breast adenocarcinoma cell line) cell lysates were used as positive controls for E-cadherin. (**B**): The blot presents the localisation of E-cadherin in the presence or absence of IGF-I treatment in RT4 cells using cellular fractionation. Lamin and Tubulin exist only in nuclei and cytoplasm, respectively, and they are an indicator of the efficiency of protein separation. "T": total cell lysates; "C": cytoplasmic extract; "N": nuclear extract. (**C**): The graph shows the mean of fold change of the optical density measurements of E-cadherin in response to increased dosage of IGF-I (from 0 to 100ng/ml for 48 hours) from three experiments each performed at least in triplicate; and error bars demonstrate the standard error of the mean of experiments (n=3). "*": $p<0.05$. (**D**): The graph represents the mean of fold change of the optical density measurements of E-cadherin in cytoplasmic extracts in response to treatment with and without the presence of IGF-I (at 50ng/ml for 48 hours), from three experiments each performed at least in triplicate; and error bars demonstrate the standard error of the mean of experiments (n=3).

No visible (see Figure 75-**A**) or statistical (see Figure 75- **B** & **C**) changes in the abundance of β-catenin were observed in RT4 or T24 cells with the treatment of IGF-I. However, the treatment of exogenously added IGF-I at 50ng/ml for 48 hours led to nuclear translocation of β-catenin in both cell lines with an induction in the fold change of cytoplasmic β-catenin normalised to this protein in total cell lysates found between control and IGF-I-treated cells being 50% ($p<0.05$; see Figure 75-**F**) in RT4 cells and 20% ($p<0.05$; see Figure 75-**G**) in T24 cells.

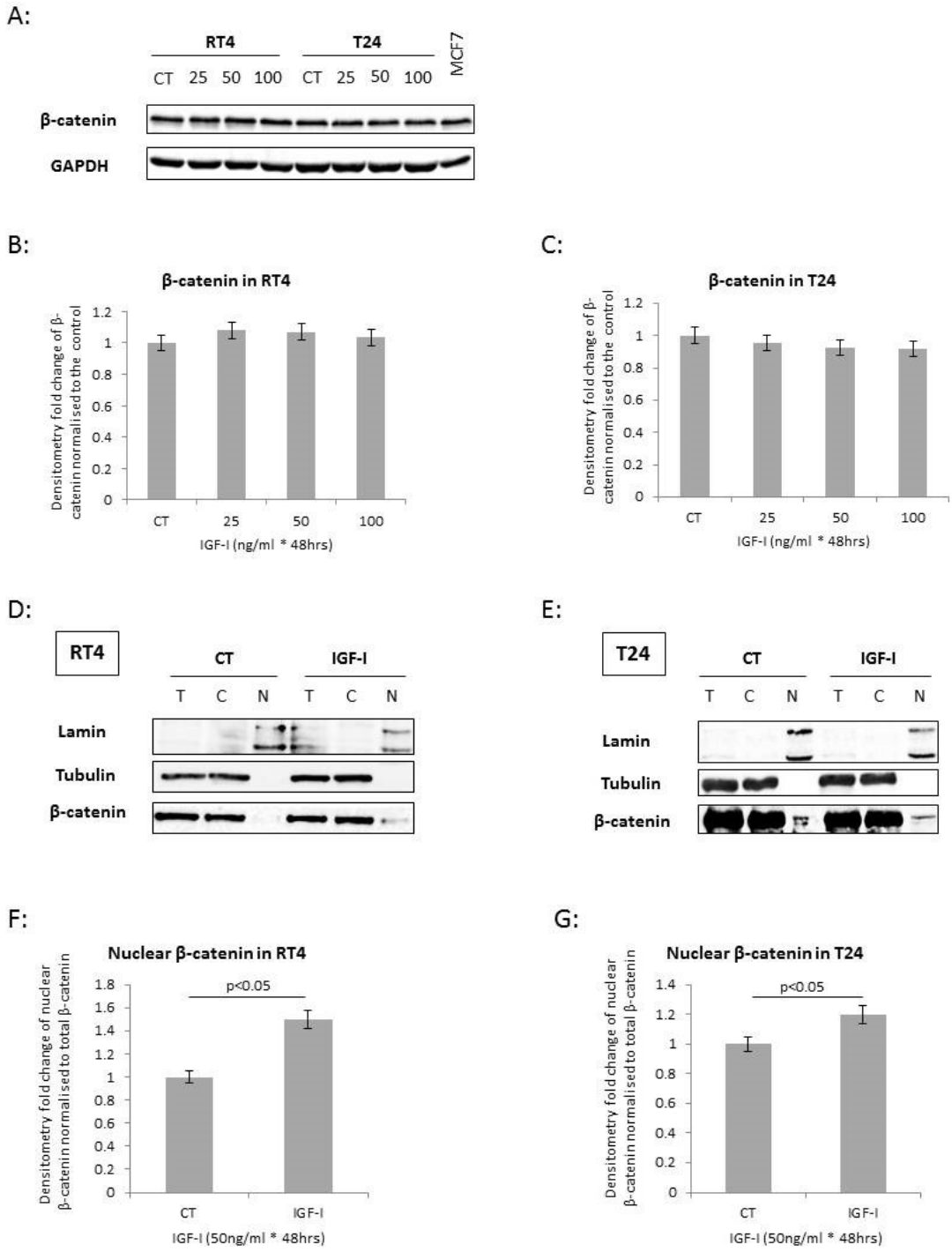

Figure 75: effect of IGF-I on β-catenin in RT4 and T24 cells

RT4 and T24 cells were seeded in 6-well plates at a density of 0.1 and 0.05x10^6 cells/well, respectively, in GM for 24 hours and serum starved with SFM for another 24 hours. Then cells were separated according to different treatments ("CT": untreated cells as a control group; "25", "50", "100": cells treated with IGF-I at the concentration of 25, 50, and 100ng/ml for 48 hours, respectively; "IGF-I": cells treated with IGF-I at the certain concentration of 50ng/ml for 48 hours). After 48 hours of treatment, cells were harvested to investigate the changes in protein abundance and localisation using WB and cellular fractionation analysis, accordingly. All blots demonstrate typical results from three experiments each performed at least in triplicate (n=3).

(**A**): The blot shows the abundance of β-catenin in RT4 and T24 cells in response to an increased dosage of IGF-I treatment. Samples from whole lysates were loaded equally at 60μg for protein detection, and GAPDH was assessed as reference protein. Proteins from MCF7 (a human breast adenocarcinoma cell line) cell lysates were used as positive controls for β-catenin. (**B**) & (**C**): The graphs show the mean of fold change of the optical density measurements of β-catenin in RT4 and T24 cells, respectively, in response to increased dosage of IGF-I (from 0 to 100ng/ml for 48 hours) from three experiments each performed at least in triplicate; and error bars demonstrate the standard error of the mean of experiments (n=3). (**D**) & (**E**): The blots present the localisation of β-catenin in the presence or absence of IGF-I treatment in RT4 and T24 cells, respectively, using cellular fractionation. Lamin and Tubulin exist only in nuclei and cytoplasm, respectively, and they are an indicator of the efficiency of protein separation. "T": total cell lysates; "C": cytoplasmic extract; "N": nuclear extract. (**F**) & (**G**): The graphs present the densitometry fold change of cytoplasmic β-catenin normalised to total β-catenin in the total cell lysates in RT4 and T24 cells, respectively, in response to treatment with and without the presence of IGF-I (at 50ng/ml for 48 hours), with error bars representing the standard error of the mean of experiments (n=3).

Similar to N-cadherin, ZEB-1 was expressed only in T24 cells. Moreover, treatment with IGF-I induced an increase in the levels of ZEB-1 in T24 cells (by 28.8% when treated with IGF-I at 50ng/ml for 48 hours, $p<0.05$; see Figure 76-**C**) compared with the control, with no induction of this protein in RT4 cells (see Figure 76-**A**). Existing only in the nuclei of T24 cells, the levels of ZEB-1 increased in both whole lysates and nuclear extracts (see Figure 76-**B**). Moreover, the treatment with IGF-I at 50ng/ml for 48 hours led to an enhancement in the fold change of nuclear ZEB-1 by 20% ($p<0.05$; see Figure 76-**D**) normalised to the untreated control.

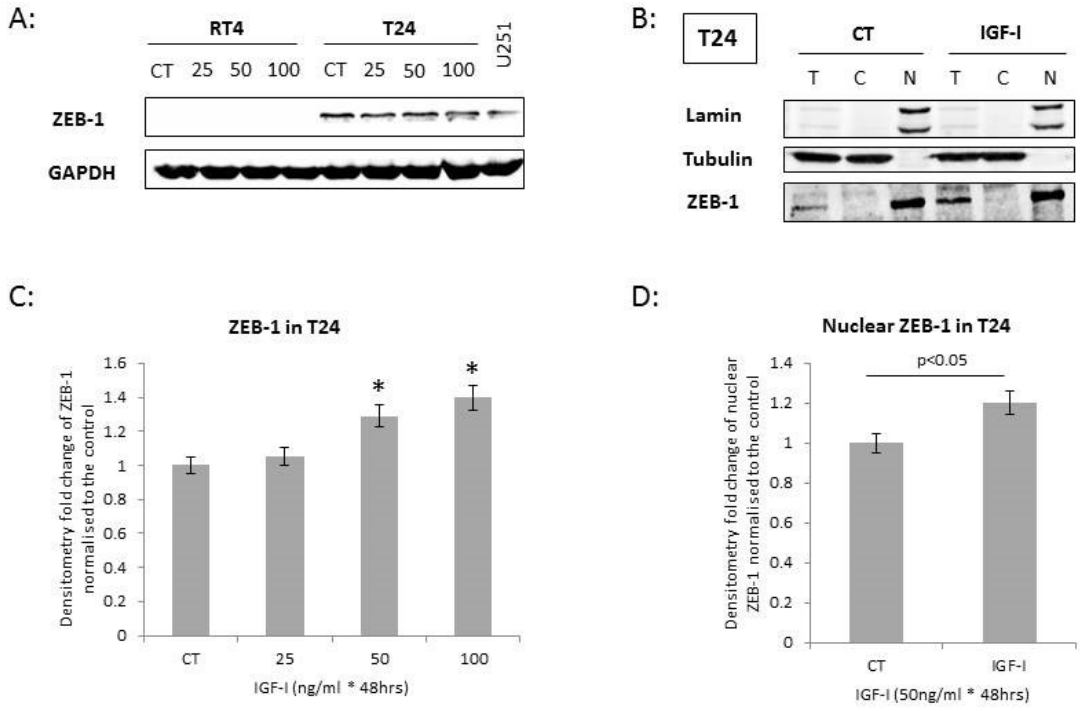

Figure 76: effect of IGF-I on ZEB-1 in RT4 and T24 cells

RT4 and T24 cells were seeded in 6-well plates at a density of 0.1 and 0.05x10^6 cells/well, respectively, in GM for 24 hours and serum starved with SFM for another 24 hours. Then cells were separated according to different treatments ("CT": untreated cells as a control group; "25", "50", "100": cells treated with IGF-I at the concentration of 25, 50, and 100ng/ml for 48 hours, respectively; "IGF-I": cells treated with IGF-I at the certain concentration of 50ng/ml for 48 hours). After 48 hours of treatment, cells were harvested to investigate the changes in protein abundance and localisation using WB and cellular fractionation analysis, accordingly. All blots demonstrate typical results from three experiments each performed at least in triplicate (n=3).

(**A**): The blot shows the abundance of ZEB-1 in RT4 and T24 cells in response to an increased dosage of IGF-I treatment. Samples from whole lysates were loaded equally at 60µg for protein detection, and GAPDH was assessed as reference protein. Proteins from U251 (a human glioblastoma cell line) cell lysates were used as positive controls for ZEB-1. (**B**): The blot presents the localisation of ZEB-1 in the presence or absence of IGF-I treatment in T24 cells using cellular fractionation. Lamin and Tubulin exist only in nuclei and cytoplasm, respectively, and they are an indicator of the efficiency of protein separation. "T": total cell lysates; "C": cytoplasmic extract; "N": nuclear extract. (**C**): The graph shows the mean of fold change of the optical density measurements of ZEB-1 in response to increased dosage of IGF-I (from 0 to 100ng/ml for 48 hours) from three experiments each performed at least in triplicate; and error bars demonstrate the standard error of the mean of experiments (n=3). "*": $p<0.05$. (**D**): The graph represents the mean of fold change of the optical density measurements of ZEB-1 in nuclear extracts in response to treatment with and without the presence of IGF-I (at 50ng/ml for 48 hours), from three experiments each performed at least in triplicate; and error bars demonstrate the standard error of the mean of experiments (n=3).

With the treatment of IGF-I, the abundance of FOXO3a was increased in both RT4 and T24 cells (see Figure 77-**A** & **B**) with an induction by 33.8% ($p<0.05$; see Figure 77-**C**) and 23.0% ($p<0.05$; see Figure 77-**D**), respectively, compared to the control. Along with the increased expression in whole cell lysates, decreased levels of nuclear FOXO3a were observed in both cell lines (see Figure 77-**E** & **F**), and a significant reduction by 40% ($p<0.05$; see Figure 77-**G**) and 30% ($p<0.05$; see Figure 77-**H**) was found in RT4 and T24 cells, respectively, in the fold change of nuclear FOXO3a normalised to this protein in total cell lysates of control and IGF-I-treated cells.

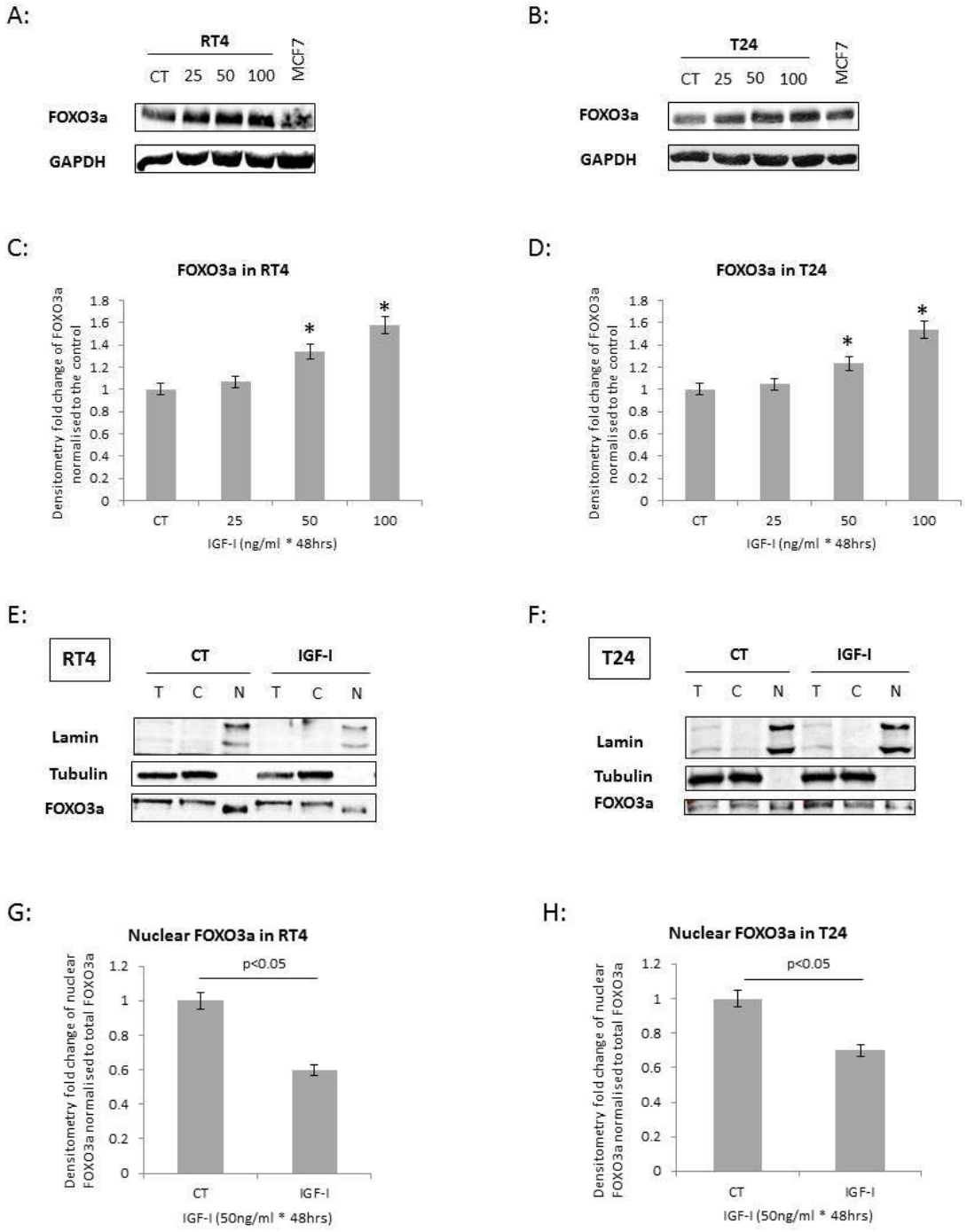

Figure 77: effect of IGF-I on FOXO3a in RT4 and T24 cells

RT4 and T24 cells were seeded in 6-well plates at a density of 0.1 and $0.05x10^6$ cells/well, respectively, in GM for 24 hours and serum starved with SFM for another 24 hours. Then cells were separated according to different treatments ("CT": untreated cells as a control group; "25", "50", "100": cells treated with IGF-I at the concentration of 25, 50, and 100ng/ml for 48 hours, respectively; "IGF-I": cells treated with IGF-I at the certain concentration of 50ng/ml for 48 hours). After 48 hours of treatment, cells were harvested to investigate the changes in protein abundance and localisation using WB and cellular fractionation analysis, accordingly. All blots demonstrate typical results from three experiments each performed at least in triplicate (n=3).

(**A**) & (**B**): The blots show the abundance of FOXO3a in RT4 and T24 cells, respectively, in response to an increased dosage of IGF-I treatment. Samples from whole lysates were loaded equally at 60μg for protein detection, and GAPDH was assessed as reference protein. Proteins from MCF7 (a human breast adenocarcinoma cell line) cell lysates were used as positive controls for β-catenin. (**C**) & (**D**): The graphs show the mean of fold change of the optical density measurements of FOXO3a in RT4 and T24 cells, respectively, in response to increased dosage of IGF-I (from 0 to 100ng/ml for 48 hours) from three experiments each performed at least in triplicate; and error bars demonstrate the standard error of the mean of experiments (n=3). (**E**) & (**F**): The blots present the localisation of FOXO3a in the presence or absence of IGF-I treatment in RT4 and T24 cells, respectively, using cellular fractionation. Lamin and Tubulin exist only in nuclei and cytoplasm, respectively, and they are an indicator of the efficiency of protein separation. "T": total cell lysates; "C": cytoplasmic extract; "N": nuclear extract. (**G**) & (**H**): The graphs present the densitometry fold change of nuclear FOXO3a normalised to total FOXO3a in the total cell lysates in RT4 and T24 cells, respectively, in response to treatment with and without the presence of IGF-I (at 50ng/ml for 48 hours), with error bars representing the standard error of the mean of experiments (n=3).

Levels of FOXA1 was also elevated by exogenous IGF-I in RT4 cells both visually (see Figure 78-**A**) and statistically (by 42.5% when treated with IGF-I at 50ng/ml for 48 hours, $p<0.05$; see Figure 78-**C**) compared to the control, with a slight yet not significant decrease found in T24 cells (see Figure 78-**B** & **D**). Both RT4 (see Figure 78-**E**) and T24 (see Figure 78-**F**) cells showed a slight decrease of nuclear FOXA1 expression with IGF-I treatment (at 50ng/ml for 48 hours) compared to the control, but the difference in the fold change of nuclear FOXA1 normalised to this protein in total cell lysates of control and IGF-I-treated cells was not significant in either cell line (see Figure 78-**G** & **H**).

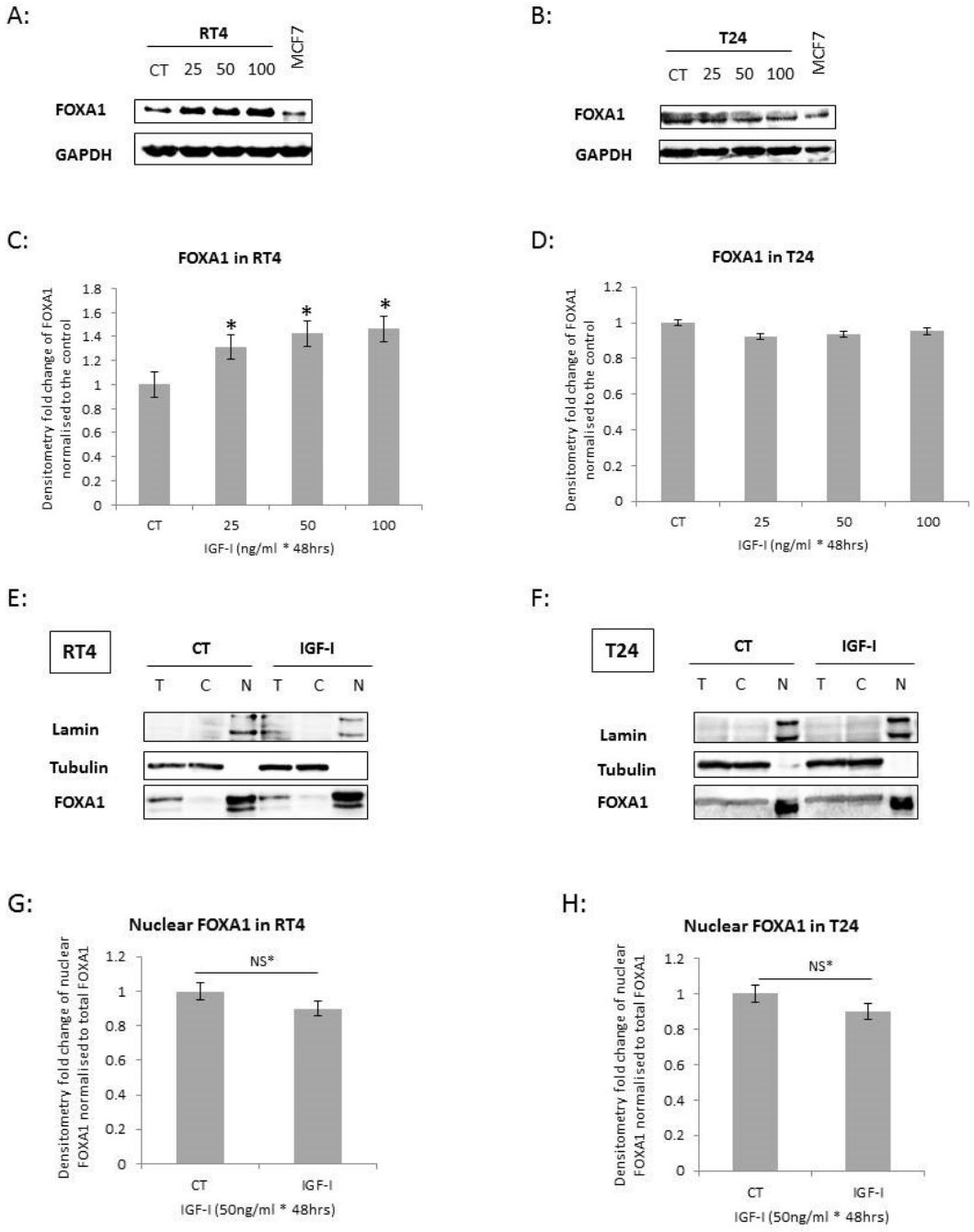

Figure 78: effect of IGF-I on FOXA1 in RT4 and T24 cells

RT4 and T24 cells were seeded in 6-well plates at a density of 0.1 and 0.05x10^6 cells/well, respectively, in GM for 24 hours and serum starved with SFM for another 24 hours. Then cells were separated according to different treatments ("CT": untreated cells as a control group; "25", "50", "100": cells treated with IGF-I at the concentration of 25, 50, and 100ng/ml for 48 hours, respectively; "IGF-I": cells treated with IGF-I at the certain concentration of 50ng/ml for 48 hours). After 48 hours of treatment, cells were harvested to investigate the changes in protein abundance and localisation using WB and cellular fractionation analysis, accordingly. All blots demonstrate typical results from three experiments each performed at least in triplicate (n=3).

(**A**) & (**B**): The blots show the abundance of FOXA1 in RT4 and T24 cells, respectively, in response to an increased dosage of IGF-I treatment. Samples from whole lysates were loaded equally at 60µg for protein detection, and GAPDH was assessed as reference protein. Proteins from MCF7 (a human breast adenocarcinoma cell line) cell lysates were used as positive controls for β-catenin. (**C**) & (**D**): The graphs show the mean of fold change of the optical density measurements of FOXA1 in RT4 and T24 cells, respectively, in response to increased dosage of IGF-I (from 0 to 100ng/ml for 48 hours) from three experiments each performed at least in triplicate; and error bars demonstrate the standard error of the mean of experiments (n=3). (**E**) & (**F**): The blots present the localisation of FOXA1 in the presence or absence of IGF-I treatment in RT4 and T24 cells, respectively, using cellular fractionation. Lamin and Tubulin exist only in nuclei and cytoplasm, respectively, and they are an indicator of the efficiency of protein separation. "T": total cell lysates; "C": cytoplasmic extract; "N": nuclear extract. (**G**) & (**H**): The graphs present the densitometry fold change of nuclear FOXA1 normalised to total FOXA1 in the total cell lysates in RT4 and T24 cells, respectively, in response to treatment with and without the presence of IGF-I (at 50ng/ml for 48 hours), with error bars representing the standard error of the mean of experiments (n=3). "NS*": not significant.

Significant increases in the levels of 14-3-3 β was observed in RT4 cells when treated with IGF-I at 50ng/ml ($p<0.05$) and 100ng/ml ($p<0.05$) for 48 hours compared to the control (see Figure 79-**B**), with no changes found in T24 cells (see Figure 79-**C**). No 14-3-3 β was detected in the nuclear extracts in either RT4 or T24 cells, and an induction of cytoplasmic expression of this protein was observed in both cell lines (see Figure 79-**D** & **E**). Statistically, when treated with IGF-I at 50ng/ml for 48 hours, a significant enhancement by 40% ($p<0.05$; see Figure 79-**F**) and 20% ($p<0.05$; see Figure 79-**G**) was found in RT4 and T24 cells, respectively, in the densitometry fold change of cytoplasmic 14-3-3 β expression compared to the control.

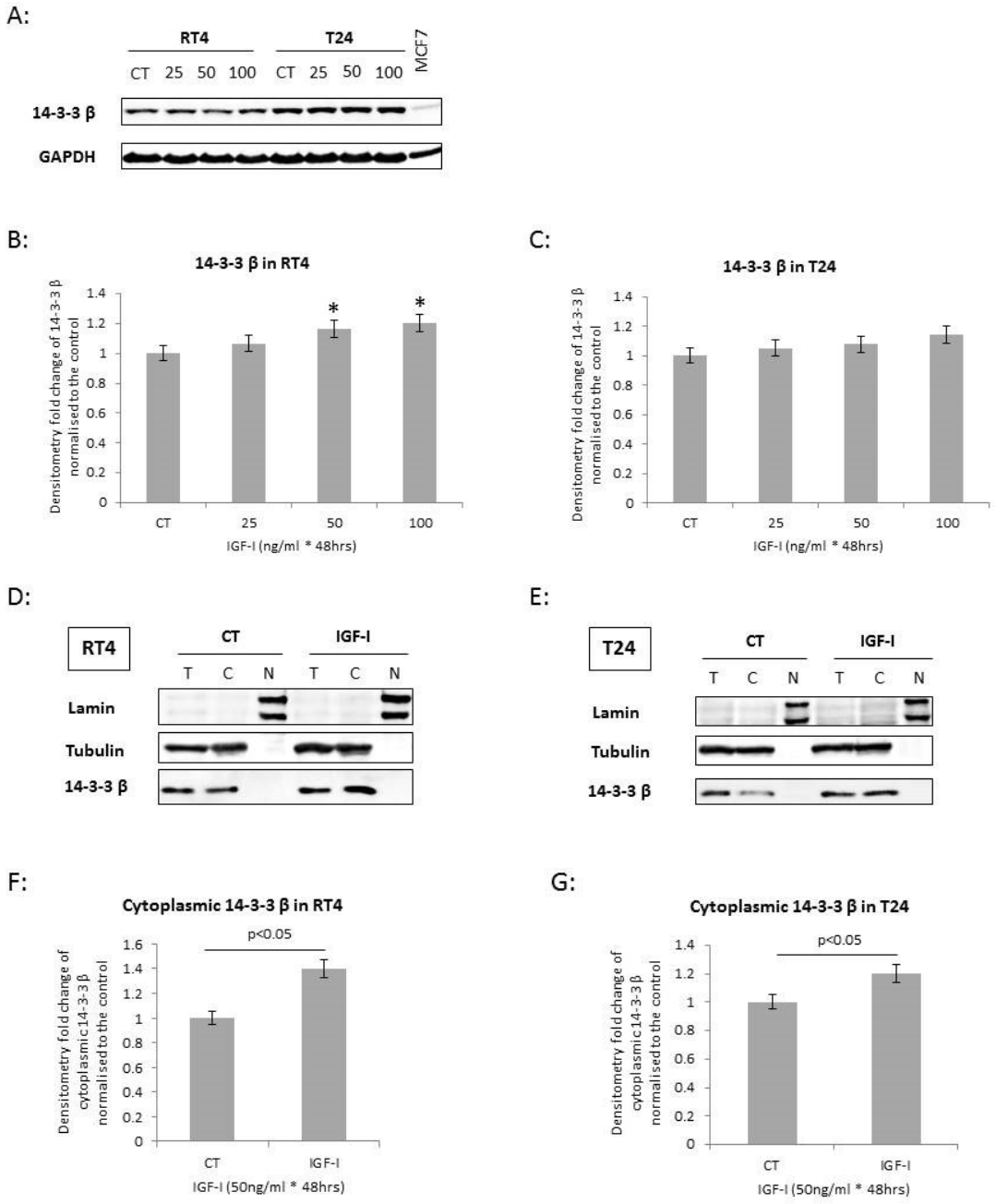

Figure 79: effect of IGF-I on 14-3-3 β in RT4 and T24 cells

RT4 and T24 cells were seeded in 6-well plates at a density of 0.1 and 0.05x10^6 cells/well, respectively, in GM for 24 hours and serum starved with SFM for another 24 hours. Then cells were separated according to different treatments ("CT": untreated cells as a control group; "25", "50", "100": cells treated with IGF-I at the concentration of 25, 50, and 100ng/ml for 48 hours, respectively; "IGF-I": cells treated with IGF-I at the certain concentration of 50ng/ml for 48 hours). After 48 hours of treatment, cells were harvested to investigate the changes in protein abundance and localisation using WB and cellular fractionation analysis, accordingly. All blots demonstrate typical results from three experiments each performed at least in triplicate (n=3).

(**A**): The blot shows the abundance of 14-3-3 β in RT4 and T24 cells in response to an increased dosage of IGF-I treatment. Samples from whole lysates were loaded equally at 60μg

for protein detection, and GAPDH was assessed as reference protein. Proteins from MCF7 (a human breast adenocarcinoma cell line) cell lysates were used as positive controls for β-catenin. (**B**) & (**C**): The graphs show the mean of fold change of the optical density measurements of 14-3-3 β in RT4 and T24 cells, respectively, in response to increased dosage of IGF-I (from 0 to 100ng/ml for 48 hours) from three experiments each performed at least in triplicate; and error bars demonstrate the standard error of the mean of experiments (n=3). (**D**) & (**E**): The blots present the localisation of 14-3-3 β in the presence or absence of IGF-I treatment in RT4 and T24 cells, respectively, using cellular fractionation. Lamin and Tubulin exist only in nuclei and cytoplasm, respectively, and they are an indicator of the efficiency of protein separation. "T": total cell lysates; "C": cytoplasmic extract; "N": nuclear extract. (**F**) & (**G**): The graphs present the densitometry fold change of cytoplasmic 14-3-3 β normalised to total 14-3-3 β in the total cell lysates in RT4 and T24 cells, respectively, in response to treatment with and without the presence of IGF-I (at 50ng/ml for 48 hours), with error bars representing the standard error of the mean of experiments (n=3).

5.5 Discussion

Accumulating evidence indicates a relationship between IGF-activity and the promotion of EMT in bladder cancer: in this study two bladder cancer cell lines the RT4 (with an epithelial-like phenotype) and T24 (with a mesenchymal-like phenotype) were used to investigate this suggested role of IGF-I.

Promoting effects of IGF-I on cell events, such as cell proliferation and invasion, have been reported in many cancer types such as breast (Sarkissyan, Sarkissyan et al. 2014). As summarised in Table 28, the results of my study showed that exogenous IGF-I induced a significant increase of cell proliferation in T24 cells, but it did not affect RT4 cells, whilst the increase induced by IGF-I observed in RT4 cells which was shown in the TTI assay was due to the high sensitivity of this technique in measuring DNA synthesis. Similarly, the ability of T24 cells to migrate was enhanced by the treatment of IGF-I with RT4 cells showing no stimulation of migration. IGF-I promoted cell invasion in both RT4 and T24 cell lines. Regarding colony formation in soft agar, in response to the treatment of IGF-I, both RT4 and T24 cells exhibited larger colonies but increased colony forming efficiency was only found in T24 cells. These data suggest the association between higher IGF activity and increased risk of progression of bladder cancer.

With the promoting effects of IGF-I on bladder cancer development identified, the signalling pathway(s) through which it may act was investigated. Two

signalling pathways, including IGF-IR/PI3K/Akt and IGF-IR/MAPK/ERK, were examined (Hermanto, Zong et al. 2000, Liu, Li et al. 2011, Zhu, Qi et al. 2011).

A study of bladder cancer biopsies showed up-regulated IGF-IR in bladder cancer compared with non-malignant bladder (Rochester, Patel et al. 2007), and IGF-IR knockdown via microRNA-145 was suggested to inhibit bladder cancer progression (Zhu, Xu et al. 2014). However, the correlations between IGF-IR level and tumour grade in bladder cancer remains unclear. In my study, the basal levels of the insulin-like growth factor receptor 1 (IGF-IR) and the insulin receptor (IR) were found to be much higher in the epithelial-like RT4 cell line than that in the mesenchymal-like T24 cells, Short-exposure-to-IGF-I treatment (from 5 to 30 minutes) showed a more rapid phosphorylation of the IGF-IR in RT4 cells (from 5 minutes) than that in T24 cells (with no obvious phosphorylation of IGF-IR observed until 30 minutes), which suggests the abundance of the IGF-IR plays an important role in facilitating the quick response to IGF-I in cells (Pandini, Vigneri et al. 1999).

Rapid stimulation of phopho-Akt (p-Akt) activation from 5 to 30 minutes was observed in both RT4 and T24 cells in response to IGF-I. In contrast, no stimulation of phospho-MAPK (p-MAPK) activation was observed in either RT4 or T24 cells, implying that the IGF-IR/PI3K/Akt might be the dominant signalling pathway in bladder cancer. As I observed that p-Akt was activated by IGF-I earlier than any detected change in the IGF-IR in T24 cells, it suggests the activation of IGF-IR was transient or the sensitivity in its detection by Western blotting poor, or that other tyrosine kinase receptors, such as the IR,

may also be playing a role in the aggressive bladder cancer cells; this would be worth further investigation.

To confirm that IGF-I exerts its effects through the IGF-IR/PI3K/Akt axis in bladder cancer, AG1024 and LY294002, a specific inhibitor of IGF-IR and PI3K, respectively, were used to block the signalling pathway and the following effects on cell proliferation, invasion, migration and colony formation were examined with results briefly summarised in Table 28.

Inhibiting the IGF-IR using AG1024 induced a significant decrease in cell growth as well as an increase in cell death in T24 cells, with no significant changes observed in RT4 cells. Both the invasive and colony forming ability was impaired when the IGF-IR was inhibited in RT4 and T24 cells. Moreover, the migratory ability was impeded in T24 cells following the inhibition of the IGF-IR. Similarly, inhibiting PI3K using LY294002 significantly decreased cell colony formation in both RT4 and T24 cells with the migratory ability of T24 cells reduced.

Therefore, the IGF-IR/PI3K/Akt axis is considered to be the dominant signalling pathway involved in the promotion of bladder cancer progression induced by exogenously added IGF-I. The results with T24 cells showing a stronger response to IGF-I treatment with less basal IGF-IR expression suggest that the examination of endogenous levels of IGF-I in bladder cancer cells is required.

IGF-I also influenced EMT in bladder cancer (Table 28) with the results briefly summarised in Table 29. It induced changes in the levels of EMT markers in bladder cancer with the down-regulation of E-cadherin, an epithelial marker, in RT4 cells and up-regulation of N-cadherin, a mesenchymal marker, in T24 cells, indicating its links to EMT during the progress of cancer aggressiveness (Morali, Delmas et al. 2001, Ahmad, Morton et al. 2011). Up-regulation of the levels of ZEB-1, an EMT-inducing transcription factor that has been reported in the development of many types of cancer, including breast (Walsh and Damjanovski 2011), was also observed in T24 cells. β-catenin is absent in the nuclear component of RT4 cells and is present in small amounts in the nuclear component of T24 cells. IGF-1 stimulated translocation of β-catenin into the nucleus in both cell lines which could lead to its binding to transcription factors (TCF) and, therefore, promote the expression of target oncogenes involved in Wnt signalling pathway (Ahmad, Morton et al. 2011). Nuclear β-catenin is considered as a metastasis inducer in colon cancer by conferring resistance to the FOXO3a-mediated apoptosis which was reversed by XAV-939, an inhibitor of Wnt-β-catenin signalling (Tenbaum, Ordonez-Moran et al. 2012). The decrease in FOXO3a was reported in urothelial carcinoma tumour samples with higher aggressiveness (Shiota, Song et al. 2010). However, increased levels of FOXO3a were observed in both RT4 and T24 cells with decreased expression in the nuclear extracts following IGF-I treatment, which suggests IGF-I induced cancer progression through inhibiting the binding of β-catenin and FOXO3a in cell nuclei. FOXA1 is also reported to be low in high-grade bladder cancer (DeGraff, Clark et al. 2012) which was confirmed in this study with reduced levels of FOXA1 found in mesenchymal-like T24 cells. In

response to IGF-I treatment, T24 cells showed a further reduction in FOXA1 levels. However, in RT4 cells a significant increase in the level of this protein was observed in whole lysates with a trace of, but not a significant induction of expression in the cytoplasmic cell extracts. It has been reported that knockdown of FOXA1 in RT4 cells led to decreased E-cadherin and increased cell proliferation (DeGraff, Clark et al. 2012), and as a cell line propagated from a well-differentiated tumour, RT4 cells demonstrated higher FOXA1 expression (DeGraff, Clark et al. 2012). Therefore, it would be interesting to further investigate the role FOXA1 in IGF activity in bladder cancer. It has also been reported that insulin/IGF induced activation of Akt results in phosphorylation of FOXO proteins leading to their binding to 14-3-3 proteins which then retains the FOXO proteins in the cytoplasm and thus promotes cell survival by reducing the nuclear actions of FOXO proteins (Jin, George Fantus et al. 2008). It was observed that 14-3-3 β was expressed at high levels in both RT4 and T24 cells with localisation mainly in the cytoplasm, and IGF-I-induced an enhancement in the levels of this protein compared to the control; consistent with a supportive role for 14-3-3 β in EMT of bladder cancer through the binding of FOXO3a .

Table 28: a summary of the effects of IGF-I, AG1024 and LY294002 on cell phenotype and EMT in bladder cancer cells

		Cell proliferation	Cell invasion	Cell migration	Cell colony formation	EMT
IGF-I	RT4	NE	√ (+)	NE	√ (+)	√ (+)
	T24	√ (+)	√ (+)	√ (+)	√ (+)	√ (+)
AG1024 (IGF-IR inhibitor)	RT4	NE	√ (-)	/	√ (-)	/
	T24	√ (-)	√ (-)	√ (-)	√ (-)	/
LY294002 (PI3k inhibitor)	RT4	/	√ (-)	/	/	/
	T24	/	√ (-)	√ (-)	/	/

"√ (+)": promoting effect; "√ (-)": inhibiting effect; "NE": no effect. "/": not performed in this study.

Table 29: a summary of the effects of IGF-I on EMT-related molecules in bladder cancer cells

	N-cadherin	E-cadherin	β-catenin	ZEB-1	FOXO3a	FOXA1	14-3-3 β
RT4	NE	√ (-)	NE; nuclear trans-location	NE	√ (+); decreased levels in the cell nuclei	√ (+)	√ (+); increased levels in the cytoplasm
T24	√ (+)	NE	NE; increased levels in the cell nuclei	√ (+)	√ (+); decreased levels in the cell nuclei	√ (-) (NS*)	NE; increased levels in the cytoplasm

"√ (+)": increased in total protein levels; "√ (-)": decreased in total protein levels; "NE": no effect on total protein levels; "NS*": not significant.

In summary, exogenously added IGF-I exerts promoting effects on bladder cancer development by enhancing the proliferative, invasive, migratory and colony forming abilities of bladder cancer cells, and these effects are more potent in mesenchymal-like T24 cells than that in epithelial-like RT4 cells. The IGF-IR/PI3K/Akt is the dominant signalling pathway by which the above effects of IGF-I are mediated, and inhibitors targeting components in this signalling pathway shed light on potential therapeutic drugs for bladder cancer treatment. A relationship between IGF-I and regulation of EMT molecules implies a promoting role for IGF-I in bladder cancer progression.

Chapter 6- Final Discussion

6.1 Summary of Main results

In humans, bladder cancer is the most common malignancy of the urinary tract. With its high incidence and recurrence, poor prognoses after progression, as well as great costs to both patients and the society, bladder cancer has become a major clinical issue that requires more understanding in order to impact treatment strategies to improve outcome.

Epithelial-to-mesenchymal transition (EMT) facilitates metastatic progression of many cancer types including bladder (McConkey, Choi et al. 2009), and accumulating evidence indicates an association of EMT with IGF-activity in many cancers such as colorectal (Yao, Su et al. 2016). Therefore, this study aimed to investigate whether the IGF-axis influenced EMT in bladder cancer progression.

As a member of the IGF system, IGFBP-2 is the second most abundant IGFBP in human serum with contradictory results about its role in cancer, being reported as a promoter (Perks, Vernon et al. 2007, Uzoh, Holly et al. 2011, Foulstone, Zeng et al. 2013, Gao, Sun et al. 2016) but also an inhibitor (Hoflich, Lahm et al. 1998, Frommer, Reichenmiller et al. 2006).

To investigate the role of IGFBP-2 in bladder cancer development, we manipulated its levels in specific bladder cancer cell lines and examined any phenotypic changes that occurred.

Knocking down IGFBP-2 using specific siRNA was performed in IGFBP-2-abundant epithelial-like RT4 cells. With the reduction in IGFBP-2 expression, a significant increase in cell proliferation and promotion of cell invasion, as well as colony formation, was observed, along with a decrease in the levels of E-cadherin (an epithelial marker) along with β-catenin translocation to the nucleus. Exogenous IGFBP-2 was added to IGFBP-2-null mesenchymal-like T24 and TCCSUP cells, and this led to a significant decrease in cell growth, invasion, migration, colony formation as well as the expression of N-cadherin (a mesenchymal marker). These data suggested that IGFBP-2 was playing a critical inhibitory role in bladder cancer exerting anti-proliferative, -invasive, -migratory, -colony-forming as well as -EMT effects in cancer progression.

Chemo-sensitivity to cisplatin in bladder cancer was also investigated using epithelial-like RT4 and mesenchymal-like T24 cells representing cancer types with less and more aggressiveness, respectively. With the same manipulations of the levels of IGFBP-2 using siRNA transfection or exogenous addition, the results demonstrated that higher levels of IGFBP-2 were associated with enhanced sensitivity to cisplatin suggesting IGFBP-2 may be used as a marker of chemo-sensitivity to cisplatin in bladder cancer. However, in contrast the inhibition of IGFBP-2 using gene silencing was reported to enhance cell sensitivity to cisplatin in a cisplatin-resistant bladder cancer subline (BIU87-CisR) (Zhu H 2015). Therefore, further studies on additional cell lines are required.

How the levels of IGFBP-2 are regulated and in which way(s) IGFBP-2 acts as a tumour suppressor in bladder cancer, either an IGF-dependent or -independent, were then assessed.

Based on studies of epigenetic changes in cancer (Han, Wolff et al. 2012, Tahara, Shibata et al. 2014), aberrant hypermethylation of the gene promoter of *IGFBP-2* was considered to contribute to the loss of IGFBP-2 in advanced bladder cancer. This conclusion was supported by the data of my study: the re-expression of IGFBP-2 in IGFBP-2-null T24 cell line following treatment with AZA, a commonly used demethylating agent, and the detection of relevant changes in the methylation status of the promoter region of *IGFBP-2* gene in T24 cells using Combined Bisulphite Restriction Assay (COBRA). Moreover, in T24 cells, dosing with AZA led to similar phenotypic changes that were observed on addition of exogenous IGFBP-2, including a reduction in the levels of N-cadherin, a mesenchymal marker, along with significantly decreased cell proliferation, colony formation and increased cell death.

Differences in cell responses to AZA treatment were found between TCCSSUP and T24 cells, and this likely reflects the heterogeneity among cell lines with similar phenotypes, whilst another study demonstrated differences in the sensitivity of T24 and TCCSUP cell lines in response to cisplatin (Falso, Buchholz et al. 2012). These data suggest further studies on additional cell lines and other epigenetic changes, such as histone modification, are required.

To understand the working mechanism of IGFBP-2 in bladder cancer, we used a number of strategies: we used NBI-31772, an inhibitor of IGF/IGFBP

interactions, along with exogenously added human recombinant IGF-I as well as manipulation of IGFBP-2 levels in RT4 and T24 cells by siRNA transfection and adding exogenous IGFBP-2, respectively. These data indicated that IGFBP-2 acted in both IGF-dependent and -independent manner in bladder cancers despite the cancer phenotype (Frommer, Reichenmiller et al. 2006, Wheatcroft and Kearney 2009, Uzoh, Holly et al. 2011). The intrinsic effects of IGFBP-2 via binding to integrin receptors have been reported in many cancers such as prostate (Uzoh, Holly et al. 2011), and should be further investigated in bladder cancer.

Having established that the exogenous addition of IGF-I promoted cell proliferation and migration of T24 cells in this study, and the conclusion that IGFBP-2 exerted some of its effects partly through an interaction with IGFs in both cell lines, we next compared the effects of exogenously added IGF-I on bladder cancer cell phenotypes using epithelial-like RT4 and mesenchymal-like T24 cell lines.

Following the addition of IGF-I, enhanced proliferation, invasion, migration as well as colony formation were observed. And these effects were more potent in T24 (of a mesenchymal phenotype) than in epithelial-like RT4 cells. Moreover, the regulation of EMT molecules by IGF-I, such as nuclear translocation of β-catenin which can lead to more aggressive cancer, was also observed, suggesting that IGF-I plays a role in bladder cancer progression (Walsh and Damjanovski 2011, Liao, Wang et al. 2014, Sarkissyan, Sarkissyan et al. 2014).

Further investigation into how exogenous IGF-I exerts these effects demonstrated rapid stimulation of phospho-Akt (p-Akt) in both RT4 and T24 cells in comparison with no activation of phospho-MAPK (p-MAPK) in either RT4 or T24 cell lines. And inhibition of PI3K using LY294002, a specific PI3K inhibitor, blocked these effects induced by IGF-I.

This indicated that the IGF-IR/PI3K/Akt might be the dominant signalling pathway in mediating IGF-I actions, and that specific inhibitors targeting its components may provide potential particular therapeutic drugs for bladder cancer treatment (Bergqvist, Holgersson et al. 2017, Xu, Wang et al. 2017).

6.2 Future work

Considering the heterogeneity that exists in tumours, including those of the bladder, studies on a more expansive panel of bladder cancer cell lines would be required to fully understand the mechanism of progression. In addition, I have already obtained ethics approval to access a cohort of bladder tumours, and in future work a pilot translational tissue study would be performed. We could assess the levels of the key molecules we have identified as playing a role in bladder cancer progression, such as IGFBP-2, the IGF-IR, p-Akt and markers of EMT, such as nuclear β-catenin that has been shown to confer resistance to FOXO3a-mediated apoptosis induced by PI3K and Akt inhibitors in colon cancer (Tenbaum, Ordonez-Moran et al. 2012). Thus further studies to examine the associations between these molecules would be valuable to

confirm the findings of my *in vitro* studies and to determine their association with any clinicopathological features of bladder cancer progression.

My study examined the impact of blocking the IGF-IR and of adding in exogenous IGF-I; these were informative experiments, and future work measuring levels of endogenously produced IGFs and other IGFBPs would complete the picture.

To better understand the relationship between IGFBP-2 and cell chemosensitivity to cisplatin in bladder cancer, well-developed stable clinically relevant cisplatin-resistant cell lines and doses of cisplatin administered at a pulsed low-level treatment strategy would be needed to mimic the clinic setting.

6.2.1 A co-culture model at the development stage

Poor prognoses are related to advanced bladder cancers when disease includes muscle invasion. I have also been developing a co-culture model to investigate bladder cancer invasion behaviour by growing BdSMC (see 2.1.2), a primary human bladder smooth muscle cell line in combination with the aggressive mesenchymal-like IGFBP-2-null T24 cells. Using this co-culture model, I have also been assessing if cross-talk exists between the T24 and epithelial-like IGFBP-2-abundant RT4 cells.

A preliminary migration assay was performed (as described in 2.9) to investigate the migration of T24 cells in the presence of RT4 or BdSMC cells. As shown in Figure 80, the migration of T24 cells was inhibited in the presence

of RT4 cells, and this inhibition was more marked when T24 cells were cultured in the presence of BdSMC cells.

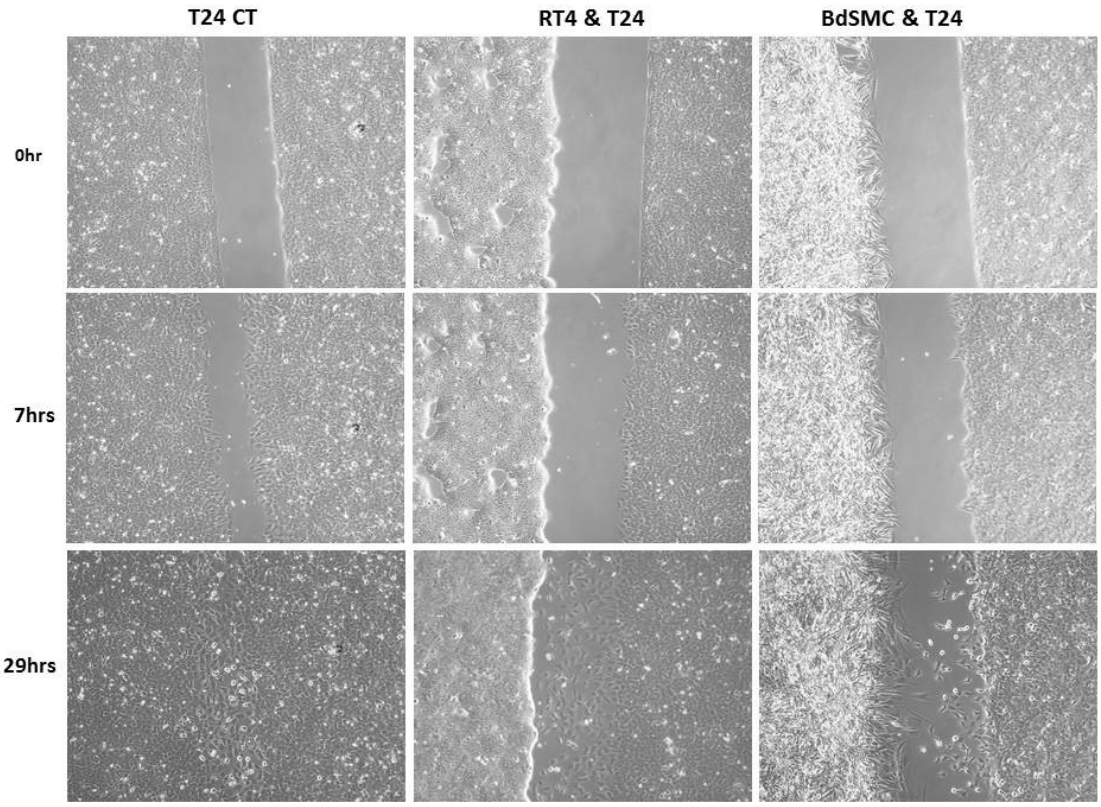

Figure 80: co-culture of T24, RT4 and BdSMC cells

Cells were seeded at a certain density (T24: 0.028x10^6, RT4: 0.0525 x10^6; BdSMC: 0.0315 x10^6 cells) into each chamber in GM and allowed to grow for approximately 24 hours to reach about 80% confluence. Cell reached 90-95% confluence during an additional 24 hours in SFM. The inserts were then removed leaving an observed gap, and gap closure was recorded for up to 30 hours. Images of cell gaps were taken at different times with relative labels. "0hr": the start point after the removal of inserts; "7hrs", "29hrs": 7 and 29 hours after the removal of inserts. All images demonstrate the results from one experiment performed in duplicate (n=1). All images shown are at x10 magnification.

Optimisation of this co-culture model, such as cell seeding density, is required in the first instance. Then, as we found that components of the IGF axis played a critical role in bladder cancer progression including cell migration and invasion, future work would use this model to investigate whether manipulating components of the IGF axis, such as IGFBP-2, affects the

behaviour of bladder cancer cells in the presence of normal bladder muscle cells.

Chapter 7- References

Abba, M. L., N. Patil, J. H. Leupold and H. Allgayer (2016). "MicroRNA Regulation of Epithelial to Mesenchymal Transition." J Clin Med **5**(1).

Acloque, H., M. S. Adams, K. Fishwick, M. Bronner-Fraser and M. A. Nieto (2009). "Epithelial-mesenchymal transitions: the importance of changing cell state in development and disease." J Clin Invest **119**(6): 1438-1449.

Adam Pickard, S. S. M. (2015). "HPV16 Down-Regulates the Insulin-Like Growth Factor Binding Protein 2 to Promote Epithelial Invasion in Organotypic Cultures."

Agrawal, N., P. V. Dasaradhi, A. Mohmmed, P. Malhotra, R. K. Bhatnagar and S. K. Mukherjee (2003). "RNA interference: biology, mechanism, and applications." Microbiol Mol Biol Rev **67**(4): 657-685.

Ahmad, I., J. P. Morton, L. B. Singh, S. M. Radulescu, R. A. Ridgway, S. Patel, J. Woodgett, D. J. Winton, M. M. Taketo, X. R. Wu, H. Y. Leung and O. J. Sansom (2011). "beta-Catenin activation synergizes with PTEN loss to cause bladder cancer formation." Oncogene **30**(2): 178-189.

Al Moustafa, A. E. (2013). "Epithelial-mesenchymal transition and its regulators are major targets of triple-negative breast cancer." Cell Adh Migr **7**(5): 424-425.

Alexander, R. E., L. Wang, A. Lopez-Beltran, R. E. Emerson, R. Montironi, J. A. Pedrosa, H. Z. Kaimakliotis, M. O. Koch and L. Cheng (2015). "Human papillomavirus (HPV)-induced neoplasia in the urinary bladder: a missing link?" Histol Histopathol: 11715.

American Cancer Society, A. (2016). "Bladder Cancer Overview."

Amling, C. L. (2001). "Diagnosis and management of superficial bladder cancer." Curr Probl Cancer **25**(4): 219-278.

Azar, W. J., S. H. Azar, S. Higgins, J. F. Hu, A. R. Hoffman, D. F. Newgreen, G. A. Werther and V. C. Russo (2011). "IGFBP-2 enhances VEGF gene promoter activity and consequent promotion of angiogenesis by neuroblastoma cells." Endocrinology **152**(9): 3332-3342.

Azar, W. J., S. Zivkovic, G. A. Werther and V. C. Russo (2014). "IGFBP-2 nuclear translocation is mediated by a functional NLS sequence and is essential for its pro-tumorigenic actions in cancer cells." Oncogene **33**(5): 578-588.

Babjuk, M., A. Bohle, M. Burger, O. Capoun, D. Cohen, E. M. Comperat, V. Hernandez, E. Kaasinen, J. Palou, M. Roupret, B. W. van Rhijn, S. F. Shariat, V. Soukup, R. J. Sylvester and R. Zigeuner (2017). "EAU Guidelines on Non-Muscle-invasive Urothelial Carcinoma of the Bladder: Update 2016." Eur Urol **71**(3): 447-461.

Bachelder, R. E., S. O. Yoon, C. Franci, A. G. de Herreros and A. M. Mercurio (2005). "Glycogen synthase kinase-3 is an endogenous inhibitor of Snail transcription: implications for the epithelial-mesenchymal transition." J Cell Biol **168**(1): 29-33.

Baselga, J. (2011). "Targeting the phosphoinositide-3 (PI3) kinase pathway in breast cancer." Oncologist **16 Suppl 1**: 12-19.

Baxter, R. C. (2014). "IGF binding proteins in cancer: mechanistic and clinical insights." Nat Rev Cancer **14**(5): 329-341.

Beattie, J., K. Phillips, J. H. Shand, M. Szymanowska, D. J. Flint and G. J. Allan (2008). "Molecular interactions in the insulin-like growth factor (IGF) axis: a surface plasmon resonance (SPR) based biosensor study." Mol Cell Biochem **307**(1-2): 221-236.

Bedi, U., V. K. Mishra, D. Wasilewski, C. Scheel and S. A. Johnsen (2014). "Epigenetic plasticity: a central regulator of epithelial-to-mesenchymal transition in cancer." Oncotarget **5**(8): 2016-2029.

Berg, U., P. Bang and C. Carlsson-Skwirut (2007). "Calpain proteolysis of insulin-like growth factor binding protein (IGFBP) -2 and -3, but not of IGFBP-1." Biol Chem **388**(8): 859-863.

Bergmann, U., H. Funatomi, M. Yokoyama, H. G. Beger and M. Korc (1995). "Insulin-like growth factor I overexpression in human pancreatic cancer: evidence for autocrine and paracrine roles." Cancer Res **55**(10): 2007-2011.

Bergqvist, M., G. Holgersson, I. Bondarenko, E. Grechanaya, A. Maximovich, G. Andor, M. Klockare, M. Thureson, M. Jerling and J. Harmenberg (2017). "Phase II randomized study of the IGF-1R pathway modulator AXL1717 compared to docetaxel in patients with previously treated, locally advanced or metastatic non-small cell lung cancer." Acta Oncol **56**(3): 441-447.

Bienz, M. (2005). "beta-Catenin: a pivot between cell adhesion and Wnt signalling." Curr Biol **15**(2): R64-67.

Biernacka, K. M., C. C. Uzoh, L. Zeng, R. A. Persad, A. Bahl, D. Gillatt, C. M. Perks and J. M. Holly (2013). "Hyperglycaemia-induced chemoresistance of prostate cancer cells due to IGFBP2." Endocr Relat Cancer **20**(5): 741-751.

Bosschieter, J., A. Hentschel, C. D. Savci-Heijink, J. Patrick van der Voorn, L. Rozendaal, A. N. Vis, B. W. G. van Rhijn, B. I. Lissenberg-Witte, E. E. Fransen van de Putte, R. J. A. van Moorselaar and J. A. Nieuwenhuijzen (2018). "Reproducibility and Prognostic Performance of the 1973 and 2004 World Health Organization Classifications for Grade in Non-muscle-invasive Bladder Cancer: A Multicenter Study in 328 Bladder Tumors." Clin Genitourin Cancer.

Bringuier, P. P., R. Umbas, H. E. Schaafsma, H. F. Karthaus, F. M. Debruyne and J. A. Schalken (1993). "Decreased E-cadherin immunoreactivity correlates with poor survival in patients with bladder tumors." Cancer Res **53**(14): 3241-3245.

Bryan, R. T. (2015). "Cell adhesion and urothelial bladder cancer: the role of cadherin switching and related phenomena." Philos Trans R Soc Lond B Biol Sci **370**(1661): 20140042.

Bryan, R. T., P. A. Atherfold, Y. Yeo, L. J. Jones, R. F. Harrison, D. M. Wallace and J. A. Jankowski (2008). "Cadherin switching dictates the biology of transitional cell carcinoma of the bladder: ex vivo and in vitro studies." J Pathol **215**(2): 184-194.

Bryan, R. T. and C. Tselepis (2010). "Cadherin switching and bladder cancer." J Urol **184**(2): 423-431.

Byrne, R. R., S. F. Shariat, R. Brown, M. W. Kattan, R. J. Morton, T. M. Wheeler and S. P. Lerner (2001). "E-cadherin immunostaining of bladder transitional cell carcinoma, carcinoma in situ and lymph node metastases with long-term followup." J Urol **165**(5): 1473-1479.

Cai, Z., N. Chattopadhyay, W. J. Liu, C. Chan, J. P. Pignol and R. M. Reilly (2011). "Optimized digital counting colonies of clonogenic assays using ImageJ software and customized macros: comparison with manual counting." Int J Radiat Biol **87**(11): 1135-1146.

Cancer Genome Atlas Research, N. (2014). "Comprehensive molecular characterization of urothelial bladder carcinoma." Nature **507**(7492): 315-322.

Cancer Research UK, C. (2016). "Bladder Cancer Overview - About the Bladder."

Cancer Research UK, C. (2016). "Bladder Cancer Overview - Diagnosing Bladder Cancer."
Cancer Research UK, C. (2016). "Bladder Cancer Overview -Treating Bladder Cancer."
Cancer Research UK, C. (2016). "Bladder cancer statistics."
Carmona, F. J., V. Davalos, E. Vidal, A. Gomez, H. Heyn, Y. Hashimoto, M. Vizoso, A. Martinez-Cardus, S. Sayols, H. J. Ferreira, J. V. Sanchez-Mut, S. Moran, M. Margeli, E. Castella, M. Berdasco, O. A. Stefansson, J. E. Eyfjord, E. Gonzalez-Suarez, J. Dopazo, M. Orozco, I. G. Gut and M. Esteller (2014). "A comprehensive DNA methylation profile of epithelial-to-mesenchymal transition." Cancer Res **74**(19): 5608-5619.
Cauberg Evelyne, C. C., J. J. de la Rosette and T. M. de Reijke (2011). "Emerging optical techniques in advanced cystoscopy for bladder cancer diagnosis: A review of the current literature." Indian J Urol **27**(2): 245-251.
Chavan, S., F. Bray, J. Lortet-Tieulent, M. Goodman and A. Jemal (2014). "International variations in bladder cancer incidence and mortality." Eur Urol **66**(1): 59-73.
Chen, H. F. and K. J. Wu (2016). "Epigenetics, TET proteins, and hypoxia in epithelial-mesenchymal transition and tumorigenesis." Biomedicine (Taipei) **6**(1): 1.
Chen, J., Q. Han and D. Pei (2012). "EMT and MET as paradigms for cell fate switching." J Mol Cell Biol **4**(2): 66-69.
Chen, X., J. Zheng, Y. Zou, C. Song, X. Hu and C. C. Zhang (2013). "IGF binding protein 2 is a cell-autonomous factor supporting survival and migration of acute leukemia cells." J Hematol Oncol **6**(1): 72.
Chiba, T., O. Yokosuka, K. Fukai, Y. Hirasawa, M. Tada, R. Mikata, F. Imazeki, H. Taniguchi, A. Iwama, M. Miyazaki, T. Ochiai and H. Saisho (2005). "Identification and investigation of methylated genes in hepatoma." Eur J Cancer **41**(8): 1185-1194.
Choi, W. Y., M. Gemberling, J. Wang, J. E. Holdway, M. C. Shen, R. O. Karlstrom and K. D. Poss (2013). "In vivo monitoring of cardiomyocyte proliferation to identify chemical modifiers of heart regeneration." Development **140**(3): 660-666.
Christoph, F., S. Weikert, C. Kempkensteffen, H. Krause, M. Schostak, K. Miller and M. Schrader (2006). "Regularly methylated novel pro-apoptotic genes associated with recurrence in transitional cell carcinoma of the bladder." Int J Cancer **119**(6): 1396-1402.
Clayton, P. E., I. Banerjee, P. G. Murray and A. G. Renehan (2011). "Growth hormone, the insulin-like growth factor axis, insulin and cancer risk." Nat Rev Endocrinol **7**(1): 11-24.
De Wever, O., P. Pauwels, B. De Craene, M. Sabbah, S. Emami, G. Redeuilh, C. Gespach, M. Bracke and G. Berx (2008). "Molecular and pathological signatures of epithelial-mesenchymal transitions at the cancer invasion front." Histochem Cell Biol **130**(3): 481-494.
Degraff, D. J., A. A. Aguiar and R. A. Sikes (2009). "Disease evidence for IGFBP-2 as a key player in prostate cancer progression and development of osteosclerotic lesions." Am J Transl Res **1**(2): 115-130.

DeGraff, D. J., P. E. Clark, J. M. Cates, H. Yamashita, V. L. Robinson, X. Yu, M. E. Smolkin, S. S. Chang, M. S. Cookson, M. K. Herrick, S. F. Shariat, G. D. Steinberg, H. F. Frierson, X. R. Wu, D. Theodorescu and R. J. Matusik (2012). "Loss of the urothelial differentiation marker FOXA1 is associated with high grade, late stage bladder cancer and increased tumor proliferation." PLoS One **7**(5): e36669.

Diaz-Lopez, A., J. Diaz-Martin, G. Moreno-Bueno, E. P. Cuevas, V. Santos, D. Olmeda, F. Portillo, J. Palacios and A. Cano (2015). "Zeb1 and Snail1 engage miR-200f transcriptional and epigenetic regulation during EMT." Int J Cancer **136**(4): E62-73.

Doble, B. W. and J. R. Woodgett (2007). "Role of glycogen synthase kinase-3 in cell fate and epithelial-mesenchymal transitions." Cells Tissues Organs **185**(1-3): 73-84.

Dobruch, J., S. Daneshmand, M. Fisch, Y. Lotan, A. P. Noon, M. J. Resnick, S. F. Shariat, A. R. Zlotta and S. A. Boorjian (2016). "Gender and Bladder Cancer: A Collaborative Review of Etiology, Biology, and Outcomes." Eur Urol **69**(2): 300-310.

Dung V. Nguyen, S. L. C., Lynn C. Shaw, Jennifer L. Kielczewski, Hannah E. Korah, Maria B. Grant (2013). "An ocular view of the IGF–IGFBP system." Growth Hormone & IGF Research.

Dupont, C., D. R. Armant and C. A. Brenner (2009). "Epigenetics: definition, mechanisms and clinical perspective." Semin Reprod Med **27**(5): 351-357.

Eble, J. N., Sauter, G., Epstein, J. I., Sesterhenn, I. A. (2004). "World Health Organization Classification of Tumours. Pathology and Genetics of Tumours of the Urinary System and Male Genital Organs." IARC Press Lyon.

El Tayebi, H. M. and A. I. Abdelaziz (2016). "Epigenetic regulation of insulin-like growth factor axis in hepatocellular carcinoma." World J Gastroenterol **22**(9): 2668-2677.

Endogenous, H., G. Breast Cancer Collaborative, T. J. Key, P. N. Appleby, G. K. Reeves and A. W. Roddam (2010). "Insulin-like growth factor 1 (IGF1), IGF binding protein 3 (IGFBP3), and breast cancer risk: pooled individual data analysis of 17 prospective studies." Lancet Oncol **11**(6): 530-542.

Falso, M. J., B. A. Buchholz and R. W. White (2012). "Stem-like cells in bladder cancer cell lines with differential sensitivity to cisplatin." Anticancer Res **32**(3): 733-738.

Ferlay, J., I. Soerjomataram, R. Dikshit, S. Eser, C. Mathers, M. Rebelo, D. M. Parkin, D. Forman and F. Bray (2015). "Cancer incidence and mortality worldwide: sources, methods and major patterns in GLOBOCAN 2012." Int J Cancer **136**(5): E359-386.

Forbes, B. E., P. McCarthy and R. S. Norton (2012). "Insulin-like growth factor binding proteins: a structural perspective." Front Endocrinol (Lausanne) **3**: 38.

Fottner, C., T. Minnemann, S. Kalmbach and M. M. Weber (2006). "Overexpression of the insulin-like growth factor I receptor in human pheochromocytomas." J Mol Endocrinol **36**(2): 279-287.

Foulstone, E., S. Prince, O. Zaccheo, J. L. Burns, J. Harper, C. Jacobs, D. Church and A. B. Hassan (2005). "Insulin-like growth factor ligands, receptors, and binding proteins in cancer." J Pathol **205**(2): 145-153.

Foulstone, E. J., L. Zeng, C. M. Perks and J. M. Holly (2013). "Insulin-like growth factor binding protein 2 (IGFBP-2) promotes growth and survival of breast epithelial cells: novel regulation of the estrogen receptor." Endocrinology **154**(5): 1780-1793.

Foulstone, E. J., L. Zeng, C. M. Perks and J. M. Holly (2013). "(paper in the blue folder) - Insulin-like growth factor binding protein 2 (IGFBP-2) promotes growth and survival of breast epithelial cells: novel regulation of the estrogen receptor." Endocrinology **154**(5): 1780-1793.
Froesch, E. R., H. Buergi, E. B. Ramseier, P. Bally and A. Labhart (1963). "Antibody-Suppressible and Nonsuppressible Insulin-Like Activities in Human Serum and Their Physiologic Significance. An Insulin Assay with Adipose Tissue of Increased Precision and Specificity." J Clin Invest **42**: 1816-1834.
Frommer, K. W., K. Reichenmiller, B. S. Schutt, A. Hoeflich, M. B. Ranke, G. Dodt and M. W. Elmlinger (2006). "IGF-independent effects of IGFBP-2 on the human breast cancer cell line Hs578T." J Mol Endocrinol **37**(1): 13-23.
Fukushima, T. and H. Kataoka (2007). "Roles of insulin-like growth factor binding protein-2 (IGFBP-2) in glioblastoma." Anticancer Res **27**(6A): 3685-3692.
Gallagher, E. J. and D. LeRoith (2010). "The proliferating role of insulin and insulin-like growth factors in cancer." Trends Endocrinol Metab **21**(10): 610-618.
Gao, S., Y. Sun, X. Zhang, L. Hu, Y. Liu, C. Y. Chua, L. M. Phillips, H. Ren, J. B. Fleming, H. Wang, P. J. Chiao, J. Hao and W. Zhang (2016). "IGFBP2 Activates the NF-kappaB Pathway to Drive Epithelial-Mesenchymal Transition and Invasive Character in Pancreatic Ductal Adenocarcinoma." Cancer Res **76**(22): 6543-6554.
Genua, M., S. Q. Xu, S. Buraschi, S. C. Peiper, L. G. Gomella, A. Belfiore, R. V. Iozzo and A. Morrione (2012). "Proline-rich tyrosine kinase 2 (Pyk2) regulates IGF-I-induced cell motility and invasion of urothelial carcinoma cells." PLoS One **7**(6): e40148.
Gheidari, F., B. Bakhshandeh, L. Teimoori-Toolabi, A. Mehrtash, M. Ghadir and S. Zeinali (2014). "TCF4 silencing sensitizes the colon cancer cell line to oxaliplatin as a common chemotherapeutic drug." Anticancer Drugs **25**(8): 908-916.
Ghosh, M., S. J. Brancato, P. K. Agarwal and A. B. Apolo (2014). "Targeted therapies in urothelial carcinoma." Curr Opin Oncol **26**(3): 305-320.
Ghoshal, K. and S. Bai (2007). "DNA methyltransferases as targets for cancer therapy." Drugs Today (Barc) **43**(6): 395-422.
Gos, M., J. Miloszewska and M. Przybyszewska (2009). "Epithelial-mesenchymal transition in cancer progression." Postepy Biochem **55**(2): 121-128.
Graham, T. R., H. E. Zhau, V. A. Odero-Marah, A. O. Osunkoya, K. S. Kimbro, M. Tighiouart, T. Liu, J. W. Simons and R. M. O'Regan (2008). "Insulin-like growth factor-I-dependent up-regulation of ZEB1 drives epithelial-to-mesenchymal transition in human prostate cancer cells." Cancer Res **68**(7): 2479-2488.
Gray, S. G., A. M. Baird, F. O'Kelly, G. Nikolaidis, M. Almgren, A. Meunier, E. Dockry, D. Hollywood, T. J. Ekstrom, A. S. Perry and K. J. O'Byrne (2012). "Gemcitabine reactivates epigenetically silenced genes and functions as a DNA methyltransferase inhibitor." Int J Mol Med **30**(6): 1505-1511.
Griffiths, T. R. and J. K. Mellon (2000). "Human papillomavirus and urological tumours: II. Role in bladder, prostate, renal and testicular cancer." BJU Int **85**(2): 211-217.
Guarino, M., B. Rubino and G. Ballabio (2007). "The role of epithelial-mesenchymal transition in cancer pathology." Pathology **39**(3): 305-318.

Gunlusoy, B., Y. Ceylan, T. Degirmenci, Z. Kozacioglu, T. Yonguc, H. Bozkurt, O. Aydogdu and V. Sen (2015). "Urothelial bladder cancer in young adults: Diagnosis, treatment and clinical behaviour." Can Urol Assoc J **9**(9-10): E727-730.
Han, H., E. M. Wolff and G. Liang (2012). "Epigenetic alterations in bladder cancer and their potential clinical implications." Adv Urol **2012**: 546917.
Hassler, M. R., A. Klisaroska, K. Kollmann, I. Steiner, M. Bilban, A. I. Schiefer, V. Sexl and G. Egger (2012). "Antineoplastic activity of the DNA methyltransferase inhibitor 5-aza-2'-deoxycytidine in anaplastic large cell lymphoma." Biochimie **94**(11): 2297-2307.
Hay, E. D. (1995). "An overview of epithelio-mesenchymal transformation." Acta Anat (Basel) **154**(1): 8-20.
Heidegger, I., P. Massoner, N. Sampson and H. Klocker (2015). "The insulin-like growth factor (IGF) axis as an anticancer target in prostate cancer." Cancer Lett **367**(2): 113-121.
Hellawell, G. O., G. D. Turner, D. R. Davies, R. Poulsom, S. F. Brewster and V. M. Macaulay (2002). "Expression of the type 1 insulin-like growth factor receptor is up-regulated in primary prostate cancer and commonly persists in metastatic disease." Cancer Res **62**(10): 2942-2950.
Henning, A., M. Wehrberger, S. Madersbacher, A. Pycha, T. Martini, E. Comploj, K. Jeschke, C. Tripolt and M. Rauchenwald (2013). "Do differences in clinical symptoms and referral patterns contribute to the gender gap in bladder cancer?" BJU Int **112**(1): 68-73.
Hermanto, U., C. S. Zong and L. H. Wang (2000). "Inhibition of mitogen-activated protein kinase kinase selectively inhibits cell proliferation in human breast cancer cells displaying enhanced insulin-like growth factor I-mediated mitogen-activated protein kinase activation." Cell Growth Differ **11**(12): 655-664.
Hoelzinger, D. B., L. Mariani, J. Weis, T. Woyke, T. J. Berens, W. S. McDonough, A. Sloan, S. W. Coons and M. E. Berens (2005). "Gene expression profile of glioblastoma multiforme invasive phenotype points to new therapeutic targets." Neoplasia **7**(1): 7-16.
Hoflich, A., H. Lahm, W. Blum, H. Kolb and E. Wolf (1998). "Insulin-like growth factor-binding protein-2 inhibits proliferation of human embryonic kidney fibroblasts and of IGF-responsive colon carcinoma cell lines." FEBS Lett **434**(3): 329-334.
Holly, J. M. and C. M. Perks (2012). "Insulin-like growth factor physiology: what we have learned from human studies." Endocrinol Metab Clin North Am **41**(2): 249-263, v.
Horibata, S., T. V. Vo, V. Subramanian, P. R. Thompson and S. A. Coonrod (2015). "Utilization of the Soft Agar Colony Formation Assay to Identify Inhibitors of Tumorigenicity in Breast Cancer Cells." J Vis Exp(99): e52727.
Huangyang, P. and Y. Shang (2013). "Epigenetic regulation of epithelial to mesenchymal transition." Curr Cancer Drug Targets **13**(9): 973-985.
Hwang, J. A., Y. Kim, S. H. Hong, J. Lee, Y. G. Cho, J. Y. Han, Y. H. Kim, J. Han, Y. M. Shim, Y. S. Lee and D. H. Kim (2013). "Epigenetic inactivation of heparan sulfate (glucosamine) 3-O-sulfotransferase 2 in lung cancer and its role in tumorigenesis." PLoS One **8**(11): e79634.

International Collaboration of Trialists, Medical Research Council Advanced Bladder Cancer Working Party, E. O. f. R. and, Treatment of Cancer Genito-Urinary Tract Cancer Group, Australian Bladder Cancer Study Group, National Cancer Institute of Canada Clinical Trials Group, Finnbladder, Norwegian Bladder Cancer Study Group, Club Urologico Espanol de Tratamiento Oncologico Group, G. Griffiths, R. Hall, R. Sylvester, D. Raghavan and M. K. Parmar (2011). "International phase III trial assessing neoadjuvant cisplatin, methotrexate, and vinblastine chemotherapy for muscle-invasive bladder cancer: long-term results of the BA06 30894 trial." J Clin Oncol **29**(16): 2171-2177.

Jabbari, K. and G. Bernardi (2004). "Cytosine methylation and CpG, TpG (CpA) and TpA frequencies." Gene **333**: 143-149.

Jemal, A., F. Bray, M. M. Center, J. Ferlay, E. Ward and D. Forman (2011). "Global cancer statistics." CA Cancer J Clin **61**(2): 69-90.

Jin, T., I. George Fantus and J. Sun (2008). "Wnt and beyond Wnt: multiple mechanisms control the transcriptional property of beta-catenin." Cell Signal **20**(10): 1697-1704.

Jogie-Brahim, S., D. Feldman and Y. Oh (2009). "Unraveling insulin-like growth factor binding protein-3 actions in human disease." Endocr Rev **30**(5): 417-437.

Kalluri, R. and E. G. Neilson (2003). "Epithelial-mesenchymal transition and its implications for fibrosis." J Clin Invest **112**(12): 1776-1784.

Kalluri, R. and R. A. Weinberg (2009). "The basics of epithelial-mesenchymal transition." J Clin Invest **119**(6): 1420-1428.

Kaneko, G., E. Kikuchi, K. Matsumoto, J. Obata, S. Nakamura, A. Miyajima and M. Oya (2011). "Neoadjuvant gemcitabine plus cisplatin for muscle-invasive bladder cancer." Jpn J Clin Oncol **41**(7): 908-914.

Karantanos, T., P. G. Corn and T. C. Thompson (2013). "Prostate cancer progression after androgen deprivation therapy: mechanisms of castrate resistance and novel therapeutic approaches." Oncogene **32**(49): 5501-5511.

Kirkali, Z., T. Chan, M. Manoharan, F. Algaba, C. Busch, L. Cheng, L. Kiemeney, M. Kriegmair, R. Montironi, W. M. Murphy, I. A. Sesterhenn, M. Tachibana and J. Weider (2005). "Bladder cancer: epidemiology, staging and grading, and diagnosis." Urology **66**(6 Suppl 1): 4-34.

Kisielewska, J., J. Ligeza and A. Klein (2008). "The effect of tyrosine kinase inhibitors, tyrphostins: AG1024 and SU1498, on autocrine growth of prostate cancer cells (DU145)." Folia Histochem Cytobiol **46**(2): 185-191.

Knowles, M. A. and C. D. Hurst (2015). "Molecular biology of bladder cancer: new insights into pathogenesis and clinical diversity." Nat Rev Cancer **15**(1): 25-41.

Ko, J. A., R. Yanai and T. Nishida (2009). "IGF-1 released by corneal epithelial cells induces up-regulation of N-cadherin in corneal fibroblasts." J Cell Physiol **221**(1): 254-261.

Kramer, N., A. Walzl, C. Unger, M. Rosner, G. Krupitza, M. Hengstschlager and H. Dolznig (2013). "In vitro cell migration and invasion assays." Mutat Res **752**(1): 10-24.

Le Roith, D. (1997). "Seminars in medicine of the Beth Israel Deaconess Medical Center. Insulin-like growth factors." N Engl J Med **336**(9): 633-640.

Lee, J., H. Jeon, S. M. Yoo, J. Park and M. S. Lee (2015). "The role of Kaposi's sarcoma-associated herpesvirus infection in the proliferation of human bladder cancer cells." Tumour Biol.

Li, C., J. Li, D. Wu and G. Han (2015). "The involvement of survivin in insulin-like growth factor 1-induced epithelial-mesenchymal transition in gastric cancer." Tumour Biol.

Li, H., L. Xu, L. Zhao, Y. Ma, Z. Zhu, Y. Liu and X. Qu (2015). "Insulin-like growth factor-I induces epithelial to mesenchymal transition via GSK-3beta and ZEB2 in the BGC-823 gastric cancer cell line." Oncol Lett **9**(1): 143-148.

Li, Y., C. Ma, X. Shi, Z. Wen, D. Li, M. Sun and H. Ding (2014). "Effect of nitric oxide synthase on multiple drug resistance is related to Wnt signaling in non-small cell lung cancer." Oncol Rep **32**(4): 1703-1708.

Liao, G., M. Wang, Y. Ou and Y. Zhao (2014). "IGF-1-induced epithelial-mesenchymal transition in MCF-7 cells is mediated by MUC1." Cell Signal **26**(10): 2131-2137.

Liu, G., Y. J. Liu, W. J. Lian, Z. W. Zhao, T. Yi and H. Y. Zhou (2014). "Reduced BMP6 expression by DNA methylation contributes to EMT and drug resistance in breast cancer cells." Oncol Rep **32**(2): 581-588.

Liu, S., Y. Li, T. Lin, X. Fan, Y. Liang and U. Heemann (2011). "High dose human insulin and insulin glargine promote T24 bladder cancer cell proliferation via PI3K-independent activation of Akt." Diabetes Res Clin Pract **91**(2): 177-182.

Liu, X. J., Q. Xie, Y. F. Zhu, C. Chen and N. Ling (2001). "Identification of a nonpeptide ligand that releases bioactive insulin-like growth factor-I from its binding protein complex." J Biol Chem **276**(35): 32419-32422.

Livingstone, C. (2013). "IGF2 and cancer." Endocr Relat Cancer **20**(6): R321-339.

Loh, Y. N., E. L. Hedditch, L. A. Baker, E. Jary, R. L. Ward and C. E. Ford (2013). "The Wnt signalling pathway is upregulated in an in vitro model of acquired tamoxifen resistant breast cancer." BMC Cancer **13**: 174.

Lorenzatti, G., W. Huang, A. Pal, A. M. Cabanillas and C. G. Kleer (2011). "CCN6 (WISP3) decreases ZEB1-mediated EMT and invasion by attenuation of IGF-1 receptor signaling in breast cancer." J Cell Sci **124**(Pt 10): 1752-1758.

Lu, L., D. Katsaros, A. Wiley, I. A. Rigault de la Longrais, H. A. Risch, M. Puopolo and H. Yu (2006). "The relationship of insulin-like growth factor-II, insulin-like growth factor binding protein-3, and estrogen receptor-alpha expression to disease progression in epithelial ovarian cancer." Clin Cancer Res **12**(4): 1208-1214.

Lucca, I., T. Klatte, H. Fajkovic, M. de Martino and S. F. Shariat (2015). "Gender differences in incidence and outcomes of urothelial and kidney cancer." Nat Rev Urol **12**(10): 585-592.

Lukacz, E. S., C. Sampselle, M. Gray, S. Macdiarmid, M. Rosenberg, P. Ellsworth and M. H. Palmer (2011). "A healthy bladder: a consensus statement." Int J Clin Pract **65**(10): 1026-1036.

Mackay, K. B., S. A. Loddick, G. S. Naeve, A. M. Vana, G. M. Verge and A. C. Foster (2003). "Neuroprotective effects of insulin-like growth factor-binding protein ligand inhibitors in vitro and in vivo." J Cereb Blood Flow Metab **23**(10): 1160-1167.

Mahnken, A., I. Kausch, A. C. Feller and S. Kruger (2005). "E-cadherin immunoreactivity correlates with recurrence and progression of minimally

invasive transitional cell carcinomas of the urinary bladder." Oncol Rep **14**(4): 1065-1070.
Malouf, G. G., J. H. Taube, Y. Lu, T. Roysarkar, S. Panjarian, M. R. Estecio, J. Jelinek, J. Yamazaki, N. J. Raynal, H. Long, T. Tahara, A. Tinnirello, P. Ramachandran, X. Y. Zhang, S. Liang, S. A. Mani and J. P. Issa (2013). "Architecture of epigenetic reprogramming following Twist1-mediated epithelial-mesenchymal transition." Genome Biol **14**(12): R144.
Manara, M. C., L. Landuzzi, P. Nanni, G. Nicoletti, D. Zambelli, P. L. Lollini, C. Nanni, F. Hofmann, C. Garcia-Echeverria, P. Picci and K. Scotlandi (2007). "Preclinical in vivo study of new insulin-like growth factor-I receptor--specific inhibitor in Ewing's sarcoma." Clin Cancer Res **13**(4): 1322-1330.
Martyn-Hemphill, C., D. Mak, M. S. Khan, B. J. Challacombe and C. V. Bishop (2013). "Recent advances in diagnosis and treatment of transitional cell carcinoma of the bladder." Int J Surg **11**(9): 749-752.
Massari, F., M. Santoni, C. Ciccarese, M. Brunelli, A. Conti, D. Santini, R. Montironi, S. Cascinu and G. Tortora (2015). "Emerging concepts on drug resistance in bladder cancer: Implications for future strategies." Crit Rev Oncol Hematol **96**(1): 81-90.
McCaig, C., C. M. Perks and J. M. Holly (2002). "Intrinsic actions of IGFBP-3 and IGFBP-5 on Hs578T breast cancer epithelial cells: inhibition or accentuation of attachment and survival is dependent upon the presence of fibronectin." J Cell Sci **115**(Pt 22): 4293-4303.
McConkey, D. J., W. Choi, L. Marquis, F. Martin, M. B. Williams, J. Shah, R. Svatek, A. Das, L. Adam, A. Kamat, A. Siefker-Radtke and C. Dinney (2009). "Role of epithelial-to-mesenchymal transition (EMT) in drug sensitivity and metastasis in bladder cancer." Cancer Metastasis Rev **28**(3-4): 335-344.
Metalli, D., F. Lovat, F. Tripodi, M. Genua, S. Q. Xu, M. Spinelli, L. Alberghina, M. Vanoni, R. Baffa, L. G. Gomella, R. V. Iozzo and A. Morrione (2010). "The insulin-like growth factor receptor I promotes motility and invasion of bladder cancer cells through Akt- and mitogen-activated protein kinase-dependent activation of paxillin." Am J Pathol **176**(6): 2997-3006.
Mhawech-Fauceglia, P., G. Fischer, A. Beck, R. T. Cheney and F. R. Herrmann (2006). "Raf1, Aurora-A/STK15 and E-cadherin biomarkers expression in patients with pTa/pT1 urothelial bladder carcinoma; a retrospective TMA study of 246 patients with long-term follow-up." Eur J Surg Oncol **32**(4): 439-444.
Michel, C., D. Vordos, C. Dumont, V. Basset, F. Meyer, F. Gaudez, P. Meria, A. Cortesse, P. Mongiat-Artus, A. de la Taille, S. Culine, F. Desgrandchamps and A. Masson-Lecomte (2018). "[Impact of neoadjuvant chemotherapy on the peri-operative morbidity of radical cystectomy for muscle invasive bladder cancer]." Prog Urol.
Mireuta, M., A. Darnel and M. Pollak (2010). "IGFBP-2 expression in MCF-7 cells is regulated by the PI3K/AKT/mTOR pathway through Sp1-induced increase in transcription." Growth Factors **28**(4): 243-255.
Mitra, A. P. and R. J. Cote (2009). "Molecular pathogenesis and diagnostics of bladder cancer." Annu Rev Pathol **4**: 251-285.
Miyake, H., I. Hara, K. Yamanaka, M. Muramaki, M. Gleave and H. Eto (2005). "Introduction of insulin-like growth factor binding protein-2 gene into human

bladder cancer cells enhances their metastatic potential." Oncol Rep **13**(2): 341-345.
Miyako, K., L. J. Cobb, M. Francis, A. Huang, B. Peng, J. E. Pintar, H. Ariga and P. Cohen (2009). "PAPA-1 Is a nuclear binding partner of IGFBP-2 and modulates its growth-promoting actions." Mol Endocrinol **23**(2): 169-175.
Montironi, R. and A. Lopez-Beltran (2005). "The 2004 WHO classification of bladder tumors: a summary and commentary." Int J Surg Pathol **13**(2): 143-153.
Moore, L. M., K. M. Holmes, S. M. Smith, Y. Wu, E. Tchougounova, L. Uhrbom, R. Sawaya, J. M. Bruner, G. N. Fuller and W. Zhang (2009). "IGFBP2 is a candidate biomarker for Ink4a-Arf status and a therapeutic target for high-grade gliomas." Proc Natl Acad Sci U S A **106**(39): 16675-16679.
Morali, O. G., V. Delmas, R. Moore, C. Jeanney, J. P. Thiery and L. Larue (2001). "IGF-II induces rapid beta-catenin relocation to the nucleus during epithelium to mesenchyme transition." Oncogene **20**(36): 4942-4950.
Morris, M. R., D. Gentle, M. Abdulrahman, N. Clarke, M. Brown, T. Kishida, M. Yao, B. T. Teh, F. Latif and E. R. Maher (2008). "Functional epigenomics approach to identify methylated candidate tumour suppressor genes in renal cell carcinoma." Br J Cancer **98**(2): 496-501.
Morrison, C. D., P. Liu, A. Woloszynska-Read, J. Zhang, W. Luo, M. Qin, W. Bshara, J. M. Conroy, L. Sabatini, P. Vedell, D. Xiong, S. Liu, J. Wang, H. Shen, Y. Li, A. R. Omilian, A. Hill, K. Head, K. Guru, D. Kunnev, R. Leach, K. H. Eng, C. Darlak, C. Hoeflich, S. Veeranki, S. Glenn, M. You, S. C. Pruitt, C. S. Johnson and D. L. Trump (2014). "Whole-genome sequencing identifies genomic heterogeneity at a nucleotide and chromosomal level in bladder cancer." Proc Natl Acad Sci U S A **111**(6): E672-681.
Motawi, T. K., S. M. Rizk, T. M. Ibrahim and I. A. Ibrahim (2016). "Circulating microRNAs, miR-92a, miR-100 and miR-143, as non-invasive biomarkers for bladder cancer diagnosis." Cell Biochem Funct.
Murai, T., S. Yamada, B. C. Fuchs, T. Fujii, G. Nakayama, H. Sugimoto, M. Koike, M. Fujiwara, K. K. Tanabe and Y. Kodera (2014). "Epithelial-to-mesenchymal transition predicts prognosis in clinical gastric cancer." J Surg Oncol **109**(7): 684-689.
Nagata, M., S. Muto and S. Horie (2016). "Molecular Biomarkers in Bladder Cancer: Novel Potential Indicators of Prognosis and Treatment Outcomes." Dis Markers **2016**: 8205836.
Natsuizaka, M., S. Ohashi, G. S. Wong, A. Ahmadi, R. A. Kalman, D. Budo, A. J. Klein-Szanto, M. Herlyn, J. A. Diehl and H. Nakagawa (2010). "Insulin-like growth factor-binding protein-3 promotes transforming growth factor-{beta}1-mediated epithelial-to-mesenchymal transition and motility in transformed human esophageal cells." Carcinogenesis **31**(8): 1344-1353.
Nickel, A. and S. C. Stadler (2015). "Role of epigenetic mechanisms in epithelial-to-mesenchymal transition of breast cancer cells." Transl Res **165**(1): 126-142.
Nurwidya, F., F. Takahashi, I. Kobayashi, A. Murakami, M. Kato, K. Minakata, T. Nara, M. Hashimoto, S. Yagishita, H. Baskoro, M. Hidayat, N. Shimada and K. Takahashi (2014). "Treatment with insulin-like growth factor 1 receptor inhibitor reverses hypoxia-induced epithelial-mesenchymal transition in non-small cell lung cancer." Biochem Biophys Res Commun **455**(3-4): 332-338.

Oh, J. K. and E. Weiderpass (2014). "Infection and cancer: global distribution and burden of diseases." Ann Glob Health **80**(5): 384-392.
Pandini, G., R. Vigneri, A. Costantino, F. Frasca, A. Ippolito, Y. Fujita-Yamaguchi, K. Siddle, I. D. Goldfine and A. Belfiore (1999). "Insulin and insulin-like growth factor-I (IGF-I) receptor overexpression in breast cancers leads to insulin/IGF-I hybrid receptor overexpression: evidence for a second mechanism of IGF-I signaling." Clin Cancer Res **5**(7): 1935-1944.
Paradzik, M., V. Bucevic-Popovic, M. Situm, C. J. Jaing, M. Degoricija, K. S. McLoughlin, S. I. Ismail, V. Punda-Polic and J. Terzic (2014). "Association of Kaposi's sarcoma-associated herpesvirus (KSHV) with bladder cancer in Croatian patients." Tumour Biol **35**(1): 567-572.
Parkin, D. M. (2006). "The global health burden of infection-associated cancers in the year 2002." Int J Cancer **118**(12): 3030-3044.
Parkin, D. M. (2008). "The global burden of urinary bladder cancer." Scand J Urol Nephrol Suppl(218): 12-20.
Patil, S. S., R. Railkar, M. Swain, H. S. Atreya, R. R. Dighe and P. Kondaiah (2015). "Novel anti IGFBP2 single chain variable fragment inhibits glioma cell migration and invasion." J Neurooncol **123**(2): 225-235.
Perks, C. M., C. Burrows and J. M. Holly (2011). "Intrinsic, Pro-Apoptotic Effects of IGFBP-3 on Breast Cancer Cells are Reversible: Involvement of PKA, Rho, and Ceramide." Front Endocrinol (Lausanne) **2**: 13.
Perks, C. M. and J. M. Holly (2008). "IGF binding proteins (IGFBPs) and regulation of breast cancer biology." J Mammary Gland Biol Neoplasia **13**(4): 455-469.
Perks, C. M. and J. M. Holly (2015). "Epigenetic regulation of insulin-like growth factor binding protein-3 (IGFBP-3) in cancer." J Cell Commun Signal **9**(2): 159-166.
Perks, C. M., E. G. Vernon, A. H. Rosendahl, D. Tonge and J. M. Holly (2007). "IGF-II and IGFBP-2 differentially regulate PTEN in human breast cancer cells." Oncogene **26**(40): 5966-5972.
Pickard, A. and D. J. McCance (2015). "IGF-binding protein 2 (IGFBP2) – oncogene or tumour suppressor?" Frontiers in Endocrinology **6**.
Praveen Kumar, V. R., P. Sehgal, B. Thota, S. Patil, V. Santosh and P. Kondaiah (2014). "Insulin like growth factor binding protein 4 promotes GBM progression and regulates key factors involved in EMT and invasion." J Neurooncol **116**(3): 455-464.
Ramis-Conde, I., M. A. Chaplain, A. R. Anderson and D. Drasdo (2009). "Multi-scale modelling of cancer cell intravasation: the role of cadherins in metastasis." Phys Biol **6**(1): 016008.
Reinert, T., C. Modin, F. M. Castano, P. Lamy, T. K. Wojdacz, L. L. Hansen, C. Wiuf, M. Borre, L. Dyrskjot and T. F. Orntoft (2011). "Comprehensive genome methylation analysis in bladder cancer: identification and validation of novel methylated genes and application of these as urinary tumor markers." Clin Cancer Res **17**(17): 5582-5592.
Renehan, A. G., J. Frystyk and A. Flyvbjerg (2006). "Obesity and cancer risk: the role of the insulin-IGF axis." Trends Endocrinol Metab **17**(8): 328-336.
Rinaldi, S., R. Cleveland, T. Norat, C. Biessy, S. Rohrmann, J. Linseisen, H. Boeing, T. Pischon, S. Panico, C. Agnoli, D. Palli, R. Tumino, P. Vineis, P. H. Peeters, C. H. van Gils, B. H. Bueno-de-Mesquita, A. Vrieling, N. E. Allen, A. Roddam, S. Bingham, K.

T. Khaw, J. Manjer, S. Borgquist, V. Dumeaux, I. Torhild Gram, E. Lund, A. Trichopoulou, G. Makrygiannis, V. Benetou, E. Molina, I. Donate Suarez, A. Barricarte Gurrea, C. A. Gonzalez, M. J. Tormo, J. M. Altzibar, A. Olsen, A. Tjonneland, H. Gronbaek, K. Overvad, F. Clavel-Chapelon, M. C. Boutron-Ruault, S. Morois, N. Slimani, P. Boffetta, M. Jenab, E. Riboli and R. Kaaks (2010). "Serum levels of IGF-I, IGFBP-3 and colorectal cancer risk: results from the EPIC cohort, plus a meta-analysis of prospective studies." Int J Cancer **126**(7): 1702-1715.

Rinderknecht, E. and R. E. Humbel (1976). "Amino-terminal sequences of two polypeptides from human serum with nonsuppressible insulin-like and cell-growth-promoting activities: evidence for structural homology with insulin B chain." Proc Natl Acad Sci U S A **73**(12): 4379-4381.

Rochester, M. A., N. Patel, B. W. Turney, D. R. Davies, I. S. Roberts, J. Crew, A. Protheroe and V. M. Macaulay (2007). "The type 1 insulin-like growth factor receptor is over-expressed in bladder cancer." BJU Int **100**(6): 1396-1401.

Roddam, A. W., N. E. Allen, P. Appleby, T. J. Key, L. Ferrucci, H. B. Carter, E. J. Metter, C. Chen, N. S. Weiss, A. Fitzpatrick, A. W. Hsing, J. V. Lacey, Jr., K. Helzlsouer, S. Rinaldi, E. Riboli, R. Kaaks, J. A. Janssen, M. F. Wildhagen, F. H. Schroder, E. A. Platz, M. Pollak, E. Giovannucci, C. Schaefer, C. P. Quesenberry, Jr., J. H. Vogelman, G. Severi, D. R. English, G. G. Giles, P. Stattin, G. Hallmans, M. Johansson, J. M. Chan, P. Gann, S. E. Oliver, J. M. Holly, J. Donovan, F. Meyer, I. Bairati and P. Galan (2008). "Insulin-like growth factors, their binding proteins, and prostate cancer risk: analysis of individual patient data from 12 prospective studies." Ann Intern Med **149**(7): 461-471, W483-468.

Rodrigues, D., C. Jeronimo, R. Henrique, L. Belo, M. de Lourdes Bastos, P. G. de Pinho and M. Carvalho (2016). "Biomarkers in bladder cancer: A metabolomic approach using in vitro and ex vivo model systems." Int J Cancer.

Russo, V. C., B. S. Schutt, E. Andaloro, S. I. Ymer, A. Hoeflich, M. B. Ranke, L. A. Bach and G. A. Werther (2005). "Insulin-like growth factor binding protein-2 binding to extracellular matrix plays a critical role in neuroblastoma cell proliferation, migration, and invasion." Endocrinology **146**(10): 4445-4455.

Sachdev, D. and D. Yee (2007). "Disrupting insulin-like growth factor signaling as a potential cancer therapy." Mol Cancer Ther **6**(1): 1-12.

Samani, A. A., S. Yakar, D. LeRoith and P. Brodt (2007). "The role of the IGF system in cancer growth and metastasis: overview and recent insights." Endocr Rev **28**(1): 20-47.

Sandhu, M. S., J. M. Gibson, A. H. Heald, D. B. Dunger and N. J. Wareham (2004). "Association between insulin-like growth factor-I: insulin-like growth factor-binding protein-1 ratio and metabolic and anthropometric factors in men and women." Cancer Epidemiol Biomarkers Prev **13**(1): 166-170.

Sarkissyan, S., M. Sarkissyan, Y. Wu, J. Cardenas, H. P. Koeffler and J. V. Vadgama (2014). "IGF-1 regulates Cyr61 induced breast cancer cell proliferation and invasion." PLoS One **9**(7): e103534.

Savagner, P., B. Boyer, A. M. Valles, J. Jouanneau and J. P. Thiery (1994). "Modulations of the epithelial phenotype during embryogenesis and cancer progression." Cancer Treat Res **71**: 229-249.

Serel, T. A., T. Turan, S. Soyupek, Z. Aybek and H. Perk (2003). "Urine and serum free IGF-1 levels in patients with bladder cancer: a brief report." Urol Res **31**(5): 297-299.
Sfakianos, J. P., L. Lin Gellert, A. Maschino, G. T. Gotto, P. H. Kim, H. Al-Ahmadie and B. H. Bochner (2014). "The role of PTEN tumor suppressor pathway staining in carcinoma in situ of the bladder." Urol Oncol **32**(5): 657-662.
Shelton, L. M., P. Mukherjee, L. C. Huysentruyt, I. Urits, J. A. Rosenberg and T. N. Seyfried (2010). "A novel pre-clinical in vivo mouse model for malignant brain tumor growth and invasion." J Neurooncol **99**(2): 165-176.
Shen, X., G. Xi, L. A. Maile, C. Wai, C. J. Rosen and D. R. Clemmons (2012). "Insulin-like growth factor (IGF) binding protein 2 functions coordinately with receptor protein tyrosine phosphatase beta and the IGF-I receptor to regulate IGF-I-stimulated signaling." Mol Cell Biol **32**(20): 4116-4130.
Sherif, A., L. Holmberg, E. Rintala, O. Mestad, J. Nilsson, S. Nilsson, P. U. Malmstrom and G. Nordic Urothelial Cancer (2004). "Neoadjuvant cisplatinum based combination chemotherapy in patients with invasive bladder cancer: a combined analysis of two Nordic studies." Eur Urol **45**(3): 297-303.
Shimasaki, S. and N. Ling (1991). "Identification and molecular characterization of insulin-like growth factor binding proteins (IGFBP-1, -2, -3, -4, -5 and -6)." Prog Growth Factor Res **3**(4): 243-266.
Shiota, M., Y. Song, A. Yokomizo, K. Kiyoshima, Y. Tada, H. Uchino, T. Uchiumi, J. Inokuchi, Y. Oda, K. Kuroiwa, K. Tatsugami and S. Naito (2010). "Foxo3a suppression of urothelial cancer invasiveness through Twist1, Y-box-binding protein 1, and E-cadherin regulation." Clin Cancer Res **16**(23): 5654-5663.
Siddik, Z. H. (2003). "Cisplatin: mode of cytotoxic action and molecular basis of resistance."
Siegel, R. L., K. D. Miller and A. Jemal (2015). "Cancer statistics, 2015." CA Cancer J Clin **65**(1): 5-29.
Simons, C. C., P. A. van den Brandt, C. D. Stehouwer, M. van Engeland and M. P. Weijenberg (2014). "Body size, physical activity, early-life energy restriction, and associations with methylated insulin-like growth factor-binding protein genes in colorectal cancer." Cancer Epidemiol Biomarkers Prev **23**(9): 1852-1862.
Singer, C. F., M. Mogg, W. Koestler, M. Pacher, E. Marton, E. Kubista and M. Schreiber (2004). "Insulin-like growth factor (IGF)-I and IGF-II serum concentrations in patients with benign and malignant breast lesions: free IGF-II is correlated with breast cancer size." Clin Cancer Res **10**(12 Pt 1): 4003-4009.
Singh, K. P., J. Treas, T. Tyagi and W. Gao (2012). "DNA demethylation by 5-aza-2-deoxycytidine treatment abrogates 17 beta-estradiol-induced cell growth and restores expression of DNA repair genes in human breast cancer cells." Cancer Lett **316**(1): 62-69.
Sjodahl, G., K. Lovgren, M. Lauss, O. Patschan, S. Gudjonsson, G. Chebil, M. Aine, P. Eriksson, W. Mansson, D. Lindgren, M. Ferno, F. Liedberg and M. Hoglund (2013). "Toward a molecular pathologic classification of urothelial carcinoma." Am J Pathol **183**(3): 681-691.
Smith, B. N. and N. A. Bhowmick (2016). "Role of EMT in Metastasis and Therapy Resistance." J Clin Med **5**(2).

Son, H. and A. Moon (2010). "Epithelial-mesenchymal Transition and Cell Invasion." Toxicol Res **26**(4): 245-252.
Stanton, M. L., L. Xiao, B. A. Czerniak and C. C. Guo (2013). "Urothelial tumors of the urinary bladder in young patients: a clinicopathologic study of 59 cases." Arch Pathol Lab Med **137**(10): 1337-1341.
Stewart, C. E. and P. Rotwein (1996). "Growth, differentiation, and survival: multiple physiological functions for insulin-like growth factors." Physiol Rev **76**(4): 1005-1026.
Subramani, R., R. Lopez-Valdez, A. Arumugam, S. Nandy, T. Boopalan and R. Lakshmanaswamy (2014). "Targeting insulin-like growth factor 1 receptor inhibits pancreatic cancer growth and metastasis." PLoS One **9**(5): e97016.
Sun, J. W., L. G. Zhao, Y. Yang, X. Ma, Y. Y. Wang and Y. B. Xiang (2015). "Obesity and risk of bladder cancer: a dose-response meta-analysis of 15 cohort studies." PLoS One **10**(3): e0119313.
Suzuki, M. M. and A. Bird (2008). "DNA methylation landscapes: provocative insights from epigenomics." Nat Rev Genet **9**(6): 465-476.
Tahara, T., T. Shibata, M. Okubo, T. Ishizuka, M. Nakamura, M. Nagasaka, Y. Nakagawa, N. Ohmiya, T. Arisawa and I. Hirata (2014). "DNA methylation status of epithelial-mesenchymal transition (EMT)--related genes is associated with severe clinical phenotypes in ulcerative colitis (UC)." PLoS One **9**(10): e107947.
Taliaferro-Smith, L., E. Oberlick, T. Liu, T. McGlothen, T. Alcaide, R. Tobin, S. Donnelly, R. Commander, E. Kline, G. P. Nagaraju, L. Havel, A. Marcus, R. Nahta and R. O'Regan (2015). "FAK activation is required for IGF1R-mediated regulation of EMT, migration, and invasion in mesenchymal triple negative breast cancer cells." Oncotarget **6**(7): 4757-4772.
Tanaka, T., K. Miyazawa, T. Tsukamoto, T. Kuno and K. Suzuki (2011). "Pathobiology and chemoprevention of bladder cancer." J Oncol **2011**: 528353.
Tenbaum, S. P., P. Ordonez-Moran, I. Puig, I. Chicote, O. Arques, S. Landolfi, Y. Fernandez, J. R. Herance, J. D. Gispert, L. Mendizabal, S. Aguilar, S. Ramon y Cajal, S. Schwartz, Jr., A. Vivancos, E. Espin, S. Rojas, J. Baselga, J. Tabernero, A. Munoz and H. G. Palmer (2012). "beta-catenin confers resistance to PI3K and AKT inhibitors and subverts FOXO3a to promote metastasis in colon cancer." Nat Med **18**(6): 892-901.
Thiery, J. P. and C. T. Lim (2013). "Tumor dissemination: an EMT affair." Cancer Cell **23**(3): 272-273.
Thissen, J. P., J. M. Ketelslegers and L. E. Underwood (1994). "Nutritional regulation of the insulin-like growth factors." Endocr Rev **15**(1): 80-101.
Tiwari, N., A. Gheldof, M. Tatari and G. Christofori (2012). "EMT as the ultimate survival mechanism of cancer cells." Semin Cancer Biol **22**(3): 194-207.
Tomiyama, L., T. Sezaki, M. Matsuo, K. Ueda and N. Kioka (2015). "Loss of Dlg5 expression promotes the migration and invasion of prostate cancer cells via Girdin phosphorylation." Oncogene **34**(9): 1141-1149.
Torre, L. A., F. Bray, R. L. Siegel, J. Ferlay, J. Lortet-Tieulent and A. Jemal (2015). "Global cancer statistics, 2012." CA Cancer J Clin **65**(2): 87-108.
Turo, R., W. Cross and P. Whelan (2012). "Bladder cancer." Medicine **40**(1): 14-19.
Uzoh, C. C., J. M. Holly, K. M. Biernacka, R. A. Persad, A. Bahl, D. Gillatt and C. M. Perks (2011). "Insulin-like growth factor-binding protein-2 promotes prostate

cancer cell growth via IGF-dependent or -independent mechanisms and reduces the efficacy of docetaxel." Br J Cancer **104**(10): 1587-1593.
Vallo, S., M. Michaelis, F. Rothweiler, G. Bartsch, K. M. Gust, D. M. Limbart, F. Rodel, F. Wezel, A. Haferkamp and J. Cinatl, Jr. (2015). "Drug-Resistant Urothelial Cancer Cell Lines Display Diverse Sensitivity Profiles to Potential Second-Line Therapeutics." Transl Oncol **8**(3): 210-216.
Van Batavia, J., T. Yamany, A. Molotkov, H. Dan, M. Mansukhani, E. Batourina, K. Schneider, D. Oyon, M. Dunlop, X. R. Wu, C. Cordon-Cardo and C. Mendelsohn (2014). "Bladder cancers arise from distinct urothelial sub-populations." Nat Cell Biol **16**(10): 982-991, 981-985.
van der Horst, G., L. Bos and G. van der Pluijm (2012). "Epithelial plasticity, cancer stem cells, and the tumor-supportive stroma in bladder carcinoma." Mol Cancer Res **10**(8): 995-1009.
van Kessel, K. E., T. C. Zuiverloon, A. R. Alberts, J. L. Boormans and E. C. Zwarthoff (2015). "Targeted therapies in bladder cancer: an overview of in vivo research." Nat Rev Urol **12**(12): 681-694.
van Rhijn, B. W., M. Burger, Y. Lotan, E. Solsona, C. G. Stief, R. J. Sylvester, J. A. Witjes and A. R. Zlotta (2009). "Recurrence and progression of disease in non-muscle-invasive bladder cancer: from epidemiology to treatment strategy." Eur Urol **56**(3): 430-442.
Varol, N., E. Konac, I. H. Onen, S. Gurocak, E. Alp, A. Yilmaz, S. Menevse and S. Sozen (2014). "The epigenetically regulated effects of Wnt antagonists on the expression of genes in the apoptosis pathway in human bladder cancer cell line (T24)." DNA Cell Biol **33**(7): 408-417.
Vedula, S. R., A. Ravasio, C. T. Lim and B. Ladoux (2013). "Collective cell migration: a mechanistic perspective." Physiology (Bethesda) **28**(6): 370-379.
von der Maase, H., L. Sengelov, J. T. Roberts, S. Ricci, L. Dogliotti, T. Oliver, M. J. Moore, A. Zimmermann and M. Arning (2005). "Long-term survival results of a randomized trial comparing gemcitabine plus cisplatin, with methotrexate, vinblastine, doxorubicin, plus cisplatin in patients with bladder cancer." J Clin Oncol **23**(21): 4602-4608.
Wallace, D. M., R. T. Bryan, J. A. Dunn, G. Begum, S. Bathers and G. West Midlands Urological Research (2002). "Delay and survival in bladder cancer." BJU Int **89**(9): 868-878.
Walsh, L. A. and S. Damjanovski (2011). "IGF-1 increases invasive potential of MCF 7 breast cancer cells and induces activation of latent TGF-beta1 resulting in epithelial to mesenchymal transition." Cell Commun Signal **9**(1): 10.
Wang, H., Q. Li, X. Niu, G. Wang, S. Zheng, G. Fu and Z. Wang (2017). "miR-143 inhibits bladder cancer cell proliferation and enhances their sensitivity to gemcitabine by repressing IGF-1R signaling." Oncol Lett **13**(1): 435-440.
Wang, Q. H., Z. G. Ji, H. Z. Li, H. Fan, Z. G. Chen, B. B. Shi and Y. Fang (2016). "Clinicopathologic Comparison of Urothelial Bladder Carcinoma in Young and Elder Patients." Pathol Oncol Res **22**(1): 67-70.
Waterland, R. A. and K. B. Michels (2007). "Epigenetic epidemiology of the developmental origins hypothesis." Annu Rev Nutr **27**: 363-388.

Weber, M. M., C. Fottner, S. B. Liu, M. C. Jung, D. Engelhardt and G. B. Baretton (2002). "Overexpression of the insulin-like growth factor I receptor in human colon carcinomas." Cancer **95**(10): 2086-2095.
Wheatcroft, S. B. and M. T. Kearney (2009). "IGF-dependent and IGF-independent actions of IGF-binding protein-1 and -2: implications for metabolic homeostasis." Trends Endocrinol Metab **20**(4): 153-162.
Wiley, A., D. Katsaros, S. Fracchioli and H. Yu (2006). "Methylation of the insulin-like growth factor binding protein-3 gene and prognosis of epithelial ovarian cancer." Int J Gynecol Cancer **16**(1): 210-218.
Williams, C. S., B. Zhang, J. J. Smith, A. Jayagopal, C. W. Barrett, C. Pino, P. Russ, S. H. Presley, D. Peng, D. O. Rosenblatt, F. R. Haselton, J. L. Yang, M. K. Washington, X. Chen, S. Eschrich, T. J. Yeatman, W. El-Rifai, R. D. Beauchamp and M. S. Chang (2011). "BVES regulates EMT in human corneal and colon cancer cells and is silenced via promoter methylation in human colorectal carcinoma." J Clin Invest **121**(10): 4056-4069.
Wolff, E. M., Y. Chihara, F. Pan, D. J. Weisenberger, K. D. Siegmund, K. Sugano, K. Kawashima, P. W. Laird, P. A. Jones and G. Liang (2010). "Unique DNA methylation patterns distinguish noninvasive and invasive urothelial cancers and establish an epigenetic field defect in premalignant tissue." Cancer Res **70**(20): 8169-8178.
World Health Organization, W. (1973). "Histological Typing of Urinary Bladder Tumours.".
Wu, B., X. Cao, X. Liang, X. Zhang, W. Zhang, G. Sun and D. Wang (2015). "Epigenetic regulation of Elf5 is associated with epithelial-mesenchymal transition in urothelial cancer." PLoS One **10**(1): e0117510.
Wu, Y., M. Sarkissyan and J. V. Vadgama (2016). "Epithelial-Mesenchymal Transition and Breast Cancer." J Clin Med **5**(2).
Xu, Y. C., X. Wang, Y. Chen, S. M. Chen, X. Y. Yang, Y. M. Sun, M. Y. Geng, J. Ding and L. H. Meng (2017). "Integration of Receptor Tyrosine Kinases Determines Sensitivity to PI3Kalpha-selective Inhibitors in Breast Cancer." Theranostics **7**(4): 974-986.
Yafi, F. A., S. North and W. Kassouf (2011). "First- and second-line therapy for metastatic urothelial carcinoma of the bladder." Curr Oncol **18**(1): e25-34.
Yamada, K. M. and M. Araki (2001). "Tumor suppressor PTEN: modulator of cell signaling, growth, migration and apoptosis." J Cell Sci **114**(Pt 13): 2375-2382.
Yang, J. and R. A. Weinberg (2008). "Epithelial-mesenchymal transition: at the crossroads of development and tumor metastasis." Dev Cell **14**(6): 818-829.
Yao, C., L. Su, J. Shan, C. Zhu, L. Liu, C. Liu, Y. Xu, Z. Yang, X. Bian, J. Shao, J. Li, M. Lai, J. Shen and C. Qian (2016). "IGF/STAT3/NANOG/Slug signaling axis simultaneously controls epithelial-mesenchymal transition and stemness maintenance in colorectal cancer." Stem Cells.
Yao, X., D. Li, D. M. Xiong, L. Li, R. Jiang and J. X. Chen (2013). "A novel role of ribonuclease inhibitor in regulation of epithelial-to-mesenchymal transition and ILK signaling pathway in bladder cancer cells." Cell Tissue Res **353**(3): 409-423.
Yau, S. W., W. J. Azar, M. A. Sabin, G. A. Werther and V. C. Russo (2015). "IGFBP-2 - taking the lead in growth, metabolism and cancer." J Cell Commun Signal.
Yazawa, T., H. Sato, H. Shimoyamada, K. Okudela, T. Woo, M. Tajiri, T. Ogura, N. Ogawa, T. Suzuki, H. Mitsui, J. Ishii, C. Miyata, M. Sakaeda, K. Goto, K. Kashiwagi,

M. Masuda, T. Takahashi and H. Kitamura (2009). "Neuroendocrine cancer-specific up-regulating mechanism of insulin-like growth factor binding protein-2 in small cell lung cancer." Am J Pathol **175**(3): 976-987.
Yin, W. Y., M. C. Lee, N. S. Lai and M. C. Lu (2015). "BK virus as a potential oncovirus for bladder cancer in a renal transplant patient." J Formos Med Assoc **114**(4): 373-374.
Yu, H. and T. Rohan (2000). "Role of the insulin-like growth factor family in cancer development and progression." J Natl Cancer Inst **92**(18): 1472-1489.
Yun, S. J. and W. J. Kim (2013). "Role of the epithelial-mesenchymal transition in bladder cancer: from prognosis to therapeutic target." Korean J Urol **54**(10): 645-650.
Zeisberg, M. and E. G. Neilson (2009). "Biomarkers for epithelial-mesenchymal transitions." J Clin Invest **119**(6): 1429-1437.
Zeng, L., C. Jarrett, K. Brown, K. M. Gillespie, J. M. Holly and C. M. Perks (2013). "Insulin-like growth factor binding protein-3 (IGFBP-3) plays a role in the anti-tumorigenic effects of 5-Aza-2'-deoxycytidine (AZA) in breast cancer cells." Exp Cell Res **319**(14): 2282-2295.
Zha, J. and M. R. Lackner (2010). "Targeting the insulin-like growth factor receptor-1R pathway for cancer therapy." Clin Cancer Res **16**(9): 2512-2517.
Zhang, X., C. Han and J. He (2015). "Recent Advances in the Diagnosis and Management of Bladder Cancer." Cell Biochem Biophys.
Zhao, X. and E. A. Flynn (2012). "Small cell carcinoma of the urinary bladder: a rare, aggressive neuroendocrine malignancy." Arch Pathol Lab Med **136**(11): 1451-1459.
Zhou, J., J. Wang, Y. Zeng, X. Zhang, Q. Hu, J. Zheng, B. Chen, B. Xie and W. M. Zhang (2015). "Implication of epithelial-mesenchymal transition in IGF1R-induced resistance to EGFR-TKIs in advanced non-small cell lung cancer." Oncotarget **6**(42): 44332-44345.
Zhou, Z., Y. Guo, Y. Liu, F. Zhang, Y. Wang, B. Shen, Y. Qin and J. Qiu (2015). "Methylation-mediated silencing of Dlg5 facilitates bladder cancer metastasis." Exp Cell Res **331**(2): 399-407.
Zhu, C., X. Qi, Y. Chen, B. Sun, Y. Dai and Y. Gu (2011). "PI3K/Akt and MAPK/ERK1/2 signaling pathways are involved in IGF-1-induced VEGF-C upregulation in breast cancer." J Cancer Res Clin Oncol **137**(11): 1587-1594.
Zhu H, Y. F., Shi X, Wang D (2015). "Inhibition of BP-2 improves the sensitivity of bladder cancer cells to cisplatin via upregulating the expression of maspin."
Zhu, J., X. Pan, Z. Zhang, J. Gao, L. Zhang and J. Chen (2012). "Downregulation of integrin-linked kinase inhibits epithelial-to-mesenchymal transition and metastasis in bladder cancer cells." Cell Signal **24**(6): 1323-1332.
Zhu, Z., T. Xu, L. Wang, X. Wang, S. Zhong, C. Xu and Z. Shen (2014). "MicroRNA-145 directly targets the insulin-like growth factor receptor I in human bladder cancer cells." FEBS Lett **588**(17): 3180-3185.
Zielinska, H. A., A. Bahl, J. M. Holly and C. M. Perks (2015). "Epithelial-to-mesenchymal transition in breast cancer: a role for insulin-like growth factor I and insulin-like growth factor-binding protein 3?" Breast Cancer (Dove Med Press) **7**: 9-19.

Chapter 8- Appendix

8.1 Manuscripts arising from this work

- Review: Bladder Cancer and Viruses – What's the Truth behind the Myth? [In preparation]
- Effect of IGF-1 on Bladder Cancer Cells [In preparation]
- Insulin-Like Growth Factor Binding Protein 2 (IGFBP-2) Inhibits Growth, Invasion and Colony Formation of Bladder Cancer Cells [In preparation]

8.2 Presentations

- Poster presentation:
  - The SOCS postgraduate academic day, Dec 7th 2012, UoB

    Poster title: Interactions between the E-cadherin/β-catenin and IGF/PI3K pathways in Bladder Cancer
  - The SOCS postgraduate academic day, Dec 10th 2013, UoB

    Poster title: Interactions between the E-cadherin/β-catenin and IGF/PI3K pathways in Bladder Cancer
- Oral presentation:
  - Postgraduate seminar talk, Oct 15th 2013, UoB

    Talk title: Interactions between the E-cadherin/β-catenin and IGF/PI3K pathways in Bladder Cancer
  - Postgraduate seminar talk, May 28th 2014, UoB

Talk title: Interactions between the E-cadherin/β-catenin and IGF/PI3K pathways in Bladder Cancer

- The SOCS postgraduate academic day, Dec 16th 2014, UoB

  Talk title: Insulin-Like Growth Factor Binding Protein 2 (IGFBP-2) Inhibits Growth and Invasion of Bladder Cancer Cells

- Gordon Research Conferences: IGF & Insulin System in Physiology & Disease (to be held), March 11th 2015, Ventura, CA, USA

  Talk title: Insulin-Like Growth Factor Binding Protein 2 (IGFBP-2) Inhibits Growth, Invasion and Colony Formation of Bladder Cancer Cells

8.3 Conferences and Awards

- Gordon Research Conferences: IGF & Insulin System in Physiology & Disease (to be held), March 11th 2015, USA – A talk to be given.
- Alumni Foundation Award - £500
- BACR/CRUK Student Award - £1000
- Gordon Research Conferences Travel Award - $500